

**Electronic Drive for Low Wattage
Metal Halide Lamps**
Focused on
Acoustic Resonance in HID Lamps

vorgelegt von

M.Sc. Farhang Ghasemi Afshar

von der Fakultät IV Elektrotechnik und Informatik
der Technischen Universität Berlin
zur Erlangung des akademischen Grades
Doktor der Ingenieurwissenschaften
Dr.-Ing.

genehmigte Dissertation

Promotionsausschuss:

Vorsitzender: Prof. Dr.-Ing. E. Obermeier

Gutachter: Prof. Dr. rer. nat. H. Kaase

Gutachter: Prof. Dr. rer. nat. K. D. Weltmann

Tag der wissenschaftlichen Aussprache: 6.11.2008

Berlin 2009

D 83

Abstract

In this work the concept of acoustic resonance (AR) in High Intensity Discharge (HID) lamps theoretically and experimentally is studied. A fundamental investigation is carried out in order to get a better understanding of physical backgrounds which are responsible in excitation of acoustic resonances and acoustic instabilities in such lamps.

The existing theories, which have introduced during the last four decades is explored. Based on the theory of acoustic streaming, a new hypothesis about the possible physical reasons for the excitation of acoustic instabilities and the temporal response of the discharge is given. To support the discussed hypothesis a real case of acoustic instability is investigated. A numerical method to solve the wave equations inside the lamp's arc tube which accounts for the temperature distribution of the filling gas is then introduced. In contrast to the classic method, which solves the wave equation in a cylindrical arc tube considering a homogenous sound velocity, the method mentioned in this work, considers the exact geometry of the arc tube and the sound velocity distribution as well. Some different practical methods in order to detect, to avoid or to establish acoustic resonances are then discussed.

There are some phenomena in High Intensity Discharge (HID) lamps which have the potential to make the discharge unstable. Discharge instability, can lead to some transients in light intensity, or in its periodic form, to annoying light flickering. Instabilities appear in a very vast range. Depending on the strength of the source of instability, it varies from a very slight deflection of sodium sheath to extreme deviations of conducting channel from its normal position which can extinguish the lamp as well. In order to detect the existence of such phenomena and predict their potential power, their effects and consequences on the light intensity can be analyzed. This has been carried out by using a tuned model of the human eye-brain system, to predict the perceptibility of the transient changes of light. The concept of *light flicker factor* based on eye-brain model as a measure of discharge instabilities will be introduced. The implementing method of the model and a proper measuring system for light flicker factor is being discussed. Some laboratory experiments to support this method of measurement are presented. In order to avoid the acoustic instabilities in metal halide (MH) lamps a proper method is to supply the lamp with a low frequency square wave (LFSW) current. Due to the topology of electronic ballasts for such an application, there is a high frequency ripple in the current or voltage waveform. It is known that such ripples with sufficient energy at the proper frequency are able to excite acoustic resonance in MH lamps. The threshold value for high frequency ripples in order to excite an acoustic mode and destabilize the lamp is under debate. This threshold is lamp dependent and should be measured experimentally for each lamp type. This work addresses an automated experimental method to determine the threshold value of the power ripple in a frequency range of 10-400 kHz. The experimental results show that less than 1% of power ripple at the resonance frequency is sufficient to excite a detectable (perceptible to the human eye) acoustic instability. The experimental results of this work, in the process of a standardization of low frequency square wave electronic ballasts in the range of 20 to 150W, are already used.

ACKNOWLEDGEMENTS

This thesis is a result of a cooperative work between technical university of Berlin (Fachgebiet Lichttechnik TU Berlin) and R&D department of OSRAM GmbH (HID D-B) in Berlin.

I would like to deeply thank the generous help and friendship of many people without whom this work would not be completed.

I am very grateful for continual support and valuable advice of my supervisors Prof. Dr. rer. nat. H. Kaase and Dr. Ing. F. Serick from technical university of Berlin (TU Berlin). Without their care and consideration before and during this work, this thesis would likely not have matured.

I would like to extend profound thanks to Dr. M. Tüshaus, my supervisor from OSRAM GmbH and director of this project, for his significant support, valuable help, guidance and his very helpful comments.

I like to thank all my colleagues in R&D department of OSRAM GmbH in Berlin and Munich and in technical university of Berlin, for their theoretical and technical support.

I would like to especially thank Dr. S. Lichtenberg, A. Lembcke, S. Boldt and Dr. B. Koch for their friendship and invaluable help for this work and especially for editing and reviewing of this work and my other publications. Also thanks to J. Mühlshlegel for his technical support in constructing the experimental setup.

Thanks to Dr. S. Boluriaan, Dr. T. Hartmann, Dr. E. Honary, W. Moskowitz, Dr. K. Stockwald and Dr. B. Siessegger for their very helpful inputs and informative negotiations.

I highly appreciate valuable supports of Dr. C. Allgeier, Dr. B. Freisinger and H. Hubert all from OSRAM GmbH.

I am really grateful to Prof. H. Mohseni, my professor and advisor in Tehran university, who encouraged and helped me continue my education. For sure without his very supportive aids this was not possible.

Very special thanks to my wonderful wife Sara Honary who powerfully supported me, gave me hope and energy and spent all her valuable time together with me. I am indebted to her because of her endless patience, significant kindness and her helpfulness when it was most required.

Last but not least, I wish to thank my parents for providing me with the opportunity to be where I am. I thank them for their love, support, patience and their confidence through entire my life. I thank them for all they taught me directly or indirectly.

I dedicate this work to my wife and my parents to honour their love.

Contents

1	Introduction	1
1.1	Research Motivation and Practical Purpose	2
1.2	Definition of the Problem	4
1.3	Problem Solving Procedure	5
1.4	Structure of the Dissertation	5
2	Intermittent Vision of the Human Eye and the Modeling Approach	6
2.1	Introduction	7
2.2	Definition of Light Flicker Factor	8
2.3	Signal Processing in Retina	10
2.3.1	Construction of Retina	10
2.3.2	Information Flow in Retina	10
2.4	Scaling Laws of Perception	12
2.4.1	Weber's Law	12
2.4.2	Weber-Fechner Law	13
2.4.3	Stevens' Power Law	13
2.5	Critical Flicker Frequency	13
2.5.1	Talbot-Plateau Law	14
2.5.2	Ferry-Porter Law	15
2.6	Intermittent vision of the Human Eye	16
2.6.1	Ives' Diffusion Theory	16
2.6.2	De Lange's Experiment	18
2.6.3	Flicker Detection Model of Sperling and Sondhi	19
2.6.4	Veringa's Diffusion Theory	20
2.6.5	Realizability of Ferry-Porter Law as a Linear System	20
2.6.6	Experiments of Kelly	21
2.6.7	Kelly's Diffusion-Inhibition Model	22
2.6.8	Studies of Rashbass	23
2.7	Human Eye Temporal Modulation Sensitivity Curve	25
2.7.1	Normalized Filter Characteristics of the Human Eye	27
2.8	Realization of the Light Flicker Meter	28
2.8.1	Model of the visual System concerning Light Transients	28
2.8.2	Realization of the Human Eye Characteristic Filter	30
2.8.3	Digital IIR Filter with Arbitrary Magnitude	35
2.8.4	Implementation of the Visual System Model	37
2.9	Experimental Arrangement and Observation	41

2.9.1	Experimental Setup	41
2.9.2	Model Performance	42
2.10	A Practical Example of Using the Proposed Model	53
3	Excitation of Acoustic Instability in High Intensity discharge Lamps	55
3.1	Introduction	56
3.2	Theory of Acoustic Resonance and Acoustic Instability	57
3.3	Theoretical Prediction of Acoustic Resonance	61
3.3.1	Damping of Acoustic Resonances	62
3.3.2	Hypothesis About the Wall Effect	62
3.3.3	Hypothesis About the Pressure Effect	63
3.3.4	Analytical Solution	63
3.3.5	Effective Sound Velocity	64
3.3.6	Numerical Solution	65
3.3.7	Arc Tube's Geometry	66
3.3.8	Calculation of Eigenfrequencies	66
3.3.9	Concerning Temperature Distribution	67
3.3.10	Example of an AR Calculation	67
3.3.11	Importance of Acoustic Modes	75
3.3.12	Calculation of Acoustic Streaming	81
3.4	Acoustic Resonance and Acoustic Streaming in a Cylindrical Arc Tube	81
3.5	Interference of Acoustic Streaming and the Discharge	83
3.6	Detection of Acoustic Resonance	85
3.6.1	Lamp current	85
3.6.2	Lamp Voltage	86
3.6.3	Lamp Impedance / Conductance	86
3.6.4	Lamp Power	86
3.6.5	Visual Detection and Optical Methods	87
3.6.6	Measurement of Emitted Sound	87
3.6.7	Measurement of the Temperature	87
3.6.8	Optogalvanic Detection of Acoustic Resonance	88
3.6.9	Other Considerations about detection of Acoustic Resonance	88
3.7	Avoidance of Acoustic Instabilities	89
3.7.1	Lamp Related Factors	89
3.7.2	Optimized Ballasting Methods	91
3.8	Benefits of Acoustic Resonance Operation	96
3.8.1	Arc Straightening	96
3.8.2	Color Mixing of Vertically Operated HID Lamps	99
3.8.3	Beam Switching	102
3.8.4	Strength Test of Ceramic Arc Tube and Outer Bulb	102
3.8.5	Determination of Instantaneous Gas Temperature of rare Gas Flashlamp	102
4	Allowed Level of the power ripple in LFSW Ballasts	104
4.1	Introduction	105
4.2	HID Ballast Topology (LFSW)	106
4.2.1	Functionality of Different Blocks in a LFSW Ballast	107

4.2.2	Full Bridge Inverter and Ignition Stage	119
4.2.3	Full Bridge Two-Stage Driver Topology	120
4.2.4	Three-Stage Driver Topology	121
4.2.5	Half Bridge Two-Stage Driver Topology	122
4.2.6	Integration of Buck and Boost Stages	123
4.2.7	Two Stage Driver Topology with 2 nd LC Stage	123
4.2.8	Two Stage Driver Topology with Coupled Inductors Filter	124
4.2.9	Pseudo-Random Switching Frequency	125
4.2.10	Modulated Switching Frequency	126
4.3	Methodology for Measurement of Acceptable Level of the Power Ripple	126
4.3.1	Criterion and Concept of the Experiment	126
4.3.2	Experimental Setup	127
4.3.3	Experimental procedure	128
4.3.4	Results	132
4.4	Effect of Ripple Superposition on the Lamp Power	136
4.5	Conclusion and Discussion	136
5	Temporal Response of Acoustic Resonance Instabilities	140
5.1	Introduction	141
5.2	Concept of the Experiment	143
5.3	Experimental Setup	143
5.4	Procedure of the Measurement	144
5.5	Experimental Results	146
5.6	Evaluation of the Experimental Results	149
6	Experimental Results and Conclusion	153
6.1	Experimental Results	154
6.1.1	Measurements' Results for 35 W Metal Halide Lamps	156
6.1.2	Measurements' Results for 70 W Metal Halide Lamps	158
6.1.3	Measurements' Results for 150 W Metal Halide Lamps	161
6.1.4	Measurements' Results for 250 W Metal Halide Lamps	163
6.2	Conclusion	166
	Appendices	169
A	Coefficients of IIR Filter	169
B	Acoustic Resonance Frequencies for HQI TS 150W WDL	170
C	LabVIEW Program to determine the Allowed Level of the Power Ripple	172
D	List of Publications	175
	References	177

List of Figures

1.1	PTi 150; HCI T 150W WDL; voltage waveform	2
1.2	PTi 150; HCI T 150W WDL; current waveform	2
1.3	PTi 150; HCI T 150W WDL; power waveform	2
1.4	PTi 150; HCI T 150W WDL; Spectrum Analysis with respect to the Power Ripple.	3
2.1	Input and output of the Light Flicker Meter.	7
2.2	Schematic diagram of retina	11
2.3	Retina response to a sinusoidal flickering light.	12
2.4	Scotopic, Mesopic and Photopic vision of the human eye	15
2.5	Dependence of CFF on adaptation level.	16
2.6	Ives' Diffusion Theory	17
2.7	Double flash test of Rashbass.	24
2.8	Bandpass filter characteristics of the human eye.	28
2.9	Realization of the human eye characteristic.	30
2.10	Process of crossover by splitting parent chromosomes.	32
2.11	A comparison between filter characteristics.	34
2.12	Impulse response of the filter, simulating eye response to the flash light stimulus.	37
2.13	Comparison of model and desired filter characteristics.	37
2.14	Block diagram of the light flicker meter.	38
2.15	The method which is used to determine the DC value of luminance signal	39
2.16	Adding the original signal with a DC signal.	40
2.17	Experimental arrangement which is used to measure the light flicker factor.	41
2.18	Model performance test.	43
2.19	An example of input signal with a sinusoidal flickering part of 10 Hz and 0.15% modulation depth.	44
2.20	Flicker factor for the signal of Figure 2.19.	45
2.21	Response of the flicker model to double flash stimuli.	46
2.22	Probabilistic method to determine the threshold of flicker detection.	47
2.23	Schematic diagram of a current pulses to create flickering light.	49
2.24	Brief flash test.	50
2.25	Comparison between sensitivity curves; derived from Henger and modified version of this work.	51
2.26	Experimental test of the model.	53
2.27	Input light signal before and after applying high frequency ripple.	54
2.28	Flicker factor signal shows the transition of the discharge between two states.	54

3.1	Positions of nodes and anti-nodes with respect to standing pressure wave.	58
3.2	Sketch of the arc tube of an OSRAM HCI T 70W ShopLight.	68
3.3	Temperature distribution inside the arc tube.	69
3.4	Calculated sound velocity distribution inside the arc tube.	70
3.5	The first longitudinal acoustic mode considering sound velocity distribution of Fig. 3.4	71
3.6	The second longitudinal acoustic mode considering sound velocity distribution of Fig. 3.4	73
3.7	The third longitudinal acoustic mode considering sound velocity distribution of Fig. 3.4	73
3.8	The fourth longitudinal acoustic mode considering sound velocity distribution of Fig. 3.4	74
3.9	The first radial and the second longitudinal acoustic mode considering sound velocity distribution of Fig. 3.4	74
3.10	The first radial and the fourth longitudinal acoustic mode considering constant sound velocity distribution inside the arc tube.	75
3.11	Normalized eigenvalues in the bracket of [0-15] for both cases of effective sound velocity and distributed sound velocity in ate lamp arc tube.	76
3.12	Calculated resonant frequencies for two cases of effective sound velocity of 500 ms^{-1} and distributed velocity as it is illustrated in Fig. 3.4	76
3.13	Comparison of the resonant frequencies for three different effective sound velocities in the arc tube.	77
3.14	The 18 th acoustic mode considering the constant effective sound velocity of 500 ms^{-1}	78
3.15	Eigenmode's level shows the importance of each eigenfrequency with respect to its potential power to excite acoustic instability. The curve between points is a smoothed moving average of order 4.	78
3.16	Comparison of eigenmode's level for effective sound velocity and distributed sound velocity of Fig. 3.4	79
3.17	The 18 th acoustic mode considering the sound velocity distribution of Fig. 3.4	80
3.18	The difference between two adjacent acoustic resonant frequency decreases for higher resonant frequencies.	80
3.19	Schematic diagram of a cylindrical arc tube when the first longitudinal acoustic mode is excited.	82
3.20	Streamline diagram of acoustic streaming velocity in a cylindrical (r, ϕ =constant, z) tube.	83
3.21	Interaction of acoustic streaming and discharge position in arc tube.	84
3.22	four snap shots of the discharge of an HQI TS 150W WDL lamp.	85
3.23	Comparison of the first and the second longitudinal acoustic modes for a vertically operated lamp.	100
3.24	Acoustic streaming and thermal conduction in a horizontally operated lamp.	101
4.1	Block diagram of a low frequency square wave ballast	107
4.2	Combination of EMI filter, full wave rectifier and boost PFC to convert the ac main voltage to a constant level bus voltage.	108
4.3	PFC conductor current in a half period of AC main line.	109

4.4	Effect of EMI filter on AC main line current.	110
4.5	Low frequency ripple on the output voltage.	111
4.6	Schematic diagram of a buck converter.	111
4.7	Operation of a buck converter with low time constant RC_{buck}	113
4.8	Linear/exponential change of buck inductor current and buck capacitor current.	114
4.9	Coupled inductors filter.	117
4.10	Schematic diagram of a buck converter with coupled inductor construction.	117
4.11	Full bridge and ignition circuitry.	119
4.12	The HID ignition circuit produces high-voltage pulses that are discontinued once the ballast circuit detects the lamp has ignited.	120
4.13	LFSW ballast topology proposed in (Nishimura and others, 1988).	121
4.14	LFSW ballast topology proposed in (Melis, 1998)	121
4.15	Half bridge topology for an HID ballast regarding (Sun and Goriki, 2000) based on (US patent application No. 08,783,557).	123
4.16	The buck type ballast using 2^{nd} LC stage.	124
4.17	Schematic diagram of experimental setup	128
4.18	Frequency response of the experimental setup with a 103Ω resistance.	129
4.19	Flow-chart of the program which automates the measurement process	130
4.20	Flow-chart of the main-block of the program.	131
4.21	Power Ripple calculated using the method suggested by Moskowitz.	132
4.22	Acceptable power Ripple versus the ripple frequency.	133
4.23	Impedance deviations versus the ripple frequency.	134
4.24	The current and voltage waveform of the lamp with a 33.1 kHz sinusoidal ripple and the corresponding power waveform.	134
4.25	Light signal (output of the Lux-meter) vs. time for different values of the power ripple.	135
4.26	Light Flicker Factor curves (semi-log) for the light signals shown in Fig. 4.25.	135
4.27	A comparison of the measurement results of two similar OSRAM HCI-T 70W NDL lamps.	137
4.28	A comparison of the method which is proposed in this work with Olsen's method (Olsen and Moskowitz, 1997).	139
5.1	Schematic diagram of changing the motion trajectory of a particle as a result of presence of an acoustic (streaming) force.	142
5.2	Voltage and current waveform of an OSRAM HCI T 70W WDL Lamp with high frequency ripple.	144
5.3	Schematic diagram of the experimental setup.	145
5.4	Flowchart of the measurement procedure	146
5.5	Acceptable power ripple versus frequency of an OSRAM HCI T 70W WDL lamp.	147
5.6	Light signal deviation vs. time for different values of the ripple durations at the frequency of 32 kHz.	148
5.7	Schematic diagram of the discharge position between electrode tips for a lamp operated horizontally.	149
5.8	Light signal deviation vs. time for different values of the ripple durations at the frequency of 70 kHz	150

5.9	Light signal deviation vs. time for different values of the ripple durations at the frequency of 175 kHz	150
5.10	Light signal deviation vs. time for different values of the ripple durations at the frequency of 250 kHz	151
5.11	Flicker factor vs. ripple duration (semi Log) for different AR frequencies. The power ripple is 20~25%.	151
5.12	Voltage and current waveform of an OSRAM HCI 70W lamp subjected to a 20ms sinusoidal ripple at the frequency of 32 kHz and power ripple of 21%.	152
5.13	Light signal (upper curve) and calculated power waveform (lower curve) for an OSRAM HCI 70W lamp subjected to a 20 ms sinusoidal ripple at the frequency of 32 kHz and power ripple of 21%.	152
6.1	Acceptable power ripple for an OSRAM HCI T 35W NDL lamp	156
6.2	Fluctuations of the lamp power for an OSRAM HCI T 35W NDL lamp operated vertically based up.	156
6.3	Relative impedance of the lamp for an OSRAM HCI T 35W NDL lamp	157
6.4	Light flicker factor for an OSRAM HCI T 35W NDL lamp	157
6.5	Acceptable power ripple for 35 W lamps	158
6.6	Acceptable power ripple for an OSRAM HCI T 70W WDL lamp	158
6.7	Fluctuations of the lamp power for an OSRAM HCI T 70W WDL lamp operated vertically based up.	159
6.8	Relative impedance of the lamp for an OSRAM HCI T 70W WDL lamp	159
6.9	Light flicker factor for an OSRAM HCI T 70W WDL lamp	160
6.10	Acceptable power ripple for 70 W lamps	160
6.11	Acceptable power ripple for an OSRAM HCI TS 150W NDL lamp	161
6.12	Fluctuations of the lamp power for an OSRAM HCI TS 150W NDL lamp operated vertically based up.	161
6.13	Relative impedance of the lamp for an OSRAM HCI TS 150W NDL lamp	162
6.14	Light flicker factor for an OSRAM HCI TS 150W NDL lamp	162
6.15	Acceptable power ripple for 150 W lamps	163
6.16	Acceptable power ripple for an OSRAM HQI TS 250W D lamp	163
6.17	Fluctuations of the lamp power for an HQI TS 250W D lamp operated vertically based up.	164
6.18	Relative impedance of the lamp for an HQI TS 250W D lamp	164
6.19	Light flicker factor for an HQI TS 250W D lamp	165
6.20	Acceptable power ripple for 250 W lamps	165
6.21	Acceptable power ripple for 150W lamps compared with PTi 150 Power Ripple.	167
B.1	Acceptable power ripple for HQI TS 150W WDL No. 1	171
B.2	Acceptable power ripple for HQI TS 150W WDL No. 1 10-30 kHz	171
C.1	LabVIWE program which is used to determine the allowed level of the power ripple	173
C.2	LabVIWE program which is used to determine the allowed level of the power ripple	174

List of Tables

2.1	Temporal Sensitivity of the Human eye in different frequencies	27
2.2	Results of a Flicker Factor threshold test for four probe persons.	48
2.3	Amplitude of the pulse train and the value of the light flicker factor for different frequencies	49
2.4	Amplitude of current pulses for flash test and the value of the light flicker factor	50
3.1	Calculation of acoustic resonance eigenvalues frequencies for a given arc tubes geometry	72
6.1	Max. and min. acoustic resonant frequency for low wattage metal halide lamps.	168
A.1	Coefficients of eight 2^{nd} order and the corresponding 40^{th} order IIR filters. . . .	169

Chapter 1

Introduction

1.1 Research Motivation and Practical Purpose

Electronic ballasts are used to transform the power of the main source and produce the voltage and the required current of the lamp. As a byproduct, the ballast typically also produces a current ripple at frequencies higher than 10 kHz.

A simultaneous measurement (oscilloscope trace) of the voltage and current of an OSRAM POWERTRONIC PTi ballast supplying an OSRAM HCI T 150 W WDL lamp is illustrated in Figures 1.1 and 1.2.

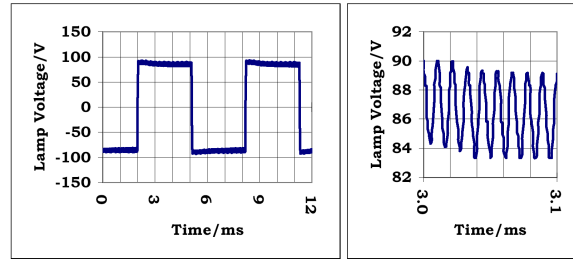


Figure 1.1: Ballast: PTi 150; Lamp: HCI T 150W WDL; voltage waveform.

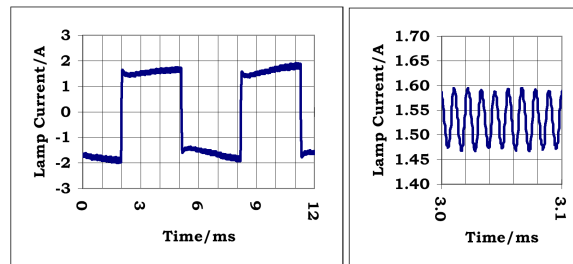


Figure 1.2: Ballast: PTi 150; Lamp: HCI T 150W WDL; current waveform.

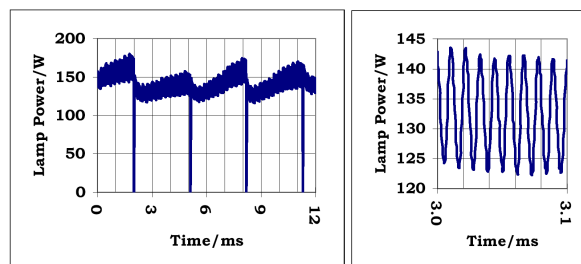


Figure 1.3: Ballast: PTi 150; Lamp: HCI T 150W WDL; power waveform.

In both figures a zoomed window with a length of 0.1 ms is illustrated to show the high frequency superimposed ripple of current and voltage. Regarding Fig. 1.1 or 1.2 the high frequency component, which is significantly noticeable, has a frequency of about 90 kHz. By multiplying the voltage and current waveforms the lamp instant power is calculated (Fig. 1.3). As it can be seen the ripple of current and voltage are transferred to the lamp power. The frequency of the power ripple is the same as that of the current or voltage waveform. The reason is that in both positive and negative low frequency cycles of the current and voltage the

high frequency ripple is superposed on a positive or negative dc level respectively. Assuming the positive low frequency half cycle

$$i(t) = I_{dc} + a \cos(\omega t) \quad (1.1)$$

$$v(t) = V_{dc} + b \cos(\omega t) \quad (1.2)$$

where ω is the ripple frequency and a and b are the amplitude of the current and voltage ripples respectively. The instant power of the lamp is then calculated as follows

$$p(t) = I_{dc}V_{dc} + [V_{dc}a + I_{dc}b] \cos(\omega t) + ab \cos^2(\omega t) \quad (1.3)$$

Since the value of a and b in comparison with I_{dc} and V_{dc} are low the term of ab is very small and can be neglected. Hence, the power ripple has a frequency equal to the current or voltage waveform.

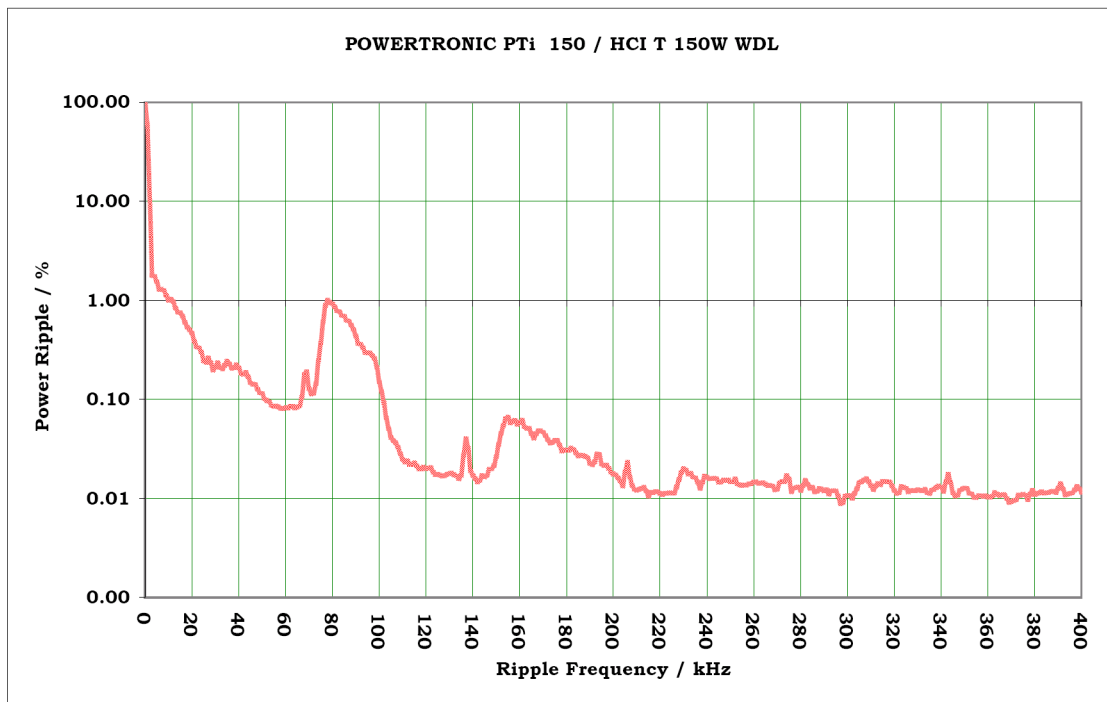


Figure 1.4: Spectrum Analysis with respect to the Power Ripple (SAPR) after (Moskowitz and Olsen, 2004) for POWERTRONIC PTi150 operating an OSRAM HCI T 150W WDL. The highest value of the power ripple is about 1% at the frequency of 78 kHz.

(Moskowitz and Olsen, 2004) proposes a method to measure ripple generated by an HID ballast. By applying the method of Moskowitz, to measured current and voltage waveforms of Figures 1.1 and 1.2, the spectrum of Power Ripple (Fig. 1.4) can be generated.

As it was expected, the significant peak of the frequency spectrum appears in the frequency range of about 75-95 kHz with the highest value at 78 kHz. The reason of this slight difference with the value of 90 kHz which is derived from Figures 1.1-1.3 is as follows:

The high frequency component which is superimposed on the current or voltage does not have a constant frequency. Depending on the position of the zoom window along the time

axis, the observed high frequency component shows a different frequency. This can be seen in frequency spectrum as well. There is not a single high frequency component along the frequency spectrum rather than there is a region (75-95 kHz) in which the high frequency components have larger amplitudes.

When the associated power with the current ripple exceeds a given threshold level of the nominal power of the lamp, the lamp can become unstable and potentially fail. As a result, the high frequency components of the lamp power spectrum should be kept under a given threshold value. Attenuation of the high frequency components needs to use extra filters which increases the cost, weight and the size of the ballast.

Although this threshold value is agreed to be 1.5% of the lamp power, the exact value of this threshold is not known. A question of how much ripple should be allowed to be passed from the ballast to the lamp at acoustic frequencies is currently under debate in the lighting community, especially in the standard¹ committees (Olsen and Moskowitz, 2005).

The main practical purpose of this research is to determine the above mentioned threshold value for different low wattage (up to and including 250 W) metal halide lamps.

1.2 Definition of the Problem

The third chapter of this work explains in details how the existence of high frequency components in the lamp power spectrum may affect the lamp discharge which can lead to the flickering phenomenon or a single change of emitted light of the lamp.

Criterion:

If the fluctuations of emitted light of the lamp is perceptible to the human eye the high frequency components of the lamp power which are responsible for these fluctuations should be removed.

Applying this criterion, fulfills two following applications:

- Obviously light flickers or some fluctuations in emitted light of a light source is not acceptable and the light system (combination of the lamp and the ballast) is not satisfactory. Therefore, applying this criterion results in avoidance of such failures.
- The minimum (the most harmless) effect of high frequency components in the lamp power is a *just perceptible* change of the emitted light. The more significant effects which are accompanied with larger amplitudes of high frequency components firstly appear as a just perceptible change of light when their amplitudes are still low. Hence, applying this criterion can definitely avoid the occurrence of more significant effects of high frequency components as well.

problem:

¹Such as ELMAPS, European Lamp Manufacturers Association in the Preparation of Standards.

The question is to find a method to investigate the effect of high frequency components in power spectrum of low wattage metal halide lamps. The purpose of this investigation is to define the acceptable power ripple of the lamp in such a way that the light intermittent is not perceptible to the human eye.

1.3 Problem Solving Procedure

To solve the above mentioned problem, it is necessary to design and implement a measuring system based upon the criterion which is formerly discussed.

In this regard, the first logical step is to implement a model which simulates the human vision with respect to the eye-brain response to the intermittent stimuli. The desired model should be able to decide between perceptible and imperceptible changes of light. It is expected that the model would be encountered with both periodic and aperiodic light intermittent. This implies that the response of the model should be valid for the both mentioned input signals.

The second step is design and implementation of a measuring system which is able to add a specific frequency component to the frequency spectrum of the lamp power or remove it. The desired system should be able to superimpose a given (with respect to its frequency and its amplitude) high frequency ripple on the lamp current and check its effect on the emitted light of the lamp. The effect of high frequency ripple on the electrical parameters of the lamp such as lamp impedance are investigated as well. An automated measuring system then scans whole frequency region of the interest to determine the lamp response to the high frequency components of its power spectrum.

1.4 Structure of the Dissertation

In the second chapter a methodology which is used to design a model which accounts for the human vision system to detect perceptible light intermittent is given. Afterwards the model implementation and modifications procedures are explained.

The third chapter is dedicated to theoretical explanation of Acoustical Resonances (ARs) in HID lamps and their desired and undesired effects on light sources. The purpose of this section is to review the existing theoretical explanation about the acoustic resonance phenomenon and introduce some hypotheses as a theoretical contribution in this topic.

In the fourth chapter firstly some different types of low frequency square wave ballasts for low wattage HID lamps are introduced. Some methods to attenuate the high frequency components which flow from ballast into the lamp is discussed. Afterwards the implementation of a practical method to evaluate the effect of high frequency components of the power spectrum of HID lamps is explained. Basically the main practical purpose of this investigation is covered in this chapter.

Chapter five explains a new method to measure the onset time of AR excitation in HID lamps. This investigation helps us in better understanding of the physical backgrounds of the phenomenon of acoustic resonance in HID lamps.

In the sixth chapter the results of the measurements which are carried out based on the method explained in the fourth chapter is given. The chapter gives a conclusion about the whole work as well.

Chapter 2

Intermittent Vision of the Human Eye and the Modeling Approach

2.1 Introduction

This chapter explains the development of a measuring system which simulates the human vision system with respect to the flickering light and light intermittent. It is desired to develop a system which detects if a transient light signal is perceptible to the human eye or not. In fact we need a model which accepts a light signal as an input and provides an output signal resembling the human vision response with respect to the perceptibility of transient light. It should be noted that the phrase of *light signal* which will be used frequently in this chapter refers to a time signal which is proportional to the luminance.

Transients of light signal can be divided into two types. The first type is periodic light signal in which the light signal shows continuous repeating changes. Emitted light of a glow lamp which is supplied with the network shows a periodic light signal with a frequency of doubled of the network frequency. The emitted light of a cathode ray tube is the other example of this type. When periodic transients of light signal are perceptible to the human eye then it is called a *Flickering Light*. Although the emitted light of a glow lamp, supplied with the network, changes periodically, it is not a flickering light since the light transients are not perceptible.

The second type of light transients is non-periodic changes of light signal. The example of this type is experienced when there is an immediate notch voltage in the network. In this case the emitted light of the glow lamp is decreased for a short time and then resumes to its previous base line again. Alternatively an immediate increase of the voltage may be detected when the radiated light of the glow lamp increases.

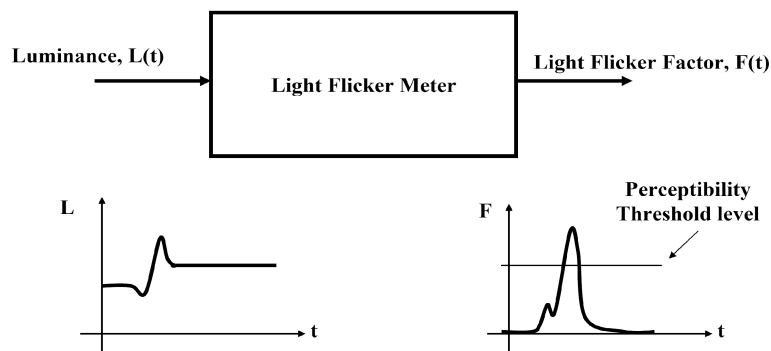


Figure 2.1: Input and output of the Light Flicker Meter.

The desired model should be able to detect both types of light transients. The output of this model which is called *Light Flicker Factor*¹ determines the level of the flickering light. In fact the model interprets the quality of the light flicker to a quantitative value. As a result any light transient can be evaluated quantitatively and can be categorized as perceptible or imperceptible to the human eye. To fulfill this idea the value of the light flicker factor will be compared with a threshold value above which the light transient is perceptible. Actually the output of the model is a positive signal which gives the flicker factor corresponding to the input signal. If the value of the light flicker factor signal exceeds a threshold level the light signal at that point is flickering or shows a perceptible transient. Fig. 2.1, schematically illustrates a flicker meter with input signal and its corresponding output as the light flicker factor.

¹In this work the phrase of Light Flicker Factor is used for both periodic and non-periodic changes of light.

The process of design and implementation of such a measuring system, based on existing models and theories about the human vision response to the light intermittent, is covered in this chapter.

Although this model and measuring system is designed to check the excitation of acoustic resonances in HID lamps, it would be used for any application in which the light transient with respect to the human eye perceptibility is important. In fact any distortion of the discharge in HID lamps may result in some kind of instability of the conducting channel. Some phenomena such as self magnetic forces generated by the discharge current, movement of the arc attachment on the electrode, dimming (in some cases) and non-optimized electrode design can result in discharge instability in HID lamps.

Helical instability is a result of self magnetic forces of the discharge current. The discharge current has two components, axial and azimuthal. The azimuthal component, generates an axial magnetic field and the axial component of current, generates an azimuthal magnetic field. The result is a helical (spiral) field. The current is guided along the twists of the spiral, or the lines of magnetic forces. This process favors the helical arc configuration in contrast to the wall stabilizing forces which lead to cylindrical form. In a normal operation the stabilizing forces balance the magnetic forces. In high frequency operation, the process results in a movement of the discharge around a fixed point. This becomes more visible when the lamp is dimmed at high frequency operation (Fellows, 2003).

Movement of the arc attachment on the electrode causes the electrode instability. For massive electrodes this can be a somewhat random movement of the attachment on the surface of the electrode (Lichtenberg and others, 2002). For electrodes with winding, this could be a movement between winding and electrode tip, especially in high frequencies (Fellows, 2003).

Existence of significant re-ignition peak ² on the voltage waveform might be a source of the light flicker. If the re-ignition time for each electrode is different, then the electric current and consequently the intensity of the emitted light will be different for each half cycle. For network frequency supply of 50/60 Hz this leads to a flickering light of the same frequency (Fromm and Hohlfeld, 1993).

Mentioned effects and processes can change the shape or the position of the discharge in the arc tube or even both. These changes can be periodic or just a single transient. Any single or periodic changes of shape and/or position of the discharge, can consequently affect the emitted light of the lamp. In order to be able to evaluate these light transients, 'light flicker factor' is being defined. This is a quantity which illustrates the discharge instability with respect to the human eye sensitivity to the light transients. This means, instabilities which lead to the light fluctuations, for which human eye shows more sensitivity, are interpreted as more serious ones.

2.2 Definition of Light Flicker Factor

"Light flicker refers to quick, repeated changes in light intensity - that light appears to flutter and be unsteady" (CCOH)³. The light intensity can be interpreted as a photometrical quantity such as *luminous flux*, *luminance* or even *illuminance* depending on the application. **Percep-**

²The finite integral $\int (U - U_s) dt$ over Δt determines the significance of the re-ignition peak. Where U is the voltage waveform, U_s is the steady state value of the voltage in a half cycle and Δt is the time duration of the re-ignition peak (Fromm and Hohlfeld, 1993).

³Canadian National Center for Occupational Health and Safety.

tibility to the human eye is an important concept, which is tightly related to the light unsteadiness. In this work flickering is defined as any change of the luminance which is detectable by the human eye. Before discussing the proposed method to quantify the light flicker, it is helpful to review some previous attempts in this regard.

To express the light flickering quantitatively, different equations have been used. Some of them are pointed out in (Lindner, 1992) as follows:

$$F = \frac{\phi_{\max} - \phi_{\min}}{\phi_{\max} + \phi_{\min}} \quad (2.1)$$

where F is the flicker factor and ϕ_{\max} and ϕ_{\min} show the maximum and minimum value of the luminous flux consequently (Lindner, 1992). Assume a simple form of luminous flux:

$$\phi(t) = \phi_{mean} + a \cos(2\pi ft) \quad (2.2)$$

Using such a basic definition (2.1), flicker factor provides us only with some information about the amplitude of the unsteadiness of the light. What we calculate for F , using equation (2.1), would be equal for two luminous flux signals, with the same ϕ_{mean} and a , but different frequencies. The other shortcoming of this definition is its dependence on the length of the light signal. If we consider some local extremum in the investigated signal, then only the global extremum would appear in the calculation and others will be ignored.

Two other expressions for light flickering mentioned in (Lindner, 1992) are defined as follows:

$$F = \frac{\phi_{\max} - \phi_{\min}}{\phi_{\min}} \quad (2.3)$$

with the same parameters like equation (2.1), and

$$F = \frac{A_1}{A_1 + A_2} \quad (2.4)$$

where A_1 is the area under $\phi(t)$ above ϕ_{mean} and A_2 is the area under ϕ_{mean} . All above definitions which try to interpret the light flicker as a quantity are not representative due to the nature of human eye filtering which will be explained later in this chapter. The concept of filtering nature of the human eye is considered in European standard EN 50006, by defining F_{10} flicker factor (Henger, 1986).

$$F_{10} = \sqrt{\sum m^2(f_i)G^2(f_i)} \quad (2.5)$$

Where $m(f_i)$ is the temporal modulation depth of the light intensity (luminance) which is calculated using the i^{th} Fourier component of the luminance signal as follows

$$m(f_i) = \frac{L_{i,\max} - L_{i,\min}}{L_{i,\max} + L_{i,\min}} \quad (2.6)$$

$G(f_i)$ is the value of the normalized filter characteristics of the human eye with respect to the frequency f_i .

Pabst in his paper (Pabst, 1986) suggests a light flicker-meter to measure the F_{10} flicker factor with the following definition:

$$F_{10} = \frac{1}{\phi(0)} \sqrt{\sum_i \phi^2(f_i) G^2(f_i)} \quad 100\% \quad (2.7)$$

where $\phi(f_i)$ is the i^{th} Fourier component of the luminous flux, $\phi(0)$ is the DC term (mean value) of the luminous flux and $G(f_i)$ is the same as in equation (2.5).

Before discussing about the model and its design process, a short introduction to the human eye vision system namely the retina is given. The purpose of this section is to recall the reasons for which the human eye perceives some transients of light signal while does not detect some others. This chapter is continued with investigating some laws governing the human vision and reviewing the previous researches with respect to the human intermittent vision. Afterwards the proposed model which is developed based on experiments and model of Rashbass (Rashbass, 1970) and UIE voltage flicker meter (EN 61000-4-15 , 1998) is being discussed.

2.3 Signal Processing in Retina

“The retina is a family piece of tissue, barely half a millimeter⁴ thick, that lines the inside of the eyeball” (Kolb, 2003).

The human vision is a quite complex system, with many chemical and physical processes. To understand the functionality of the retina it is necessary to know about its anatomy and physiology. However, discussing about its details is out of scope of this work. After a very brief introduction to the retina’s construction, the information flow in the retina which explains the filter characteristics of the vision is explained.

2.3.1 Construction of Retina

There are three major layers constructing the retina. The first layer contains photoreceptors. This layer lies against the back of the eyeball. There are two types of photoreceptors, cones and rods. The total number of rods is much more than the total number of cones. Rod photoreceptors are responsible for low-light vision while cone photoreceptors are used for day-light bright color vision (Kolb, 2003). The population of rods and cones strongly changes over the surface of the retina. In fovea there are only cones. On this area the retina has its best resolution and very detailed information of an image can be detected on this area. In fact cones are distributed over whole area of the retina with the maximum population in fovea (Hubel, 1989).

In the second layer which is called *inner nuclear layer*, lie *horizontal cells*, *bipolar cells* and *amacrine cells* (Kolb, 2003).

The third layer which is actually the surface layer of the retina contains the *ganglion cells*.

2.3.2 Information Flow in Retina

Within the retina, information passes from the photoreceptors to the bipolar cells and then on to the ganglion cells. At each stage along this most direct visual pathway (illustrated in Fig.

⁴According to (Hubel, 1989) the thickness of the retina is about a quarter of a millimeter.

2.2), the responses are modified by the activation of lateral connections involving horizontal and amacrine cells. Thus the analysis of visual stimuli begins even in the retina (Dubuc, -).

When a light stimuli strikes the surface of the retina, Photoreceptors transduce the light energy into a change in membrane potential. Both cones and rods response to light with a slow hyperpolarizing response (Kolb, 2003). It should be pointed out that in biology, hyperpolarizing means the absolute value of the cell's membrane potential increases.

This analogue signal which is produced by photoreceptors, propagates through the other cells (horizontal, bipolar and amacrine cells) toward the ganglion cells (Fig. 2.2).

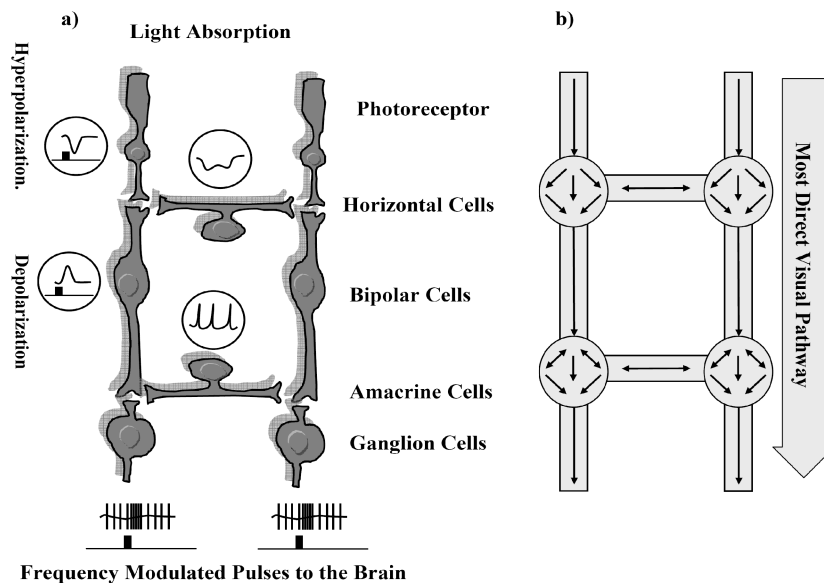


Figure 2.2: a) Schematic diagram of three layers of retina with action potentials for each part. b) Flow of information between different cells within retina (Haitz, 1986).

At this level the input analogue signal to the ganglion cells is converted to digital information. The output of the ganglion cells is an action potential. “*Action potential*” is the technical term used to describe a nerve impulse. It consists of a brief, reversible polarization that propagates along an axon” (Dubuc, -).

The amplitude or intensity of action potentials is always constant. In fact they are digital (all or nothing) events. When the intensity of a stimulus is below the neuron's excitation threshold, nothing happens. If the intensity of the stimulus exceeds this threshold value, the action potential is triggered. No matter the stimulus is just exceeded the threshold level or it is quite larger than the threshold, the action potential will be triggered.

Since the amplitude of action potentials is constant, consequently, the only way a neuron can transmit information is by varying the *frequency* of its action potentials (Dubuc, -). This means when a light signal strikes the retina, the event is transmitted to the brain due to the change of the frequency of the action potentials of ganglion cells.

Fig. 2.3 schematically shows a typical response of the retina to a sinusoidal flickering light. When the frequency of the flicker is low (a and b in Fig. 2.3) the resolution of the ganglion cells frequency is sufficient to code the light fluctuations. In contrast, for light flickers with higher frequencies (c and d in the same figure) the frequency of the action potentials of ganglion

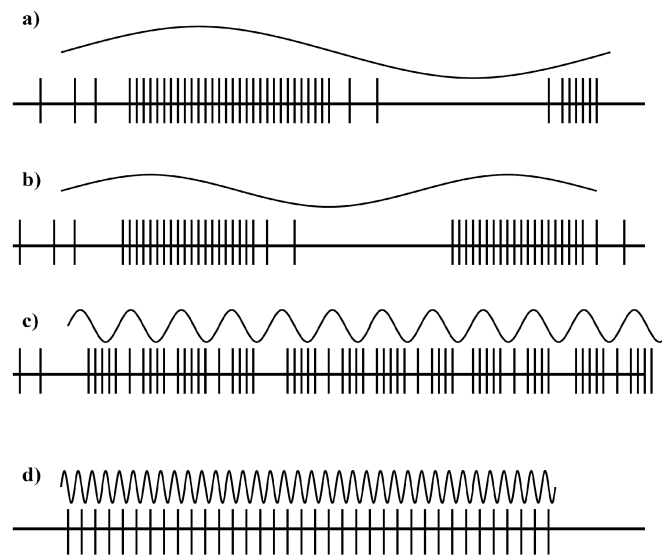


Figure 2.3: Retina response to a sinusoidal flickering light, after (Rackensperger and Grüsser, 1966), cited by (Haitz, 1986).

cells is not sufficient to sample all transients of light signal. As a result a flickering light with sufficiently high frequency appears as a continuous light to the human eye.

In addition, the whole process of changing the light stimulus to electrical signal (especially in the stage of photoreceptors) is a relatively slow process. Hence, the light transients only up to a limited frequency are perceptible to the human eye and very fast changes of light can not be detected.

2.4 Scaling Laws of Perception

2.4.1 Weber's Law

According to the Weber's Law⁵, just-noticeable differences⁶, JND's, in the intensity of various stimuli are proportional to the intensity of initial stimulus (for some range of stimuli).

$$k = \frac{\Delta I}{I} \quad (2.8)$$

where ΔI shows the difference threshold, I stands for the base line of the magnitude of stimulus (or initial stimulus intensity) and k is a constant (Schieber, 2006).

For instance, if a luminance of 100 cd/m^2 must be increased by 5 cd/m^2 in order for the difference to be perceptible, then an increase of 10 cd/m^2 would be necessary for a luminance of 200 cd/m^2 to be perceptible.

Weber's law can be rewritten in the following form as well (Kuge, 2002)

⁵Named after the German psychophysicist, Ernst Heinrich Weber (1795-1878).

⁶This term is also known as Difference Threshold.

$$dp = k \frac{dI}{I} \quad (2.9)$$

where dp shows the differential change in perception, dI stands for differential increase of stimulus, k is a constant and I is the amplitude of the instant stimulus.

According to (Ives, 1922) Kennelly and Whiting in 1907, stated that their observations are in accordance with Weber-Fechner⁷ stimulus-sensation law, considering the ‘sensation of visibly flickering illumination’. This means that they considered P as flicker sensation and I as sensation of visibly flickering illumination and ΔI as a change of flicker amplitude or modulation depth of stimulus.

2.4.2 Weber-Fechner Law

In the 1860’s Fechner elaborated on Weber’s law and suggested that the psychological response P might be built up from JND’s and could therefore be described with the formula⁸

$$P = k \cdot \ln \frac{I}{I_0} \quad (2.10)$$

where k is another constant and I_0 is that threshold of stimulus below which it is not perceived at all. This logarithmic relationship suggests that if stimulus is multiplied by a factor like α , its corresponding perception will be added with a constant value of $k \cdot \ln(\alpha)$. It should be noted that this law is accepted as a general law of stimulus-sensation, not only for light and vision, but for instance for sound and hearing as well.

2.4.3 Stevens’ Power Law

Stevens’ power law proposes the relationship between the magnitude of a physical stimulus and its perceived intensity. According to this law, the magnitude of a subjective sensation (Ψ) increases proportional to a power of the stimulus intensity (I) (Stevens, 1975)

$$\Psi = kI^\alpha \quad (2.11)$$

In this equation k is a constant, and α indicates how fast the magnitude of the sensation grows as the stimulus intensity increases. For example this value for brightness (5° in dark) is about 0.33 (Montag, 2002 I.). Note that, brightness is the perception elicited by the luminance of a visual target. Regarding Stevens’ power law, if the luminance of a target increases with a factor of 10, its brightness to the human eye will be approximately duplicated.

2.5 Critical Flicker Frequency

Critical Flicker Frequency (CFF) is the frequency at which in the vision system fusion occurs and flickering light source appears as a continuous light. A typical value for CFF is about 30-40 Hz and there are many factors which can affect the flicker perceptibility of the human eyes. Some important factors which affect the CFF value are as follows:

⁷It is important to state that in (Ives, 1922) the definition of Weber-Fechner law is as follows: $\Delta S = \frac{\Delta I}{I}$ which is another form of Weber Law as it is defined in (2.9).

⁸source : <http://de.wikipedia.org/wiki/Weber-Fechner-Gesetz>

- *Size and retinal position of the test stimulus*

Due to the non-homogenous population of rod and cone receptors on the surface of retina and their different temporal response, the sensitivity of retina varies with size and position of the stimulus. For small fields about 1° , fovea is the most sensitive and for large fields the peripheral is the most sensitive (Brundrett, 1992). The most sensitivity to the flicker (highest CFF) has been found by Hylkelma with a 10° test field located 30° away from fovea (Brundrett, 1992).

- *Intensity of stimulus*

Under different light levels (scotopic, mesopic and photopic as is illustrated by Fig. 2.4) the human eye shows different responses to the light transients. The reason is that in scotopic vision more rods photoreceptors are involved while in photopic vision the contribution of cone photoreceptors dominates. These two types of photoreceptors have different temporal properties which determines their time response to the flickering stimulus, hence the sensitivity of the eye to the flickering light changes from scotopic to photopic level.

According to (Perlman, 2005), "The maximal frequency of stimulation that can be perceived as flickering, show low CFF in dim illumination (scotopic-mesopic) that rises with stimulus intensity until a plateau phase of about 15 Hz is reached. Under cone vision conditions, high intensity stimuli can be perceived as flickering at frequencies of 30 and even 50 Hz (Conner and MacLeod, 1976). However, when special care is taken to selectively desensitize the cones and thus, reveal the rod function under bright illumination, flicker fusion frequencies are achieved at 28 Hz (Conner and MacLeod, 1976)."

The effect of intensity of stimulus will be explained under the Ferry-Porter law (2.6.2) as well.

- *Spectral composition of the test stimulus*

This item is important under scotopic vision and deals with very low intensities of light which is out of scope of this work.

- *Age of the test subject*

Sensitivity to the flicker increases up to 20 years old and slowly declining with further increase in age. This reduction of sensitivity is due to decrement of the light intensity reaching the retina as a result of thickening and discoloring⁹ of the lens and the decreasing size of pupil (Brundrett, 1992).

2.5.1 Talbot-Plateau Law

Talbot-Plateau Law¹⁰ describes the brightness of an intermittent light source which has a frequency above CFF (Hentschel, 2002).

⁹The normal clear lens getting milky or cloudy as a natural process of aging, caused by years of exposure to sun light.

¹⁰Also known as Talbot's Law

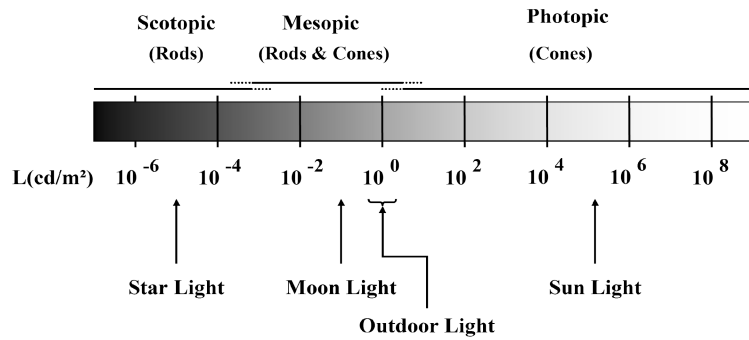


Figure 2.4: Scotopic, Mesopic and Photopic vision of the human eye, after (Rinalducci and others, 1999), cited by (Elholma and others, 2004).

$$L_m = \frac{1}{T} \int_0^T L(t) dt \quad (2.12)$$

where $L(t)$ is the intermittent luminance as a function of time. This law states that above CFF, subjectively fused intermittent light and objectively steady light (of equal color and brightness) will have exactly the same luminance. In other words, brightness sensation from the intermittent light source is the same as if the light perceived during the various periods of stimulation had been uniformly distributed over the whole time. The Talbot-Plateau Law applies only above the CFF, and shows a linearity of vision system at flicker fusion.

2.5.2 Ferry-Porter Law

Critical Flicker Frequency CFF is proportional to the logarithm of the luminance of flickering stimulus $L(t)$. It can be expressed as

$$CFF = a \cdot \text{Log}(L_m) + b \quad (2.13)$$

where a and b are constants and L_m is the mean value of Luminance (adaptation level), regarding Talbot equation (2.12).

Considering square wave light signal and L_m between 2 and 300 cd/m^2 , constant values are about 12 Hz and 33 Hz for a and b respectively (Hentschel, 2002). This basic law shows that critical flicker frequency changes logarithmically with the luminance. The higher the mean value of light intensity is the larger the value of the critical frequency, as it is shown in Fig. 2.5. In the other words, human eye shows more sensitivity to the light transients in the higher light intensities, with the proper amplitude of higher frequency components. A practical usage of this law is that if a monitor is flickering decreasing its intensity level will possibly eliminate the flickering.

Ferry-Porter law shows the frequency at which in the human vision system fusion takes place and beyond that, periodic changes of the light signal is imperceptible. Note that this law deals only with higher frequency region beyond which the fusion effect will occur in the vision system of the human. It has been shown that the Ferry-Porter law, is valid only in a range of stimulus intensity (Kelly, 1961). By increasing the intensity some kind of saturation takes place, and slope of the curve decreases gradually. In Kelly's experiment (Kelly, 1961) with wide

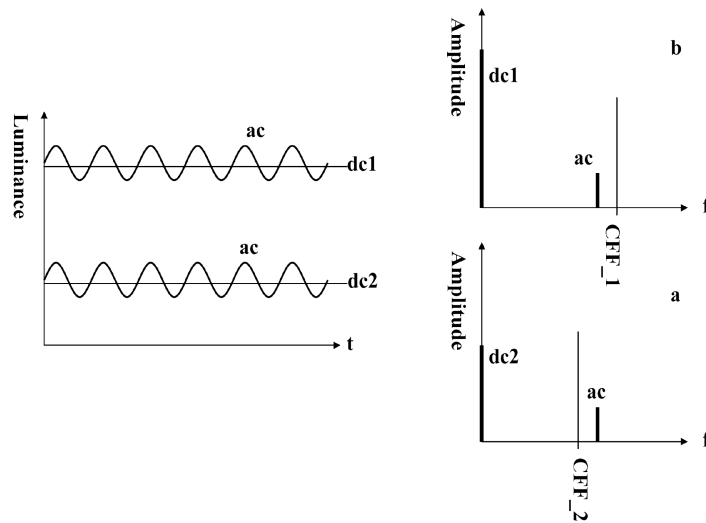


Figure 2.5: Dependence of CFF on adaptation level. Two light signals with the same ac component but different dc components. a. When dc value is low, according to the Ferry-Porter law CFF is low, which could be less than the frequency of ac component, in this case the light signal appears as a constant light. b. Increasing the light intensity (dc value) increases CFF to the values which could be greater than ac component's frequency. Therefore the light fluctuations could be noticeable. This will be happened only if the ratio of ac/dc remains greater than the necessary threshold, as Weber-Law suggests.

stimulus, from about 0.1 to 10,000 td¹¹, and 100% depth modulation, Ferry-Porter law is valid only in the region of 5 to 500 td.

2.6 Intermittent vision of the Human Eye

2.6.1 Ives' Diffusion Theory

In 1922, Ives proposed a model, concerning the diffusion of photochemical product in a receptor cell (Ives, 1922). He proposed a model of intermittent vision with two important concepts. Firstly, that there is a Logarithmic relationship between stimulus and its response (Ferry-Porter law). And secondly the validity of Talbot-Plateau's law, which states, the response (sensation) shall be the same for the same mean illumination, no matter in steady or intermittent, for the frequencies greater than CFF. For his theory he suggested three stages:

- *Stage I*

exciting process, a photochemical reversible reaction of such a nature that the equilibrium value under steady illumination is proportional to the logarithm of the stimulus.

¹¹Convexional retinal illuminance (trolands) is the product of the pupil area (mm^2) times target illuminance (cd/m^2). For a pupil area of 1 mm^2 the value of retinal illuminance and target illuminance are the same i.e. 1 td = 1 cd. It is meant as a method for correcting photometric measurements of luminance values impinging on the human eye by scaling them by the effective pupil size. Source: <http://en.wikipedia.org/wiki/Troland> and <http://de.wikipedia.org/wiki/Troland>

- *Stage II*

conduction process, according to Fourier diffusion law, as developed to cover conduction accompanied with leakage and re-composition of diffused substance.

- *Stage III*

perception process, in which the criterion of perception is that the time rate of change of transmitted reaction must exceed a constant critical value. Fig. 2.6 illustrates stage I and II.

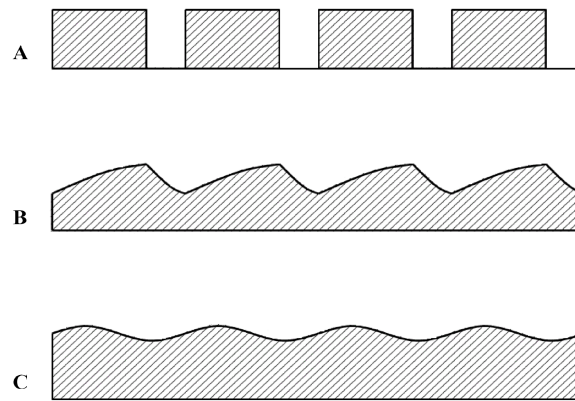


Figure 2.6: Ives' Diffusion Theory, A. Stimulus, B. Reaction of photochemical C. Reaction at far side of conducting medium (Ives, 1922).

For the first stage he proposed the following equation in order to cover such kind of logarithmic and reversible behavior of the photochemical.

$$C \frac{d\theta}{dt} + be^\theta = f(I, t) \quad (2.14)$$

Where C is the capacity of the cell, θ is the potential or concentration of ions in the cell, b is a constant and $f(I, t)$ stands for the stimulus. The equation states that energy is being received by the system, at a rate determined by $f(I, t)$, is being stored (capacity of the cell), and being lost in such a way that in steady state $d\theta/dt$ goes to zero, or the potential remains constant.

A general equation for stimulus with the steady value of ΦI can be expressed as follows¹²:

$$f(I, t) = \Phi I + A \sin(\omega t) + B \sin(2\omega t) + C \sin(3\omega t) + \dots \quad (2.15)$$

In order to realize the concept of the second stage he started with Fourier diffusion equation

$$\frac{\partial f}{\partial t} = c \frac{\partial^2 f}{\partial x^2} - \rho \cdot f \quad (2.16)$$

where c is the diffusion constant and ρ shows the recombination rate of the photochemical before reaching the cell membrane. Ives proposes that the excited photochemical substance must be carried from its exciting position by diffusion to the position of the stimulation. Ives

¹² ΦI is the steady of intermittent illumination, caused by the light source of I which is chopped with a rotating sector disk with an open fraction of Φ .

considered periodic sinusoidal¹³ boundary condition, and found a response function dominated by the terms of the form of

$$\exp\left(-k\left[(\omega^2 + \rho^2)^{1/2} + \rho\right]^{1/2}\right) \quad (2.17)$$

Ives showed that for all ρ greater than 10, provided ω greater than 20, and subsequently the term of $-k\left[(\omega^2 + \rho^2)^{1/2} + \rho\right]^{1/2}$ would be proportional to ω . Therefore the final response (amplitude sensitivity function) at high frequencies would be approximately proportional to

$$e^{-k\omega} \quad (2.18)$$

As a special case of stimulus, Ives considered an alternating uniform light and completely dark intervals. Then considering the criterion noted under stage III, the relationship between frequency and amplitude, obeys the following equation:

$$\omega = k \ln \frac{I\Phi(1 - \Phi)F}{k'} \quad (2.19)$$

in order for such a stimulus to be perceptible. Where $\omega = 1/\tau$ stands for critical rotational angle, F is the form factor, Φ shows the ON fraction of the stimulus signal, k and k' are constants and I stands for intensity of Stimulus. Equation (2.19) which obeys Ferry-Porter law, shows that with a light flickering with higher frequencies, human eye needs higher amplitude of the stimulus to percept the light fluctuations. In other words, according to this equation, human eye sensitivity decreases with increasing flicker frequency, in a logarithmic manner. This is what represented by equation (2.18).

2.6.2 De Lange's Experiment

In 1958 H. De Lange published the results of his experiments investigating the dynamic nature of the human fovea-cortex system with the task of finding the attenuation characteristics $\eta(\omega)$ of the human visual system (De Lange, 1958). In his experiment he used four different shapes of stimuli, containing approximate sinusoidal form, for a 2° test field on a large surrounding field and central fixation. In this method which is applicable to any linear system¹⁴, $\eta(\omega)$ as the ratio of output amplitude to the input amplitude as a function of the frequency for sinusoidal input is obtained. Assume that input signal is

$$L(t) = B_a(1 + r \sin(\omega t)) \quad (2.20)$$

means the ripple or modulation depth of test field luminance is $100 \times r\%$, and the absolute change of luminance is $r B_a$. This luminance changes will be attenuated to $r_0 B_a$ because of the attenuation characteristics of the human eye, hence $\eta(\omega) = r_0/r$. Since it is not possible to measure the change of the luminance at the output of the system, a relative measurement should be carried out. Regarding De Lange measurements, at the frequencies around zero no attenuation occurs. This means that in this range the visual system is able to follow the light

¹³In the case of high frequency stimulus, photochemical response is a sharp saw tooth. In a general case, the saw tooth signal is unsymmetrical. According to Ives theory, this signal -through diffusion- would be mapped into a sinusoidal (therefore symmetrical) signal with a highly attenuated amplitude. see Fig. 2.6.

¹⁴Talbot-Plateau law implies the linearity of the human vision system at CFF frequency range.

changes, while it is slow¹⁵. Therefore at $\omega = 0$, η is unity (no attenuation¹⁶) and $r_0 = r$, r_0 is defined as the critical value of the threshold mechanism (percentage variation of the quantity).

This attenuation characteristic describes the behavior of the system in different frequencies, and indicates in which frequency regions the system attenuates the input signal and where it would be amplified and to what extent. He measured the attenuation characteristics for white light of the right hand system fovea brightness perception of observer with 2° test field, large surrounding field with the same luminance as the test field, and central fixation. He used four different waveforms as the stimuli, and found a very important linearity in the vision system. For modulation depth above 2% ($r > 0.02$) the attenuation for all waveforms are very steep. This results in a dependency of the attenuation approximately only on the fundamental Fourier component in high frequencies and the assumption that the adaptation level, B_a is constant. Therefore most flicker theories are supposed to predict sine-wave modulation threshold, as a practical use of this experimental fact.

As a model to resemble the eye vision system, De Lange proposed an electrical analog consists of several RC low-pass integrators in cascade (De Lange, 1958). For the lowest adaptation level (0.375 photons), he suggested a four RC units, in which all units have the same time-constant, but every unit has a 10 times greater R and 10 times smaller C in comparison with the preceding unit. For the highest adaptation level, (400 photons), the electrical analog consists of 10 RC units connected in cascade together with two extra units, having inductors as well. Some years later, D.H. Kelly in his discussion about this kind of model, pointed out that such cascaded linear models do not fit the sine-wave flicker thresholds and also the Ferry-Porter law (Kelly, 1969).

2.6.3 Flicker Detection Model of Sperling and Sondhi

In 1964, Fuortes and Hodgkin, suggested an electrical model to account for the light transients response in the eye of *Limulus*¹⁷ (Fuortes and Hodgkin, 1964). Based on this model, in 1967, Sperling and Sondhi, developed and published a new model accounting for human eye (Sperling and Sondhi, 1968). Their model consists of three RC based parametrically controllable filters, a gain factor and a threshold detector unit. The model predicts the psychophysical results of flicker detection experiments of De Lange at above 10 Hz, the Ferry-Porter and Weber laws (in their applicable ranges), and the effect of light adaptation. This model uses a block of parametric-feedback filter¹⁸ consisting of n RC stages, a delayed feed forward filter, and a low-

¹⁵With this consideration and according to the attenuation characteristics, obtained by De Lange or Kelly, it is clear that these curves show an amplification in the frequency region around 10 Hz.

¹⁶Practically the value of r at $f = 1$ has been chosen as the critical value.

¹⁷"Why study *Limulus* (known also as horseshoe crab) vision? Horseshoe crabs, being very closely related to spiders, use their compound eyes to locate mates. The system is optimal for neuroethological study because it has simple connectivity and uses principles that are found in higher organisms. Thus, findings can be applied to other systems as well. Until relatively recently— in fact, as late as 1982— popular opinion was that the primary sensory modality that horseshoe crabs use to find mates was something other than vision because the eyes are very primitive." Source: <http://instruct1.cit.cornell.edu/courses/bionb424/students/cma32/behavior.html>
"Within certain limits, neurons behave as linear filters. That is, they act in a predictable way (linearly) in response to a given stimulus as long as it is both above threshold and below saturation. A cell thus helps create a neural code for vision based on simple on/off properties." Source: <http://instruct1.cit.cornell.edu/courses/bionb424/students/cma32/linearfiltering.html>

¹⁸It should be recalled that using feed-back in the model, is due to cover the non-linearity behavior of the human vision system. As it is pointed out, in spite of *Limulus* vision system which is linear, the human vision

pass filter consisting of p RC stages. The detection model needs to be adjusted regarding its parameters, which are: the gain factor K , n time-constant for feedback filter, p time-constant for feed forward filter, the time-constant of delay stage, and finally the threshold value of the detector. Such a model can translate a luminance analog signal to "Yes" or "No" or "1" and "0" digital signal, which predicts the perceptibility of light transients such as flickers and flashes.

According to their paper, the shortage of this model is its overestimation for the flickers with the frequencies below 10 Hz or single pulses.

2.6.4 Veringa's Diffusion Theory

About 40 years after Ives' attempts, in 1970, Veringa, apparently unaware of Ives' work, developed a very similar diffusion theory. Concerning a different boundary conditions, he suggested a transfer function like

$$G_v(s) = C_1 \operatorname{sech}\{[2\tau(s + \rho)]^{1/2}\} \quad (2.21)$$

as a model of diffusion phenomenon. In this equation τ is the time-constant of the diffusion process and ρ is served as the recombination rate. Veringa tried to find a solution for the diffusion equation which would fit to De Lange data (De Lange, 1958) of eye response to the flickering light. This is the main and the single difference between Ives and Veringa's approach. Since these two methods are very similar, this model is known as *Ives - Veringa diffusion model* (Kelly, 1969).

2.6.5 Realizability of Ferry-Porter Law as a Linear System

Paley-Wiener Criterion

Necessary and sufficient for a square integrable amplitude function $|G(\omega)| : R \rightarrow R^+$ to be realizable by a non anticipative linear dynamical system with a response function $g(t) : R \rightarrow R$ is Paley-Wiener criterion (Dagnelie, 1992; Mason and Zimmerman, 1960)

$$\int_0^\infty \frac{\ln [|G(\omega)|]}{1 + \omega^2} d\omega < \infty \quad (2.22)$$

Kelly, using Paley-Wiener Criterion, discussed that Ives' model could not be realized as a linear system (Kelly, 1969).

Realizability

According to Kelly's discussion, let's define the 'Amplitude Sensitivity Function' in the following form:

$$|G(\omega)| = \exp(-k|\omega|^a) \quad (2.23)$$

where $\omega = 2\pi f$ is the flicker frequency and k and a are constant. This kind of linear model, considering $a = 1$, rigorously obeys the Ferry-Porter law (compare with equation (2.18) in Ives' theory). By checking Paley-Wiener criterion for such a system we get

system shows some nonlinear properties.

$$\int_0^{\infty} \frac{\ln [|G(\omega)|]}{1 + \omega^2} d\omega = \int_0^{\infty} \frac{-k\omega^a}{1 + \omega^2} d\omega = \frac{-k\pi}{2 \cos(a\pi/2)} \quad (2.24)$$

Therefore the criterion could not be satisfied if $a = 1$ as it is considered by Ives in his theory. Because in this case the right-hand of the equation (2.24) goes to ∞ . For this reason *Ives' diffusion model in a linear causal system is not realizable.*

2.6.6 Experiments of Kelly

The experiments of Kelly were very similar to De Lange's attempts. The main difference is in the test field size and the nature of the stimulus pattern. Kelly has carried out his investigations using a 68° *Ganzfeld* or *edgeless* spatial pattern as stimulus. The waveform of the stimulus, has two components: a sine wave of absolute amplitude mB and a constant term B , which can be written as

$$f(t) = B(1 + m \cos(\omega t)) \quad (2.25)$$

Comparing (2.25) and (2.20), shows that both stimuli, except their terminologies, are identical. According to Kelly's definitions

- B is adaptation level.
- m is relative amplitude and m^{-1} is amplification or relative amplitude sensitivity¹⁹ (both dimensionless).
- mB stands for absolute amplitude and $(mB)^{-1}$ for absolute sensitivity.

Kelly (Kelly, 1961) made his experiment using white light at 6 different adaptation levels, from 0.06 to 9300 td which covers both scotopic (0.06 td) and photopic vision. The frequency of the stimuli has been changed from 1.6 to 75 Hz for the highest adaptation level and up to 12.7 Hz for the lowest one. A comparison between Kelly's and De Lange's experimental results, despite of the test field size, shows a considerable similarity in the highest sensitivity region of the relative amplitude sensitivity. In contrast, in the low frequency region, there is a significant difference. Kelly's curve illustrates a band-pass filter while attenuation characteristics curve found by De Lange has a low-pass characteristic.

It seems that the reason of this difference lies in the fact that the pupil reacts to the change of light up to 3 Hz (Brundrett, 1992), when the test field is very small, like De Lange experiment, the reaction of pupil is negligible, but with large fields, pupil synchronous is significant. Therefore the attenuation of the sensitivity in low frequencies could be a result of the pupil synchronization.

Kelly's data suggest that the total bandwidth of the band-pass filter and frequency of maximum sensitivity, increase with roughly the same rate, in such a way that bandwidth is about 4.5 times frequency of maximum sensitivity at all adaptation levels. (Kelly, 1961) pointed out that the sensitivity to the flicker, like many other measures of sensitivity, increases with decreasing adaptation level, if measured in terms of "absolute amplitude threshold"²⁰, $(mB)^{-1}$.

¹⁹To make it more clear, as an example, $m^{-1} = 15$ means that the adaptation level is 15 times the amplitude of the superimposed sine ripple.

²⁰Absolute amplitude threshold and absolute sensitivity are the same.

Plotting absolute amplitude sensitivity against frequency shows a stronger type of linearity of the vision system. All curves of Kelly's data, approach a common asymptote at high frequencies. A single curve can present the high frequency cut-off (CFF) over nearly entire photopic range. Along this curve the high frequency threshold, depends only on the absolute amplitude mB , which is a product of adaptation level and relative amplitude (Kelly, 1961).

Thus, the condition of constant adaptation level for the linearity, which discussed by (De Lange, 1958), can be removed. For this reason, all periodic waveforms with the same fundamental Fourier amplitude have the same CFF, regardless of adaptation level (Kelly, 1969).

Based on this explanation, and Kelly's experiments, Ferry-Porter law can be written in the following form

$$CFF = a \log(mB) + b \quad (2.26)$$

with a and b as constants and mB as the absolute amplitude.

2.6.7 Kelly's Diffusion-Inhibition Model

In two succeeding papers, (Kelly, 1969; Kelly, 1971), Kelly proposed two complementary models to simulate the flicker response and inhibition behavior of the human vision, based on diffusion equation (2.16) like Ives' theory and his experimental data. His model consists of two stages. The first part accounts for diffusion process, which is responsible for fusion phenomenon in the eye. The second part models the inhibition in the eye and adds some non-linearity due to using feedback in the model. The diffusion part models the behavior of the eye with respect to high frequencies. By using the solution of the diffusion equation suggested by Veringa and assuming $\rho = 0$, he pointed out that the diffusion stage can be modeled with a simple equation.

$$|G_1(j\omega)| = C \exp(-|\omega\tau|^{1/2}) \quad (2.27)$$

where C is a model constant and τ stands for the time-constant of diffusion process. Later on he pointed out that using Laplace transform, it can be shown that equation (2.27) is a solution for diffusion equation.

For the inhibition part, accounting for low frequencies, he suggested a more complicated model with a variable gain integrator in a feedback loop. The magnitude of the model is

$$|G_2(j\omega)| = \left[\frac{(\omega^2 + \alpha^2)^2}{(\omega^2 + K^2)^2 + 2K^2(K^2 - \omega^2) + K^4} \right]^{r/4} \quad (2.28)$$

Where K and r are model variables, depending on adaptation level, and $\tau = 0.5$ s and $\alpha = 11$ rad/s has been chosen to get the best fit to the Kelly's experimental data.

The total model contains both parts in cascade, and therefore the model has the following form

$$|G(j\omega)| = C \left[\frac{(\omega^2 + \alpha^2)^2}{(\omega^2 + K^2)^2 + 2K^2(K^2 - \omega^2) + K^4} \right]^{r/4} \cdot \exp(-|\omega\tau|^{1/2}) \quad (2.29)$$

The outgoing signal from this transfer function should be evaluated with an amplitude detector unit in order to be able to decide about the perceptibility of the input stimulus.

2.6.8 Studies of Rashbass

In 1970, C. Rashbass, conducted a series of interesting experiments of perceptibility of brief rectangular and double flash signals (Rashbass, 1970). He discovered that the threshold intensity of a 2 ms rectangular signal is about 0.18 times the baseline intensity. This threshold decreases in a logarithmic manner by increasing the duration of the flash signal. For longer flashes, the threshold intensity continues to decrease but more slightly up to about 64 ms, and after that the threshold will be again increased. In his double flash experiment he pointed out that the threshold intensity of two equal 2 ms flashes depends on the time interval between them. As interval between flashes increases the vision system shows a behavior passing from total summation to partial summation. By increasing the time interval between two flashes, higher intensity is needed for the observer to detect the changes. This addresses that the eye doesn't integrate completely and there is only a partial summation of light signal. At about 65 ms interval, the intensity threshold is again equal to the one flash test. This phenomenon suggests that after receiving the first stimulus, the eye needs more time to be ready to accept the second stimulus, which is known as mutual inhibition.

In a more general experiment, Rashbass considered two succeeding brief flashes, with magnitudes A and B with variable interval. If A is plotted against B, any combination of two flashes, as it is shown in Fig. 2.7, will be represented as a point in (A,B) co-ordinate system. Near the origin of this co-ordinate system, the magnitude of both flashes is low, and consequently, the combination is under the threshold. Far from the origin one or both flashes will be large, and the combination will be perceptible.

Depending on time interval between two flashes there is a curve enclosing the origin, which separates the perceptible and imperceptible combination of the flashes. The general shape of this curve is an ellipse which changes by time interval separating two flashes.

$$A^2 + B^2 + 2ABL_T = 1 \quad (-1 \leq L_T \leq 1) \quad (2.30)$$

Where L_T , is a function of the time interval between two flashes. Regarding his experiment, he pointed out that any model which is supposed to simulate the behavior of the human eye should satisfy the following conditions:

1. The flashes interact differently at different intervals of time, much larger than the flash duration.
2. Ellipses are symmetrical by rotation of 180° about the origin, which means that changing the sign of whole stimulus pattern leaves the threshold unchanged.
3. Symmetry by reflection in the line $A=B$, which means at any particular interval flashes can be interchanged without changing the threshold.

The model supposed by Rashbass has three parts to cover the mentioned conditions:

1. Different time intervals between two brief flashes, means different frequencies of impulses, therefore for the first condition to be satisfied, the model needs to have a filter (which is explained previously). As a task of simplicity the filter will be assumed to be linear.
2. The second part in the model contributes the equivalence of $(A,B) = (B,A)$. This element is supposed to be a simple squaring, which gives the elliptical relationship to the inputs A and B and at the same time has the property of sign elimination.

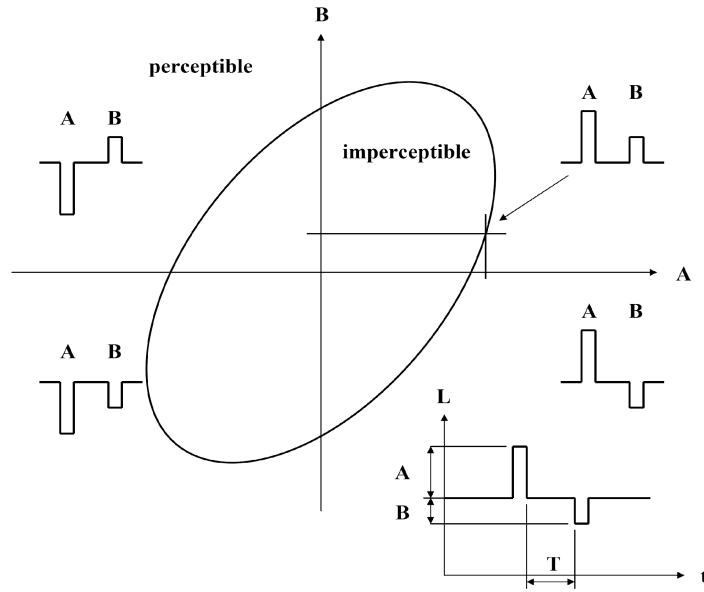


Figure 2.7: Double flash test of Rashbass. A flash with an amplitude greater than the base line is defined as a positive flash, and when the light is decreased for a short time a negative flash is introduced. The graph which is illustrated in lower part of this figure, sketches the luminance signal against time. The first flash is a positive flash with an amplitude of A and the second one is a negative flash with amplitude of B . The time interval between two flashes is T . In the first quarter both flashes are positive and in fourth quarter both are negative flashes. In second and third quarters one flash is positive and the other is negative. All points which are located inside the ellipse represent imperceptible couples of flashes. Other combinations of two flashes which are located outside the ellipse are perceptible stimuli. The shape of ellipse is a function of the time interval between two flashes.

3. The third part of the model which satisfies the independency from the sequence of the flashes, $(A, B) = (B, A)$, is an integrator over the whole waveform.

It can be easily shown that such kind of model is able to simulate the results obtained from his experiment. He discussed that:

The impulse response of the linear filter is supposed to be $\phi(t)$, therefore its response to the brief flash with magnitude A will be, $A \cdot \phi(t)$. By defining the unit of intensity of flashes as the threshold flash, and let the value required to be reached by integral at threshold be 1 then the threshold will be:

$$\int_0^{\tau} [\phi(t)]^2 dt = 1 \quad (2.31)$$

where τ is a time period greater than the stimulus duration. Assuming the second flash with magnitude B and time delay T the filter response will be, $B \cdot \phi(t - T)$, and since the filter is assumed to be linear, then the response of the system will be:

$$\int_0^{\tau} [A\phi(t) + B\phi(t - T)]^2 dt \quad (2.32)$$

which leads to

$$A^2 + B^2 + 2AB \int_0^\tau \phi(t)\phi(t - T) dt \quad (2.33)$$

which is resulted when (2.31) is applied in calculations. Now by comparing (2.30) and (2.33) one can see that

$$L_T = \int_0^\tau \phi(t)\phi(t - T) dt \quad (2.34)$$

which is a function of T and independent of the magnitude of A and B. At threshold the output of the system is considered to be 1, therefore

$$A^2 + B^2 + 2ABL_T = 1 \quad (2.35)$$

which is nothing else an ellipse centered in the origin of the (A, B) co-ordinate system, covering all symmetries which are described earlier. He found the magnitude of filter characteristics, with auto-correlation method. Using ellipses which he found in his experiments for different time intervals, and equations (2.34) and (2.35) he sketched the auto-correlation function of the impulse response function. For this, the x axis is time interval in ms and y axis is L_T value calculated from (2.35).

The minimum frequency in his calculated filter magnitude is 5 Hz, which determines the time-constant which is used in integration part of his model. This means the model calculate a running mean value over $\tau = 200$ ms.

It is well known that subjects need a considerable time, in order to reach the highest sensitivity to temporal modulation. The value of τ in Reashbass model, which is so called build-up time is considered to be up to 1 second or more in (Graint and Hammond, 1931). Koenderink and Van Doorn in 1974 and 1977 measured this time and found a value of 330 to 500 ms (Koenderink and Van Doorn, 1977). They suggested a formally identical scheme like Rashbass but by introducing noise signals. They found that if the duration of noise signal is less than one third or half of a second, then the detection threshold is reached if the noise energy (noise power integrated over time) exceeds a certain level. In other word, by noise duration less than about 330 – 500 ms the threshold power decreases by increasing the time duration of the noise signal, which shows the integration time is not still complete. After this build-up time, increasing the duration of noise has no effect on threshold power which illustrates that the build-up time is already passed. What the method of Van Doorn and Koenderink suggests is a variance estimator, the bandwidth of which can be measured with sine wave modulations (like De Lange or Kelly curves) and with an integration time of one third to half of a second.

2.7 Human Eye Temporal Modulation Sensitivity Curve

There are several sources for the human eye temporal modulation sensitivity²¹ curve.

- Rashbass (Rashbass, 1970)
- DIN or UIE (DIN EN 61000-3-3, 2002)

²¹This curve is also known as Attenuation Characteristics (AC) in some literature like (De Lange, 1958).

- De Lange (De Lange, 1958)
- Kelly (Kelly, 1961)
- Kelly-Henger (Henger, 1986)

The characteristic suggested by Rashbass, is not a direct measurement of the temporal modulation sensitivity of the human eye. Rashbass derived this curve (4 Hz to 20 Hz) mathematically using the results of a double flash test (Rashbass, 1970).

The curve which is used in DIN or UIE (up to 25 Hz) shows the threshold of the voltage deviations, for which the light deviation of an incandescent lamp is perceptible (DIN EN 61000-3-3, 2002).

De Lange curves only account for small field photopic amplitude sensitivity. According to these curves, human eye shows its highest sensitivity around 8-9 Hz with the relative amplitude of about $m = 0.8\%$. Hence, such a sensitivity curve is valid only for a small part of the retina around the fovea (De Lange, 1958).

D.H. Kelly, used a wide (68° diameter) uniformly flickering field, and found sine-wave flicker thresholds in terms of depth of temporal modulation of luminance. He measured this threshold for six different adaptation levels (B) in a frequency range of about 80 Hz. Regarding Kelly's measurements, the highest sensitivity to the flicker occurs at about 8 Hz for lower adaptation level and at about 18 Hz for higher adaptation level. The threshold modulation for the former is about $m = 5\%$ and for the latter is between $m = 1\%$ and $m = 0.5\%$.

It is well known that human eye shows more sensitivity to the flicker in the periphery than at the fovea (Brundrett, 1992). Therefore by expanding the area of the stimulus on the retina, more sensitivity can be measured. Henger (Henger, 1986) carried out a series of experiments on the human eye including the periphery. As it was expected, Henger's experiments showed more sensitivity of the human eye to the flickering light. According to Henger's experimental data, a threshold of about 0.3% at the frequencies around 10 Hz is recognizable. As Henger made his measurement under 200 cd/m^2 adaptation level, he suggested to set the threshold to $m = 0.2\%$ for higher luminance such as 10000 cd/m^2 (Henger, 1986). The value of $F_{10} = 0.15\%$ is suggested by Pabst in (Pabst, 1986).

There is a logarithmic behavior between adaptation level and relative amplitude sensitivity which can be illustrated using Kelly's experiment. From *Table I* of (Kelly, 1961), neglecting the highest and lowest adaptation levels and choosing the maximum amplitude sensitivity vs. adaptation level, this logarithmic regression can be established:

$$m^{-1} = 15.7 \ln(B) + 28.5 \quad (2.36)$$

with m^{-1} as amplitude modulation sensitivity (relative amplitude sensitivity), and B in trolands as adaptation level. The coefficient of determination $R^2 = 0.994$ shows a good curve fitting for this equation. If we consider for an adaptation level of 200 cd/m^2 , the threshold of relative amplitude m is 0.3% then regarding (2.17), for an adaptation level²² of 20000 cd/m^2 , m should be reduced to 0.25%.

²²It should be noted that such a high adaptation level can not be reached practically (because of the eye restrictions). Therefore m can not be measured experimentally and it has to be found out mathematically using extrapolation.

The assumption that $m = 0.15\%$ like in (Pabst, 1986), leads to some overestimation in the evaluations. On the other hand, this guaranties that the curve is applicable to the very sensitive eyes as well. Depending on the application this threshold value should be set.

2.7.1 Normalized Filter Characteristics of the Human Eye

As it is explained in previous sections and according to (Rovamo and others, 1999), "at high luminance levels, sensitivity to a flickering spot rises with increasing temporal frequency across the low frequency range, peaks around 10 Hz and then decreases steeply." Thus, the flicker sensitivity function has a band-pass shape in bright light²³.

Freq.	Sens.								
0	0.010	20	0.650	40	0.164	60	0.030	80	0.005
1	0.152	21	0.613	41	0.153	61	0.028	81	0.004
2	0.303	22	0.576	42	0.143	62	0.025	82	0.004
3	0.459	23	0.544	43	0.132	63	0.023	83	0.004
4	0.620	24	0.517	44	0.122	64	0.020	84	0.003
5	0.755	25	0.489	45	0.111	65	0.018	85	0.003
6	0.850	26	0.460	46	0.103	66	0.016	86	0.003
7	0.918	27	0.430	47	0.096	67	0.014	87	0.003
8	0.962	28	0.400	48	0.088	68	0.013	88	0.002
9	0.981	29	0.371	49	0.081	69	0.011	89	0.002
10	1.000	30	0.341	50	0.074	70	0.010	90	0.002
11	0.979	31	0.321	51	0.068	71	0.009	91	0.002
12	0.959	32	0.300	52	0.063	72	0.009	92	0.002
13	0.933	33	0.281	53	0.058	73	0.008	93	0.002
14	0.900	34	0.263	54	0.053	74	0.007	94	0.002
15	0.868	35	0.245	55	0.048	75	0.007	95	0.001
16	0.820	36	0.230	56	0.044	76	0.006	96	0.001
17	0.772	37	0.215	57	0.041	77	0.006	97	0.001
18	0.729	38	0.199	58	0.037	78	0.005	98	0.001
19	0.689	39	0.182	59	0.034	79	0.005	99	0.001

Table 2.1: Temporal Sensitivity of the Human eye (Sens.) in different frequencies (Freq.), based on (Kelly, 1961; Henger, 1986). The characteristic curve is slightly modified in this work.

Since the lowest attenuation (i.e. the highest amplitude modulation sensitivity, m^{-1}) occurs around 10 Hz, therefore the magnitude of the filter can be considered as 'unity' at this frequency. This corresponds to the highest sensitivity of the eye to the flickering light at this frequency. Using this concept, the temporal modulation sensitivity curve will be normalized with respect to its largest value.

The curve illustrated in Fig. 2.8 is derived using Henger's proposed curve and is modified in this work. The value of the human eye sensitivity as a function of the frequency of the flickering light is given in Table 2.1 as well.

²³At low luminance levels sensitivity to flicker in a spot of the moderate size first remains constant but then decreases steeply as a function of temporal frequency (Rovamo and others, 1999). Hence, the flicker sensitivity function has a low-pass shape in dim light.

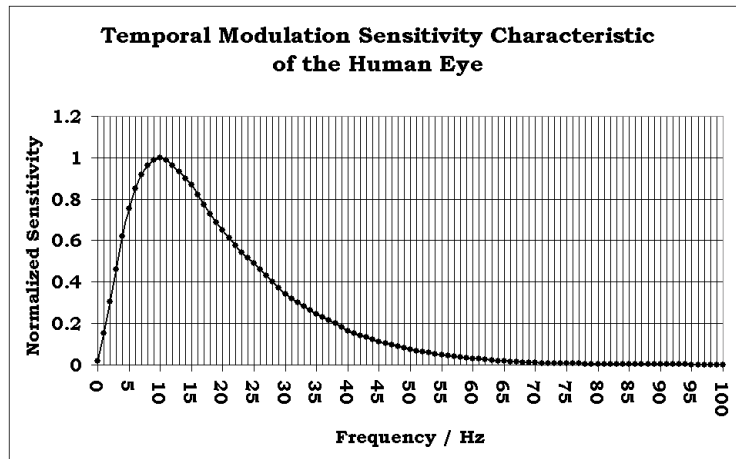


Figure 2.8: Bandpass filter characteristics of the human eye, based on (Kelly, 1961; Henger, 1986). The characteristic curve is slightly modified in this work.

2.8 Realization of the Light Flicker Meter

2.8.1 Model of the visual System concerning Light Transients

As it is mentioned, there are many studies that aim at the development of a model, which can account for vision system response to the transients of light.

As long as a fundamental contribution was provided by Rashbass and the model which is used in this work is based on his model, it is worth to briefly recall his method one more time. He considered two succeeding brief flashes, with magnitudes A and B with variable interval. Rashbass developed a relatively simple model based on his experiments. The model proposed by him, has three stages. The first stage is a bandpass filter which models the attenuation characteristics of the human eye. The second stage is a simple squaring unit, which gives the elliptical relationship to the flashes A and B, and at the same time gives the sign independency to the model. Now it is known that this part simulates the non-linear eye-brain perception mechanism (Wang and Devaney, 2004). The last part is an integrator, over the whole waveform and accounts for independency of the double flash sequence. The model calculates a running mean value over the time. If the input signal is a function of time like $L(t)$, and after passing through the filter is linearly transformed into $L_f(t)$, the model can be expressed as:

$$O(t) = \int_0^{\tau} [L_f(t)]^2 dt \quad (2.37)$$

where $O(t)$ is the output of the model and τ is a time constant²⁴ greater than the stimulus duration. Changing the third stage of the model originally developed by Rashbass, from integrator to a low-pass filter forms the eye-brain simulating unit of the 'IEC Flicker Meter' (EN 61000-4-15, 1998).

The filter which is suggested by the above mentioned standard is a sliding mean filter having a time constant of 0.3 s. This filter is implemented as a first order low-pass filter with

²⁴The model of Rashbass accounts for transient changes that are complete in 100 ms. The lowest frequency in weighting filter calculated by Rashbass was 5 Hz. For this reason, the time constant for integrator part of model was 200 ms.

the cut off frequency of 0.53 Hz (McKim, 1992). Such a low-pass filter simulates the perceptual storage effect in the brain. This means that the brain remembers the previous perturbation and immediately relates with the new one (Gomez and Morcoz, 2002). In other words by starting of the light flickers, brain starts to store the information of the flicker, after a time constant, there are sufficient information stored in the brain and the highest level of sensitivity is achieved. On the other hand, by removing the flickers, there are still some information about the flicker in the memory. As a result of this phenomenon the sensitivity of the vision system to the flicker attenuates (gradually decreases) with the same time constant.

For perceptible periodic flicker, at the beginning, flicker is not perceptible, but brain starts to store the information which are interpreted as flickering effect. After passing a time constant, flicker would be perceptible to the visual system which means that the brain interprets the incoming light signal as a flickering light based on the previous information which is stored in it. By using the above mentioned filter, this time constant is about $\tau = 1.5$ s. The output of such a system simulates the instantaneous perception of the human eye to the light flicker or any transient change of light intensity. The output of this filter is known as Instantaneous Flicker Level (IFL) (Wang and Devaney, 2004). In order to determine the total gain of the model, for any perceptible flicker or light transient, the output of the model is set to unity.

Without loss of generality it is possible to calculate the gain factor of the overall model with a 10 Hz sinusoidal input signal. For a luminance signal with the form of equation (2.25), at the frequency of 10 Hz a relative amplitude of $m = 0.15\%$, is sufficient to make the flicker perceptible. Therefore the luminance signal can be considered as:

$$L(t) = B [1 + 0.0015 \cos(2\pi 10s^{-1} \cdot t)] \quad (2.38)$$

Since the signal passes through a band-pass filter, its DC term will be eliminated. The gain of weighting filter at 10 Hz is considered to be unity, which means no attenuation of the modulating signal at this stage occurs. Therefore the output of the first stage of the model is:

$$L_1(t) = B [0.0015 \cos(2\pi 10 s^{-1} \cdot t)] \quad (2.39)$$

In the second stage the signal will be squared:

$$L_2(t) = \frac{1}{2}(0.0015B)^2 [1 + \cos(2\pi 20s^{-1} \cdot t)] \quad (2.40)$$

Finally this signal will be filtered with a low-pass filter. This removes the alternating term. As a threshold of the perceptibility the result is assumed to be unity. Hence, in the last part, the output signal is multiplied by the gain factor G:

$$1 = \frac{1}{2} \cdot G \cdot (0.0015B)^2 \quad (2.41)$$

$$G = \frac{2}{(0.0015B)^2} \quad (2.42)$$

If we apply a signal such as (2.38) to the model, and set the total gain of the model to above value, after a time constant of about 1.5 s, the output of the model will reach the unity.

2.8.2 Realization of the Human Eye Characteristic Filter

Pabst's Filter

(Pabst, 1986) proposes a filter combination (Fig. 2.9) which fits to the data of Hofmann-Kelly (Hofmann, 1982) curve. The filter is combined of two identical band pass filters and two lowpass filters all in cascade formation. Bandpass filters have the center frequency of 10 Hz with $Q=0.4$ and $A=-0.32$. Lowpass filters are Tchebychev filters with cut off frequency of 25 Hz and 50 Hz for the first and second filter respectively and a ripple value of 0.5 db and a gain factor of $A=-1$ for both. An overall gain factor finally compensates the total gain of the filter and makes it equal to unity.

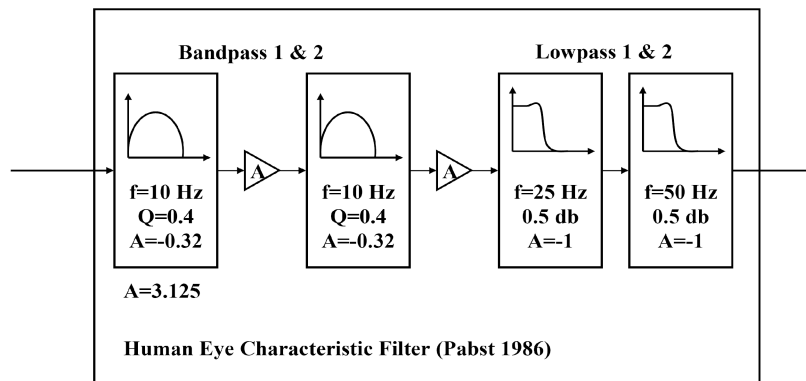


Figure 2.9: Realization of the human eye characteristic filter after (Pabst, 1986) using analog filters.

The corresponding IIR digital filters using ‘Bilinear Transformation’ are calculated and presented by Pabst as well.

Using Genetic Algorithm to fit Pabst filter to Kelly-Henger Curve

”Genetic algorithms are a part of evolutionary computing, which is a rapidly growing area of artificial intelligence. Idea of evolutionary computing was introduced in the 1960s by Ingo Rechenberg in his work *Evolution strategies (Evolutionstrategie* in original). His idea was then developed by other researchers. Genetic Algorithms (GAs) were invented by John Holland and developed by him and his students and colleagues. This lead to Holland’s book *Adaption in Natural and Artificial Systems* published in 1975” (Obitko, 1998).

As it is already noted the selected human eye characteristic curve for this work is Kelly-Henger (Henger, 1986). As long as a filter is already designed by Pabst, the idea is to find a filter with the same structure which is fitted to the proposed curve of Henger. In fact the filters’ parameters should be changed in such a way that the new filter has a characteristic curve which is fitted to a desired curve. Any parameter of individual filter has its own effect on the whole filter. For example, maybe we need to change the center frequency of one Bandpass filter or cut off frequency of one lowpass filter in Pabst’s filter. As long as two bandpass filters are identical and each filter has three parameters, the whole filter is defined with totally nine parameters. Investigating the effect of each parameter on the filter characteristic is a quite complicated task.

Alternatively this could be carried out using genetic algorithm. The parameters which must be changed to get the desired filter are as follows:

1. Center frequency of bandpass filters (G1).
2. Quality factor of bandpass filters (G2).
3. Gain factor of bandpass filters (G3).
4. Cutoff frequency of the first lowpass filter (G4).
5. Passband ripple of the first lowpass filter (G5).
6. Gain factor of the first lowpass filter (G6).
7. Cutoff frequency of the second lowpass filter (G7).
8. Passband ripple of the second lowpass filter (G8).
9. Gain factor of the second lowpass filter (G9).

Before explaining the algorithm it is worth to give some definitions used in the proposed genetic algorithm.

- **Gene:** Each filter parameter is considered as a gene (here G1 to G9).
- **Chromosome:** Each chromosome represents a filter and is composed of a strain of genes.
- **Population:** A set of filters being evaluated.
- **Initial Population:** It is necessary to create an initial population to serve as the starting point for the genetic algorithm. This initial population is usually created randomly.
- **Fitness Evaluation:** Fitness evaluation involves defining an objective or fitness function against which each chromosome is tested for suitability for the environment under consideration. As the algorithm proceeds we would expect the individual fitness of the "best" chromosome to increase as well as the total fitness of the population as a whole.
- **Crossover:** The process of crossover creates a new chromosome (filter) from parents. During this process two chromosomes are divided to some parts and a new chromosome by random combination of these parts are created.

The Genetic Algorithm (GA)

As it is illustrated in Fig. 2.10, each chromosome represents nine filter parameters. As long as the whole filter is combined of three different filters (as is shown in Fig. 2.9), each chromosome is divided into three sub-chromosomes namely X1, Y1 and Z1. X1 represents the bandpass filter parameters while Y1 and Z1 corresponds the parameters of two lowpass filters. Two chromosomes p1 and p2 belong to current generation and are supposed to be parents which contribute to create a new generation chromosome.

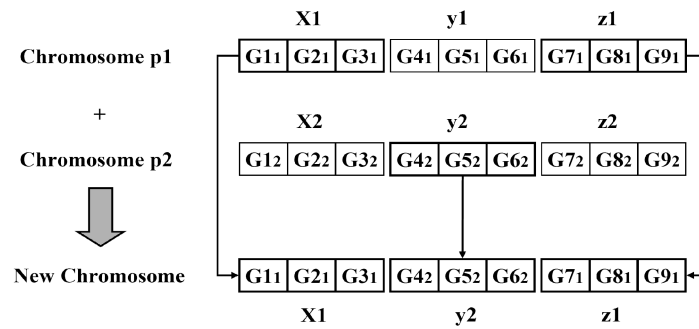


Figure 2.10: Process of crossover by splitting parent chromosomes and merging the sub-chromosomes to create new generation.

The first step to implement the genetic algorithm is creating the first generation or initial population. This process is normally carried out as a random process. In our case the initial population can be created using the values of Pabst's filter. Hence we start the procedure with a good population and the genetic algorithm will be used as an optimization process. The first generation is considered to have 1000 chromosomes. The way to create the first generation is to select the values which are used in Pabst's filter and change all variables linearly within a range of 10%. As an example we change the center frequency of bandpass filter which is 10 Hz, from 9.5 Hz to 10.5 Hz and the same for all other parameters. In this way the initial population with 1000 individuals is created. Afterwards all chromosomes must be evaluated in order to see how fit they are with respect to the desired filter characteristics. In the first step of evaluation, the corresponding filter for given parameters is created. The fast Fourier transform (FFT) of the time domain impulse response of the filter gives the filter characteristics.

The fitness evaluation is carried out by comparing the filter characteristics of each chromosome with desired characteristics. The point by point error is calculated as a point by point subtraction of two characteristics. The summation of squares of all errors then is considered as the total error for one chromosome. The square function removes the effect of the error sign for each point. It is usual to define a fitness value between 0 and 1. When the error value is zero (desired pattern) the fitness value is 1 and the aim of GA is to find chromosomes which have the highest possible fitness values. To define a fitness value between 0 and 1 the calculated error values are subtracted with their minimum value. As a result the minimum error value will be changed to zero. All error values are then divided to the maximum value which normalizes all of them between 0 and 1. The fitness value is defined as the subtraction of unity and calculated error values. Therefore the fitness value of unity corresponds to the minimum error value and the chromosome which represents the maximum error value has a fitness value of zero.

Using the above explained method, all chromosomes of the initial population are evaluated. The first generation then is created with the criterion that the more fitted chromosomes have a better chance to contribute to the new generation while the poorer chromosomes have a lower chance. To implement this idea we copy the chromosomes of the initial population to a new population. There are more identical copies of chromosomes with the higher fitness values and lower number of copies of poor chromosomes. As an example if the fitness value of a chromosome is one, we put 40 copies of it into the new population, and there is no copy of chromosomes with fitness value of zero. For other fitness values the numbers of copies are

calculated as a non-linear interpolation of the fifth²⁵ power of the fitness value between 0 and 40. For example if a chromosome has a fitness value of 0.8 there are 13 copies of it in the new population.

After creation of the new population the process of crossover should be carried out to create the new generation. The process of crossover which is used in this GA is as followed. A new chromosome is created by merging three sub-chromosomes. Any sub-chromosome is randomly selected from its own area of new population. This means inside new population there are three areas; one area for all x chromosomes one for all y-chromosomes and one for all z-chromosomes. After selection of one sub-chromosome from new population, that chromosome then is omitted from whole chromosomes set and then the process of selection for the next sub-chromosome is carried out. This avoids selection of one chromosome many times. In fact for fitted chromosomes the selection chance is already high as long as they are copied many times (with respect to their fitness values) into the new population.

By creating 1000 new chromosomes based on explained crossover method, the new generation is created. As long as the most fitted chromosomes of the previous generation have more chance to contribute creating this new generation there is a hope to find more fitted chromosomes in new generation. The explained procedure then is continued to create more and more generations. In any step there is a chance to get more and more fitted chromosomes. The following steps summarize the genetic algorithm used for this application:

1. Create initial population (N individuals).
2. Evaluate all individuals of population (Fitness value between 0 and 1).
3. Create new population in which the more fitted chromosomes are copied more frequently in the new population (M > N individuals).
4. Create new generation, by randomly selection of N chromosomes of new population.
5. Go to the second step.

The whole procedure is continued until the best chromosome with the sufficiently high fitted value is found. In fact, in the second step after evaluating process, always the best chromosome will be saved in the memory. It is likely that after some iteration better chromosomes are found and they will transfer to the next generations. This way it is possible to modify the filter which is originally designed by Pabst to fit the curve of Hofmann-Kelly in such a way that it fits to the desired curve of Henger-Kelly.

The following is the result of an attempt of using GA to modify the human eye characteristics filter.

We start with the initial values used by (Pabst, 1986)

G1	G2	G3	G4	G5	G6	G7	G8	G9
10 Hz	0.4	1	25 Hz	0.5 db	1	50 Hz	0.5 db	1

After creation of the initial population as it is explained and applying the proposed GA to this population and after some iteration the result is converged to some better fitted chromosomes. At this point the iteration is stopped and a fitted chromosome is used to create

²⁵Note that these values are set empirically. In fact there are no specific rules to define fitness function.

another initial population with the hope that a better starting point is reached which may lead to a faster convergence of the algorithm. Finally a good fitted chromosome is found with the following values.

G1	G2	G3	G4	G5	G6	G7	G8	G9
9.965 Hz	0.494	1.128	24.89 Hz	0.657 db	0.908	63.85 Hz	0.876 db	0.988

It is worth to recall that the results of several attempts of genetic algorithm with exactly the same initial parameters are not the same. This is a result of random selection of chromosomes during this procedure. For this reason, successful attempts of GA lead to finding good fitted patterns which could be similar but are not necessarily identical.

There are some points should be considered about the application of this method:

1. As a general rule, the method of genetic algorithm, because of its nature, is not a perfect method for applications of finding the exact design parameters. It is more applicable to find a general pattern when there are many design parameters.
2. Besides the crossover technique there is another process which is called mutation. The process of mutation changes one or more gene in a chromosome randomly. This process is not involved in the explained GA.
3. There are many parameters in implementing of GA which can affect its performance. For example the definition of its fitness evaluation function or the criterion which is used to create the new population. As a result it could be possible that after many iterations still there are not satisfying patterns inside populations.

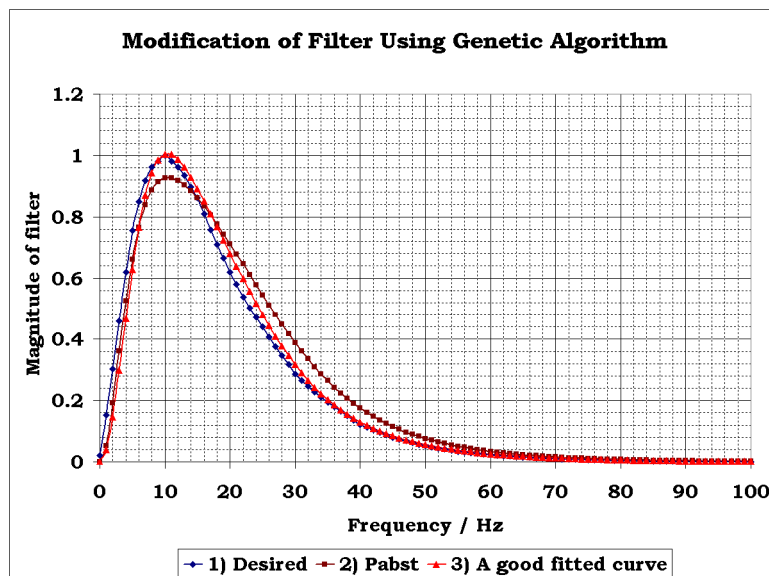


Figure 2.11: A comparison between filter characteristics. 1. Desired curve. 2. Pabst's filter. 3. Modified filter characteristic using proposed genetic algorithm.

Fig. 2.11 compares the characteristic filters of the desired curve with Pabst's proposed filter and a modified filter using genetic algorithm.

Although GA seems to be a solution to design the desired filter, as it is explained, it is not the optimum way to solve this problem. In fact it is very difficult, if it is not impossible, to find a filter with the same structure as Pabst's filter which is fitted exactly to our desired filter characteristics using GA.

For this reason the desired filter is designed as digital IIR filter with arbitrary magnitude using Matlab software. The method and the procedure which is used to design the filter are explained in the following section.

2.8.3 Digital IIR Filter with Arbitrary Magnitude

Data from Kelly-Henger (Henger, 1986) or others provide only a small part of the magnitude of the transfer function and contains no phase information. Considering a minimum-phase spectrum for the transfer function, yields an impulse response function with the minimum onset delay that can be physically realized. For this reason, the eye characteristic filter is realized as a minimum-phase filter (Dagnelie, 1992).

At the low frequency end, observation of several modulation cycles at modulation depth near threshold has to be carried out. This especially for frequencies much less than 1 Hz is tedious.

At the high frequency end, reaching 100% threshold at the Critical Flicker Frequency (CFF) is the barrier. By raising the adaptation level, regarding Ferry-Porter law (Hentschel, 2002), higher CFF can be obtained. However physical limitations of equipments and retinal physiology are restrictions. Therefore for both low and high end frequencies, the extrapolation has to be fulfilled. Kelly's model (Kelly, 1971) for high frequencies meets the Paley-Wiener criterion (Mason and Zimmerman, 1960). Therefore such a model can be physically realized and extrapolation toward high frequency can be carried out using Kelly's model for high frequencies:

$$|T(f)| = A \exp\{-(\pi f)^{1/2}\} \quad (2.43)$$

where $|T(f)|$ is the magnitude of filter transfer function and this extrapolation is used for frequencies greater than the CFF.

The extrapolation toward low frequencies needs some other considerations. Assuming the human eye characteristics as a band pass filter suggests that $|T(0)| = 0$. However, practically $\log[|T(f)|]$ should be analytic, otherwise $\arg[T(f)]$ can not be calculated using Hilbert transform. $T(f) \neq 0$ provides that the \arg function is kept single valued and continuous, and this is a sufficient condition for Hilbert transform. (Victor, 1989) expressed that the condition of $T(f) \neq 0$ will be met when the assumption of the minimum-phase is fulfilled and this is another reason to choose the filter as a min-phase. Thus to be able to compute the phase characteristics, one needs to set $T(0)$ to a small positive value. This value has been suggested by (Dagnelie, 1992), as follows

$$|T(0)| = \frac{|T(0.5)|}{8} \quad (2.44)$$

If we use the suggested method of Dagnelie, a prior linear extrapolation is needed to find $|T(0)|$. This leads to:

$$|T(f)| = 0.1523 f + 0.0049 \quad \text{where } 1 \leq f \leq 4 \text{ Hz} \quad (2.45)$$

and $|T(0)| = 0.01$ will be calculated.

The other condition which should be met is that the first derivative of $|T(f)|$ at zero should be zero. This is the necessary condition for $\log|T(f)|$ to have the continuous first derivative.

A digital IIR filter can cover the minimum phase condition. Using existing software like LabVIEW²⁶ or MATLAB²⁷, for arbitrary magnitude, desired filter can be designed. Using the data illustrated in Fig. 2.8, and the extrapolation of data, 101 known values of the desired filter magnitude are derived. Magnitude data are spread in a range of $f = 0$ to $f = 100$ Hz with a frequency interval of 1 Hz. This means the Nyquist frequency is 100 Hz and therefore the sample frequency of the filter would be $f_s = 200$ Hz. The designed filter is a digital IIR filter of 16th order. The filter is composed of eight 2nd order filters in a cascade arrangement and the following general form:

$$Y_i = \frac{1}{a_0} \left(\sum_{j=0}^{N_b-1} b_j X_{i-j} - \sum_{k=1}^{N_a-1} a_k Y_{i-k} \right) \quad (2.46)$$

where $N_b - 1$ is the forward filter order, b_i are the forward filter coefficients, $N_a - 1$ is the feedback filter order, a_i are the feedback filter coefficients, X_i is the input signal and Y_i is the output signal.

To capture light transients signals containing fast changes of light, such as light flashes, the sample rate of 200 Hz is too low. Rashbass in (Rashbass, 1970), showed that flashes with 2 ms width and about 18% height with respect to the adaptation level are perceptible²⁸. For such waveforms, the sample rate should be increased. A sample frequency of $f_s = 4$ kHz, provides 8 samples for a 2 ms flash which is adequate to represent the signal. By extrapolating the data found by Rashbass (Rashbass, 1970), a 1 ms (4 samples for $f_s = 4$ kHz) rectangular flash, in order to be perceptible for the human eye, should have the height of 21.6%. Our laboratory experiments show that the light transients caused by discharge instabilities are not so sharp and fast and the sample frequency of $f_s = 4$ kHz is sufficient for this purpose.

In order to change the sample frequency of the filter, the order of its coefficients should be changed. If we change a_i to a_{ni} and b_i to b_{ni} , and set all coefficients of order $ni - n + 1$ to $ni + n - 1$ to zero, then the sample frequency of the filter will be multiplied by n .

In appendix A, TABLE A.1 shows the forward and feedback coefficients of eight second order IIR filters with both 200 Hz and 4 kHz sampling frequencies. In case of $f_s = 4$ kHz, all forward and feedback coefficients between two given values are zero.

Applying this method has a side effect on the filter spectrum magnitude as well. For any duplication of sample frequency, the method will add a copy of filter spectrum, in the reverse order, at the end of original spectrum. Concerning $n = 20$, sample frequency of filter will be multiplied by 20. At the same time the spectrum contains 20 adjacent spectrums of original filter, either identical, or in a reverse order with respect to the frequency. Only the first spectrum, i.e. up to the Nyquist frequency or $f_s/2$ is meaningful for us. Therefore the spectrum in the frequency region greater than the Nyquist frequency should be eliminated. To implement this, another lowpass filter with cut off frequency equal to the Nyquist frequency, should be added in series to the filter. The low-pass filter has also the new sample frequency.

²⁶Digital Filter Design Toolkit.

²⁷Filter Design and Analysis Toolbox.

²⁸In experiments of Rashbass, the subject saw a uniform circular green field of light, diameter 17° which he fixated centrally. The retinal illumination (adaptation level) was estimated to be 700 td.

This filter should be designed with a very sharp transition from pass-band to stop-band, to cut the additional part of the spectrum, without changing the useful part. This filter is a Butterworth of order 10, with cut off frequency of 100 Hz and sample frequency of 4 kHz.

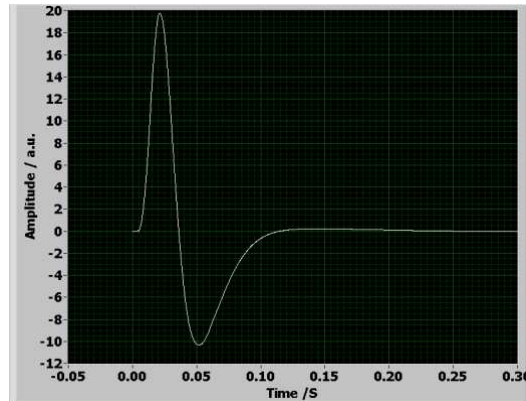


Figure 2.12: Impulse response of the filter, simulating eye response to the flash light stimulus.

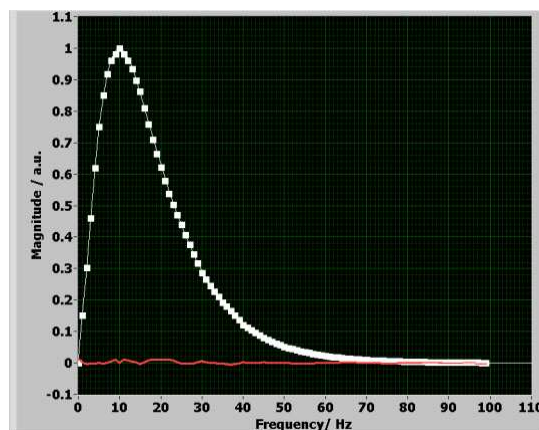


Figure 2.13: Comparison of model and desired filter characteristics. Filled squares are desired values, the fitted curve is the characteristic of the designed filter and the curve around zero is the error. Root Mean Squared Error is $RMSE=0.003$.

Combination of these two filters makes a new band-pass filter, with desired sample frequency. This filter will be used as the human eye model. Fig. 2.12 shows the impulse response of the filter, which simulates the human eye response to the flash light stimulus. Impulse response of the eye model, as it is expected, shows a causal system, with two considerable peaks. Ignoring the sign of impulse response, this kind of response resembles well known Electroretinogram (ERG) of the human eye (Asi, 1992). By applying FFT to the impulse response, frequency spectrum of the filter is derived. Comparing this spectrum with the desired attenuation characteristics shows the precision of the proposed method. Fig. 2.13 illustrates this comparison.

2.8.4 Implementation of the Visual System Model

As it is explained earlier, the model of the visual system to the light transients contains three parts. Fig. 2.14 summaries the model as a block diagram. The input signal $L(t)$ is the

luminance versus time or a signal proportional with luminance. The first stage resembles the eye characteristic attenuation to the light transients. The second stage which squares the signal simulates eye-brain non-linearity property. The third block is used to emulate the storage effect in brain. The fourth block shows the gain factor which is used to set the overall gain of the model. The output of the model, light flicker factor $F(t)$, models the instantaneous perception of the vision system to the transients of luminance. To implement the model, 'LabVIEW' software is used. The result of the implementation is a so called subVI²⁹ which accepts a signal with the sample rate of 4 kHz as the input, and outputs the light flicker factor versus time with the same sample frequency.

The overall gain of the model is selected in such a way that for a perceptible light flicker, output reaches unity. The values, lower than this threshold, are interpreted as imperceptible transients.

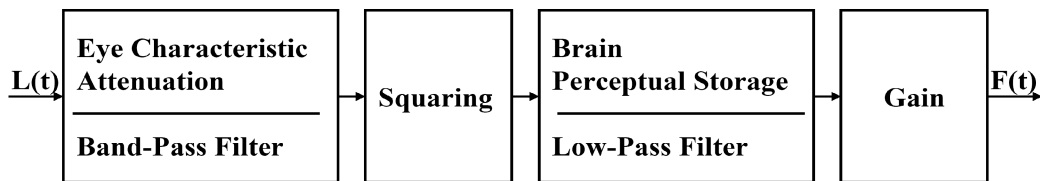


Figure 2.14: Block diagram of the light flicker meter.

Henger in (Henger, 1986) suggests a method in order to implement F_{10} in a measuring system. Merely the same procedure was carried out by Pabst (Pabst, 1986) with more details. In the model proposed by Pabst, a signal proportional to the luminous flux passes through two filters. The first filter simulates the human eye attenuation using data of (Hofmann, 1982), and the second filter accounts for the perceptual storage process of the brain. The RMS value of the output signal of the second filter will be calculated and then divided by the mean value of luminous flux. To be able to calculate the RMS value of a signal, a time interval RMS-window has to be defined. To detect the periodic changes of light signal with the low frequencies such as 2 Hz, this time interval should be at least 500 ms. According to Fig. 2.12 the impulse response of the human eye attenuation filter has a duration of about 100-120 ms. Hence, setting the RMS-window to 500 ms leads to underestimation problem when there are some fast transients in the light signal. By setting the RMS-window equal to the time constant of the second filter (1.5 s as discussed earlier); the underestimation problem will be more considerable. This means one should choose a short RMS-window to detect fast transients and a long one to get the periodic changes of the light signal.

Furthermore in Pabst's method (Pabst, 1986), the human eye weighting filter is applied to the 'luminous intensity' signal, while this attenuation characteristics is valid for the 'luminance' signal. In the method proposed in this paper, the 'luminance' signal is used; therefore the eye characteristic weighting curve is valid. This proposed method accounts for periodic and transient changes of the light signal simultaneously. It can be used for any light signal proportional to the 'luminance'. Therefore it is not necessary to use an integrating sphere. The signal can be produced by a simple photodiode ($V(\lambda)$ corrected) located in front of a light source and this makes its usage and implementation easier.

²⁹VI is a short form of Virtual Instrument.

Following section declares the different stages which are used to implement the proposed light flicker model.

1. The DC value of the light signal is determined. To do this, the initial 125 ms of the light signal is used and the mean value of all samples within this window is considered as the DC value or base line of the signal. It is important to note that this DC value is in fact the mean value of a small window at the beginning of the signal and does not account for whole signal. Fig. 2.15 illustrates two methods for determining DC value of luminance signal. The first method leads to L_{dc} and is proposed for this application. The second method is to use the area under the curve to find the mean value of the signal which is noted as L_{dc1} . As can be seen, for luminance signals which change stepwise, the difference between L_{dc1} and the value of signal after transient (b) is significantly lower than the same difference (a), concerning L_{dc} as the mean value. Considering L_{dc1} as DC value of the signal leads to a lower flicker value since the relative change of signal then is being smaller.

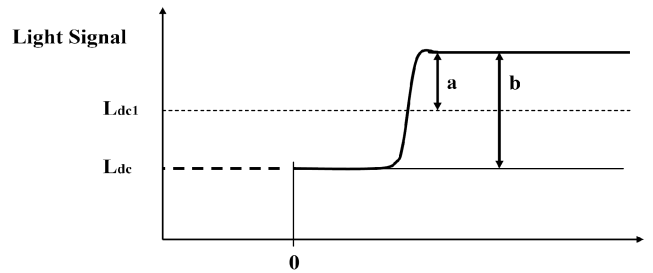


Figure 2.15: The method which is used to determine the DC value of luminance signal.

2. As long as a high order IIR digital filter (human eye characteristic filter) is used to filter the input signal, the output of the filter only after passing some initial time is valid. This is the result of using feedback in filter structure. According to (2.46) to get the first output of the filter, Y_0 , the value of $Y_{(1-Na)}$ is needed. The feedback filter order in this case is 40 which means to get the first value of the filter response the value with the order of (-39) is needed. As long as this value does not exist, this behavior of the filter leads to some transient responses at the beginning of the response signal of filter which are obviously invalid. It should be recall that the proposed filter is composed of eight filters in cascade form which increases the invalid part by a factor of eight. To avoid this malfunction it is possible to add some zeroes to the beginning of the signal and ignore their response in the output signal. This means the response of the signal appears after transient values of the filter and the initial part of the filter response can be removed without losing any information of the input signal. As it is formerly explained a lowpass filter resembles the brain perceptual storage process in the proposed model. The response of this lowpass filter to the transients which are generated by the first filter is a very slow signal which needs about 1.5 s to be vanished. Therefore the input signal is added with a pure DC signal which has the same value as the base line of the original signal and is determined in the first step. To stay in a safe margin the length of this signal is set to 8 s. To get the response of the model then the first 8 s of the response including initial transients of the filters is removed.

3. A potential problem which may appear by padding the DC signal to the beginning of the original signal is as follows. Consider that the first point of the original signal has a significant deviation from determined DC value. In this case after padding the DC signal to the original signal, at the point in which two signals are connected to each other, a significant change of light signal is then appeared which is not realistic.

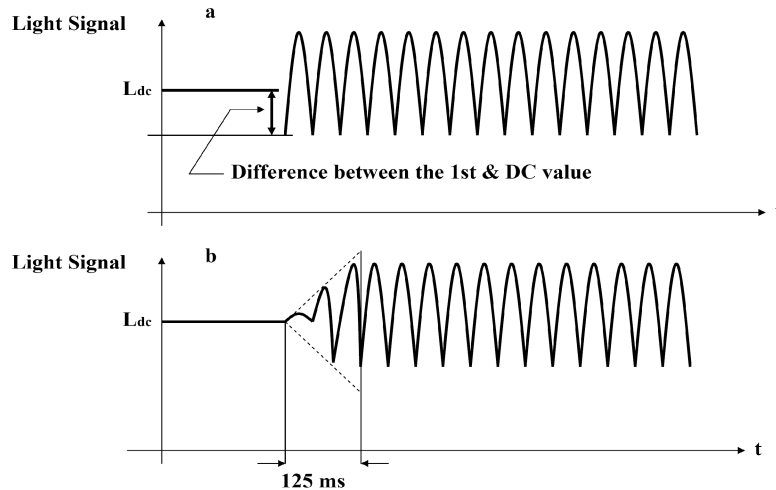


Figure 2.16: Adding the original signal with a DC signal. a. Shows the case that there is a significant difference between the first value of the signal and the DC value. b. Shows a DC padding which changes the initial part of signal to make these two values equal.

Obviously the model will interpret it as a light transient and gives a big value of flicker factor. To avoid this problem the AC term of the signal is multiplied with a ramp (between 0 and 1) within a small window (125 ms) which starts at the beginning of the original signal. This way the first value of the signal and the DC padded signal have the same value and after 125 ms the AC value of the signal reaches its original value. This method is more important when the model is using to determine the flicker factor of such light signals which have a significant AC term with higher frequencies. For example if an HID lamp is operated with convectional ballast, the light signal has a significantly large 100 Hz AC term. According to what is explained formerly this kind of flicker is not perceptible to the human eye. But if this light signal is padded with a DC signal, the difference between the first value of signal and its DC value is quite high. The result is a virtual light transient and leads to a false response of the model. Fig. 2.16 illustrates the method of DC padding to avoid virtual light transient. The only disadvantage of this method is that some information of the first 125 ms of the signal will be lost which for most applications is not decisive.

4. Before applying the signal to the first filter its DC value is removed. The reason is that the first filter is not an ideal bandpass filter and DC value of the signal can pass through it. It is already explained (in IIR filter designation) that the magnitude of filter at $f = 0$ can not be zero.
5. The output of the first filter then is squared and filtered with the second filter to imitate the perceptual storage effect of brain.

6. The output of the second filter is multiplied by a gain factor which is a function of DC value of the luminance signal L_{dc} . Equation (2.42) can be rewritten in the following form.

$$G = \frac{2}{(0.0015 \cdot L_{dc})^2} \quad (2.47)$$

7. For many applications the maximum value of the flicker signal is important. Because this value corresponds that part of the luminance signal which, contains the most serious transient. To give a single value of flicker factor for whole signal the maximum value of the flicker factor signal is determined.

2.9 Experimental Arrangement and Observation

2.9.1 Experimental Setup

The lamp is installed in an integrating sphere. As it is schematically illustrated in Fig. 2.17, a Lux-meter sensor gets the light intensity signal, and this will be converted into a voltage signal (0-10 V) through the Lux-meter (LMT System Flash Meter SF100). By using a 16-bit A/D card (National Instruments PCI 6014), the signal is then be captured by the computer. This signal is used as input signal of the eye-brain model and therefore the flicker factor of the signal can be determined.

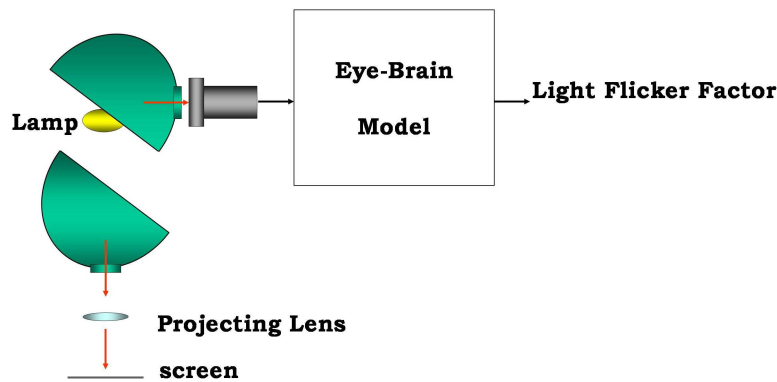


Figure 2.17: Experimental arrangement which is used to measure the light flicker factor and to observe a projection of the discharge simultaneously. To show the lamp position, the integrating sphere is illustrated in its open position.

A projection system makes it possible to observe the shape of the discharge during the measurement. This is very useful to check the performance of the whole measuring system, by comparing the light flicker factor and the degree of discharge instability which can be seen on the screen. The light sensor, which is used in this system, is a fast $V(\lambda)$ corrected photometer (LMT System-Photometer head SP 05 F00). This photometer head does not have a cosine correction and measures only the perpendicular light incidence, with a deviation of max. 10° . In addition, a short tube to avoid stray light from other directions is included. In the integrating sphere a shutter is located in front of the photometer head to avoid direct light into the photometer

head. Therefore what can be seen by the photometer head is a relatively small area on the shutter directly in front of photometer head.

It is assumable that on this area spatial distribution of light intensity is constant. Assuming that this area has a surface of A , and the luminous intensity perpendicular to the shutter and reflecting from its surface is I_{out} . The luminance of the area will be:

$$L = \frac{I_{out}}{A} \quad (2.48)$$

On the other side, the illuminance on the photometer head is:

$$E = \frac{I_{in}}{d^2} \quad (2.49)$$

where I_{in} is the incident luminous intensity and d is the distance between shutter and the photometer head. Structure of the photometer head makes it reasonable to consider that approximately whole incidence light into the photometer head is coming from this area. This means $I_{in} = I_{out}$ and therefore:

$$E \propto L \quad (2.50)$$

Proportionality of illuminance E and luminance L , in this case, allows us to use the output signal of the lux-meter as a signal which is proportional to the luminance.

2.9.2 Model Performance

Sinusoidal Mono-frequent Signals

Regarding the previous discussion about the perceptibility threshold, for an input signal with the form of equation (2.19) the flicker factor should be unity, as the perceptibility threshold. Fig. 2.19 illustrates the input signal. Up to $t = 2$ s, the luminance is constant. After the initial 2 seconds, a sinusoidal flicker with the frequency of 10 Hz and relative amplitude of 0.15% is added to the signal and remains for a 2-second interval. Fig. 2.20 shows the behavior of the model to the input signal. The flicker factor remains zero up to 2 seconds, as long as there is no transient. After that, it goes up with a time constant of 1.5 s (perceptual storage effect of brain), and reaches its final value of one. By terminating the superimposed flicker, the model response goes to zero with the same time constant. This means, after omission of flicker, the sensitivity of the eye decreases gradually. Therefore after termination of a flickering signal and in a time interval less than 1.5 s, visual system should be more sensitive to the flicker, because it doesn't need to pass the whole perceptual storage time from the beginning.

The model provides a similar response to the input signals with other frequencies as well. The only difference is the value of the modulation depth for different light transient frequencies in order to reach the flicker factor equal to unity. As an example if the input signal is a sinusoidal waveform with the frequency of 5 Hz, an amplitude modulation depth of about 0.20% is needed to make the flicker perceptible. This value for a flicker with the frequency of 20 Hz is about 0.23% and for a flicker frequency of 50 Hz increases up to 2.02%.

To evaluate the performance of the model when the input signal is a periodic flicker the following procedure is carried out. In a given frequency the modulation depth of the input signal is adjusted in such a way that the value of the flicker factor is unity. In other words the

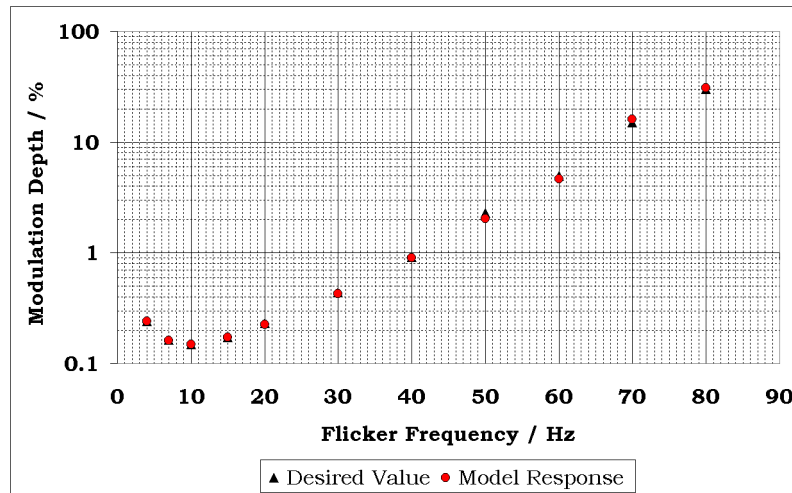


Figure 2.18: Model performance test. A comparison between desired threshold values (triangles) and modulation depth of the input signal to the model which leads to unity flicker factor (circles).

threshold of the flicker perceptibility in given frequencies is determined using the model. As long as these values are already known from Table 2.1, a comparison can be carried out easily. The values of Table 2.1 are normalized with respect to the value of 10 Hz which is considered as 0.15%. Therefore by dividing 0.15 to each value of the table the value of the modulation depth for any frequency can be calculated. As it is illustrated in Fig. 2.18 desired values and model responses are quite similar for whole range of frequency.

Double Flash Test

It is already pointed out that the proposed flicker model of this work is designed based on studies of Rashbass. In fact the model of Rashbass is established in such a way that it imitates the behavior of the human eye to double flash stimuli. Therefore a good test of model performance is to evaluate its response to double flashes. To check this, double flash signal is applied to the model as an input signal. Both flashes are considered to be rectangle pulses with pulse width of 2 ms and a time interval of 23 ms between two pulses. The amplitude of pulses are varied between -10% and 10% with respect to the base-line. Such pulses are illustrated in Fig. 2.23. For each couple of flashes the maximum value of flicker factor is determined. The minimum value of flicker factor would be zero when both amplitudes are zero. When both flashes have the maximum amplitude with opposite signs, the maximum value of flicker factor is reached.

Fig. 2.21 illustrates a surface diagram in which the value of flicker factor as a function of the relative amplitude of the first and second flashes is sketched.

The contours on the surface show the points with constant flicker factor. As it can be seen such contours have elliptical shape. The contour with the value of unity represents the threshold value of flash combination at which the stimuli would be perceptible. For the points inside this contour the flicker factor is less than unity while for the other points the value of flicker factor exceeds unity and the flash combination is considered as perceptible light intermittent. This is what expected from the model and shows that it resembles the results of the experiment of Rashbass perfectly.

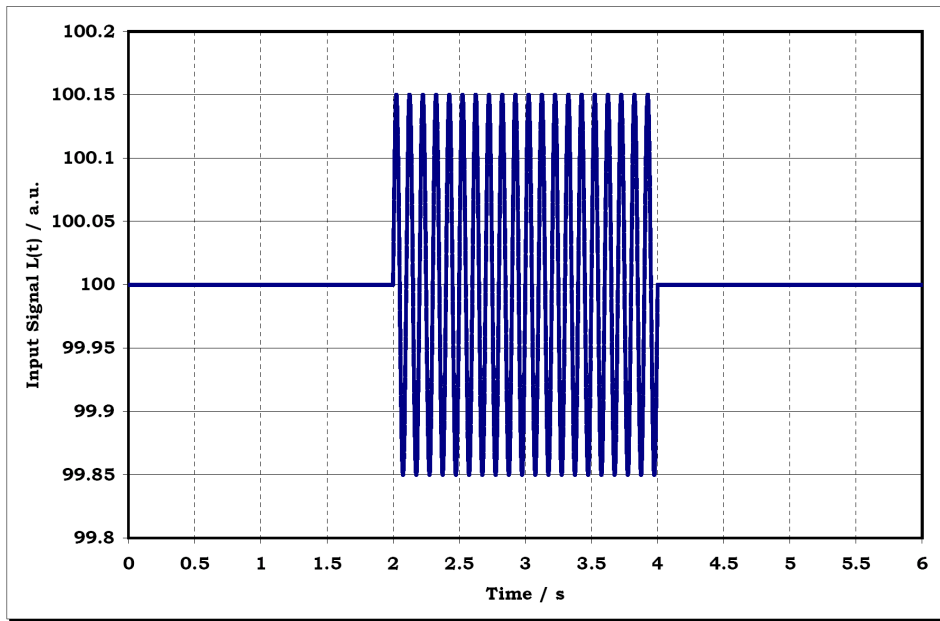


Figure 2.19: An example of input signal with a sinusoidal flickering part of 10 Hz and 0.15% modulation depth.

Linearity of the Model

The model accounts for the relative changes of luminance signal with respect to its base-line. This leads to independency of the model output to the absolute value of the base-line of the signal. The advantage of this property is that the model output does not depend on the light sensor. Using two light sensors, with different sensing areas, results in different values of luminance for a unique light signal. Actually the amplitude of the luminance signal is proportional to the sensor area. Considering the relative value of light transient, with respect to its base-line, leads to an identical model response for both input signals as it is expected. The linearity of the model is also important when the factor of amplification of the sensor circuit is changed. Hence the model can be used with any type of sensor regardless to its amplifying coefficient. Regarding equation (2.42) the output of the model is multiplied by a factor of B^{-2} which eliminates the effect of absolute value of the base-line. It must be noted that there is still a non-linearity inside the model to simulate the eye-brain perception mechanism. We consider a sinusoidal input signal with given amplitude, which is superposed on a DC signal (base line). If the amplitude of the sinusoidal signal is doubled while the DC value is constant the flicker factor is increased with a factor of four. As it is expected, this implies that the non-linear behavior of the model with respect to the ratio of the amplitude of the transient part to its base line value still exists.

The model linearity then was checked with different values of base-line while the relative value of the transient was kept constant (for single frequency sinusoidal input signals). As it was expected the response of the model was exactly the same for all signals.

It is important to point out that the sensitivity of the human eye to the light transients depends on adaptation level. This means the base line of the luminance signal changes the sensitivity of the eye. This is already explained under Ferry-Porter Law. The proposed model of this work, in order not to be more complicated, does not account for this law. To overcome

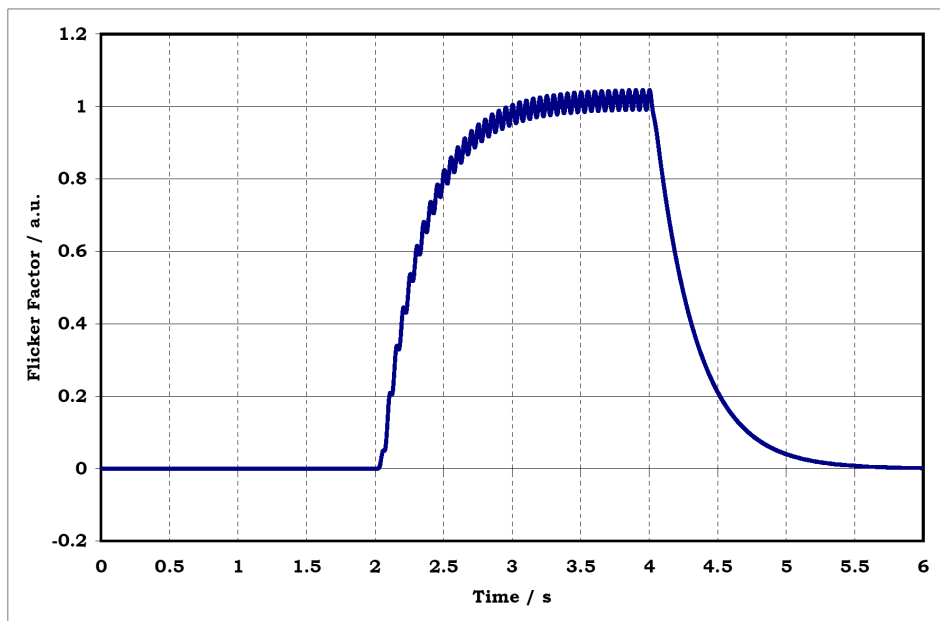


Figure 2.20: Flicker factor for the signal of Figure 2.19.

the possible disadvantage of this simplification the human eye characteristic filter with the highest possible sensitivity (0.15% at 10 Hz as it is suggested in (Henger, 1986)) is considered for the model. This model is generally used to evaluate the emitting light of the lamp directly. For this reason the model is supposed to work with very high values of luminance. At this range of luminance the human eye shows the highest sensitivity to luminance deviations and light transients. This consideration may lead to some kind of overestimation when the base line of luminance or adaptation level is low. As a result the model response for applications in which the base line of luminance is higher is more accurate.

Psychophysical Measurements to Modify the Model

Psychophysical³⁰ methods and procedures are useful in determining threshold values. For a perfect observer, threshold is an exact point above which the stimulus can just be detected and below it, it is not detectable. Human is not a perfect observer and often thresholds are defined in probabilistic terms: for example, half the points presented would be detected and half would not. So under certain psychophysical techniques, threshold can be considered the point where 50% of the stimuli are detected (Kalloniatis and Luu, 2005).

A direct method of calibration of the model and evaluating of its performance is a direct measurement. In this test, a probing person is asked to look into the integrating sphere. While the light inside the sphere is flickering the probe person is asked to decide whether the flicker is perceptible to his eyes or not. A simultaneous measurement of the flicker factor helps us to evaluate the response of the test person and the output of the model. It is expected that when flicker factor exceeds unity the test person perceives the flicker and when the flicker factor is

³⁰Psychophysics is the scientific study of the relationship between stimuli (specified in physical terms) and the sensations and perceptions evoked by these stimuli. The term psychophysics is used to denote both the substantive study of stimulus-response relationships and the methodologies used for this study (Montag, 2002 II.).

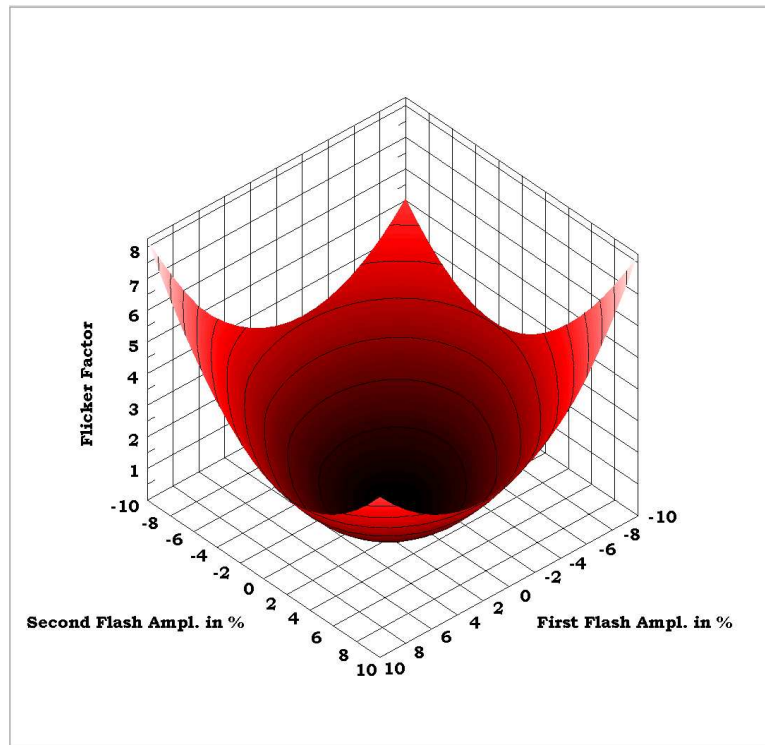


Figure 2.21: Response of the flicker model to double flash stimuli.

bellow unity the flicker is imperceptible for normal test person.

The procedure is to produce flickering light with different frequencies and different flickering factors. To cover a relatively wide range of flicker frequencies, the frequencies of 5, 10, 30 and 50 Hz are selected. For any flicker frequency 6 different values of flicker factor is considered. The first stimulus has a quite low value of flicker factor and the light flicker is not perceptible for a normal human eye. The last stimulus in contrast has a relatively high flicker factor in such a way that the light flicker is perceptible for all observers. The other four stimuli are set to have a flicker factor around unity. As a result when the subject is encountered with the first or to the last stimulus he can clearly decide about the flickering or non-flickering light. In contrast to these two stimuli the four other ones are not so easy for the subject to decide about their perceptibility.

Therefore the subject finds himself in a challenging situation to decide whether the light is flickering or not. This procedure leads to different decisions of test person for the same stimuli with the same flicker factors when the flicker factor is around unity. To find the threshold value, any stimulus is presented 10 times to the test person. The answers of the test person are gathered and it will then be determined that how many times the stimuli are detected as flickering and how many times as non-flickering light. Usually for stimuli with the flicker factor much bellow unity 100% of answers are non-flickering light, or 0% flickering light is detected. The same is for stimuli with relatively high flicker factor; actually all 10 times the answer is “the light is flickering”. For other stimuli the percentage of flicker detection is calculated as well. The threshold value for a test person is defined the value at which 50% of his answers are YES and 50% are NO. Fig. 2.22 illustrates a characteristic test result of such a threshold measurement with 6 stimuli.

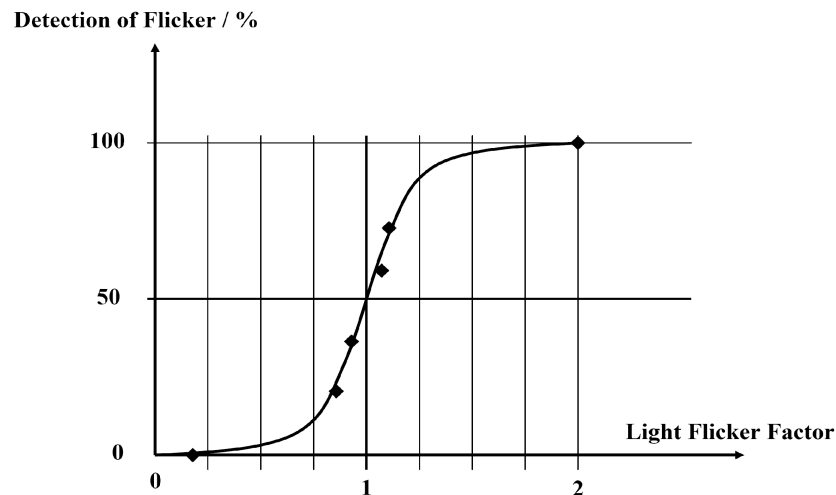


Figure 2.22: Probabilistic method to determine the threshold of flicker detection.

The order of the stimuli is changed randomly and the subject is asked to decide about the perceptibility of the light flicker. Changing the order of the stimuli in a random manner avoid the test person to be able to remember the order of perceptible/imperceptible stimuli. In this way the response of the test person to each stimulus is just what he sees at any test moment.

When the subject gives the answer about the perceptibility or imperceptibility of the stimulus he is asked not to look into the integrating sphere for a short moment. During this time the test person has a time to relax his eyes and furthermore the condition of the flickering light is changed without letting the test person to see the possible transients between two flickering light. As a result the test person has no clue to guess about the flicker situation and should decide just upon his perception.

In order to make a flickering light with a given value of the flicker factor the following method is used. An OSRAM 70W HCI lamp is used as the light source. The lamp is supplied with a low frequency square waveform current with a frequency of 200 Hz. A function generator (THURLBY THANDAR INSTRUMENTS TGA 1240) is used to generate the desired current waveform. The output signal of the function generator is amplified using a power amplifier (FM Elektronik FM1295) which is set to current mode. The current waveform which is generated by function generator is a DC signal which is superimposed with a square pulse with a given frequency, amplitude and pulse width. The offset of the DC signal determines the lamp power and the baseline of the light signal inside the integrating sphere. As long as the power amplifier amplifies the current signal with a factor of 2, setting the DC offset to 400 mV results in an 800 mA lamp current corresponding to a lamp power of 56 W. Adding a square pulse to this DC current results in a brief flash light which is added to the base line light. The flash intensity can be set by varying the amplitude and the duration (pulse width) of this superposed pulse. To reduce the number of parameters the pulse duration is set to 500 μ s and is kept constant during the experiment. The value of the flicker factor is adjusted by changing the amplitude of the pulse.

As long as the flicker factor is a signal its average value as it is shown in Fig. 2.23 is considered as the single value of the flicker factor.

The result of a flicker factor threshold test is given in Table 2.2. The test is carried out with

Flicker Factor Threshold				
Test Person	5 Hz	10 Hz	30 Hz	50 Hz
1	1.75	1.92	1.00	0.68
2	1.10	1.28	1.10	0.5
3	1.70	1.58	1.42	0.44
4	1.21	1.4	0.70	0.4
Average	1.44	1.545	1.06	0.505

Table 2.2: Results of a Flicker Factor threshold test for four probe persons.

four probe persons in an age range of 26 to 39 years. As it was expected the averaged measured values except for 50 Hz are around unity. This means that the model has a relatively good performance. The perceptibility of 50 Hz flickering light is described as inconvenient light and obviously the flicker itself is not perceptible to observers. As it is understood from table 2.2 the threshold level for 50 Hz flickering light should be doubled. This means the values of the human eye characteristic attenuation curve (Henger, 1986) should be modified for the higher frequencies. There are two important points to be noted in this regard:

Firstly, the nature of the human eye characteristic attenuation is a subjective parameter with relatively wide deviations.

Secondly, the values measured by Kelly or Henger are interpolated to get value for non-measured frequencies. This is always a question of fitting method and it is not possible to fit a curve to such points with equal error for all measured points. As a result the error of the used curve at 50 Hz was not unexpected.

Generation of Periodic Flickering Light

To create a periodic flickering light such pulses (which are described in the previous section) with given amplitudes and frequencies are superimposed on the current signal. Table 2.3 summarizes the amplitude of the current pulses regarding Fig. 2.23 which are used to drive the lamp in order to get a given light flicker factor at a given frequency. The corresponding flicker value for each current pulse train is given in the same table as well. The value of flicker factor for each frequency and amplitude which is given in Table 2.3, is the average value of 10 measurements. For any stimulus, to which the test person is encountered to decide about flicker perceptibility, the value of the flicker factor is determined simultaneously. The final value for the flicker factor is determined by averaging all values. The reason is that there are slight deviations of flicker factor with the same pulse amplitude during the experiment. This could be a result of different lamp responses (just slightly) to current pulses or some changes of circuit components for example as a function of temperature.

As can be seen from table 2.3 the values of flicker factor for all flicker frequencies are selected in such a way that the first value is quite below unity and the last one is well greater than unity. The other four flicker factor values are around unity.

It should be noted that the human eye characteristic filter is subjective and changes from one test person to other. As a result it is not expected to get the same response for different test persons when they are encountered into the identical flickering light.

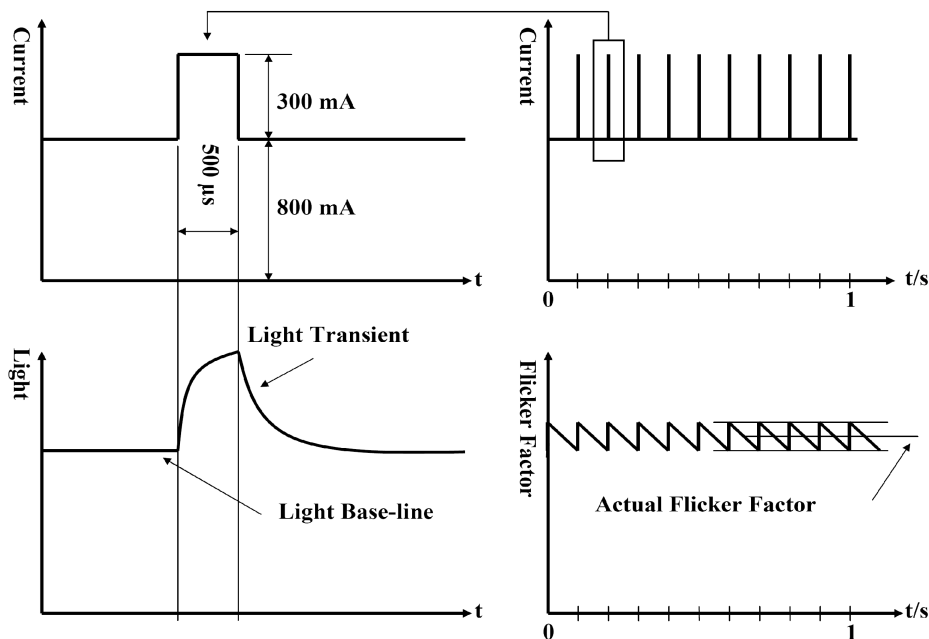


Figure 2.23: Up: Schematic diagram of a current pulse (Pulse width $500 \mu s$, Amplitude 300 mA), and a current waveform with 10 Hz periodic pulses to create flickering light. Down: Corresponding light signal when an HID lamp is operated with a pulse current waveform, and light flicker factor signal when the lamp is operated with a 10 Hz pulse train.

Generation of transient flash Light

The other experiment which is carried out to evaluate the model performance is a *single flash* test. Same as the previous test, light flashes are created by adding a rectangle pulse to the lamp current. The pulse width is kept constant ($500 \mu s$) and the value of the light flicker factor is set by adjusting the pulse amplitude.

In this experiment the probe person is encountered with repetitive light flashes with a low repetition frequency during a 50 s observation time. The time interval between flashes is changed randomly in a range of 3 to 10 s . As a result the subject does not know how many flashes exist during the observation time. The subject is asked to press a push button when perceives a transient change of light. The response of the test person and the light signal are

5 Hz		10 Hz		30 Hz		50 Hz	
Amp. [mA]	Flicker						
120	0.54	80	0.49	120	0.48	400	0.35
150	0.87	100	0.77	150	0.75	500	0.54
180	1.19	120	1.08	180	1.04	600	0.78
200	1.51	150	1.71	210	1.41	700	1.05
220	1.81	180	2.37	250	2.00	800	1.32
500	9.62	300	6.68	300	2.86	1000	2.03

Table 2.3: Amplitude of the pulse train ($500 \mu s$ pulse width) superimposed on the DC current (800 mA) and the value of the light flicker factor for different frequencies.

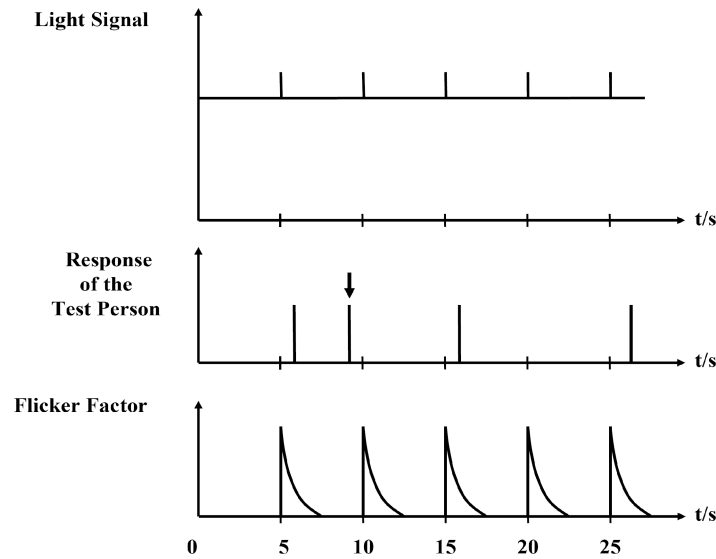


Figure 2.24: Up: The light signal versus time with brief flashes every 5 seconds. Middle: Response of the test person to light flashes. Down: Flicker factor determined by model.

Amp. [mA]	Flicker
50	0.506
60	0.703
70	1.004
80	1.307
100	2.044
110	2.47

Table 2.4: Amplitude of current pulses ($500 \mu\text{s}$ pulse width) superimposed on the DC current (800 mA) for flash test and the value of the light flicker factor.

recorded with a digital oscilloscope. Any light flash is recognizable as a brief pulse superimposed on a base line of the light signal. The response of the test person is also a voltage pulse which is generated by pressing the push button. The synchronal responses of the test person with existing light flashes show that those flashes are perceptible to that test person. As it is shown in Fig. 2.24, the value of flicker factor is determined for any light flash as well. The average value of flicker factor for all flashes during 50 s observation time is considered as the value of flicker factor. If there are some responses of the test person where there is no light flash this means that for any reason the observer could not decide correctly. This can be happened after an eye twinkling or as a result of eye tiredness or when the eye is glared during the test. This case is marked with a vertical arrow in Fig. 2.13. If some flashes are not detectable for the observer then there is no response of the observer corresponding to those flashes (Fig. 2.24, 2nd and 4th flashes are not recognized as a light transient by observer).

As long as the time intervals between light flashes are changed randomly, therefore the number of flashes within 50 s observation time is not always the same. The test is carried out several times (at least 20 times for any pulse amplitude) in order to have sufficient data for evaluation. Same as the periodic stimuli test, the light flashes have six different values of flicker factor.

The response of the test person then is used to determine the threshold value of perceptibility. The flicker factor value at which 50% of flash stimuli are perceptible is defined as the threshold value. This experiment has been carried out for two observers. The threshold values of 0.99 and 1.3 are the results of this experiment.

Modification Method

The value of the flicker factor at 50 Hz must be doubled which means a factor of 2. Furthermore, the lowest value of flicker factor at 30 Hz for the fourth test person which is 0.7 suggests that a factor of 1.42 is needed to increase it to unity. In this way for all cases a flicker factor threshold is never below unity. Applying this modification changes the average values for 30 Hz and 50 Hz to 1.5 and 1.01 respectively. To implement this idea we need to find a curve with the following correction coefficients. At 10 Hz there is no change i.e. the coefficient is 1, at 30 Hz a coefficient of 1.19, at 50 Hz a coefficient of 1.42 is needed. The correcting curve is supposed to be 1 at higher frequencies as well therefore the coefficients are considered to be reduced gradually to 1 at 70 Hz. The coefficients are root squared because there is a square function in our model. Having four desired values $\{(10,1), (30,1.19), (50,1.42), (70,1)\}$ it is possible to find a third order polynomial function which fits to these points.

$$Coef = -0.000014375 f^3 + 0.00134375 f^2 - 0.0255625 f + 1.135625 \quad 10 \leq f \leq 70$$

By using above function correction coefficients for all frequencies between and including 10 Hz to 70 Hz are calculated. The maximum value is 1.42 and the minimum value is 1. Fig. 2.25 shows the modified and the original curves of the human eye sensitivity characteristics with respect to the flickering light.

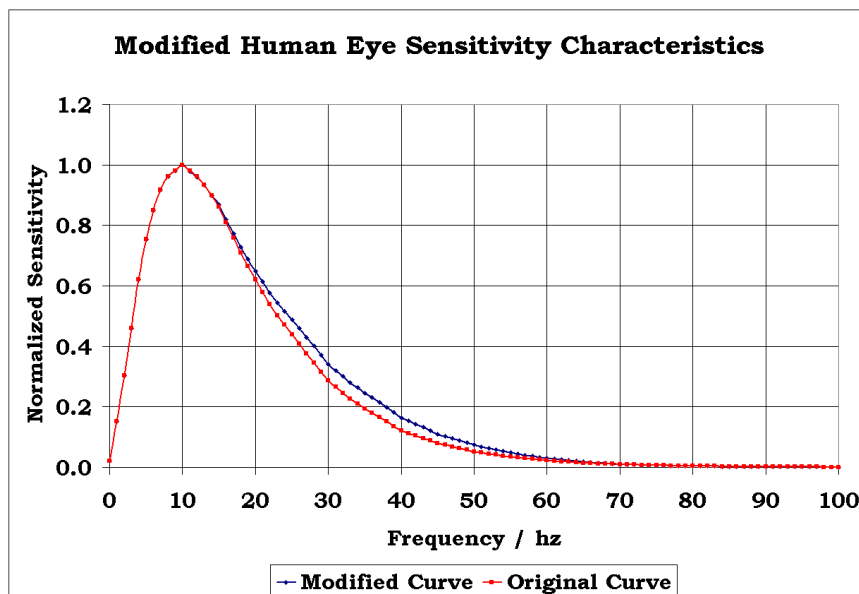


Figure 2.25: Comparison between sensitivity curves; derived from (Henger, 1986) and modified version which is used in this work.

Interpretation of the Light Flicker Factor

The value of the Light flicker factor translates the perception strength of the human vision system to the flickering or intermittent light. As explained formerly, the values below unity correspond the imperceptible changes of the light signal. The value equal to unity shows a just perceptible transient of light signal. For the light signals which contain perceptible intermittent, the value of the flicker factor exceeds unity.

As shown in Fig. 2.15, the second block of the model squares the signal. The effect of this block on the output of the model is a 2^{nd} order amplification of the amplitude of the alternating term of the input signal. As a result if the amplitude of the alternating term of the input signal (such as (2.25)) increases with a factor of 2 while its base line is kept constant, the flicker factor increases with a factor of 4.

Considering Stevens' power law, this behavior of the model suggests that the perception strength of the flicker grows with a power of two ($\alpha = 2$ in Eq. (2.11)) as the flicker stimulus increases.

A comparison of this value for perceptibility of the brightness ($\alpha = 0.33$) could be interesting. The lower value of α for brightness helps the vision system be active in a greater upper-range of luminance. An increment of the stimulus with a given value percepts as a lower incremental value. As a result the lower value of α increases the upper threshold of the visual system to the brightness. This phenomenon is in accordance with the functionality of the visual system. On the other hand the perception of the flicker increases with the power of two as the flickering stimulus increases. Hence, the perception of the flicker grows with a higher rate comparing to the physical increment of its stimulus. This phenomenon forces the person to avoid exposure his eyes to the flickering light which may bother the visual system.

According to (Brundrett, 1992), Ailleret investigated the effect of the flicker disturbance, he found that the magnitude of the flicker relative to the threshold value was more important than the exposure time i.e. the annoyance varied linearly with the time but with the square of the modulation depth

$$annoyance \propto \int_{t_1}^{t_2} (flicker \ modulation \ relative \ to \ 20 \ Hz)^2 dt \quad (2.51)$$

Since in the proposed model of this work the sensitivity curve which is suggested in (Henger, 1986; Kelly, 1961) is used it is reasonable to rewrite the equation of Ailleret as

$$annoyance \propto \int_{t_1}^{t_2} (flicker \ modulation \ relative \ to \ 10 \ Hz)^2 dt \quad (2.52)$$

As it is explained under "Normalized Filter Characteristics of the Human Eye" and according to (Rovamo and others, 1999), at high luminance levels, sensitivity to flickering spot peaks around 10 Hz. Hence the value of 20 Hz in (2.51) is changed to 10 Hz.

As an example consider the following situation: The first stimulus is a flickering light with modulation depth of 5% at 5 Hz. The second is a flickering light with modulation depth of 10% at 12 Hz. For the first stimulus using the normalized values of Table 2.1 the relative modulation with respect to 10 Hz is equal to $5\% \times 0.755 = 3.78\%$ and for the second stimulus is $10\% \times 0.959 = 9.59\%$. Therefore, for equal exposure time the annoyance of the second stimulus is 6.4 times more serious than the first one. As can be seen, although the modulation depth of

the second stimulus is only two times of the first one, its effect to the human eye is more than 6 times.

2.10 A Practical Example of Using the Proposed Model

One of the most important phenomena which can make the discharge of an HID lamp unstable is acoustic resonance. A relatively secure method to supply low wattage metal halide lamps with electronic ballast, is using low frequency square-wave current. Superimposing of high frequency ripple over this square-wave, can excite acoustic resonance in the arc tube, and make the discharge unstable or change its shape-position. Fig. 2.26 (left), shows the discharge channel of a HQI-TS 150 W lamp which is supplied with a 200 Hz square-wave. The discharge is stable with a normal shape and position. In contrast, Fig. 2.26 (right) shows the same lamp with the same current waveform but superimposed with a 20 kHz sinusoidal ripple, with about 5-6% amplitude depth. As it can be seen in the picture, the discharge channel slightly changes its position, and there is a significant deformation in its shape.

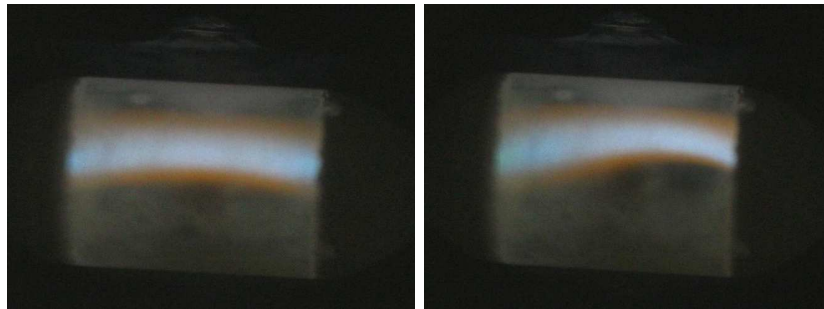


Figure 2.26: Experimental test of the model. Discharge channel of an HQI-TS 150 W lamp, in its normal position (left) which is stable and after applying power ripple at an AR frequency (right) which is deformed as a result of AR instability.

By acquisition of the light signal, before and after superimposing the ripple, we can check any deviation of discharge of its original state. Fig. 2.27 shows the light signal of the lamp in a 5-second interval. Up to $t = 0$ s the lamp current has no ripple, at this time the ripple has been added to the current waveform. As it can be seen, at the beginning (after $t = 0$ s), the light intensity shows some significant fluctuations and after that gradually will be flattened and shows some kind of stability in its new state. The perceptibility of these transients, based on the eye-brain model has been detected. Fig. 2.28 illustrates the flicker factor in this time interval. The flicker factor for two stable situations, i.e. before applying the ripple and after termination of transients, is zero which was expected. As it can be seen, the flicker factor reaches a value of about 14, and this means that the transition of discharge channel from one state to the other is perceptible for the human eye since it exceeds unity strongly.

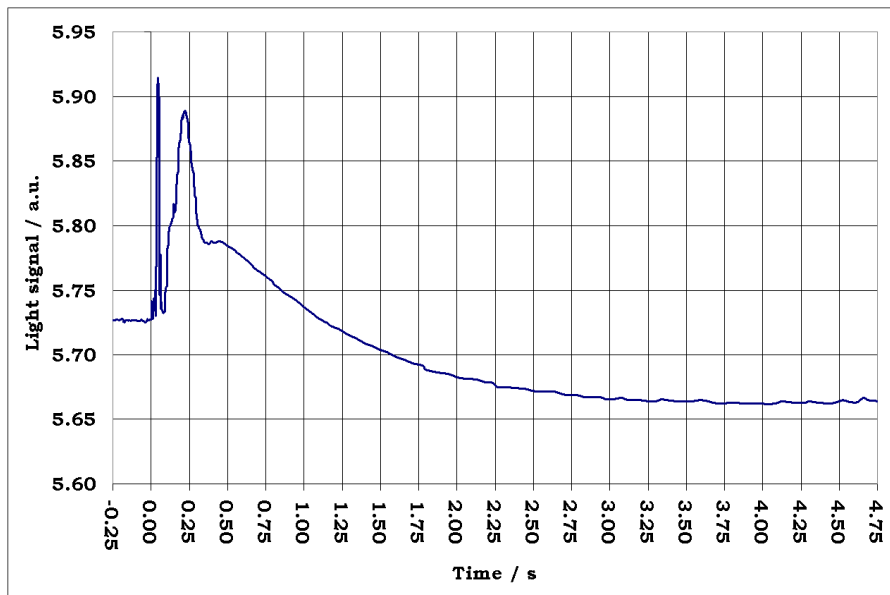


Figure 2.27: Input light signal before and after applying high frequency ripple at $t=0$ s.

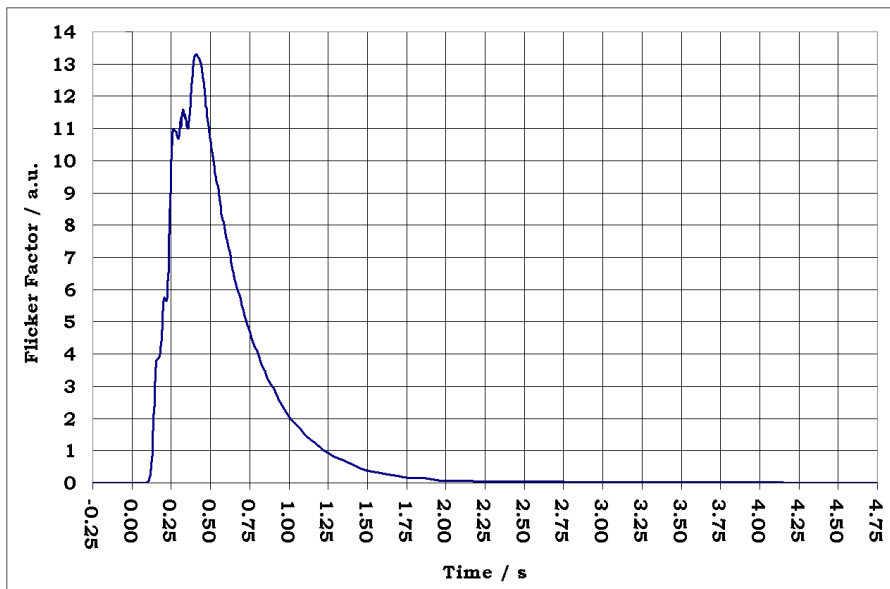


Figure 2.28: Flicker factor signal shows the transition of the discharge between two states.

Chapter 3

Excitation of Acoustic Instability in High Intensity discharge Lamps

3.1 Introduction

Excitation of Acoustic Resonances (ARs) in High Intensity Discharge (HID) lamps was reported by Buckley and Gerue in 1962-63 (Galo and Courtney, 1967) and Strickler and Steward in 1963 (Witting, 1978). They have studied the discharge instabilities that occur in compact xenon arc lamps which are operated with a modulated current. The experiment of Buckley and Gerue illustrated that the excitation frequency decreased as the bulb size increased. "This qualitative observation led Buckley and Gerue to the conclusion that resonances involving acoustical pressure waves were responsible for the lamp excitation" (Galo and Courtney, 1967). Regarding Campbell's experiment with mercury lamps, it was noticed that the arc extinguished due to a frequency scanning in the range of 60-10,000 Hz. "Subsequent analysis by Kenty revealed this effect was produced by acoustic resonance which occurred when the gas in the arc tube was subject to the half wavelength resonance" (Campbell, 1969). Acoustic Resonances with sufficient acoustic energy cause some undesired effects in HID lamps. Such effects range from a nearly imperceptible movement to extreme displacement of the discharge which can lead to total destruction of the lamp. Instability of the discharge, light flickering, fluctuation of the electrical parameters, extinguishing of the lamp, even lamp explosion are commonly noticed and reported by researchers such as (Scholz, 1970; Fellows, 2003; Garcia and others, 2004). Deterioration of the electrodes as a result of acoustic resonances which reduces the lamp life and also the deviation of the light color due to the change of the chemical balance of the lamp filling (Anton and others, 2003; Epron and others, 1998) should be noted as other malfunctions of acoustic resonances in HID lamps. Additionally, "there is a high possibility of ballast damage due to the high voltage caused by a discharge is extinguishing" (Correa and others, 2004) which should be considered by ballast designers.

On the other hand, straightening of the discharge, in horizontally operated lamps (Allen, 1992), and suppression of the color de-mixing due to the segregation of the filling material, in vertically operated lamps (Shen, 2002), are desired effects of acoustic resonances. A careful design of electronic ballast can gain mentioned advantages of acoustic resonance. In this section the theory of acoustic resonance and acoustic streaming will be discussed. A new hypothesis based on these two theories is then developed to explain the acoustic instabilities as a result of excitation of acoustic resonances. The chapter will be followed by the mathematical calculations of acoustic resonances. A numerical method of capturing acoustic resonance frequencies and resonance shapes/modes which accounts for temperature distribution in the arc tube is presented. To show the relationship between acoustic streaming and acoustic resonance, analytical solutions for these two phenomena in a simple cylindrical geometry is given. The proposed theory is then used to explain the observed behavior of the discharge when the lamp is excited with a known resonant frequency as a real case study. Regarding undesirable effects of acoustic resonances different AR detection and avoidance methods are discussed. Finally the positive and useful effects of acoustic resonances and different approaches to excite them will be introduced.

3.2 Theory of Acoustic Resonance and Acoustic Instability

There is a common explanation of the physical backgrounds of acoustic resonance phenomenon in HID lamps which is accepted by many researchers in this field. In this section, firstly, this widely accepted theory of acoustic resonance is discussed. Afterwards, a new hypothesis which aims to declare the physical reasons of acoustic instability will be introduced. It is worth to emphasize that what is meant under the phrase of *Acoustic Instability* is the discharge instability which occurs as a result of excitation of *Acoustic Resonance* inside the lamp's arc tube. It is possible to establish acoustic resonance in arc tube without exciting acoustic instability. Existing theory only explains how acoustic resonances are established. The theory of acoustic instability, which is introduced here, is an attempt to explain how acoustic resonance may lead to the discharge instability in HID lamps.

Operating of HID lamps with a periodic power leads to a modulated discharge current in the arc tube. That means the intensity of the discharge changes with the same frequency as the power. Any increase of the discharge intensity increases the pressure of the filling gas inside the arc tube. In the same manner decrement of the discharge intensity decreases the pressure. In other words, the periodic input power and the subsequent energy exchange by elastic collisions between charged particles and neutral gas are the source of pressure perturbation. The fluctuation of the pressure, which is originated in the vicinity of the discharge, propagates through the gaseous medium inside the arc tube. This propagation represents a traveling longitudinal wave with the nature of the sound (acoustic) wave¹. This is an acoustical pressure wave with spherical wave-front (Galo and Courtney, 1967).

Regarding (Aramyan and Galechyan, 1997), "Sound waves can be excited in a gas discharge by two methods: 1. by introducing sound into the discharge chamber from outside, by means of an electrodynamic generator clamped to one end of the tube, 2. by generating sound waves inside the chamber and adding an alternating component to the dc discharge. The results of experimental investigations of the influence of sound waves on the plasma parameters obtained by these two methods show that they completely agree." When the frequency of the acoustic wave is equal to or close to the eigenfrequency of the arc tube the acoustic wave will be reflected at the arc tube's wall. In this case the particle velocity perpendicular to the wall is zero. The incident and reflected traveling waves have the same frequency and travel in opposite directions. The interference of these two traveling waves introduces a standing pressure (acoustic) wave with the same frequency.

As it is shown in Fig. 3.1, characteristic of the standing waves are locations with maximum displacement (anti-nodes) and locations with zero displacement (nodes). In nodal points the amplitude of the standing wave is zero and in anti-nodes is equal to the sum of amplitudes of incident and reflected waves. In the vicinity of the inner wall of the arc tube, standing wave of the linear acoustic velocity, perpendicular to the wall, has its node, while standing pressure wave shows its anti-node at that area. This way the pressure of any point in the arc tube is a function of time, as it oscillates with input power oscillations, and position. At the pressure nodes the pressure is constant and in antinodes it is modulated with the frequency of the lamp power. This means at antinodes the pressure varies around the equilibrium pressure of the arc

¹A sound wave consists of a repeating pattern of high pressure and low pressure regions moving through a medium, which is sometimes referred to as a pressure wave.

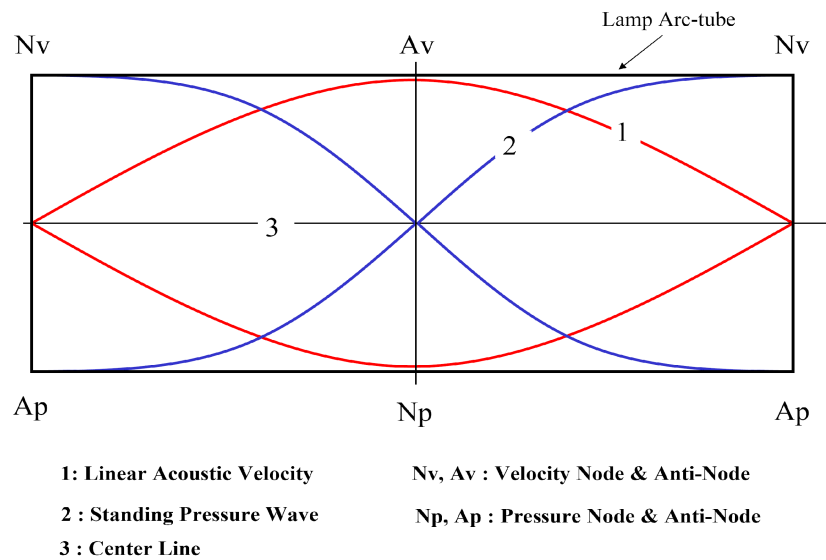


Figure 3.1: Positions of nodes and anti-nodes with respect to standing pressure wave and linear acoustic velocity in a cylindrical arc tube.

tube. In contrast to the pressure, the linear acoustic velocity varies around zero. At velocity nodes the velocity of the filling material with respect to the linear acoustic is zero (at the wall) and at antinodes it changes from a maximum positive peak to a maximum negative peak. It should be noted that the reflected acoustic wave in an arc tube has no change of phase, because the incident acoustic wave encounters a greater acoustic impedance.

Regarding related literature, existence of standing pressure waves in acoustic resonance phenomenon in HID lamps is widely accepted (de Groot and van Vliet, 1986). The above mentioned theory can not explain the reason of the discharge instability as a result of excitation of ARs.

There are some explanations about the possible reaction of the standing pressure waves and the discharge instability. "The strong oscillation in the gas density can distort the discharge path, which in turn distorts the heat input that drives the pressure wave" (Witting, 1978). Regarding (Sturm and Klein, 1992) standing pressure waves result in extra heating of the discharge channel in some positions which disturbs it.

In fact there is a gap in understanding the relationship between the standing pressure waves which is a high frequency phenomenon and arc instability in HID lamps which is a slow mechanism. "Till now the question of how an acoustic can cause visual arc instability is open" (Schäfer and Stormberg, 1982). Other and more recent investigations such as (Yan and Hui, 2004) do not give more detailed information about the physical background of the mechanism of AR instabilities as well.

A New Hypothesis: Effect of Acoustic Streaming on the Lamp Discharge

A plausible theory for the low frequency phenomenon of light flickering and visual instability of the discharge using the concept of acoustic streaming can be described as follows:

Propagation of sound in a medium is a flow of wave energy. When an object interrupts this flow the sound generates a force to push it in the direction of propagation. "This force comes from acoustic radiation pressure and is a non-linear phenomenon derived from the second order terms. The force acts not only on the ordinary objects but also on the objects in broad sense such as interface between different fluids and the medium itself in which ultrasound propagates. The latter induces non-oscillatory steady fluid motion, which is known as acoustic streaming." (Mitome, 1998).

"In a region of the fluid where a sound field exists, the pressure and the velocity vary with time, but, in general, the temporal average of these quantities are not zero. The average over time of the velocity is called *acoustic streaming*" (Hamilton and Blackstock, 1998). Mathematically speaking, acoustic streaming is defined as a second order non-linear effect where the presence of sound waves generates mean mass flow (Boluriaan and Morris, 2003).

In presence of the standing pressure waves the arc tube of an HID lamp can be considered as a standing wave resonator. In such a resonator, close to the solid boundary, shear viscosity of the filling gas induces acoustic streaming (Hamilton and others, 2003). According to the classification of acoustic streaming by Zarembo (Mitome, 1998) this kind of streaming should be classified as Rayleigh Type. In this category the vortex-like streaming is generated outside the boundary layer² in a standing wave field whose scale is comparable to the wavelength. As a general rule, establishment of acoustic streaming is a result of the dissipation of acoustic energy. Acoustic energy is converted into a momentum of the filling material in the lamp arc tube.

Inter-molecular, inter-atomic and inter-ionic forces between the electrons, atoms, ions and molecules within the arc tube lead to a finite viscosity in the discharge gas (Beasley, 1999). This type of viscosity is known as bulk viscosity. "The bulk viscosity (or the "second viscosity") is the transport coefficient that dampens the compressional motion of a fluid, beyond the damping caused by the shear viscosity. The damping is the result of energy exchange between the fluids translational degrees of freedom (acoustic waves or shock waves) and its internal degrees of freedom (molecular rotations, vibrations, metastable intermolecular bonds, and critical fluctuations)" (Gillis and others, 2005).

The bulk viscosity of the filling material is the other cause for the dissipation and conversion of the acoustic energy (Boluriaan and Morris, 2003). "Generally speaking, viscosity suppresses fluid motion but it acts as a source of driving force in generation of acoustic streaming simultaneously" (Mitome, 1998). It is worth to emphasize that the gas viscosity dissipates the acoustic energy, by converting it into mechanical momentum of filling material. If this mechanism leads to a coherent movement of filling particles, the acoustic streaming will be established. Otherwise, when the dissipated acoustic energy leads to a disordered and confused movement of particles then it can be seen as a damping effect which prevents acoustic instabilities.

The linear acoustic velocity has a time dependent oscillatory behavior with the frequency of the arc tube eigenfrequency. On the other hand, the resulting streaming represents a non-linear one-directional (or in case of a lamp arc tube circulating) time-independent movement with a much slower velocity (Sastrapradja, 2004). There is a non-curl-free acoustic field which math-

²In the vicinity of the solid boundary (boundary layer) there is another acoustic streaming loop. Depth of this layer (viscose penetration depth) depends on the fluid kinematic viscosity and the frequency of the acoustic movement. This streaming is referred as inner acoustic streaming and streaming discussed in this paper is called outer streaming.

ematically³ is the driving force of the second order acoustic streaming velocity (Sastrapradja, 2004).

Counteracting of the acoustic streaming and normal flow of the lamp fillings, mainly due to the thermal convection⁴ and the gravity force, causes acoustic instability. Excitation of acoustic resonance in the arc tube causes a mass transportation in the directions which are determined by that specific acoustic streaming mode. This can change the discharge path in the arc tube and move it to a new position. For two reasons the discharge is unstable in this new state, concerning its position or its shape, and tends to return to its original state. Firstly because of the wall stabilizing forces and secondly due to the possible changes of the eigenfrequencies of the system.

In a wall-stabilized discharge the radial temperature profile has a relatively steep tendency at the wall. Any off-center movement of the discharge toward one side leads to a steeper temperature gradient on that side and makes it less steep on the other side. Steepening of the temperature gradient leads to an increase of the heat loss and cools the discharge on that side. On the other side, the heat loss conduction decreases and allows the temperature of the discharge to rise. This mechanism (Waymouth, 1971) cancels the initial movement of the discharge and forces the discharge toward the center line of the arc tube.

Changing of the discharge path due to the acoustic streaming inside the arc tube means that the temperature distribution varies as well. This changes the sound propagation velocity and subsequently the eigenfrequencies of the system. At this point, the frequency of the input power doesn't match the new eigenfrequency and the arc tube stops resonating or resonates weakly. As a result, acoustic streaming is eliminated or weakened and the discharge path tends to resume back toward its original position. Therefore the temperature distribution reaches its former state as well and the power frequency again matches with the eigenfrequency.

This scenario explains the characteristic behavior of acoustic resonances which leads to acoustic instability and makes the lamp start to flicker. This kind of discharge instability occurs at the lower eigenfrequencies. At these frequencies the instability is more strength and changes the discharge path more widely. Therefore the disturbance of the temperature distribution is more considerable. Changes of temperature distribution in arc tube and acoustic streaming velocity both are slow mechanisms and this is a good explanation for low frequency light flicker as the discharge is presented to the acoustic resonances.

Assume that the electrical power of the lamp contains a DC level which is superimposed with a high frequency component in AR frequency. The laboratory experiments show that increasing the amplitude of the high frequency component, up to some threshold just changes the position of the discharge. In this case the discharge will remain in its new position due to weakly excited resonances. The higher the amplitude of the high frequency is the stronger the deviation of the discharge position. By reaching the threshold value the lamp starts to flicker. This observation can confirm the former proposed theory about the mechanism of discharge flickering. By slight changes of the discharge position, the temperature distribution

³It should be noted that the linear acoustic velocity is not the driving force (physically) of the acoustic streaming. This is indeed a result of the perturbation expansion. We write the velocity as: $u = u_0 + u_1 + u_2 + \dots$ then we put this in equation of motion and separate out different orders (zero order, first order, 2nd order and so on). Then the zero order quantities become the forcing function for the first order equations, and zero and first order quantities become the forcing function for the second order equations. Therefore, it is purely a mathematical manipulation.

⁴or convection currents as it is called in (Waymouth, 1971)

does not change dramatically and arc tube eigenfrequency does not change as well. Therefore the acoustic streaming remains and pushes the discharge path constantly to some direction. Reaching the threshold amplitude of the high frequency component means a relatively extreme change of the discharge path which changes the temperature distribution in lamp arc tube as well. This mechanism then can lead to light flickering as it is explained formerly.

It should be noted that there are some extreme and quick movements of the discharge by which the discharge strikes the arc tube's wall and then is reflected back. The result is a relatively non-predictable behavior of the lamp discharge. This effect may lead to a standing flicker, or will be damped by different damping mechanisms.

In some acoustic modes, there is only a deformation of the discharge, and it remains in its new state without periodic changes. This could be interpreted as an insignificant change of temperature distribution and eigenfrequencies.

3.3 Theoretical Prediction of Acoustic Resonance

The describing equation of excitation and behavior of the acoustic resonances in a cylindrical arc tube, when the filling gas is considered as an adiabatic medium, is usually assumed as

$$\frac{\partial^2(\delta p)}{\partial t^2} + \Gamma \frac{\partial(\delta p)}{\partial t} - c_{eff}^2 \nabla^2(\delta p) = (\gamma - 1) \frac{\partial N}{\partial t} \quad (3.1)$$

where δp is the local pressure fluctuations⁵, Γ the damping coefficient accounting for acoustic losses, c_{eff} the effective velocity of the sound (or wave velocity (Lama and Hammond, 1981)), $\gamma = c_p/c_v$ the specific heat ratio and N the local acoustic power. N can be written as: $N = P - P_{rad} - P_{cond}$, where P is the high frequency input electrical power, P_{rad} is the irradiative loss and P_{cond} the conduction loss all per unit volume (Schäfer and Stormberg, 1982). By assuming that the input power and the losses are sinusoidal time dependant, the solution of (3.1) in frequency domain is (Ingard, 1966)

$$\delta p(\omega) = \frac{j\omega(\gamma - 1)N(\omega)}{\omega^2 - \omega_0^2 + j\omega\Gamma} \quad (3.2)$$

where ω is the operating frequency of the lamp power supply and ω_0 denotes the eigenfrequencies of the lamp's arc tube. The magnitude of the pressure at the eigenfrequency reaches its maximum value of

$$\delta p(\omega_0) = \frac{(\gamma - 1)N(\omega_0)}{\Gamma} \quad (3.3)$$

As it can be seen there are three factors affecting the amplitude of the pressure oscillation. These factors are the input acoustic power at the eigenfrequency of the arc tube, the specific heat ratio of the gas and the damping coefficient.

Assuming a free, undamped, periodic pressure oscillation in the gas, the wave equation (3.1) will be simplified as follows:

$$\nabla^2(\delta p) = \frac{1}{c_{eff}^2} \frac{\partial^2(\delta p)}{\partial t^2} \quad (3.4)$$

⁵We shall consider the acoustic phenomena to be perturbations on a state of constant pressure p_0 (Davenport and Petti, 1985). For this reason the notation of δp is used to show the oscillating part of the local pressure.

The boundary condition is considered as

$$v_n = \text{grad}_n(\delta p) = 0 \quad (3.5)$$

which follows from the requirement that the particle velocity perpendicular to the wall, v_n , must be zero at the wall. The term $\nabla^2(\delta p)$ in equations (3.1) and (3.4) is defined as: $\nabla^2(\delta p) = \text{div}(\text{grad}(\delta p))$ where δp is a scalar field (pressure in our case) and ∇^2 is defined as Laplacian or Laplace-operator.

3.3.1 Damping of Acoustic Resonances

All fluids absorb energy from sound waves by loss through shear viscosity, bulk or "second⁶ viscosity" and heat conduction (Tanahashi, 1975). The damping coefficient (Γ in (3.1), (3.2) and (3.3)) increases as viscosity and the heat conduction increases. It should be noted that as a task of simplicity, the damping coefficient in previous section was assumed to be constant. However, as it is mentioned, this coefficient is a function of the frequency as well.

It is known that both viscosity and heat conduction are the function of the square of frequency (Yan and Hui, 2004). As a result, acoustic resonances with higher frequencies are highly damped and practically the lamp can be operated at frequencies higher than a given value without acoustic instabilities. As it is already explained the bulk viscosity damps the compressional motion of a fluid. Since the acoustic energy propagates through a periodic compression/decompression of the medium, existence of viscosity acts as an energy damper.

"Damping of acoustic waves is caused by wall or volume effects. In both cases the damping coefficient increases with increasing viscosity and decreases with increasing pressure" (de Groot and van Vliet, 1986). This is in accordance with the hypothesis of acoustic streaming. As it is explained, shear and bulk viscosities (*wall* and *volume* effects respectively) of the gas dissipate the acoustic energy (damping effect) and convert this energy into the mechanical momentum.

3.3.2 Hypothesis About the Wall Effect

The acoustic energy which is generated by discharge oscillation after reaching the arc tube's wall is divided into three parts. The first part is reflected back into the arc tube, the second part passes through the wall and makes audio noise of the resonance which at low frequency resonances can be heard and at higher frequencies can be detected with a proper microphone as it is carried out by Schäfer and Stormberg (Schäfer and Stormberg, 1982). Transferring energy from the acoustic wave to the tube's wall results in loss of energy from the wave. This part may be considered as a damping effect of acoustic energy which does not play any role in acoustic instability. Typically such wall damping dominates viscose damping (with respect to bulk viscosity) under condition of temperature, pressure, gas composition and geometrical configuration of HID lamps (Beasley, 1999). The third part of the acoustic energy as a result of the shear viscosity of the filling gas (mainly mercury) is converted to a mechanical form and establishes the so called acoustic streaming. This is also a damping effect of acoustic energy but plays a significant role in discharge instabilities.

⁶The bulk viscosity μ_B is defined as $\mu_B = \lambda + \frac{2}{3}\mu$ where λ is the second viscosity coefficient and μ is the shear viscosity. It is worth to recall that the term of "second viscosity" is the other name of the bulk viscosity and should not be confused with λ as the coefficient of the second viscosity.

3.3.3 Hypothesis About the Pressure Effect

(Giese, 1997) reports a theoretical investigation of gas filling convection in mercury HID lamps. In this work, the mass density flow for a 200 W mercury lamp with a spherical arc tube is calculated. The calculation has been carried out for two different mercury pressure values of 1 and 100 bar in the same lamp geometry. A comparison of mass density flow shows that the lamp with higher mercury pressure has a condensed discharge between the electrodes and the mass density in the cavity between plasma and arc tube's wall is very low. On the other hand the lamp with lower mercury pressure has a more distributed discharge and the mass density in the area between discharge and wall is significantly more condensed. This means the generated acoustic wave in a case of a lower pressure lamp is encountered with many particles as it is propagated through the gas. As a result, the acoustic energy of the wave is subject to a higher damping effect. In contrast, the acoustic wave which is generated with a condensed discharge in a lamp with higher mercury pressure propagates through a lower density medium and therefore is subject to lower damping coefficient.

3.3.4 Analytical Solution

The analytical solution of the wave equation (3.4) under the boundary condition (3.5) and in a cylindrical coordinates (r, φ, z) is (Morse, 1948)

$$\delta p \propto \cos(l\phi) \cos\left(\frac{\omega_z}{c_{eff}}z\right) J_l\left(\frac{\omega_r}{c_{eff}}r\right) e^{-j\omega t} \quad (3.6)$$

Where l is an integer indicates azimuthal acoustic mode, J_l is the Bessel function of the first kind and order l , ω_z indicates the angular frequency of the oscillation in z direction and ω_r is the angular oscillation frequency in radial direction. The geometry of the arc tube is considered to be symmetrical around the z axis. Therefore the problem of the wave equation is firstly solved in (r, z) plane of cylindrical coordinate system. The term of $\cos(l\phi)$ then expands the solution from two dimensions to three dimensions. In any acoustic mode the oscillation angular frequency is calculated as:

$$\omega^2 = \omega_z^2 + \omega_r^2 \quad (3.7)$$

Applying boundary condition leads to

$$\omega_z = \frac{\pi n c_{eff}}{L} \quad (3.8)$$

where L is the length of the arc tube and n is an integer which indicates the order of the longitudinal mode and

$$\omega_r = \frac{\alpha_{lm} c_{eff}}{R} \quad (3.9)$$

where R is the radius of the arc tube and α_{lm} is the m^{th} zero of

$$\frac{d}{dr} \left[J_l \left(\frac{\omega_r}{c_{eff}} r \right) \right]_{r=R} = 0 \quad (3.10)$$

The local pressure of the filling gas is a function of position (r, φ, z) , which is explicitly illustrated in (3.6) and as Laplace-operator implies in (3.4), sound velocity and time. The

first term of the right hand side of (3.6), $\cos(l\phi)$, belongs to the azimuthal modes, the second term, $\cos(\frac{\omega_z}{c_{eff}}z)$, stands for longitudinal modes and the third term, $J_l(\frac{\omega_r}{c_{eff}}r)$ stands for radial-azimuthal modes. Considering only the real part of equation (3.6) and defining A_{lmn} as the pressure amplitudes, without missing the generality, the local pressure oscillation alternatively can be rewritten in the following form (Witting, 1978).

$$\delta p = A_{lmn} \cos(l\phi) \cos\left(\frac{\omega_z}{c_{eff}}z\right) J_l\left(\frac{\omega_r}{c_{eff}}r\right) \cos(\omega t) \quad (3.11)$$

By combining equations (3.7), (3.8) and (3.9) one can calculate any resonant frequency as follows:

$$\omega = \omega_{lmn} = \sqrt{\left(\frac{\pi n c_{eff}}{L}\right)^2 + \left(\frac{\alpha_{lm} c_{eff}}{R}\right)^2} \quad (3.12)$$

where indices l , m and n stand for azimuthal, radial and longitudinal modes respectively.

3.3.5 Effective Sound Velocity

The other assumption for these calculations is that the filling gas is considered as an ideal gas, hence the effective sound velocity c_{eff} in the arc tube can be written as

$$c_{eff} = \left(\frac{c_p}{c_v} \frac{R_g \bar{T}}{\bar{M}_g}\right)^{1/2} \quad (3.13)$$

where c_p and c_v are the specific heat capacities for mono-atomic gases at constant pressure and volume respectively. R_g is molar gas constant, \bar{M}_g stands for average molar mass of the gas and \bar{T} is the effective temperature of the gas. \bar{M}_g is weighted average of molar masses of filling species with respect to their partial pressure. As it is shown in (3.1) the acoustic pressure δp , depends on the sound velocity and subsequently on the gas temperature regarding (3.13). The problem of the wave equation is analytically soluble only if the sound velocity considered as a constant parameter in whole area of the arc tube. For this reason the concept of *effective sound velocity* which is a consequence of considering a homogenous temperature distribution (isothermal) in the arc tube is used in literature (Witting, 1978; de Groot and van Vliet, 1986; Denneman, 1983).

The effective temperature should be calculated as a mean value for the whole volume of the arc tube (Witting, 1978)

$$\bar{T} = \left(\frac{1}{V}\right) \int_v T dv \quad (3.14)$$

where V is the total inner volume of arc tube and T stands for gas temperature for any volume element. To get the effective value of the temperature for any volume element the temperature should be known. For long cylindrical arc tubes such as high pressure sodium lamps, or some metal halide lamps with cylindrical arc tubes, the temperature distribution along the cylinder axis is fairly constant, the radial distribution may be considered as parabolic or cosine. A calculation of effective temperature for a cylindrical arc tube assuming the arc temperature of 4000 K and wall temperature of 1500 K with a parabolic radial distribution results in an effective temperature of $\bar{T} = 2750 K$ (Witting, 1978).

There are some difficulties regarding the concept of effective sound velocity. Firstly, it is difficult to determine the effective temperature as an average value over temperature profile of discharge in HID lamps (Keijser, 2005). Secondly it is experimentally shown that the effective sound velocity for longitudinal acoustic modes should be different from that for radial-azimuthal modes to obtain a good fit between experimental results and calculation. As an example for the longitudinal resonances in the 250W HPS lamp a velocity of 450 ms^{-1} should be taken and for the radial-azimuthal resonances 500 ms^{-1} (de Groot and van Vliet, 1986). The reason could be the different temperature profiles along the axial and the radial axes. HPS lamps have a long cylindrical arc tube therefore; their axial temperature profile is relatively constant along whole longitudinal axis. In spite of that, the temperature profile of HPS lamps along the radial axis is subject to dramatic changes from centre to the wall. Hence a unique sound velocity for both cases can not be assumed.

Witting showed that the velocity of 500 ms^{-1} for the first longitudinal resonance would yield frequencies that are 20% below the experimental data (for 150, 250 and 400W sodium lamps). Good agreements were obtained with effective sound velocity of 590 ms^{-1} (Witting, 1978). This is not in accordance with (de Groot and van Vliet, 1986) in which a lower sound velocity for longitudinal resonances is suggested.

As a general rule the actual temperature distribution of an HID lamp shows a great difference between inner wall temperature and the discharge temperature. The former is about 1100-1200 K and the latter in the range of 5000-6000 K. It is likely that if the discharge occupies only a small fraction of the total volume of the arc tube, for instance Xenon compact arc lamps, the concept of effective sound velocity gives better results. Contrarily for low wattage metal halide lamps with a relatively small arc vessel the temperature profile shows a great difference in different locations inside the arc tube. Davenport and Petti have shown that the speed of sound in a discharge lamp (low wattage metal halide) may vary by a factor of 2.2 from core (discharge) to wall (Davenport and Petti, 1985).

3.3.6 Numerical Solution

The analytical method which is formerly discussed would be applicable to simple geometries such as cylindrical arc tube with an isothermal gaseous medium. For more complicated geometries especially when the possible effect of electrodes is of interest, the analytical solution is not possible. The problem will be more complex when the temperature profile of the filling gas is desired to be considered. A good alternative is using numerical methods to solve the wave equation inside the arc tube with proper boundary conditions. Davenport and Petti introduced a numerical method using finite element method (FEM) to calculate acoustic frequencies and mode shapes for the gas in small high intensity discharge lamps (Davenport and Petti, 1985). In this section a numerical solution for AR phenomenon in HID lamps based on the work of Davenport and Petti is given. The following proposed method uses Partial Differential Equation (PDE) toolbox of MATLAB to solve the wave equation in the arc tube. Regarding (Davenport and Petti, 1985), we assume that the arc tube geometry is symmetrical around the z axis which means the local pressure oscillation has a form of

$$\delta p(r, \phi, z, t) = [\delta p(r, z) \cos(l\phi)] \cos(\omega t) \quad (3.15)$$

With this assumption we can solve the problem in two dimensional (r,z) to find the longitudinal and/or radial resonances. The azimuthal resonance as a result of axial symmetry of the arc

tube geometry is already known. Because any cross section of the arc tube perpendicular to the z axis is a circle the azimuthal resonance is considered to be $\cos(l\phi)$. Substituting (3.15) in (3.4) we get

$$\nabla^2\{\delta p(r, z) \cos(l\phi)\} \cos(\omega t) = -\frac{\omega^2}{c_{eff}^2} [\delta p(r, z) \cos(l\phi)] \cos(\omega t)$$

finally the eigenvalue problem to be solved will be

$$\nabla^2\{\delta p(r, z)\} = -\frac{\omega^2}{c_{eff}^2} [\delta p(r, z)] \quad (3.16)$$

The partial differential equation with the standard form of

$$-div\{c \cdot grad(u)\} + a \cdot u = \lambda \cdot d \cdot u \quad (3.17)$$

can be solved in 2D using PDE toolbox of MATLAB. In equation (3.17) c , a and d are coefficients of equation, u denotes the scalar field (to be found) and λ stands for the eigenvalue in any resonance mode.

By substituting $c = 1$, $a = 0$, $d = (c_{eff})^{-2}$, $\lambda = \omega^2$ and $u = \delta p$ equations (3.16) and (3.17) will be identical and the problem of acoustic resonance is soluble by PDE toolbox.

3.3.7 Arc Tube's Geometry

As it is mentioned the differential equation should be solved inside the arc tube. In reality the arc tube concerning the electrodes has a complex geometry. Using appropriate digitizing software (*Engauge Digitizer Ver. 2.12, Mark Mitchell, 2002*) the exact geometry of the arc tube is electronically digitized. The values are converted in a proper format and loaded in PDE toolbox. Geometry of the arc tube plays a significant role in AR phenomenon and in determination of AR frequencies. The advantage of this method is that the exact geometry of the arc tube without any simplifications can be used for the calculations. Fig. 3.2 illustrates an example of the real geometry of an OSRAM HCI T 70W ShopLight Lamp.

3.3.8 Calculation of Eigenfrequencies

Theoretically there are infinite number of eigenfrequencies and acoustic modes for any given geometry. The desired bracket of eigenvalues to be calculated can be determined before solving the partial differential equation problem. All eigenvalues inside the predefined bracket are determined when the PDE is solved. The eigenfrequency for any acoustic mode can be calculated as follows

$$f = \frac{1}{2\pi} (\lambda_i)^{\frac{1}{2}} \quad (3.18)$$

with λ_i as eigenvalue of the i^{th} eigenmode.

3.3.9 Concerning Temperature Distribution

If the temperature distribution in the arc tube is known, the corresponding sound velocity can be calculated using (3.13).

It should be noted that the coefficient d , which is used in definition of PDE equation can be defined as a constant or as a row vector of representing values at the triangle centers of mass. Using this property, the concept of local sound propagation velocity can be realized. We calculate the sound velocity for every small area (every triangle in FEM mesh) in the arc tube. This way, d will be a row vector defining the local sound velocity as a function of the position inside the arc tube.

3.3.10 Example of an AR Calculation

In this section an example of whole procedure of AR calculations for a lamp is presented. In the first step the geometry of the inner side of the arc tube of the lamp of interest is digitized. The selected lamp is an OSRAM HCI-T 70W Shoplight. After loading the data related to the geometry of the lamp a triangle mesh is generated to enable further numerical calculations in FEM. It should be noted that due to axisymmetrical shape of the arc tube just half of its longitudinal cross section should be considered. This way the effect of actual shape of the arc tube, concerning electrode shape and size and the distance between electrodes, can be considered. In order to be able to investigate the effect of the temperature in the arc tube, we need to define a temperature distribution inside the arc tube, as long as the actual temperature distribution is not known. To fulfil this idea, at first we solve the heat transfer partial differential equation inside the arc tube. To do this we select a region of the arc tube as the arc position. The initial temperature of this area is set to 10,000 K and all other positions are considered to have an initial temperature of 1000 K. These values of temperatures are considered as the heat source in PDE and are set empirically. Selection of governing equations for heat transfer is not critical, since the aim of this calculation is to introduce a method which accounts for temperature distribution in resonance frequency calculations. As a task of simplicity the elliptical form is selected.

$$-div(k \cdot grad(T)) = Q + h(T_{ext} - T) \quad (3.19)$$

where k is coefficient of heat conduction, Q stands for heat source, h is convective heat transfer coefficient, T_{ext} is external temperature and T is the temperature to be calculated. We solve the PDE of heat transfer when $k = 1$, $Q = 10,000$ in position of the discharge, $Q = 1000$ in other positions inside the arc tube, $h = 1$ and $T_{ext} = 200 K$. We apply the Neuman boundary conditions with heat flux and heat transfer coefficient equal to zero, which vanishes the temperature gradient on inner surfaces of arc tube. It should be noted that calculating the exact temperature distribution inside the arc tube is quite complicated and is out of scope of this work. The aim of these temperature calculations is to have an approximation of temperature distribution to show its effect on acoustic resonance phenomenon. According to (Adler, 2000) typically arc core temperatures reach about 6000 K, the vessel wall temperatures are around 1000 K and electrode tip temperatures reach values of 2000-3000 K. Temperature distribution which is calculated under above mentioned conditions is illustrated in Fig. 3.3. The temperature distribution resembles a vertically operated lamp. The temperature of the discharge has the maximum value of about 5500 K which gradually decreases toward the arc tube's wall and the

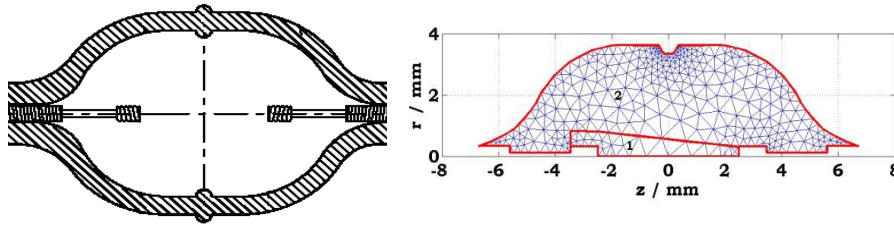


Figure 3.2: Left: Sketch of the arc tube of an OSRAM HCI T 70W ShopLight. The exact geometry of the arc tube then can be captured using a digitizing software and knowing dimensions of the arc tube. Right: Geometry of the arc tube after digitization and generation of FEM triangular mesh. There are two recognizable segments in the whole area. The first segment (1) which is located near to the electrodes is used to resemble high temperature of the discharge and the other segment (2) is used as the area with lower temperature.

wall temperature at cold spot is about 1200 K. This temperature distribution shows a good fit regarding (Adler, 2000). It should be noted that the plasma temperature in front of cathode is more than other parts (hot spot). A model based calculation of temperature profile of a Xe-lamp (Flesch and Neiger, 1999) shows that in front of the cathode the temperature drops from 8300 K to 2800 K within a distance of $120 \mu m$. As long as this hot spot occupies a very small area in arc tube its effect on sound velocity is negligible. Solving the equation of heat transfer gives the temperature values for all nodes of FEM mesh.

By averaging the temperature values of three nodes of any FEM mesh triangle, the temperature values at the triangles centers of mass are calculated. Having the temperature values for all triangles and using equation (3.13) the sound velocity distribution then is calculated. As a task of simplicity, for sound velocity calculation it is considered that the propagation medium is pure mercury gas hence the parameters used in (3.13) are $\gamma = 7/5$, $R = 8.31 J \cdot K^{-1} \cdot mol^{-1}$, $m = 0.2 kg \cdot mol^{-1}$. Fig. 3.4 shows the distribution of the sound propagation velocity corresponding to the calculated temperature distribution. Extreme changes of sound velocity with respect to the temperature distribution in the arc tube can be seen with this calculation. Now we are ready to solve the eigenmode problem inside the arc tube with known sound velocity for any triangle of FEM mesh. These values are substituted in the eigenmode partial differential equation as a row vector of coefficients which is mentioned as \mathbf{d} .

As it is mentioned in previous sections, an approximation of the effective sound propagation velocity inside the arc tube is $450\text{-}500 \text{ ms}^{-1}$ for HPS lamps (de Groot and van Vliet, 1986). This value for the small metal halide lamps varies in range of $276\text{-}617 \text{ ms}^{-1}$ (Davenport and Petti, 1985). Considering these values we assume that the effective sound propagation velocity inside the arc tube is 500 ms^{-1} . This sound velocity can be calculated for a constant temperature of 3600 K inside the arc tube when the filling gas is pure mercury. Substituting this value of sound velocity in $d = c^{-2}$ as a coefficient of the eigenmodes equation, results in very small coefficients. This may lead to some difficulties in further calculations. To avoid this problem we use the normalized sound propagation velocity distribution with respect to the effective value of sound velocity (500 ms^{-1}). Therefore \mathbf{d} will be a vector with values of $d_i = (c_i/500)^{-2}$ where c_i denotes the sound velocity in i^{th} triangle. The problem of eigenmodes then is solved with these modified values of d_i . For any eigenmode an eigenvalue will be found which satisfies the partial differential equation. Eigenvalues determine the eigenfrequencies at which acoustic resonances can be excited and these are what we are looking for. To get the correct value of

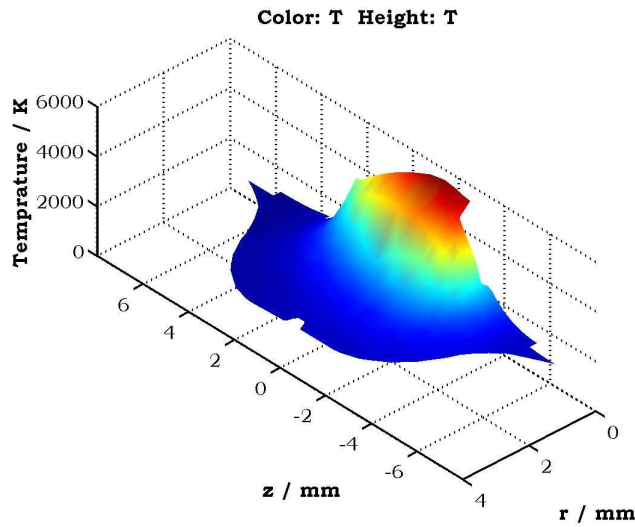


Figure 3.3: Temperature distribution inside the arc tube which is calculated considering an elliptical heat transferring situation.

eigenfrequencies two compensations should be carried out. Firstly we change the unit of the sound velocity from ms^{-1} to $mm \cdot s^{-1}$ which is the same as the dimension of the arc tube geometry.

Furthermore the effect of sound velocity normalization should be recovered as well. As the square of the sound velocity is appeared in our equation all eigenvalues should be multiplied by a correction factor of 2.5×10^{11} . Afterwards the resonance frequencies are calculated using (3.17). To apply the boundary conditions mentioned in (3.5) the Neuman boundary condition with the form of

$$n \cdot c \cdot grad(\delta p) + q \cdot (\delta p) = g \quad (3.20)$$

is used. Considering δp as the local pressure (scalar field parameter of the PDE), $q = g = 0$, and $n = c = 1$, guaranties that the gradient of the pressure perpendicular to the arc tube's wall is zero. This implies that the normal component of the linear acoustic velocity (with respect to the boundary surface) of the filling material in the vicinity of the boundaries is zero. This is applicable for all boundaries including electrodes and arc tube's wall. Along the boundary line between the electrode tips (center line of the arc tube) there is no pressure or velocity limitation, as long as this line is not a real boundary. For this line the Dirichlet boundary condition is considered.

$$h \cdot (\delta p) = r \quad (3.21)$$

Assuming $h = r = 0$, leads to elimination of any boundary limitation along the arc tube's center line. This means δp can get any value along the center line without any condition.

We solve the eigenmodes problem inside the arc tube for two conditions. Firstly, we assume the concept of the effective sound propagation velocity, and afterwards, with considering the temperature distribution inside the arc tube. The results of these calculations are illustrated in Table 3.1. As it can be seen in this table the first 30 eigenmodes for given geometry is calculated. Normalized eigenvalues for each case and for any eigenmode is calculated. The great difference

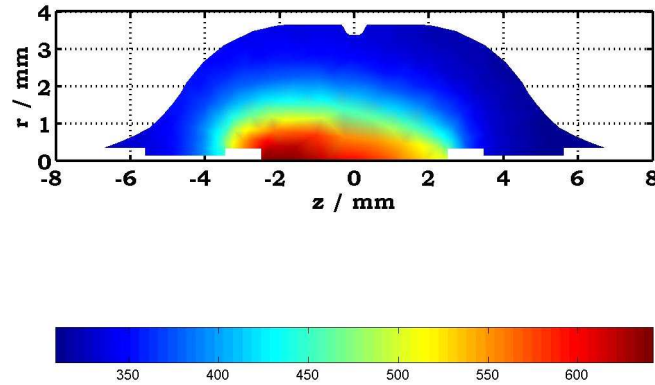


Figure 3.4: Calculated sound velocity distribution inside the arc tube considering temperature distribution of Fig. 3.3 and a pure mercury vapor gas medium for sound propagation. As it can be seen the sound propagation velocity increases with temperature.

between eigenvalues and calculated corresponding eigenfrequencies for constant effective sound velocity versus distributed sound velocity is obvious. As an example the first resonant frequency for a constant sound velocity of 500 ms^{-1} is 26.407 kHz while this value for a distributed sound velocity is 18.753 kHz. The local acoustic pressure for this resonant frequency which indicates the first longitudinal acoustic mode is illustrated in Fig. 3.5. This figure shows the acoustic mode with distributed sound velocity inside the arc tube. It should be noted that although the values of frequencies are significantly different, in both cases the local pressure distributions are quite similar with respect to their shape. This means that at this acoustic mode, a significant change of sound propagation velocity does not have any noticeable effect on resonant shape. As it can be seen in the middle of the arc tube, the acoustic pressure is always zero. At one end the amplitude of acoustic pressure is positive and at the other end is negative. Regarding (3.15) acoustic pressure has a time varying coefficient with a frequency equal to its resonant frequency. As a result the acoustic pressure which is illustrated in Fig. 3.5 changes periodically and both end experience positive and negative acoustic pressure. This means when the first longitudinal acoustic mode is excited the local pressure of the gas in the arc tube changes periodically in such a way that when at one end the pressure is increased at the other end of arc tube the pressure is decreased. The second longitudinal mode is illustrated in Fig. 3.6. As it is expected in this mode at the same time both arc tube's ends have a positive or negative acoustic pressure. The pressure of the middle area of the arc tube has always the opposite sign. A remarkable point about this mode is that the amplitude of the acoustic pressure at arc tube's end is higher than that of middle area. The third longitudinal acoustic mode is illustrated in Fig. 3.7. Such as the first longitudinal mode arc tube's ends have acoustic pressure with opposite amplitudes. It should be note that this mode is not a pure longitudinal mode and it can be seen that the pressure distribution has a downward tendency from arc tube's wall toward the lamp center line along one pressure anti-node and in the opposite direction along the other pressure anti-node. This shows that there are some effects of radial mode as well in this acoustic mode although

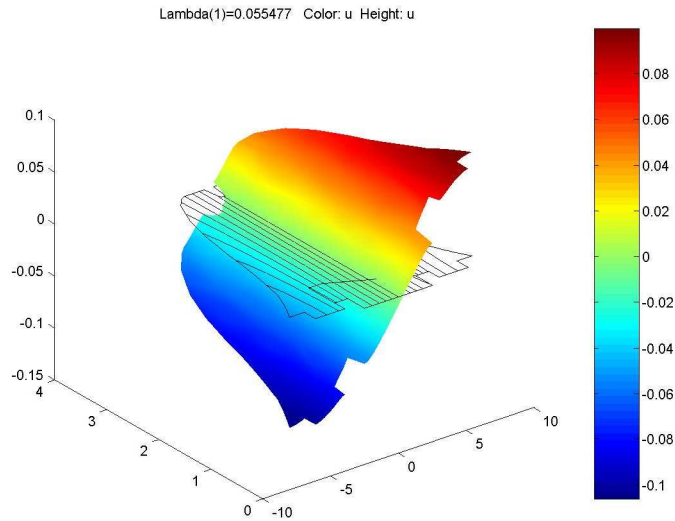


Figure 3.5: The first longitudinal acoustic mode considering sound velocity distribution of Fig. 3.4

the dominant mode is the longitudinal mode. This effect which is recognizable in the second mode as well is a result of non-constant sound velocity distribution along the radial axis.

This effect leads to a higher amplitude of acoustic pressure in the vicinity of the arc tubes wall and a lower amplitude in position of the discharge. As it is shown in Fig. 3.8 the effect of distributed temperature and the sound velocity is recognizable in the fourth longitudinal acoustic mode as well. The higher pressure amplitude at both ends of arc tube at which the temperature and the sound velocity are lower, in comparison to the area between two electrodes with higher temperature and sound velocity is obvious. The first radial acoustic mode appears together with the second longitudinal mode together. This mode corresponds to the fifth eigenmode of acoustic calculations when the temperature distribution is considered. This eigenmode is illustrated in Fig. 3.9, as it can be seen acoustic pressure changes along both radial and longitudinal axes.

Regarding Fig. 3.2 which gives the geometry of the arc tube, the aspect ratio can be considered about 14 mm: 7 mm (IL:ID). IL stands for inner length and ID is the inner diameter of the arc tube. From Fig. 3.5 it is understood that the first longitudinal mode has a pressure wavelength of 2 times Inner Length⁷. In contrast to the first longitudinal, the wavelength of first radial acoustic mode should be ID. This is due to the axisymmetrical condition with respect to the radial resonant mode. As a result the wavelength of the first radial resonant mode is 7 mm. This is comparable with the wavelength of the fourth longitudinal resonant mode which is $\frac{1}{2}$ IL or 7 mm. This property can be seen in Fig. 3.10 for a case of constant gas temperature and sound velocity propagation. The fourth longitudinal resonant mode can be seen clearly in the middle of the arc tube and along the longitudinal axis. At the same time the first radial mode is also recognizable along the radial axis.

It is worth to recall that the first radial mode occurs in the fourth resonant mode when the sound velocity is constant. That is the resonant frequency of 73.6 kHz, however this

⁷Wavelength of longitudinal resonant modes are: $2IL$, IL , $\frac{2}{3}IL$, $\frac{1}{2}IL$, $\frac{2}{5}IL$, $\frac{1}{3}IL$, ... with IL as the inner length of the arc tube

Eigenmode	Effective Sound Velocity 500 ms^{-1}		Distributed Sound Velocity $300 - 650 \text{ ms}^{-1}$	
	λ	f / kHz	λ	f/kHz
1	0.11001	26.407	0.055477	18.753
2	0.34556	46.803	0.17274	33.09
3	0.62113	62.748	0.29858	43.505
4	0.85517	73.627	0.5059	56.629
5	1.0778	82.656	0.61671	62.525
6	1.2738	89.86	0.71951	67.535
7	1.5362	98.68	0.94831	77.533
8	2.009	112.85	0.98435	78.993
9	2.2426	119.23	1.2455	88.854
10	2.5249	126.51	1.3812	93.569
11	3.1922	142.25	1.6446	102.1
12	3.2684	143.94	1.7664	105.82
13	3.4695	148.3	2.0413	113.75
14	3.8487	156.19	2.1922	117.88
15	4.0753	160.73	2.266	119.85
16	4.2228	163.61	2.4903	125.64
17	4.8302	174.98	2.6725	130.16
18	5.1723	181.07	2.7527	132.1
19	5.3566	184.27	2.9855	137.57
20	5.8089	191.89	3.2487	143.5
21	6.471	202.53	3.5208	149.39
22	6.5636	203.98	3.6362	151.82
23	7.2123	213.82	3.822	155.65
24	7.8075	222.47	4.2075	163.31
25	7.8363	222.88	4.466	168.25
26	8.2387	228.53	4.5998	170.76
27	8.4758	231.79	4.9235	176.66
28	8.5211	232.41	4.952	177.17
29	9.2623	242.31	5.2384	182.23
30	9.9259	250.84	5.4364	185.64

Table 3.1: Calculation of acoustic resonance eigenvalues frequencies for a given arc tubes geometry. The first column shows the eigenmode for each resonance. Second and fourth columns are normalized eigenvalues for sound velocity of 1 mms^{-1} . The third and the fifth columns are corresponding resonance frequencies for effective sound propagation velocity of 500 ms^{-1} and for distributed sound velocity respectively.

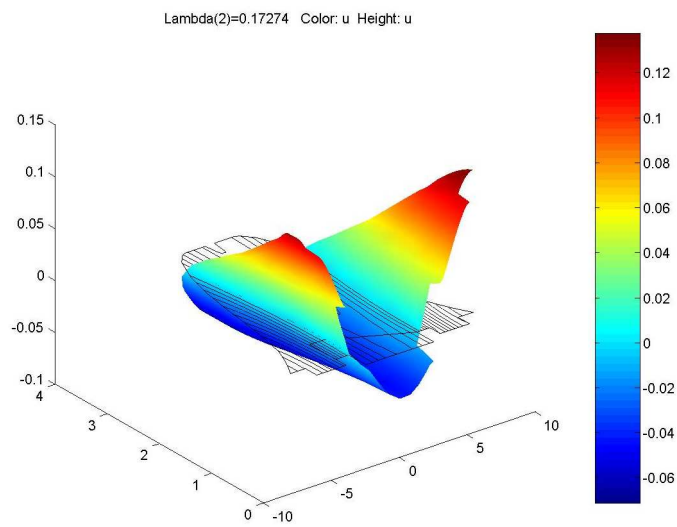


Figure 3.6: The second longitudinal acoustic mode considering sound velocity distribution of Fig. 3.4

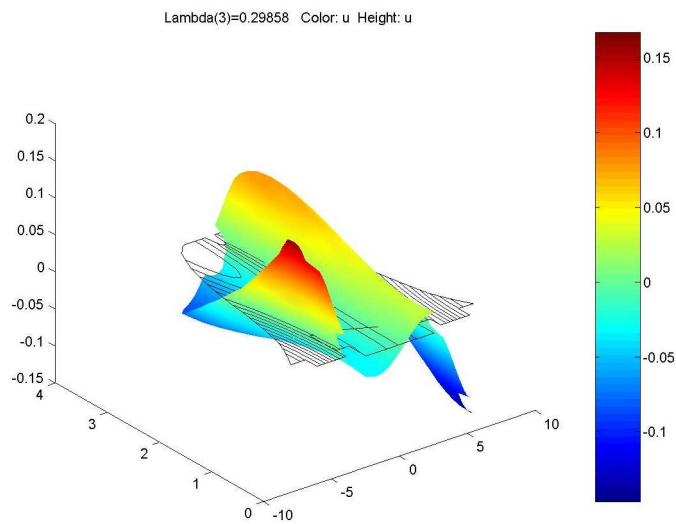


Figure 3.7: The third longitudinal acoustic mode considering sound velocity distribution of Fig. 3.4

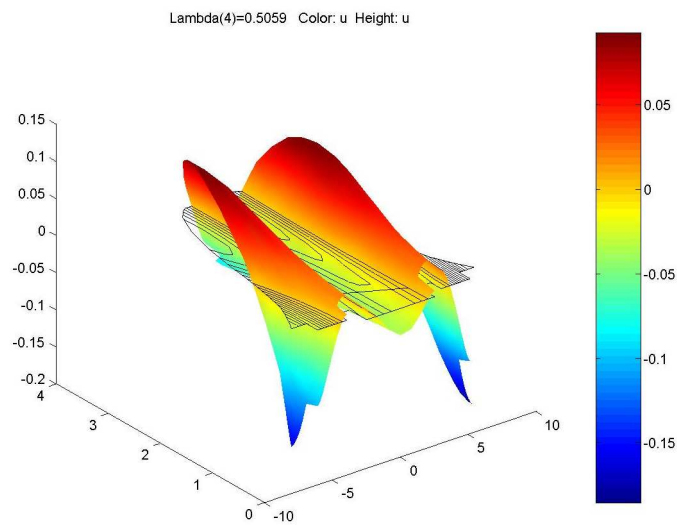


Figure 3.8: The fourth longitudinal acoustic mode considering sound velocity distribution of Fig. 3.4

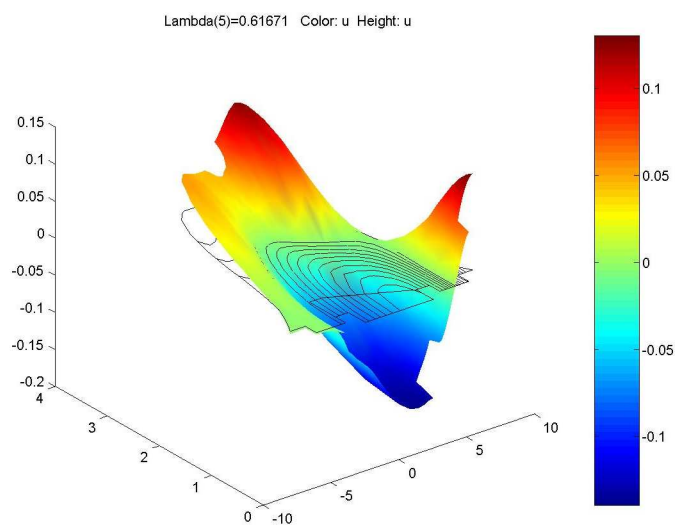


Figure 3.9: The first radial and the second longitudinal acoustic mode considering sound velocity distribution of Fig. 3.4

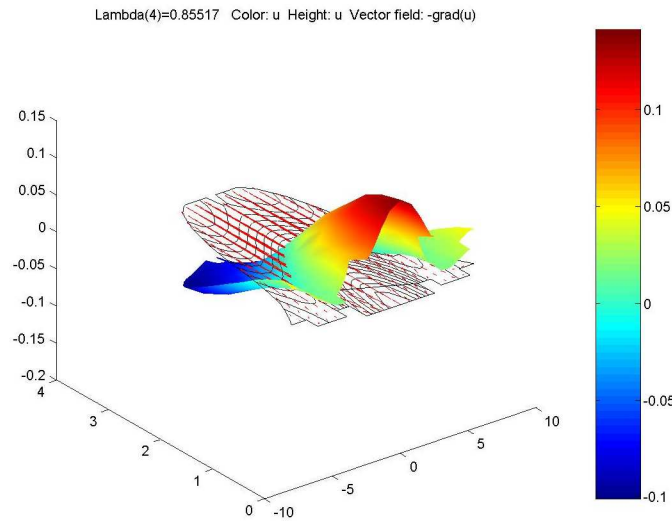


Figure 3.10: The first radial and the fourth longitudinal acoustic mode considering constant sound velocity distribution inside the arc tube.

mode appears in the fifth resonant mode under the condition of the sound velocity distribution consideration with the frequency of 62.52 kHz. To investigate the effect of the temperature distribution inside the arc tube whole eigenvalues which are located inside the bracket of [0-15] are calculated. With effective sound velocity there are 43 eigenvalues inside the given bracket, while considering the temperature distribution leads to finding more resonant modes inside the same bracket. As it is sketched in the graph of Fig. 3.11 there are 66 different eigenmodes when the sound velocity distribution has been considered.

Corresponding resonant frequencies for a constant effective velocity of 500 ms^{-1} and also for a distributed velocity as discussed formerly is sketched in Fig. 3.12. A reduction of whole resonant frequencies in the same acoustic eigenmodes and also a significant increase of the number of eigenmodes in the same frequency bandwidth appear when the temperature distribution is considered.

To evaluate the effect of the different effective sound velocities for a unique arc tube, the calculation of the resonant frequencies is carried out for three different effective sound velocities of 400, 450 and 500 ms^{-1} . As it was expected increasing the sound velocity propagation increases the resonant frequencies, which is shown in Fig. 3.13. There is linear relationship between sound velocity and the resonant frequency which is a result of normalization of the velocity which is explained previously. For this reason the effect of the sound velocity deviations especially for higher resonant frequencies is more significant. As long as the resonant frequencies are changed with the same percentage that sound velocity is changed.

3.3.11 Importance of Acoustic Modes

For any calculated acoustic mode, the oscillating component of the instant local pressure of the filling gas for any position is given. In some acoustic modes, approximately the whole region of arc tube's cross section is occupied either with positive or negative pressure and the portion for zero or near zero pressure is low. In contrast, there are some acoustic modes in which a

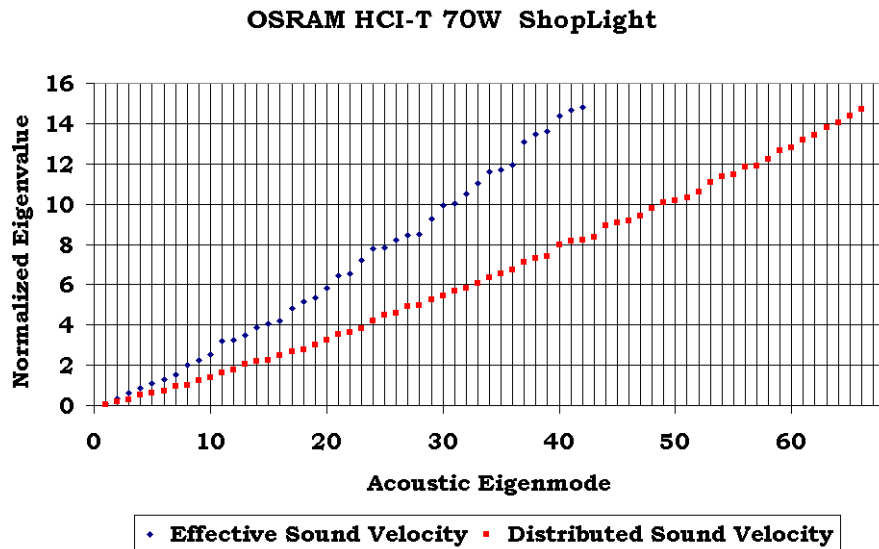


Figure 3.11: Normalized eigenvalues in the bracket of [0-15] for both cases of effective sound velocity and distributed sound velocity in a lamp arc tube.

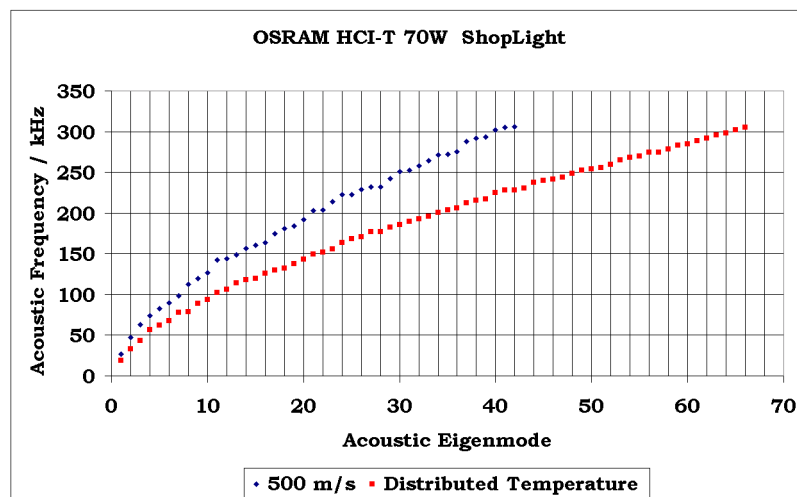


Figure 3.12: Calculated resonant frequencies for two cases of effective sound velocity of 500 m/s and distributed velocity as it is illustrated in Fig. 3.4

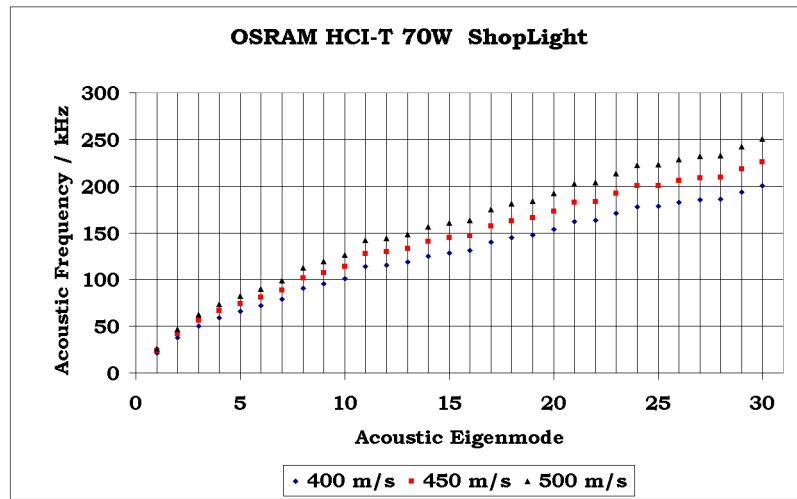


Figure 3.13: Comparison of the resonant frequencies for three different effective sound velocities in the arc tube.

significant region of the cross section has near zero pressure. In the first group it is expected that the effect of the acoustic mode in destabilizing the discharge is greater than the second group. Especially, when the area with the lower amplitude of the pressure oscillation is located in the middle of the cross section where the position of the discharge is.

As an example comparing the 18th acoustic mode which is illustrated in Fig. 3.14 with the fourth acoustic resonance of Fig. 3.8, shows the differences. It should be noted that for higher frequencies this difference is more significant. To be able to determine the importance of any acoustic mode based on above mentioned concept, any acoustic mode should be quantified. To do this we simply multiply the absolute value of the pressure amplitude by its corresponding triangle area and sum up all calculated values. By dividing the result by the area of the cross section we get an average value for the whole area. The result shows how strong the corresponding acoustic mode is and gives a quantity to compare different acoustic modes for any lamp. This value is called eigenmode's level to indicate the level of contribution of any acoustic mode in acoustic instability. From Fig. 3.15 it is understood that the effect of higher frequencies is lower than the lower frequencies. This is in a good agreement with experiment and besides the damping effect in higher frequencies, explains the reason of the lower sensitivity of HID lamps to the higher frequencies.

The other reason for this phenomenon can be explained as follows. According to Fig. 3.14, acoustic modes of higher orders contains many local positive and negative peaks (pressure nodes) which are distributed within the whole area of the cross section of the arc tube. As a result there are many local, hence, small size acoustic streaming pathes. Such local streams of filling material are not supposed to get sufficient energy to be able to affect the discharge of the lamp. Because acoustic instability requires the establishment of coherent streams with sufficient energy. As an example for comparison between higher and lower acoustic modes one can refer to Fig. 3.5 as the first acoustic mode which has only one positive and one negative local pressure. In this case stream pathes are large and many atoms and molecules can flow together and strike the discharge path.

As it is pointed out, applying the sound velocity as a function of the temperature distribution in AR calculations leads to a significant change of different resonant frequencies. This effect

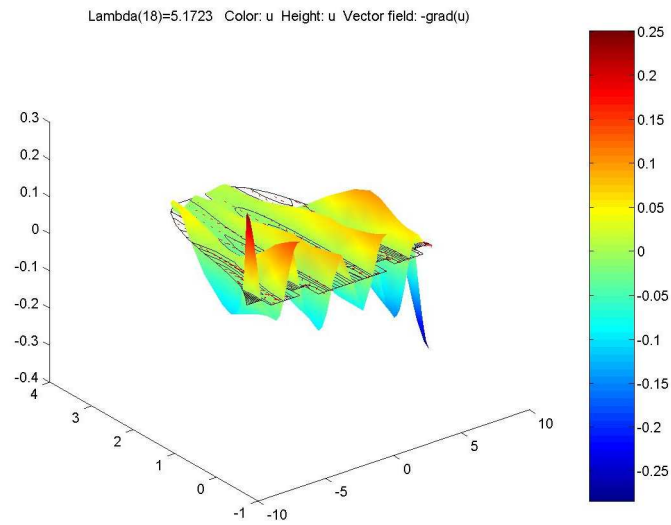


Figure 3.14: The 18th acoustic mode considering the constant effective sound velocity of 500 m s^{-1} .

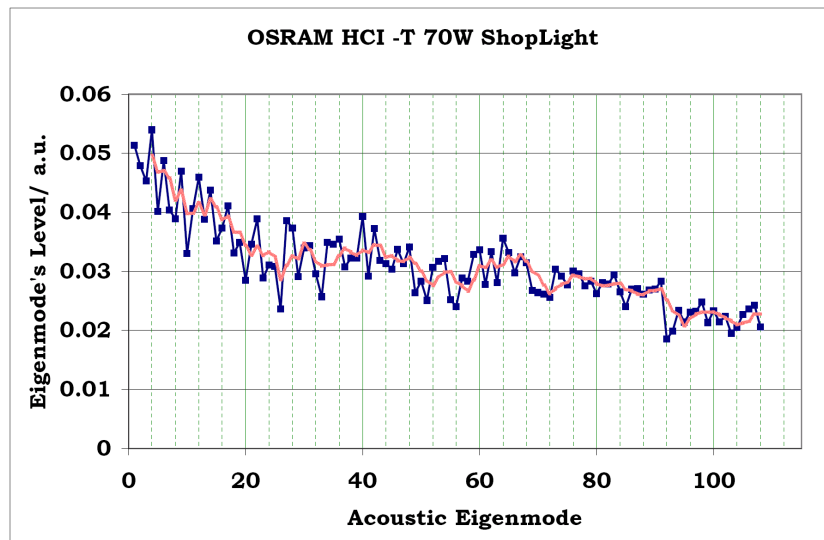


Figure 3.15: Eigenmode's level shows the importance of each eigenfrequency with respect to its potential power to excite acoustic instability. The curve between points is a smoothed moving average of order 4.

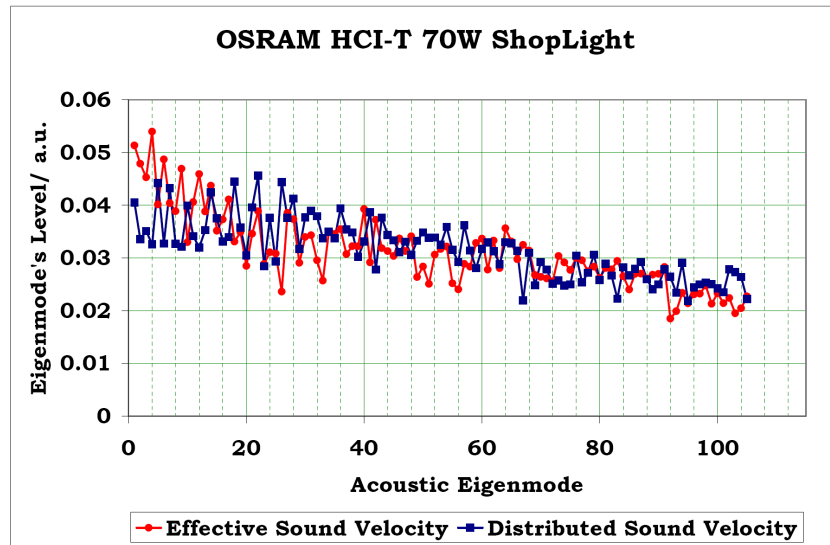


Figure 3.16: Comparison of eigenmode's level for effective sound velocity and distributed sound velocity of Fig. 3.4

can be seen by calculating the eigenmode's level, as it is illustrated in Fig. 3.16. As an example compare the 18th resonant mode for both cases. These two modes are shown in Fig. 3.14 and Fig. 3.17.

According to (de Groot and van Vliet, 1986) by increasing the frequency, the spectrum of resonant frequencies approaches a continuum, while at low frequencies the resonant frequencies are more widely spread. From Fig. 3.12 it is understood that increasing the frequency of the resonant modes leads to reduction of the difference between adjacent frequencies. In other words this means that density of acoustic resonances increases with higher frequencies. Fig. 3.18 sketches the difference between two adjacent resonant frequencies versus the number of eigenmode.

The result is in agreement with (de Groot and van Vliet, 1986) which is based on analytical solution of the wave equation in a cylindrical arc tube.

It is quite important to note that the effect of damping of acoustic resonances, Γ , is not included in the above discussion. This factor was considered to be zero (as a task of simplicity) in mentioned numerical calculation. As it is shown in (3.3) the amplitude of the local pressure fluctuations, δp , is inversely proportional to the damping coefficient, Γ . It was pointed out that increasing the frequency leads to an increase of this coefficient. Hence, at higher frequency regions the damping coefficient of acoustic resonances suppresses the actual effect of acoustic mode. However, a potential question is that at higher frequencies the value of viscosity increases, this leads to a higher damping coefficient which is responsible to convert the acoustic energy into the momentum of the filling material. It seems that this process may lead to a stronger effect of resonances at higher frequencies. The answer is: conversion of acoustic energy into the momentum of particles is the necessary but not the sufficient condition of excitation of acoustic instabilities. Since at higher frequencies (as is discussed formerly) streaming loops are small and distributed over the whole area of the arc tube, a lack of synergy leads to a significantly weaker effect on the discharge.

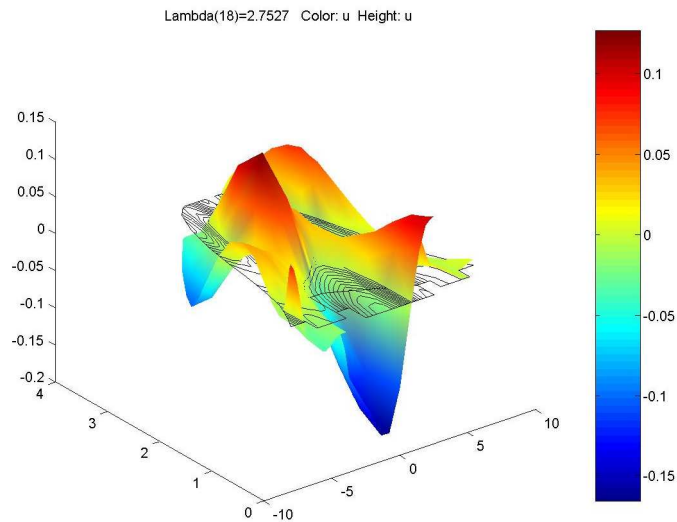


Figure 3.17: The 18th acoustic mode considering the sound velocity distribution of Fig. 3.4

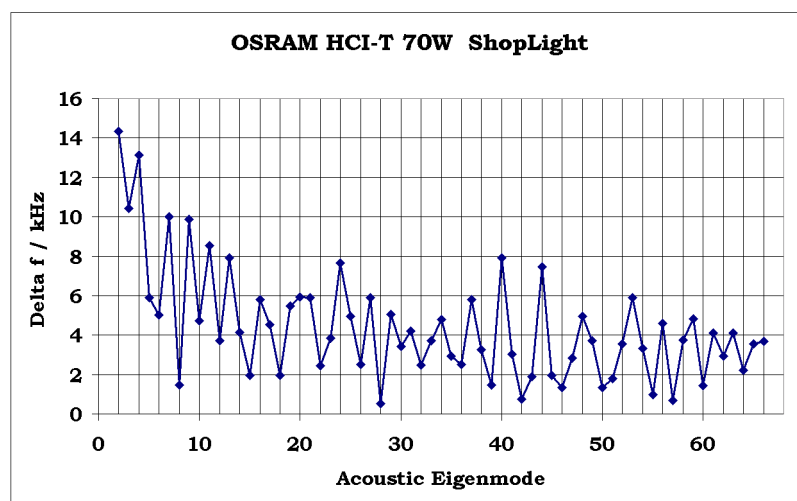


Figure 3.18: The difference between two adjacent acoustic resonant frequency decreases for higher resonant frequencies.

3.3.12 Calculation of Acoustic Streaming

There are two methods to capture the acoustic streaming velocity. The first method uses perturbation expansion technique to linearize the problem and hires the linear acoustic velocity as the force function of the non-linear acoustic streaming. The more straightforward method is solving the compressible Navier-Stokes equations in the geometry of interest (Boluriaan and Morris, 2003). The partial differential equations which govern the acoustic streaming in the arc tube of HID lamps are quite complex and there are many unknown parameters which make the problem more complex. By solving the wave equation inside the arc tube it is not possible to capture the acoustic streaming. However, such kinds of calculations lead us to get some important information about acoustic streaming. We can get the amplitude of the linear acoustic velocity and the velocity node locations, and estimate the location and magnitude of the streaming velocity. Such information are quite useful to understand and estimate the effect of acoustic resonances on discharge and excitation of acoustic instabilities in lamp's arc tube.

3.4 Acoustic Resonance and Acoustic Streaming in a Cylindrical Arc Tube

According to the theory of acoustic streaming standing pressure waves in a closed vessel can establish the acoustic streaming (Rayleigh streaming). In this section we compare the analytical solutions of the first longitudinal acoustic resonance and acoustic streaming in a closed cylindrical tube. The cylindrical tube resembles arc tube of an HID lamp and at the same time gives the possibility of the analytical solution of differential equations governing acoustic resonance and acoustic streaming. Assuming the first longitudinal acoustic mode in equation (3.11) means, $l=m=0$ and $n=1$, $\alpha_{00} = 0$ which leads to $\omega_r = 0$ and $J_0(0) = 1$. Hence, for this acoustic mode the local pressure is then calculated as

$$\delta p = A_{001} \cos\left(\frac{\pi}{L}z\right) \cos\left(\frac{\pi c}{L}t\right) \quad (3.22)$$

The linear acoustic velocity as the gradient of the local pressure can be calculated as

$$v_1 \propto \sin\left(\frac{\pi}{L}z\right) \cos\left(\frac{\pi c}{L}t\right) \quad (3.23)$$

The driving force (F_j) of streaming motion (in tensor notation) that depends on the linear acoustic field is (Lighthill, 1978)

$$F_j = -\frac{\partial \overline{\rho u_i u_j}}{\partial x_i} \quad (3.24)$$

Where ρ stands for the density of the medium and $\overline{u_i}$ and $\overline{u_j}$ are the time averaged linear acoustic velocity tensors. As a result, in order to be able to calculate the driving force of acoustic streaming two components of linear acoustic velocity is required⁸. The first component is v_1 but assuming a pure longitudinal linear acoustic motion as it is considered in (3.22) makes the second component equal to zero. In fact this is not the actual case. Existence of a strong radial temperature gradient in the tube, and also because of the boundary layer near the walls

⁸"In a standard perturbation approach to the second order, the mean density, ρ_0 and linear order acoustic velocities must be used to construct the driving force F_j ", (Boluriaan and Morris, 2003)

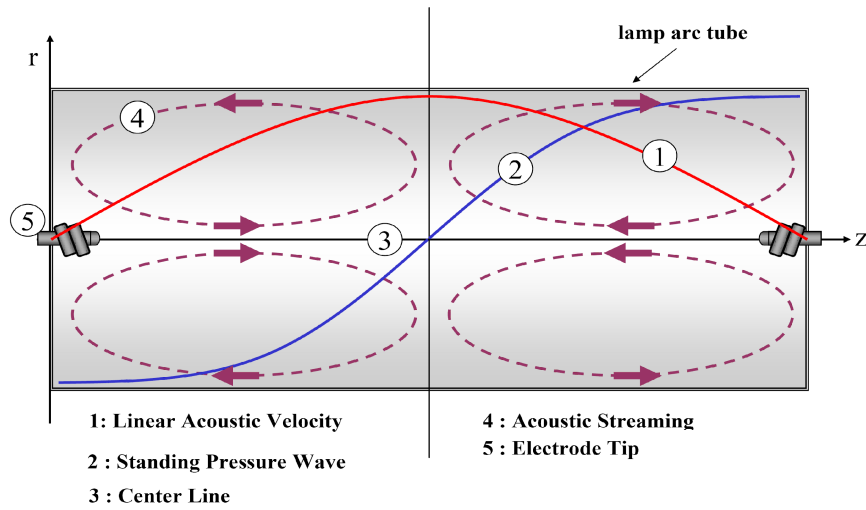


Figure 3.19: Schematic diagram of a cylindrical arc tube when the first longitudinal acoustic mode is excited. The diagram shows the standing local pressure wave, its corresponding linear acoustic velocity, the position and direction of the acoustic streaming.

where the velocity of the motion of the medium drops from the value in the sonic wave on the axis of the tube, an inhomogeneity of the acoustic field develops (Galechyan, 1995). Because of this inhomogeneity of the acoustic field the second component of the linear acoustic velocity is not zero and the vortex acoustic flow develops in the standing wave.

According to (Galechyan, 1995), "a linear acoustic flow can not actually affect the transfer process in the tube, whereas in the field of a standing sonic wave a nonlinear flow can make an appreciable contribution to transfer process but the size of inhomogeneities of acoustic field should be large." As it is mentioned previously, the nonlinear second order acoustic streaming velocity is responsible to introduce the transfer process in the arc tube.

Schuster and Matz⁹ (Schuster and Matz, 1940) treated the problem of acoustic streaming caused by standing waves in a tube (Kundt's tube) with radius R . They obtained the following profile for the streaming velocity outside the boundary layer (Boluriaan and Morris, 2003).

$$\frac{\bar{u}_2}{c_{eff}} = -\frac{3M^2}{8} \sin(2kz) \left[1 - 2\frac{r^2}{R^2} \right] \quad (3.25)$$

$$\frac{\bar{v}_2}{c_{eff}} = -\frac{3M^2}{8} kr \cos(2kz) \left[1 - \frac{r^2}{R^2} \right] \quad (3.26)$$

where \bar{u}_2 and \bar{v}_2 represent the longitudinal and radial projections of the streaming velocity in cylindrical coordinates ($r, \phi=\text{constant}, z$). M stands for Mach number, k is the acoustic wave number and c_{eff} is the sound velocity in the tube.

The streaming velocity is toward the linear acoustic velocity nodes along the boundary layer and in the opposite direction along the center line (Boluriaan and Morris, 2003). Position of

⁹The method of such classical calculations was introduced by Rayleigh (Rayleigh, 1883). "It is interesting to note that Rayleigh solution is independent of the fluid viscosity, although the driving force of Rayleigh streaming is nothing but a generation of a vortical structure inside a viscous boundary layer close to a solid object" (Boluriaan and Morris, 2003).

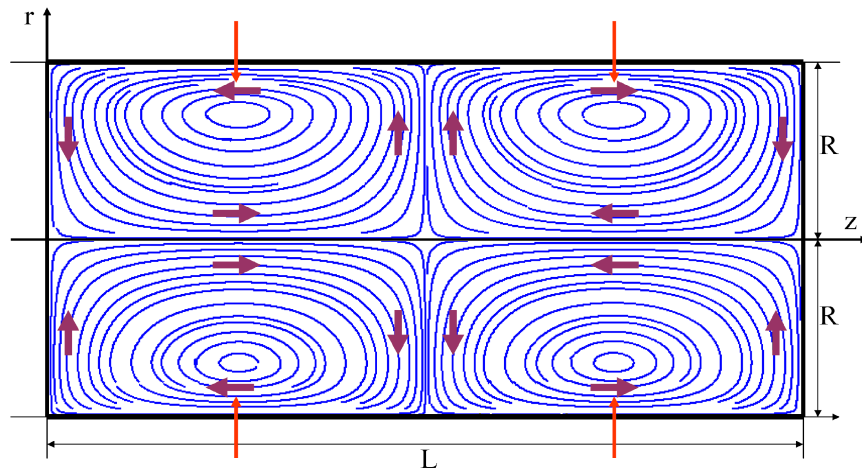


Figure 3.20: Streamline diagram of acoustic streaming velocity in a cylindrical (r , ϕ =constant, z) tube which is excited in the first longitudinal acoustic mode. Vertical arrows correspond to the positions of the maximum value of the acoustic streaming velocity.

the acoustic velocity node (N_v) and anti-node (A_v) for the upper right of the cylindrical arc tube are shown in Fig. 3.20. This motion forms a loop outside the boundary layer in which direction of the movement changes at $r/R = 0.707$. The local pressure wave, linear acoustic velocity and acoustic streaming loops for the first longitudinal acoustic mode are schematically sketched in Fig. 3.19. Regarding equations (3.25) and (3.26) there are four streaming loops inside the arc tube when the first longitudinal acoustic mode is excited. Fig. 3.20 illustrates the calculated streamlines of acoustic streaming velocity for the first longitudinal acoustic mode in a cylindrical arc tube. Along the z axis, acoustic streaming velocity reaches its maximum value at $z=L/4$ and $z=3L/4$ and along the radial direction in the vicinity of the arc tube's wall i.e. $r=R$. Thus, at these locations (which are marked with vertical arrows in Fig. 3.20), the local pressure of the filling material is decreased. Decrease of the pressure in some locations in the arc tube tends the filling material to move toward those locations to re-balance the pressure distribution. Therefore the discharge path moves toward the locations with lower local pressure as well.

3.5 Interference of Acoustic Streaming and the Discharge

Consider an HID lamp with a cylindrical arc tube which is operated in horizontal burning position and free of acoustic resonance. Due to the natural convection (gravity) the discharge is bent upward. Adding a ripple with the frequency of the first longitudinal eigenfrequency of the arc tube with sufficiently high amplitude to the lamp power leads to establishment of acoustic streaming, as it is shown in Fig. 3.19 and 3.20 in the arc tube.

As it is illustrated in Fig. 3.21, the discharge is initially located in the region of the streaming loops 1 and 2. It will be forced upward due to the direction of these two streaming loops (*case I*). If the stabilizing forces are sufficiently large, the discharge will be pushed downwards. This can occur after touching the upper wall of the arc tube by the discharge. In such case the discharge can be deflected extremely downwards. Afterwards it will be located in the region

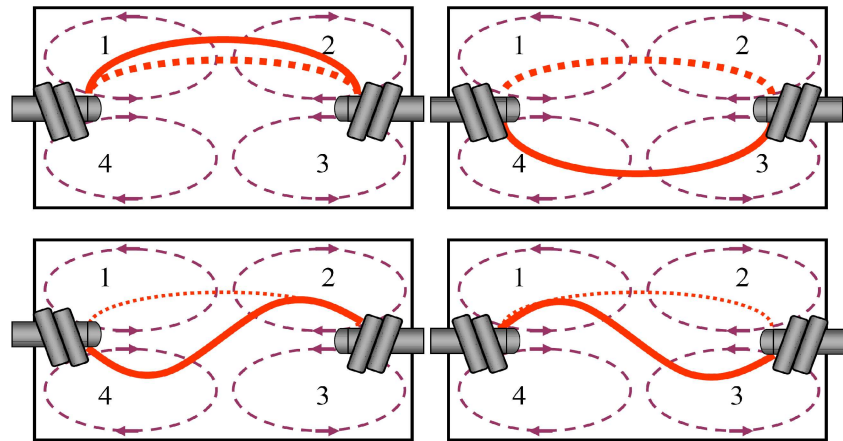


Figure 3.21: Interaction of acoustic streaming and discharge position in arc tube. In all cases the dotted line shows the original position of the discharge when there is no acoustic instability. Up-Left: *Case I* upward deflection. Up-Right: *Case II*, downward deflection. Down-Left and Down-Right: *Case III* and *Case IV*, S form instability.

of streaming loops 3 and 4 (*case II*). If the discharge is located in this position the streaming leads to a sharper bending of the discharge towards the bottom of the arc tube, since both streaming loops are downward. In this position the discharge is not stable and tends to resume back toward its original position. Both *cases (I and II)* are known as arc bowing. There are two other possible positions of the discharge. The discharge can be located partly in streaming region 2 and partly in region 4 (*case III*). This case gives an S form to the discharge. Because region 2 bends the discharge upwards and region 4 pushes it downwards. A similar situation occurs when the discharge is located in regions 1 and 3 (*case IV*). Therefore the discharge can intermittently occupy many positions in the arc tube (arc snaking). As the discharge passes through the mentioned regions, acoustic streaming gets the opportunity to entrap the discharge. Moreover, the arc attachment position on the electrode tip could be easily affected by acoustic resonances.

If for any reason, on one electrode tip, the arc attachment stays on its upper side and on the other electrode tip on its lower side, the mentioned situations of *case III or IV* can be satisfied as well. One reason of this unexpected behavior of the discharge can be the asymmetry of the electrode positions (when they are not inline). The other reason is that the movement of the discharge inside the arc tube is somewhat irregular especially after touching the arc tube's wall.

Fig. 3.22 illustrates a real case of such acoustic excitation in an HQI TS 150W WDL lamp. By superimposing high frequency power ripple of about 20% on power waveform of the lamp at a frequency of 22 kHz acoustic instability is established in the arc tube. This frequency which corresponds the first longitudinal acoustic mode has been found through measurement. The method of such measurements will be discussed in the next chapter. The result of the measurement is given in Appendix B.

The images of the lamp discharge is projected on a screen. Using a high speed camera, the movement of the lamp discharge is recorded with a rate of 1000 frames per second. Four images of Fig. 3.22 are selected from the recorded movie to show different positions of the discharge when an acoustic resonance is excited. As it is shown, the hypothesis of acoustic streaming and

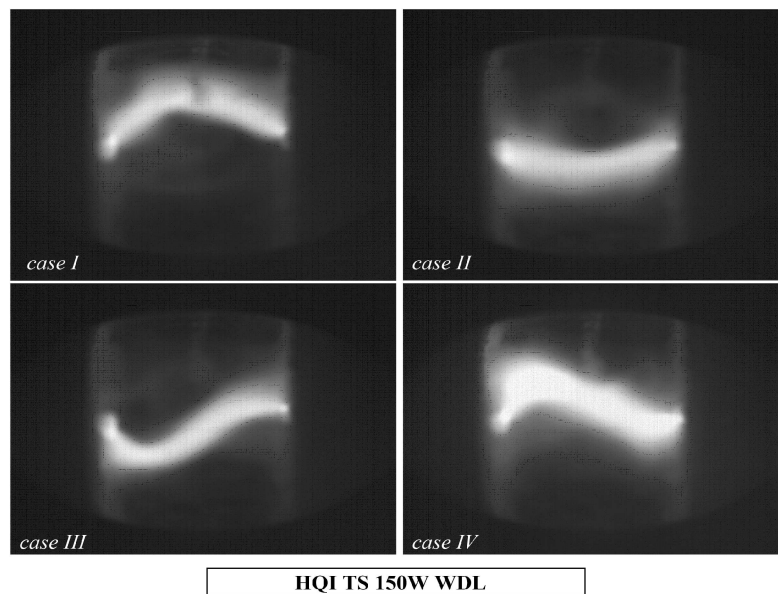


Figure 3.22: The figure shows four snap shots of the discharge of an HQI TS 150W WDL lamp. The lamp is operated with low frequency (200 Hz) square wave current which is superimposed with a high frequency (22 kHz) sinusoidal current waveform. Four cases of instability which are explained in this section are clearly recognizable in this experiment.

its interference with the discharge perfectly matches with the experimental results.

3.6 Detection of Acoustic Resonance

As it is mentioned, a very fundamental effect of AR excitation in the arc tube of HID lamps is changing of the chemical and physical balance of the filling material. This basic phenomenon leads to deviation of the electrical parameters, light instability and light flickering. There are some detecting methods for AR excitation which are established upon the mentioned effects.

3.6.1 Lamp current

The low frequency changes of current is used in (Zhou and others, 1999; Jiang and others, 2003), the proposed method is to extract AR signal out of lamp current signal using a proper low-pass filter. To eliminate the effect of line voltage fluctuations, which in turn affect the low frequency components of the lamp current, this method is combined with the line voltage feed forward (LVFF) technique. The other idea which uses the lamp current signal to detect the excitation of acoustic resonance is based on asymmetrical behavior of the lamp current waveform during AR excitation (Huynh, 1999). A common method to supply the lamp is applying a DC voltage to a half/full bridge circuit which drives the lamp. The DC voltage is derived from the AC line using a converter. This voltage contains a ripple typically at twice the AC line supply. The ripple passes through the bridge circuit and is reflected in the lamp current as well. Excitation of acoustic resonance makes this ripple of the lamp current asymmetrical as a shift in bias or frequency or both. Regarding the method proposed by Huynh a measurement of the duration of

any half cycle of the ripple signal can be used to detect the onset of AR. A significant deviation of this expected time period would be indicative of excitation of resonances in the lamp.

3.6.2 Lamp Voltage

(Statnic, 1986; Faehnrich and Rasch, 1988) report a voltage measurement of an OSRAM HQI TS 70W lamp as a function of driving frequency. According to these measurements, the effective lamp voltage shows sharp rises which characterize the instability of the discharge. The standard deviation of the lamp voltage as a quantity to detect the instability of the discharge is used in (Hsieh and others, 2005). The mentioned paper noticed that when the standard deviation of the voltage exceeds 0.3 V, the instability is recognizable. Furthermore, in presence of acoustic resonances, the lamp voltage fluctuations are dominant comparing the lamp current fluctuations.

3.6.3 Lamp Impedance / Conductance

The other electrical parameter which can be used as an index of excitation of AR is the lamp impedance. The method proposed in (Peng and others, 1997) is based on the changes of the lamp impedance. According to the calculations noticed in mentioned work, the lamp impedance shows a higher sensitivity comparing to the lamp current or lamp voltage alone. Moreover, a higher ratio of the signal to noise (typically 20 dB higher) can be achieved by measuring both voltage and current waveforms simultaneously and calculating the lamp Impedance (Calderia and others, 1999). In this way the noise signal of voltage and current signals due to the division cancels each other out.

The other benefit of using impedance as an index of AR excitation is that the impedance is independent on line voltage fluctuations such as surges and main dips (Peng and others, 1997). The method proposed in (Calderia and others, 1999) uses standard deviation of the lamp conductance as a measure of the acoustic resonance frequency and acoustic resonance strength. The proposed scheme is: “to operate the gas discharge lamp at a plurality of frequencies, at each frequency calculate the conductance a plurality of time by taking a plurality of simultaneous samples of lamp voltage and lamp current, and for each frequency calculate the standard deviation of the conductances taken at that frequency” (Calderia and others, 1999). The frequencies with small conductance standard deviation show low arc deflection and frequencies with higher standard deviations of conductance represent large arc deflections.

3.6.4 Lamp Power

According to previous explanations, it is obvious that excitation of AR is reflected in the lamp power as well. Analyzing of low frequency changes of lamp power can determine presence of AR excitation. (Garcia and others, 2004) proposes such method to detect the excitation of acoustic instabilities. The instant power of the lamp is derived by multiplying the current and voltage waveforms. A 4th order Butterworth low-pass filter with the cut-off frequency of 90 Hz is used to filter high frequency components of signal. If the filtered signal is constant then the discharge is stable otherwise the lamp is not operating stably. A more precise criterion to judge about the filtered signal with respect to the fluctuation’s threshold is not proposed by

mentioned paper. The above mentioned methods are especially suited to detect the existence of the acoustic resonances by online control in electronic ballasts.

3.6.5 Visual Detection and Optical Methods

The visual detection of the onset of the arc instabilities in the lamp (Witting, 1978; Denneman, 1983) can be considered as a simple way of evaluation. This method is especially useful in order to get a general view of the lamp sensitivity to the operating frequency in the frequency region of interest. However, for a systematic investigation of AR problem in HID lamps, it is obvious that this method is not a practical way. The method of optical evaluation is used in some different approaches. The concept of optical evaluation is to quantify the light intermittent to get a comparable value which enables us to judge about the acoustic excitation. This idea is used in (Afshar, 2006 II.; Anton and others, 2003; Dalla Costa and others, 2005; Keijser, 2005). (Olsen and Moskowitz, 1997) introduces an optical evaluation method based on the frequency spectrum of the emitted light of the lamp. In this approach the lamp is supplied with a high frequency current waveform which is greater than the highest AR frequency. This guaranties a stable operation of the lamp. A band limited noise, in the frequency range of interest, is then injected into the lamp current (or power). If in that frequency range any AR frequency exists, the spectrum of the emitted light of the lamp shows a peak value. The reason is that the discharge resonates with that frequency which is an eigenfrequency of the arc tube. By comparing the frequency spectrum of the lamp power and the emitted light, the frequencies in which the acoustic resonances are excited can be detected.

3.6.6 Measurement of Emitted Sound

Capturing acoustic resonances in HID lamps can be carried out by direct measurement of the acoustic energy which is emitted from the lamp. Schäfer and Stormberg have shown that a microphone outside the arc tube can pick up sound generated by the fundamental longitudinal AR in a high pressure mercury discharge (Schäfer and Stormberg, 1982). The sound is generated due to the arc tube oscillation inside the lamp. The pressure oscillation of the filling gas due to the electrical power fluctuation causes arc tube oscillation. The oscillation of the arc tube occurs with the same frequency as the electrical power. This way the strength of the emitted sound at different frequencies of the input power of the lamp reflects the existence or absence of acoustic resonance and its potential power as well. However, it has been shown (Schäfer and Stormberg, 1982) that a strong sound emission can occur without visual discharge instability. As it is explained under the hypothesis about the wall effect, if the ratio of the emitted acoustic energy to dissipated energy is high then the acoustic resonance does not show any discharge instability. Furthermore another disadvantage of this method is that the radiated sound may interfere with resonances outside the arc tube (Jongerijs and others, 1984).

3.6.7 Measurement of the Temperature

Small deflection of the discharge path or small changes of the internal gas flow can lead to the deviation of the temperature distribution inside the arc tube and on the arc tube's wall. Measuring of the temperature profile along the arc tube's outer wall and temperature distribution of the discharge is used in (Schäfer and Stormberg, 1982). (Olsen and Moskowitz, 2005)

reports a detection method of AR excitation based on the measurement of the hottest point on the arc tube outer wall. Regarding this experiment, excitation of AR in HID lamps can lead to a temperature deviation of the arc tube's outer wall. The experiment shows that a power ripple of less than one percent at AR frequency can deflect the discharge path which leads to a measurable wall temperature deviation (Olsen and Moskowitz, 2005). It should be noted that the method of the gas temperature measurement can be used only for the stable deviations of the discharge.

3.6.8 Optogalvanic Detection of Acoustic Resonance

The method of optogalvanic effect (OGE) to excite and detect of AR is introduced in (Jongerius and others, 1984). In this method a tuned dye laser is used to excite a known acoustic mode. The experiment has been performed in a cylindrical HPS lamp which was operated vertically. The laser beam was chopped with a mechanical chopper and was focused on the axis of the discharge. The experiment has shown that when the laser beam with a proper chop frequency is focused on an anti-node, a discharge excitation due to laser absorption occurs. Excitation of the discharge leads to a change of lamp conductance which is monitored as a deviation of the voltage (amplitude and phase) across the discharge. A measurement of the lamp voltage as a function of the chopper frequency and the target point of the laser beam was used to determine the AR excitation and its potential power. The advantage of this method is that the AR effect is detectable before excitation of the visible instability. However this approach is complicated and is not practical for more complex acoustic modes. Furthermore the resonant mode should be already known, and this is not the case for many practical applications.

3.6.9 Other Considerations about detection of Acoustic Resonance

There are some general points to address regarding detection of acoustic resonance which one should consider to prevent potential errors. The first important point is the effect of the sweeping frequency to capture acoustic resonances. Sweeping of the operating frequency may lead to two malfunctions. Firstly, it was shown that (Schäfer and Stormberg, 1982; Kramer, 2002) there is a noticeable hysteresis effect with respect to the acoustic resonance frequencies when the direction of sweeping is reversed. This means a precise detection of AR can not be expected if the frequency is swept. Secondly, if the sweep is carried out slowly for example at a rate of 20-50 ms (or slower) for any frequency step, the discharge has enough time to be deflected (as a result of AR excitation) and reaching a new position in the arc tube. If in this case the frequency is changed to a new frequency, the initial state of the discharge is not its original state. Therefore the measurement is not valid since the lamp is responding to the new frequency within an abnormal operating situation. On the other hand a fast rate sweep can lead to another error. As it is mentioned in a recent paper (Afshar, 2007) when the conditions of excitation of acoustic resonances are satisfied the arc instability occurs only after a specific duration. For this reason the sweep rate can not be selected too fast as well. Decision about the proper sweep rate is quite difficult or maybe impossible, since the onset time of acoustic instabilities depends on many parameters such as acoustic mode, and the magnitude of the power spectrum at that test frequency.

The other point is that by reaching the resonance frequencies during AR detection, it is possible that the electrical parameters of the lamp show significant changes. If this is the case

the measurement could be continued only after re-stabilization of the discharge. Such a case can happen both in sweeping methods and the methods without sweeping of the frequency. Finally it should be noted that the electrical power which is applied to the lamp is quite determinative regarding excitation of AR and its corresponding frequency. A permanent power measurement and regulation during such measurements is then necessary.

3.7 Avoidance of Acoustic Instabilities

According to the mentioned principles of acoustic resonance, it is understood that this phenomenon can be affected by lamp characteristics and electrical power by which the lamp is supplied, as well. Hence, to avoid excitation of acoustic resonances one should pay attention to different parameters of lamp as well as the supplying power waveform.

3.7.1 Lamp Related Factors

Any changes of eigenfrequencies of the lamp's arc tube directly affect the acoustic resonance phenomenon. There are some parameters which determine the eigenfrequencies of any lamp type.

Lamp Geometry

The first and maybe the most important factor is the geometry of the lamp's arc tube. It has been found that AR can not be totally eliminated through modification of the arc tube geometry (Davenport and Petti, 1985; Wada and others, 1987). However, the modification of the arc tube shape plays a significant role in reducing the potential power of acoustic resonances and shifting the resonance frequencies. The acoustic resonance can be reduced in arc tubes with conical or trumpet-shaped end (Wada and others, 1987). Acoustic resonances are more likely to be excited in spherical arc tubes or tubes with spherical end than flattened or narrow and cylindrical arc tubes. The lamps which have a small spherical arc tube such as some metal halide lamps show wide band resonance frequencies (Denneman, 1983). In contrast, cylindrical arc tubes (especially with a large aspect ratio¹⁰) are narrow band, discrete and easily recognizable (Wada and others, 1987). Increase in radius of spherical arc tubes results in increment of resonance frequency band and ARs are excited more easily (Yan and Hui, 2000). Change of geometry can help to adjust the position of AR frequencies to the desired frequency region as well. As it is reported in (Fellows and others, 1998) using a cylindrical arc tube with the aspect ratio of IL:ID about 1:1 (Inner Length to Inner Diameter) leads to maximizing the lowest acoustic resonance frequency. The aim of this upwards shift of AR frequencies is to be able to drive the lamp with a frequency above the audible and below the lowest resonance frequency. This way a high frequency operation of lamp without audible noise is possible. This application represents an example of geometry modification with respect to AR problem.

Type of Gas Filling

The other parameters affecting the AR phenomenon are type of gas filling and gas thermodynamic state variables such as pressure, temperature and gas density (Yan and Hui, 2000). The

¹⁰The aspect ratio is defined as the ratio of the arc tube's inner length to its inner radius, that is IL:ID.

sound propagation velocity is directly related to gas density and gas temperature. Therefore changing of these quantities can vary the acoustic resonance frequencies directly. The sound velocity increases with temperature increment and subsequently AR frequencies increase as well.

Burning Position

The burning position of the lamp determines the temperature distribution inside the arc tube. Usually there is a significant change of acoustic resonance frequencies and their band width when the lamp is operated vertically in comparison with horizontally operated position. Therefore the lamp sensitivity to high frequency components of its power spectrum can be affected by lamp's burning position. This property can be used especially by applications like video projections in which the burning position does not change and a stable light is quite important.

Gas Pressure

The gas pressure has an indirect effect on AR frequencies. Increasing the pressure decreases the damping coefficient accounting for acoustic resonances (de Groot and van Vliet, 1986). This leads to the conclusion that increasing the gas pressure of the arc tube increases the sensitivity of the lamp to AR and excitation threshold of ARs then is reduced. The laboratory experiments of acoustic resonance sensitivity test¹¹ for D2 automotive HID lamps (35 W) approve this conclusion. The gas pressure of D2 lamps is significantly higher than other lamps such as HCl T 35W lamps which are used in general lighting. The sensitivity test of D2 lamps show that the AR excitation threshold level at frequencies higher than 300 kHz is about 2-3 percent while this level for HCl T 35W lamps is about 4-6 percent of power ripple. According to (de Groot and van Vliet, 1986) the damping coefficient of acoustic resonances increases with increasing viscosity. On the other hand, absorption of acoustic energy due to the viscosity of the medium leads to generating of acoustic streaming. As it is formerly mentioned, viscosity suppresses the motion of the fluid but at the same time is the source of the driving force in generating acoustic streaming by converting the acoustic energy into the momentum.

(Epron and others, 1998) reports an experimental attempt to investigate the important parameters which affect AR phenomenon. The method of Epron and others is to supply the lamp with an alternating square waveform current with given frequency and duty cycle. In their experiment the frequency of the power supply was varied between 20-50 kHz. The duty cycle of the square wave current could also be varied. They experimentally showed that the higher is the gas pressure, the longer is the necessary duty cycle for the excitation of the acoustic oscillations.

Density of Atoms

The density of the mercury atoms in the arc tube of high pressure mercury lamps is another parameter which affects the AR properties of the lamp. An experimental result shows that increasing the mercury atoms density increases the lamp sensitivity to the higher frequency components (Wada and others, 1987). As Wada noted, the atomic weight of mercury is about 5 times larger than the buffer gas. The ionization voltage of mercury atoms is about two-third

¹¹The method of measurement is explained in (Afshar, 2006 II.) and will be covered in the next chapter.

of the buffer gas. The total pressure of mercury gas is about 100 times the buffer gas. Therefore in high pressure mercury lamps almost all atoms and neutrals are made from mercury. This means acoustic resonances are more likely to occur as mercury pressure increases.

In metal halide lamps it is likely that the same conclusion is valid as well. Because in such lamps the main pressure of the arc tube is provided by mercury atoms. Furthermore the partial pressure of species in arc tube of a metal halide lamp shows that mercury has a constant pressure along the whole diameter of the arc tube.

For a thorium-thallium-sodium-iodide-mercury mixture, with I:Hg ratio of 0.4, in the center of the arc tube the partial pressure of mercury is two times higher than the iodine, forty times higher than thallium, about fifty times higher than thorium and about thousand times higher than sodium partial pressure (Waymouth, 1971). In the vicinity of the arc tube's wall as the temperature is low, the partial pressure of sodium, thallium and thorium is zero; the partial pressure of iodine atoms and molecules is about one-thousandth of the mercury partial pressure (Waymouth, 1971). This is important because at the wall of the arc vessel the shear viscosity of the gas (mercury in this case) plays the main role in generating acoustic force which drives the acoustic streaming flow.

The excitation of acoustic oscillations is strongly dependent of the quantity of the mercury or sodium atoms introduced in the arc tube. For the high pressure mercury lamps, the necessary duty cycle for the excitation of the oscillation is bigger when the mass of mercury introduced in the arc tube is high (Epron and others, 1998).

The hypothesis of acoustic streaming can be used to explain the experimental results of Epron and others. When the density of the filling gas is high, the acoustic wave needs more time to establish a coherent movement of the filling atoms along the direction of acoustic streaming. Because, before introducing of the acoustic wave, there are many atoms which move in random directions. As a result, the acoustic energy of the wave should be used to change the momentum of many atoms which needs a longer time. On the other hand, when many heavy atoms like mercury atoms move coherently along a streaming path, they get sufficient energy to affect the discharge. This explains that why increasing the density of atoms makes the lamp more sensitive to acoustic resonances.

Practicability of Lamp Related Factors to Avoid ARs

Regarding above mentioned parameters which may have an effect on AR phenomenon, it seems that it is very unlikely to be able to suppress it just by lamp modifications. There are many determinative parameters such as color temperature, color rendering index, lamp life and so on, which may be badly affected by modifying the lamp with the aim of avoiding acoustic resonances.

3.7.2 Optimized Ballasting Methods

As it is discussed, the origin of acoustic instabilities is the high frequency periodic components of the power waveform with sufficiently high magnitude. The majority of ballasting methods one way or another are supposed to eliminate or reduce such high frequency components. In such a way that generated acoustic energy in the arc tube can not affect the discharge. In this section some optimized ballasting methods with the aim of eliminating of acoustic instabilities in HID lamps are introduced and briefly discussed.

DC operation

Obviously the first idea is operating the lamp with a dc current. The most important obstacle is the cataphoretic effect in which one electrode is served always as cathode and the other as anode. The result is de-mixing of the filling material toward the cathode which leads to dramatically changes in color temperature (Melis, 1998). Besides, the quick and asymmetrical etching of the cathode can occur as well (Goodenough, 1996). Due to above mentioned disadvantages; dc operation can be used only for special lamps which are designed for this operation.

Low Frequency Square Wave

A very common and widely used ballasting method is supplying the lamp with low frequency square wave (LFSW) current waveform. Theoretically this kind of ballasting spreads the voltage and current spectra in an infinite number of harmonics; however, the lamp is supplied with a dc power waveform. This way the high frequency components of the power waveform and subsequently the acoustic instabilities are eliminated. Practically, due to the commutation of switches embedded in electronic ballasts and current/voltage ripples the power waveform is not a pure dc waveform and there are still some high frequency components. However a clever selection of electronic switches and a good design of ballast can suppress such high frequencies.

High Frequency Square Wave

An alternative to LFSW is High frequency square wave (HFSW) to gain the benefits of high frequency operation as well. Theoretically this method operates the lamp with a constant instant power. However, practically this is not the case. Especially when the square wave is implemented with half-bridge circuit, due to different shapes of waveforms in the first and second half-cycles, the instant power is not constant. When the fundamental frequency component or other harmonics are sufficiently large the discharge will be unstable.

This method is used in (Ponce and others, 2004) to supply a 70 W HID lamp at 30 kHz (HFSW) from a 12 V (dc) source. Although the designed ballast was supposed to have a power crest factor¹² near unity, practically this value was about 0.7 which is not satisfactorily close to unity. It is pointed out that supplying the lamp with this kind of power waveform led to an stable lamp operation. However, the high frequency (60 kHz) power ripple with the crest factor of 0.7 seems to be too high to ensure stable operation of different lamps in different burning positions.

(Garcia and others, 2004) represents an HFSW scheme which uses a buck-boost topology as an inverter. Using this type of inverter, in one half cycle the lamp current/voltage is constant (switch is ON) while during the other half cycle it is negative exponential. This leads to a non-constant instant power. It is important to keep all frequency components of instant power less than a threshold level to avoid acoustic resonances. It is shown that the relative magnitude of frequency components with respect to the average power for proposed topology is a function of the harmonic order, duty cycle and relative power deviation. Furthermore, for a duty cycle of about 50 percent, the fundamental harmonic is kept less than 5 percent when the power deviation is up to 20 percent and other harmonics are less than the fundamental. According to this argument it is concluded that by controlling the duty cycle it is possible to keep power

¹²The crest factor in (Ponce and others, 2004) is defined as: $C_p = \frac{P_m}{P_a}$, where P_m is the maximum value of the instant power and P_a stands for the average of the lamp power.

harmonic below the threshold level. The idea is to keep the duty cycle always around 50 percent which is attainable by controlling the bus voltage (the input voltage to the inverter). (Garcia and others, 2004) reports a stable operation of a 70 W lamp at an operating frequency of 70 kHz. The disadvantage of this method is significant EMI emitted from ballast.

Spreading of Lamp Power Spectrum

Spreading the lamp power spectrum minimizes the power density of individual harmonics. Ideally if the power density of all harmonics maintained below the threshold level of AR excitation, the acoustic instability then will be avoided. To realize this concept, many experimental attempts are carried out. The most common used modulating profiles are sine wave, triangle wave and saw tooth wave.

Wada proposed a frequency-modulated sinusoidal current waveform (Wada and others, 1987) to spread the power spectrum. In Wada's experiment some trial 250W mercury lamps are operated at a center frequency of 30 to 60 kHz with a frequency modulation width of 0 to 10 kHz (with the span of 1 kHz) and modulation sweep frequency of 120 Hz. The experimental results indicated that such power spreading was not sufficient to eliminate acoustic instabilities. Obviously, the power densities of harmonics as a result of this type of power spreading exceed the threshold value of AR excitation. This result addresses some important questions about the spreading method and its related conditions. The selection of the center frequency, modulation width and modulation sweep frequency are vital variables in this regard. The other method to be mentioned in this category is non-sinusoidal lamp voltage (Stormberg and Schäfer, 1983; Koshimura and others, 1983). One alternative to high frequency sinusoidal is high frequency square wave current form. This way the current and voltage spectrum spread out but the disadvantages are limitation of lower order harmonics and EMI problem. Later it is shown that a better way of power spectrum spreading is using white noise modulation technique which can operate 250W lamps without visual instabilities (Laskai and others, 1998). In this technique the switching frequency of the lamp current or voltage is changed randomly using a band-limited white-noise signal. As a result, required modulated-wave bandwidth of this proposed method is much smaller (factor of 1/6) than the periodical modulating techniques to get the same power spectrum spreading (Laskai and others, 1998). The disadvantage of this approach is that the implementation of such electronic ballasts is not cost effective (Oh and others, 2002).

Another research shows that the mentioned method can not be used for small wattage metal halide lamps (Yan and Hui, 2000). Due to the broad band of acoustic resonance frequencies of such lamps the proposed method in (Laskai and others, 1998) is applicable only when the center frequency is located in a resonance free region. Regarding (Yan and Hui, 2000) increasing the modulation band of injected noise even may result in a more unstable operation of the lamp. In this case the power spectrum reaches unstable regions of the operating frequency as well. (Wang and others, 2004) reports a low frequency sine wave angle modulation to eliminate AR in 250W MH lamps. In this method it is proposed that the center frequency is selected at 47 kHz and the frequency of sine wave modulation signal is limited among several hundred hertz. Regarding (Wang and others, 2004) four different 250W MH lamps were operated with this method and no discharge instability was observed. This paper concluded that to get this result, the center frequency must be beyond 47 kHz and the frequency offset, lamp current and voltage must fluctuate in a proper range.

An improved modulating method is reported in (Oh and others, 2002). The mentioned paper

introduces a complex modulating method composed of two modulating signals with different waveforms and frequencies. They use a sweep frequency saw-tooth waveform as the main modulating signal which is added with a variable magnitude triangular signal. The former is the common method and the latter is already used in (Zhou and others, 1999). It is concluded (Oh and others, 2002) that using a constant modulating frequency results in a discrete distribution of spectra. Therefore excitation of AR due to fundamental frequency or its lower order harmonics with sufficient amplitude is still possible. The additional low frequency modulation makes the spectra more condense and as a result decreases the magnitude of harmonics. As it is pointed out in the mentioned paper, the spectrum has a low frequency component as well which is the frequency of the modulating signal. This low frequency must be selected carefully because the lamp power is subject to fluctuations with this frequency. Therefore it must be sufficiently low in order to be imperceptible to the human eye.

(Correa and others, 2004) reports a method which uses three different patterns of modulating signal with different modulating index in order to eliminate AR. In this work, a low frequency fluctuation of current waveform is used to detect the excitation of ARs. A digital control loop changes the modulating pattern between sinusoidal, triangular and saw-tooth or the index of the modulation to eliminate the acoustic instabilities. The paper reports some attempts to stabilize different HID lamps. A test with a CDMR-70W/830 metal halide lamp, with the central frequency of 35 kHz shows that the lamp needs about 5 minutes to be stabilized when the proposed control method is applied. The complex and white-noise modulating methods seem to be more effective than the other methods in eliminating of AR. However they are relatively complex and expensive to be used in commercial applications. In response to this disadvantage a recent paper (Chiu and others, 2006) introduces a frequency modulation method which uses 120 Hz DC bus voltage ripple as frequency modulating signal. This way the modulating signal is a sinusoidal waveform which already exists. Although the result is a low cost electronic ballast, this solution can not gain the benefits of complex or white-noise modulating methods.

Free Resonance Window

The discrete characteristic of acoustic resonance frequency spectrum offers some free resonance regions. The idea which is proposed by (Lake and Davenport, 1982) is to operate HID lamps in a resonance free frequency. To realize the concept, one requires the knowledge of resonance free zones for all lamps which are possibly supposed to be operated with that ballast. The other critical limitation is that such free resonance window(s) should be common for all lamps (concerning different lamp types and different manufactures) of interest. However this idea can be used for integrated systems in which the ballast is used only for one specific lamp. A prerequisite for this application is that the acoustic resonance frequency spectrum is not subject to significant changes along the whole lamp life. Otherwise it could be possible that a shift of AR frequencies leads to occupying the free resonance window with an adjacent resonance frequency. Any change of temperature distribution of the lamp due to different thermodynamic conditions of the gas leads to a shift of AR frequencies. It should be recalled that finding a free resonance window is not always possible. Especially for small and spherical arc tubes the AR frequency bandwidths are widened which minimize the free resonance windows with respect to their numbers and bandwidths. Furthermore, the existence of current harmonics which may have frequencies in acoustic resonance regions, in practical applications, is quite possible. Such current harmonics with sufficiently high amplitude are expected to excite acoustic resonances

and make the discharge unstable. Due to above mentioned difficulties, although the concept of free resonance window is interesting, it can not be considered as a practical and robust solution to avoid acoustic instabilities.

It is worth to recall that a combination of quasi-free resonance window and power spectrum spreading method can be used to drive the lamp stably. This method is proposed in (Kramer, 2001). In this method the lamp is operated in a frequency window which is free of fundamental and significant resonance modes but contains some weak resonance modes. For this reason we call it quasi-free resonance window. The power spectrum is spread in such a window; the absence of significant resonance modes as it is expected leads to stable operation of the lamp. The effect of resonances which tend to destabilize the discharge is not significant because they are not major resonance frequencies. Furthermore because of the reduction of power amplitude at those frequencies their effect is not perceptible. Excitation of some non-significant resonance modes which are located in the selected window can even help in straightening the discharge as it is reported in (Kramer, 2001). The mentioned work focuses on long cylindrical arc tubes. In such arc tubes the power frequency of the first azimuthal and the first radial acoustic modes are

$$f_{1^{st} azimuthal} = 1.84 \frac{c_r}{\pi D}, f_{1^{st} radial} = 3.83 \frac{c_r}{\pi D} \quad (3.27)$$

Where c_r is the effective sound velocity in radial direction and D is the inner diameter of the arc tube. As it can be seen these two frequencies are not a function of the arc tube's length, hence they are valid for other cylindrical lamps with the same inner diameter as well. The lamp is operated in a frequency window between the first azimuthal and the first radial acoustic mode. Regarding (Kramer, 2001) the typical lamp supply for such operation is a current frequency sweep from 45 to 55 kHz within a sweep time of 10 ms. The current waveform is sinusoidal and the lamp is a 70W metal halide lamp with a cylindrical arc tube and the aspect ratio of ID:IL equal to 4:19.

Lamp operation at Extra High Frequency

The other alternative is operating of HID lamps with extra high frequency. Theoretically there are infinite numbers of resonance modes. Resonances in higher frequency regions are much closer to each other and approach a continuum. This implies that there is no resonance free window in higher frequency regions as well. However, there are two factors which should be considered in this regard. Firstly, as it is formerly shown, by increasing the resonance frequency, the importance of the resonance modes is decreased. Secondly, it is known that the damping effect is increased with frequency (de Groot and van Vliet, 1986). Hence, excited acoustic modes in higher frequency regions do not have sufficient energy to make the discharge unstable. It has been shown (Yan and Hui, 2000) that this method is applicable to small wattage metal halide lamps. The mentioned paper reports a stable operation of a 35W MH lamp with a cylindrical arc tube form which is operated at 714 kHz. Due to the extra high frequency operation of ballast switches in this mode, the switching losses must be carefully treated. The other probable disadvantage of this method is EMI problems. Stable Operation of HID lamps in very high frequency around 500 kHz is reported in (Shen, 2002) as well.

High Frequency Sinusoidal Waveform Superposed with 3rd Harmonic

The method is proposed in (Koshimura and others, 1983) with the concept of approximation of lamp voltage and current waveforms to the square waveform, but using only two harmonics. The advantage is elimination of higher harmonics which are responsible for EMI problem. By comparing this method and high frequency square wave, one can see that although the problem of EMI is solved, limitation of lower order harmonics (in this case the first harmonic) is still the major obstacle. However, the idea has been used to implement a prototype of electronic ballast to supply 35 W lamps (Alonso, 2002). The first harmonic of the ballast operating frequency is about 30 kHz, the mentioned paper reports a stable operation of a 35 W lamp with ceramic arc tube. Our laboratory experiment with three different OSRAM HQI-TS 70 W lamps does not support this concept. As it was expected, operating the lamp with only first and third harmonic, 30 kHz and 90 kHz respectively, leads to strong light flickering and discharge instability.

Real Time Auto-Tracking Control

(Peng and others, 1997) introduces a topology for a so-called smart ballast which uses real time frequency tracking for AR avoidance. The idea is to operate the lamp in a free resonance window. The value of the impedance deviation as a percentage of lamp impedance is captured. For reasons which are mentioned formerly a shift of AR frequencies for different lamps and even for a unique lamp during its life is quite possible. Higher values of impedance deviation are indicative of onset of AR and it shows that the selected frequency is not the optimum. At this point the operating frequency is shifted until a stable region is reached. This concept is realized and reported in (Moo and others, 2003) as well. The only difference is the AR detection method which is based on lamp voltage deviations. The ballast is designated to supply a 70 W lamp in a frequency range between 20 kHz and 30 kHz. It is shown that this tracking method can find a free resonance window within predefined frequency bandwidth by shifting the operating frequency sequentially.

3.8 Benefits of Acoustic Resonance Operation

As it is pointed out in the introduction, the excitation of acoustic resonances may lead to some useful effects as well. In the following section some possible benefits of acoustic resonance or acoustic operation in HID lamps are pointed out.

3.8.1 Arc Straightening

It is well known that operating of HID lamps in horizontal position leads to upward bowing of the discharge. The reason is the thermal convection of filling material as a reaction of the gravity force. This effect is not desirable when the lamp optics require a straight line. Examples are automotive lamps which are installed in a precise optic to control the projecting light, or HID lamps which are used in photo-optic applications.

Furthermore, upward deflection of the discharge leads to other disadvantages which are explained as follows. This phenomenon results in a significant temperature difference between upper side and lower side of the arc tube's wall which are known as hot spot and cold spot

respectively. Extra heating of hot spot tends to shorten lamp life due to suffering the arc tube especially for quartz lamps.

Moreover, the filling material tends to condense on the arc tube's wall at the cold spot position in form of liquid drops. As a result the density of the molecules, atoms and ions which contribute in making discharge reduces hence, total efficacy of the lamp decreases. An advantage of acoustic resonance operation is arc straightening. Some acoustic modes are able to push the discharge downward and maintain it permanently in a straight position between electrodes. Actually these acoustic modes are able to arise acoustic streaming which dominates the effect of thermal convection forces. The result is an establishment of new stationary net forces which straighten the discharge. Obviously the frequency region in which the discharge can be stably straightened should be carefully selected. This is a lamp dependent factor and can be determined experimentally.

As long as the AR frequencies are spread along the frequency axis, such useful frequency regions are usually located between several unstable resonance modes. It is quite important not to achieve unstable regions during AR operating of HID lamps; otherwise the straightening would be accompanied with some undesirable effects such as light flickering. As it is mentioned, arc straightening leads to a more isothermal temperature distribution of the lamp arc tube. This way the difference between hot-spot and cold-spot temperature is reduced which can lead to minimization of fill condensation at the cold-spot. Therefore, the efficacy of the lamp will be increased due to contribution of more gaseous atoms in discharge.

The effect of acoustic operation can be dramatic. A research (Allen, 1992) shows that for a miniature xenon HID lamp, straightening the arc reduces the maximum wall temperature up to 200°C which in turns doubles the lamp efficacy. It should be noted that xenon lamps are aimed to produce instant light, for this reason the xenon pressure of such lamps should be sufficiently high to make the lamp able to emit nominal lumen instantly. Thus the xenon pressure is comparable to that of the mercury in the metal halide discharge close to double, with the result that convection in the xenon metal halide lamps is much stronger than in a miniature metal halide lamp for general lighting (Allen, 1992). If the current is constant, increasing the pressure of mercury in case of metal halide lamps for general lighting or xenon in automotive lamps leads to an increase of the wall temperature. In fact, higher density of mercury or xenon atoms in the arc tube increases the thermal conduction from discharge to the wall.

On the other hand increasing the xenon pressure means more emitted instant light, and in case of MH lamps with mercury, the increase of mercury pressure leads to a higher voltage across the discharge which may be beneficial. By decreasing the wall temperature due to arc straightening it is possible to increase the pressure of xenon or mercury without thermally overloading the arc tube's wall.

The other achievable benefit of arc straightening is that it is possible to increase the lamp power with the same arc tube's size and material. In other words, for a given lamp power arc-straightening makes it possible to reduce the size and volume of the arc tube.

To determine the frequency regions in which the discharge is straightened one method is to measure the lamp impedance as a function of operating frequency when the RMS value of the current is kept constant. As it is explained in (Afshar, 2007) when the discharge is straightened the impedance of the lamp, due to a reduction of the arc length, is decreased. The proper frequency region is then selected where the lamp impedance has a local minimum. It is also quite important to keep the discharge stable in the preferred frequency region. Flicker factor (Afshar, 2006 I.) of the emitted light when the lamp is operated in acoustic resonance mode

can be used for evaluation of the discharge stability.

As it is reported in (Allen, 1992) the widest stable band for arc-straightening at any given operating frequency for an investigated xenon lamp was 10 percent for current or voltage waveform. Furthermore, it is well known that the exact location of the stable window affected by almost all lamp parameters such as manufacturing tolerances of arc tube geometry, off axis run-out of electrodes, gas fill pressure and so on. The input power of the lamp is also important because it can change the temperature and the vapor pressure. An immediate solution to overcome such uncertainties is a frequency modulation of the lamp current. This way instead of a single frequency operation the lamp is operated in a frequency band. Frequency modulation increases the probability of meeting the stable window for all given lamps in spite of their manufacturing tolerances. Regarding (Allen, 1992) a straight stable arc, for a xenon lamp¹³ was obtained over the carrier frequency range of 32 to 48 kHz with a frequency excursion of 4.2 kHz and the modulation frequency of 0.7 kHz for a stable arc-straightening of a small (major diameter of 10 mm) xenon lamp.

During any modulation period as the instant operating frequency reaches the exact resonance frequency two times the straightening forces are maximized. The modulation frequency determines how often straightening forces are applied to the discharge. This frequency should be sufficiently high in order to prevent giving enough time to the discharge to be affected by thermal convection forces when the instant operating frequency deviated from resonance frequency. Otherwise it is expected that a light flickering occurs. Especially when the modulation bandwidth is increased to cover more tolerances of manufacturing this could be critical. Fortunately the deflection of discharge is a relatively slow process with a time constant in tens of millisecond range (Calderia and others, 1999; Afshar, 2007). The modulation frequency of 700 Hz corresponds to a period of 1.43 ms which means any 0.7 ms the straightening forces are applied to the discharge. On the other hand a very high modulation frequency could not be effective as well. In this case the time interval in which the exact resonance frequency is applied to the lamp would be below the required onset time of acoustic resonance. However the fact that the resonance frequency is not discrete and it is spread in a bandwidth is a compensating factor in this regard.

The shape of modulating frequency does not play any role for this application, it could be sinusoidal, triangular or any shape between these two (Allen, 1992). According to (Kramer, 2003) the frequency that produces arc straightening is in range above a first azimuthal acoustic mode and below a first radial acoustic mode for the resonance spectrum of the HID lamp. In contrast to Allen's proposed method, Kramer proposes an amplitude modulation to excite the proper resonance mode which can straighten the discharge. In this method the amplitude of the current/voltage is modulated with an upward swept modulating frequency while the carrier is a high frequency waveform. A very interesting property which is observed during frequency modulation is the stability broadening effect. It is observed that when frequency modulation is applied to the carrier, a remarkable modification of the frequency bands for straight stable arcs occurs (Allen, 1992). As it is formerly described frequency modulation leads to spreading of the supplied power in many frequencies. As a result the amplitude of such components which tend to make the discharge unstable is not sufficiently high and the discharge remains stable.

¹³This method was carried out with a small (major diameter of 10 mm) prolate ellipsoidal arc tube design xenon Lamp.

3.8.2 Color Mixing of Vertically Operated HID Lamps

There are some metal halide lamps, such as Philips CDM MASTERCOLOR, which have a long cylindrical ceramic arc tube (aspect ratio of about 5). These lamps have the desirable property of high efficacy, but they have the disadvantage of different color properties in horizontal and vertical operation. When such lamps are operated vertically, the emitted light along the arc tube has a different color. This is due to a non-homogenous distribution of filling material inside the arc tube which is known as color segregation. In particular, the bottom part of the discharge appears pinkish while the top part looks greenish. The reason is that the density of thallium and mercury atoms dominates at the top of discharge while at the bottom more emission of sodium atoms is observed (Kramer, 2001; Kramer, 2002). When the arc tube is long and the operation position is vertical, the forces which are induced by thermal convection are not sufficient to mix up the gas mixture thoroughly and separation of different species appears. To avoid color segregation or to minimize it the method of acoustic resonance operation, as an effective way, can be used. One idea is to establish the second longitudinal acoustic resonance mode in the arc tube as it is proposed in (Shen, 2002; Kramer, 2001) and (Kramer, 2003). Longitudinal acoustic resonance mode can move the metal halides in the lamp axially (Kramer, 2001). Kramer's research showed that when a Philips 39 W CDM lamp was operated at about 67 kHz power frequency in a vertical orientation, the liquid metal halide condensate moved from its normal position at the bottom of the lamp to a position approximately $1/3 \times L$ above the bottom. The frequency of 67 kHz corresponds the second longitudinal acoustic mode. Moreover the first longitudinal mode was less effective in reducing the color segregation. The reason of Kramer's observation can be explained with the hypothesis of acoustic streaming as follows. According to acoustic streaming theory, in a cylindrical arc tube which is excited with the second longitudinal mode, there are eight identical streaming loops. Interfering of particle movement caused by acoustic forces and that movement induced by thermal convection is the key point which explains this observation. The subject can be seen from two points of view.

Firstly, in the vicinity of the arc tube's wall, there are four regions with respect to the acoustic streaming directions. In this area movement of atoms with respect to the thermal convection is from top to bottom. For the first and the third zones the thermal force and acoustic force are additive while for the second and the fourth zones these forces are subtractive. As a result in the first and third zones condensed filling material are washed up from the wall. In contrast, due to force cancelation, filling material tends to condensate in the middle part of the second zone. However, this is not the case for the fourth zone as long as top of the arc tube is much hotter than the lower part.

Secondly, by focusing on the center line of the arc tube another supportive idea can be proposed. Along the arc tube's center line the direction of the thermal convection is upward. Focusing on the second zone it can be seen that along the center line acoustic streaming is downward; as a result a reduction of the discharge density is imaginable. This effect may lead to a temperature decrement in the middle of the second zone on the wall which helps the filling condense at this area. It should be recalled that the middle of the second zone is located at $3/8 \times L$ which is fitted very well with $1/3 \times L$ which is already reported by Kramer.

The other important observation is that the first longitudinal acoustic mode is less effective in avoiding color segregation. The first longitudinal mode establishes four streaming loops in the arc tube, while excitation of the second longitudinal mode introduces eight streaming loops. This means a better mixing of the filling gas is expected when the lamp is operated

under the second longitudinal acoustic mode. On the other hand in the second longitudinal mode the direction of the streaming loops in the 2nd and 3rd zones (in the vicinity of the wall) is toward the middle of the arc tube. Possibly this property of the second longitudinal mode plays a significant role in transporting thallium and sodium atoms and de-mixing of the filling material. Additionally, it should be noted that these two zones cover the most part of the discharge's length. Contrarily excitation of the first longitudinal mode leads to establishment of two streaming loops which transport the filling material from middle of the arc tube toward its two ends. As a result no significant de-mixing of sodium and thallium atoms is expected.

(Shen, 2002) proposes a duty cycle modulation method to excite the second longitudinal acoustic mode in the lamp. The lamp is supplied with a half bridge circuit. The switching frequency of the half bridge is in VHF range and is kept constant to avoid undesirable acoustic resonances. Applied voltage to the lamp can be changed by changing the duty cycle of switches. Therefore, modulating of the duty cycle leads to an amplitude modulation of the lamp voltage. This frequency is set in such a way that the second longitudinal resonance can be excited (e.g. 12 kHz voltage modulation). Index of the duty cycle modulation determines the strength of the amplitude modulation and the degree of color mixing. Very strong resonances may lead to instability of the discharge, i.e. a compromise between color de-mixing degree and arc stability is necessary.

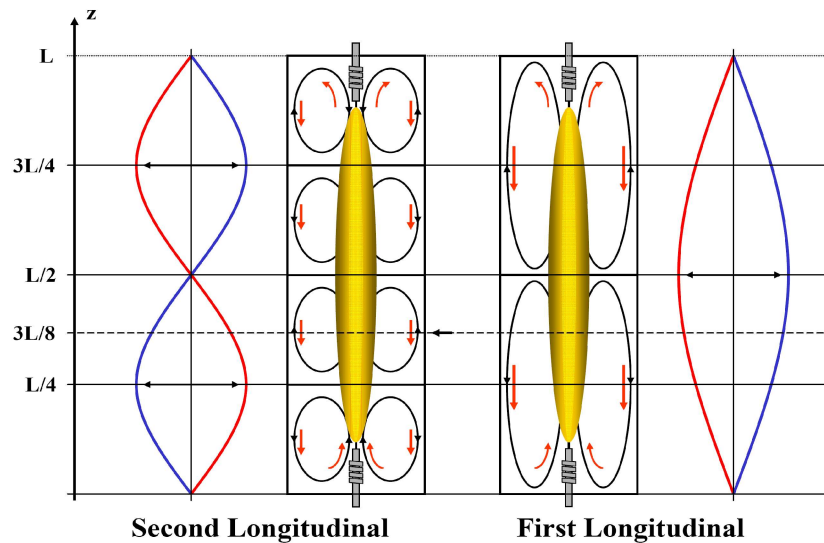


Figure 3.23: Comparison of the first and the second longitudinal acoustic modes for a vertically operated lamp with respect to the acoustic streaming loops inside the arc tube. Sinusoidal curves represent the linear acoustic velocity corresponding to the 1st and the 2nd longitudinal resonant modes. Arrows inside the arc tubes show the direction of the thermal convection. Ellipses represent position and direction of acoustic streaming loops which are excited as a result of pressure standing waves in the arc tube. On the vertical axis, positions of acoustic velocity nodes, antinodes and the position at which the filling material due to excitation of the second longitudinal mode are condensed, are indicated.

The other proposed method to reduce color segregation is reported in (Kramer, 2001). Similar to above mentioned method, in this approach an amplitude modulation with the power frequency of second longitudinal resonance mode is applied to the lamp. The amplitude mod-

ulation is carried out with a fixed frequency around the second longitudinal acoustic mode (current frequency of 12.5 kHz for a 70W cylindrical arc tube with the aspect ratio of ID:IL equal to 4:19). As a result a significant reduction in color temperature (1300 K) when the lamp is operated vertically with such amplitude modulation is reported. Alternatively the frequency of the amplitude modulation can be swept in a narrow frequency bandwidth from 12.3 kHz to about 12.5 kHz or vice versa during 2.5 ms as it is proposed in (Kramer, 2001) to capture the second longitudinal resonance with respect to the manufacturing deviations. (Kramer, 2002) suggests a method of lamp voltage measurement to find the second longitudinal acoustic mode. As it will be explained later in this chapter, this acoustic mode is important in order to obtain a mixing of the filling material in vertically operated metal halide lamps. The method is based on the assumption that when the frequency range which contains the second longitudinal acoustic frequency is scanned continuously, a relevant lamp voltage increase then indicates occurrence of this acoustic mode.

(Stockwald, 2007) proposes a method of finding second longitudinal acoustic mode, based on measurements of the lamp impedance when the lamp current experiences an amplitude modulation. The lamp impedance is measured as a function of modulation frequency and modulation index.

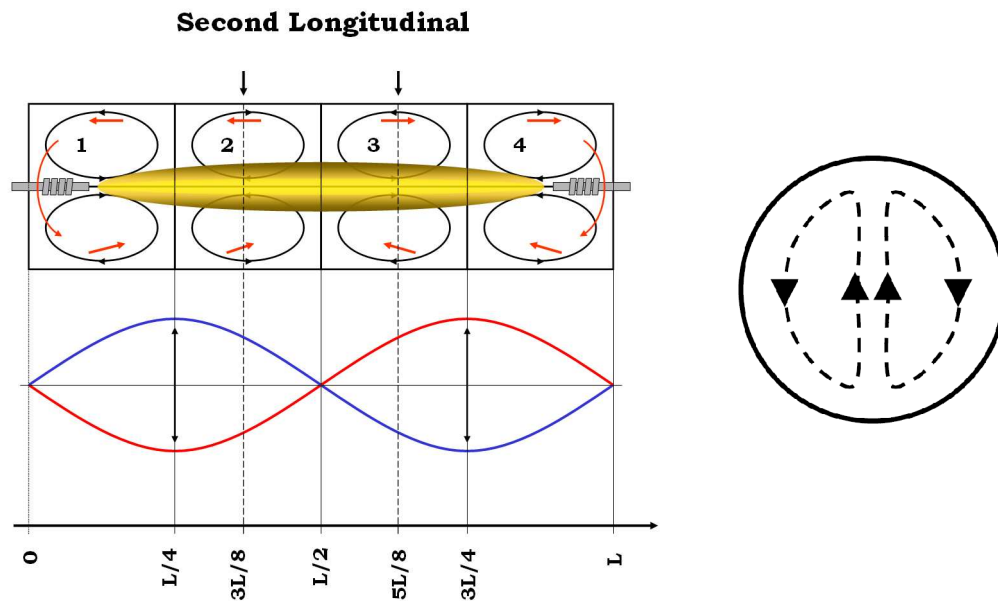


Figure 3.24: Left: The same arc tube as of Fig. 3.23 which is operated horizontally. Direction of the thermal convection is indicated with arrows in the arc tube. Locations and directions of the corresponding acoustic streaming for the 2nd longitudinal resonant mode are indicated by ellipses. Two vertical arrows located on top of the arc tube's wall show the area at which the filling material will be condensed when the 2nd longitudinal resonant mode is excited. Right: A transversal cross section of the arc tube with the direction of the thermal convection.

Horizontally operation of a cylindrical metal halide lamp when the second longitudinal resonant mode is excited leads to condensation of some filling material at $1/3 \times L$ and $2/3 \times L$ (Kramer, 2001). To explain the reason of this observation again the theory of acoustic streaming can be used. As it is schematically illustrated in Fig. 3.24, the direction of streaming loops in both 2nd and 3rd zones is in the opposite direction of the thermal convection. This means that

in the middle of these two zones, the streaming and thermal forces are subtractive. As a result the filling material will condense at $3/8 \times L$ and $5/8 \times L$ along the length of the arc tube. These values are in a good agreement with experimental observation of Kramer.

3.8.3 Beam Switching

As it discussed, excitation of acoustic resonances in the arc tube of HID lamps may lead to displacement of the discharge position. Beam switching as a useful effect of acoustic resonance can be used for some applications like automotive lighting. It is already explained how discharge straightening in HID lamps is possible. When the arc is acoustically straightened, the central point of light concentration is displaced from one point to another (Allen, 1992). In the proposed method by Allen and others, the lamp is adjusted within a reflector in such a way that the bowed discharge is located at one focal point and straightened discharge at the other focal point of the reflector. In this way just by changing the operating frequency of the lamp beam switching is realizable. (Lapatovich and others, 1996) proposes a method to deflect the discharge of an electrodeless HID lamp in order to realize beam switching in such lamps with automotive applications. This approach is quite similar to the other explained method. A second longitudinal resonant mode is excited to deflect the discharge of a small electrodeless HID lamp (cylindrical arc tube with 2 mm inner diameter and about 10 mm length). The lamp is operated with a 915 MHz carrier which is modulated with a 36 kHz modulating frequency and the modulation depth of 35 percent.

3.8.4 Strength Test of Ceramic Arc Tube and Outer Bulb

The strength of the ceramic arc tube and the glass bulb of HID lamps are quite important as a safety issues. If for any reason the ceramic arc tube of an HID lamp explodes, the outer bulb will be strongly hit with pieces of cracked arc tube. In such cases the outer bulb is supposed to withstand and not to break.

Outward deflection of the discharge heats up the arc tube extremely. Local overheating in case of a ceramic arc tube leads to extreme thermal stresses which can result in arc tube explosion. In such case it could be investigated whether the outer bulb of the lamp is sufficiently strong or not. Applying acoustic modes which deflect the discharge toward the arc tube's wall can result in destroying the arc tube. This method can be used as a proper approach to test the outer bulb.

3.8.5 Determination of Instantaneous Gas Temperature of rare Gas Flashlamp

Flashlamps are similar to all other arc lamps in that optical radiation is produced by passing an electrical current through a gas. Xenon is used in most flashlamps, since it is the most efficient inert gas for converting electrical energy to optical energy. Current is usually supplied by a charged capacitor capable of discharging large amounts of energy in a short period of time.

(Lama and Hammond, 1981) reports a method to determine the gas temperature in flashlamps based on excitation of acoustic resonances as follows. The electrical breakdown of the gas in a flashlamp which occurs after any discharge of the capacitor generates a traveling pressure wave. With the same mechanism which is discussed in this chapter, this wave can modulate

the discharge with a frequency equal to the eigenfrequency of the lamp. It is shown that (Lama and Hammond, 1981) the oscillation of the discharge which is reflected in the emitted light or the voltage waveform of the lamp has a frequency equal to the first azimuthal acoustic mode.

Regarding (3.9) as long as $\alpha_{10} = 1.84$ the first azimuthal acoustic resonance frequency (f_{100}) is:

$$f_{100} = \frac{1.84c_{eff}}{2\pi R} \quad (3.28)$$

where R is the inner radius of the arc tube and c_{eff} is the effective velocity of the sound as it is defined in (3.13). By combining equations (3.28) and (3.13) and solving for temperature as a function of the oscillating frequency we get:

$$\bar{T} = \frac{c_v \bar{M}_g}{c_p R} \left(\frac{2\pi R f_{100}}{1.84} \right)^2 \quad (3.29)$$

As a result by measuring the emitted light signal or the voltage waveform, after breakdown process, by using the above mentioned equation it is possible to find the instantaneous temperature of the gas in a cylindrical arc tube.

Chapter 4

Allowed Level of the power ripple in LFSW Ballasts

4.1 Introduction

In electronic ballasts for high intensity discharge lamps, there are two distinctly different methods to drive the lamp. The first method is operating the lamp with a high frequency sinusoidal current and the second is to driving the lamp with a low frequency square wave current (Sun and Goriki, 2000).

As it was described in detail previously, high frequency components with sufficient energy occurring in the lamp power spectrum can excite Acoustic Resonances (ARs) in HID lamps. There are many parameters which can affect the acoustic resonance frequency and its potential power to make the discharge unstable. To recall some of them we can refer to the arc tube geometry, type of the filling gas, pressure and temperature distribution of the gas and lamp burning position (a detailed description is given in chapter 3).

As a result, because of the acoustic resonance problem associated with the high frequency method, a proper and favored technique is supplying the lamp with a ‘Low Frequency Square Wave’ (LFSW) current (Sturm and Klein, 1992). To produce such a current waveform, from the AC main line or other sources e.g. batteries (for example in automotive applications), the so called ‘switch mode power supplies’ are used. The switching frequency of these power supplies usually ranges from tens to hundreds of kHz. The output voltage or current of such DC-DC converters contains a high frequency ripple which originates from their topology. The ripple frequency is equal to the converter switching frequency. When such high frequency ripples with sufficient amplitude pass to the lamp, they could be considered as a potential source of AR excitation.

The aim of this chapter is to introduce an experimental method to determine the lamp sensitivity to the high frequency power ripple. It is desired to know how the lamp reacts to the high frequency ripples with respect to the frequency and the amplitude of sinusoidal ripples which are injected to the lamp current/voltage.

There are some suggestions for level of such current/power ripples which is allowed to pass from ballast to the lamp, without exciting any acoustic instabilities in HID lamps. To points out some of them we can refer to: (Denneman, 1983) which suggests 10-15% of modulation depth of input power at fundamental acoustic frequencies and more than 25% for higher acoustic modes. (Nishimura and others, 1988) gives the maximum value of 20% for current modulation depth. Regarding (Sun, 2000) it is empirically accepted that to avoid arc instability due to acoustic resonance, the ratio of superimposed high frequency switching ripple current to the low frequency driving current has to be bellow 10%. (Keijser, 2005) shows that for metal halide lamps at certain frequencies about 3% of current modulation can lead to acoustic instabilities.

The acceptable value of the power ripple of the electronic ballasts is an open question for the industry and standard organizations (Olsen and Moskowitz, 2005). This value is a lamp characteristic and should be determined for all lamp types which are supposed to be supplied with electronic ballast. This way the most sensitive lamp to the high frequency ripples dictates the highest allowed level of the high frequency ripple of the ballast. Since the acoustic resonance phenomenon depends on the frequency, the measurement should be carried out for whole expected frequency range.

There are some different methods to detect and evaluate acoustic resonance. These methods can be categorized in three groups:

- The first group comprises methods which are based on the electrical parameters of the lamp. The method proposed in (Peng and others, 1997) is based on the change of the

impedance of the lamp. The low frequency changes of current are used in (Zhou and others, 1999) and the standard deviation of voltage is used in (Hsieh and others, 2005). Such methods are especially suited to detect the existence of the acoustic resonances by online control in electronic ballasts.

- The second group encompasses methods to predict AR by visual detection of the onset of the arc instabilities in the lamp (Witting, 1978; Denneman, 1983) or use optical evaluation (Olsen and Moskowitz, 1997). Obviously the visual detection is not a practical way to obtain the power ripple threshold in a relatively vast range of frequency.
- In the third category, detection of the AR excitation will be carried out using other methods, for example by measuring the sound emitted from the lamp (Schäfer and Stormberg, 1982; Kaiser and others, 2003) or using a Dye Laser to excite acoustic resonance and optogalvanic detection of its effect (Jongerijs and others, 1984).

A recent research (Dalla Costa and others, 2007) which is a follow up of (Dalla Costa and others, 2005) suggests a measuring method to determine the threshold value of the voltage ripple which can excite acoustic resonance in low wattage MH lamps. According to the proposed method, the existence of the acoustic resonance is detected using a photodiode and calculation of light flicker. The output signal of the photodiode is filtered with an 8th order low-pass Butterworth filter with a cut off frequency of 70Hz. The ratio of the peak to peak voltage to its steady value (when there is no AR) of this sensor circuit is defined as the light flicker.

To obtain a quantitative parameter which shows the existence and strength of the acoustic resonance is essential to determine the threshold level of the power ripple. Existing literature, as it was mentioned above, does not introduce a precise quantity for this application. This chapter proposes an experimental method based on the perceptibility of the human eye to the light transients and the so called light flicker factor as a quantitative measure in this regard.

To get a better understanding of the problem, firstly, a common topology of LFSW ballasts which are widely used to supply HID lamps is explained. Afterwards, some methods which are used to reduce the high frequency power ripple of such ballasts, based on existing literature, are discussed. The experimental method which is especially arranged to measure the allowed level of the power ripple of low wattage metal halide lamps then is described in detail. Finally the results of the experiment are discussed and the proposed approach of this work is compared with the method introduced in (Olsen and Moskowitz, 1997).

4.2 HID Ballast Topology (LFSW)

In this section some different circuitries which are used to supply the lamp with low frequency square waveform current is introduced. We start with a typical ballast topology and the functionality of each block in ballast will then be described. The origin of the high frequency ripple which is superimposed on the current/voltage waveform of the lamp in LFSW ballast is discussed. This part will be continued by introducing some methods by which the ripple of the lamp power is attenuated or existence of such ripples can not excite acoustic resonances in the lamp.

4.2.1 Functionality of Different Blocks in a LFSW Ballast

A typical HID ballast performs eight basic functions Fig. 4.1. An *electromagnetic interference (EMI) filter* in the first stage blocks ballast-generated noise. A *full-wave rectifier* provides high voltage (up to 400 V) bus voltage. A *power factor correction (PFC)* circuit ensures that the input current to the ballast remains sinusoidal and in-phase with the input voltage. A *buck converter* controls the current delivered to the lamp. A *full bridge inverter* converts the dc voltage of buck converter to the ac lamp drive. An *ignition circuit* strikes the lamp to make a conductive channel in the lamp's arc tube and start the lamp. A *control circuitry* manages each stage and finally a *protection circuitry* deactivates the ballast in the event of a lamp or ballast fault condition. The functionality of each stage is explained in the following section.

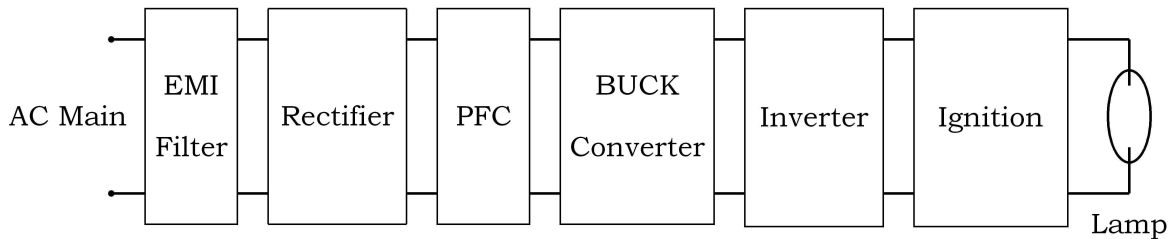


Figure 4.1: Block diagram of a low frequency square wave ballast

EMI Filter, Full-wave Rectifier and Boost PFC

EMI filter, rectifier and boost PFC as shown in Fig. 4.2, are used to output a constant voltage, typically 400 Vdc, while drawing a sinusoidal current from the main line. As long as these three stages work closely together their functionality is described conjointly in this section.

I. Circuitry and Topology

The ac main voltage is rectified by a full-wave rectifier. The rectified voltage is applied to the input of the boost converter. The transistor M_1 works as a switch which is turned on and off by a pulse-width-modulated control voltage. When the PFC switch M_1 turns on, the voltage across the boost inductor, L_{boost} , is equal to V_{in} (instantaneous input voltage to PFC module) and its current ramps up linearly to a peak value. At this moment, switch M_1 turns off and the inductor current backs down to zero. When the current reaches zero M_1 turns on again and this cycle repeats itself. In this way the converter works in a *critical conduction mode*. The reason of selecting this mode will be discussed later in this section. When M_1 is off, the current of the boost inductor flows through the boost diode, D_{boost} and charges the output capacitor C_{boost} .

More precisely, when the power switch M_1 is ON, the input voltage is applied across the boost inductor. The inductor current linearly increases with a V_{in}/L_{boost} slope. During the OFF phase of M_1 , the boost inductor voltage is $(V_{out} - V_{in})$ and the inductor current linearly decays with a $(V_{out} - V_{in})/L_{boost}$ slope. The result is a triangular current waveform which flows through L_{boost} during each ON-OFF phase of the boost switch. Since the input voltage to the boost converter, V_{in} , is sinusoidal (which is rectified), the current waveform contains of triangles with a sinusoidal envelop (Fig. 4.3). During the ON phase, the conductor current is

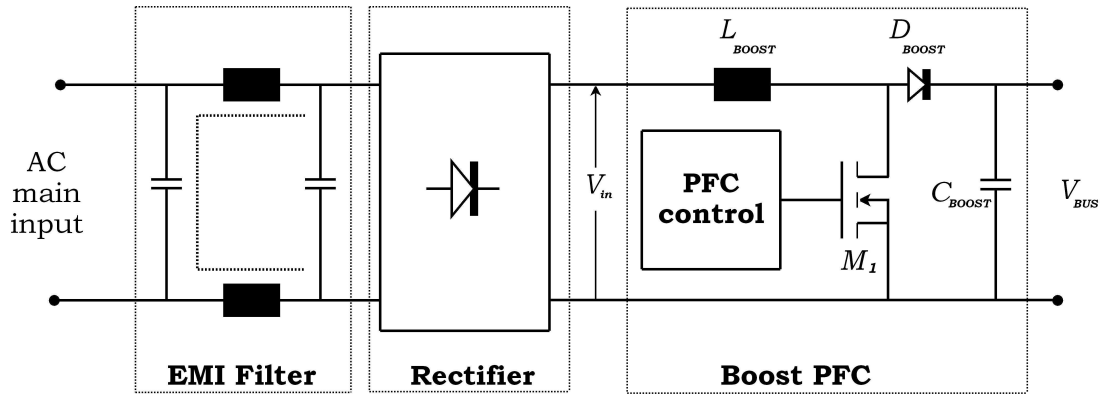


Figure 4.2: Combination of EMI filter, full wave rectifier and boost PFC to convert the ac main voltage to a constant level bus voltage.

proportional to V_{in} , therefore when the ON time of the power switch is kept constant, peak values of triangles follow the instantaneous value of the input voltage. The parameter which determines the ON time duration of M_1 is the amount of current necessary to keep the dc bus regulated at a given load power. The OFF time of M_1 is adjusted in such a way that the conductor current reaches zero at the end of each OFF time period. At the beginning and end of each input voltage cycle, the instantaneous value of voltage is low this results in lower peak value of conductor current. In the middle part of the input voltage cycle, where it reaches its maximum value, the conductor current reaches higher values (as long as the ON time duration is constant). To get a sinusoidal envelop for conductor current, and satisfying the condition of critical conductance mode, the OFF time of the power switch should be adjusted in such a way that its current reaches zero at the end of each OFF cycle. Since the frequency of switching is not constant this method is called free-running frequency.

When this current passes through the EMI filter it is then smoothed and the current waveform which is seen by the network is sinusoidal as well and is in-phase with the voltage (Fig. 4.4). The result is a power factor of about unity and very low high frequency ballast generated current harmonics. As can be seen in Fig. 4.2, the filter is a standard differential mode filter. The effect of capacitors is to tend to ‘short-out’ voltages at high (interference) frequencies. On the other hand, chokes offer a high impedance (resistance) at these frequencies.

II. Output Voltage Ripple

The output voltage over C_{boost} capacitor shows two ripples. The first one is the high frequency ripples which results from the way the output is supplied by current pulses. Since the output capacitor has a parasitic series resistor (ESR), it can not fully filter the pulsed energy source.

During the ON time, the power switch conducts and no energy is provided to the output. The output capacitor feeds the load and the product of the load current and the ESR of the capacitor forms a negative voltage. As a result the capacitor is discharged and the output voltage drops. During the OFF time, the diode drives the conductor current toward the output. The inductor current then is divided between load and output capacitor. In this case the direction of the capacitor’s current is changed (in comparison with the ON time) and the product of this current and ESR of capacitor is a positive voltage which charges the capacitor

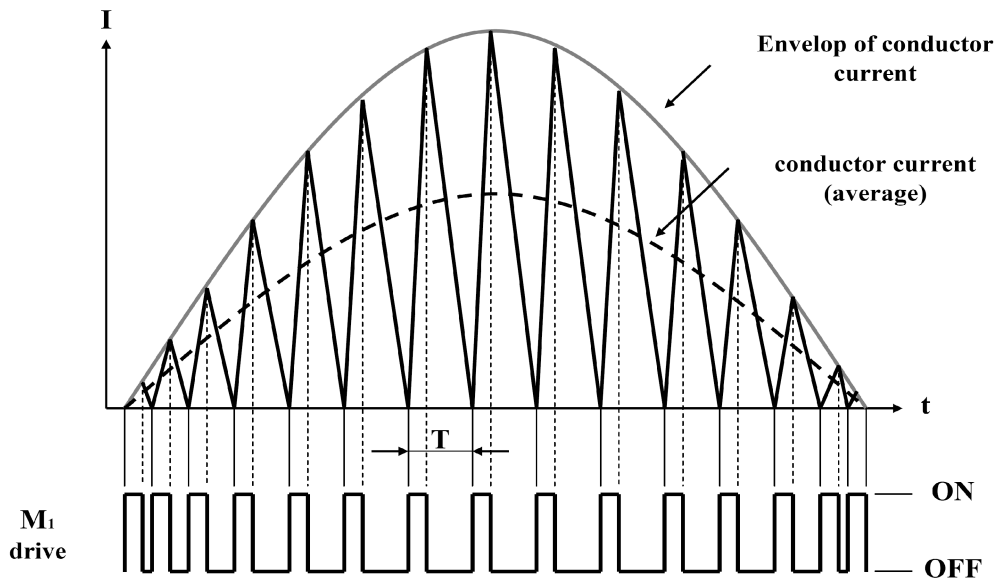


Figure 4.3: PFC conductor current in a half period of AC main line. Triangles show the current of conductor in each ON-OFF cycle (period of T and in a free-running frequency mode) of power switch. Corresponding drive to control the power switch is sketched in the lower part of graph. ON-time is always constant and OFF-time varies with instantaneous value of voltage. It should be noted that in this graph, as a task of simplicity for drawing, only a few switching cycles are shown which are not scaled with respect to the time axis. In a real case the switching frequency is much higher than the main line frequency.

and the output voltage ramps up.

The second ripple is an additional low frequency ripple which is inherent to the power factor correction. The input voltage and current waveform are sinusoidal; the power drawn by PFC stage is a squared sinusoid. On the other hand the load draws a constant power. Therefore, PFC delivers an amount of power which is equal to the load demand average value. Again the output capacitor plays a significant role, when the input energy exceeds the load demand, it is stored in the capacitor and during the time that the input energy is less than load demand the capacitor supplies it. This process is illustrated by Fig. 4.5.

III. Critical Conductance Mode

As formerly explained, PFC is designed to work in critical conductance mode. Considering a dc input current there are three modes of operations considerable for a boost converter.

1. For $\Delta I_L < 2 I_{in}$ the current of the boost inductor in both ON time and OFF time of the power switch is continuous and the converter is in continuous mode.
2. For $\Delta I_L > 2 I_{in}$ the current of the boost inductor during OFF time of the power switch goes to zero and stays at zero up to starting of ON time. Consequently the inductor current is discontinuous and converter operates in discontinuous mode.

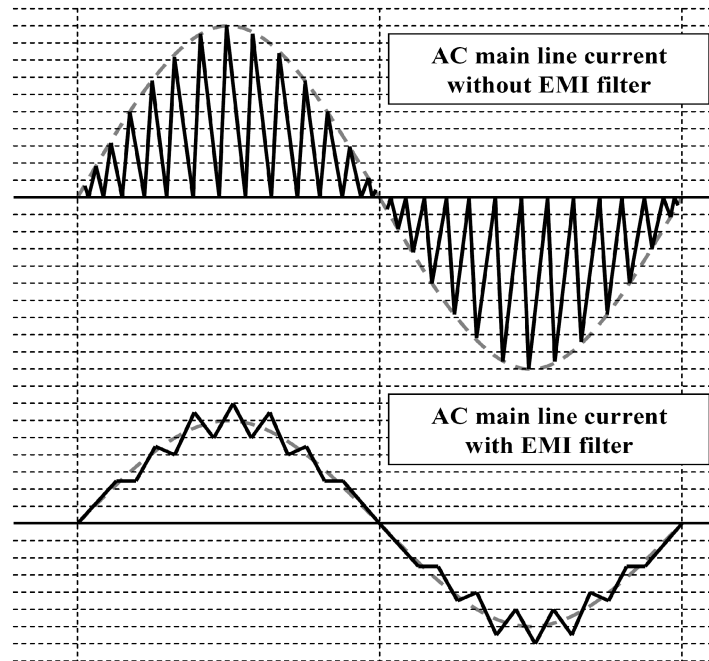


Figure 4.4: Effect of EMI filter on AC main line current.

3. If $\Delta I_L = 2 I_{in}$ the inductor current ramps up to twice the desired average value, ramps down to zero, then immediately ramps positive again. This mode of operation is called critical conduction mode or border line conduction mode.

Regarding (Ribarich, 2006) critical conduction mode is the most popular solution and standard topology for low power (below 100 W) applications. This value is pointed out by (Turchi, 2003) to be below 300 W.

(Turchi, 2003) summarizes the advantages of this mode of operation as follows :

1. *Simple Control Scheme*: The application requires few external components.
2. *Ease of Stabilization*: The boost keeps a first order converter and there is no need for ramp compensation.
3. *Zero Current Turn On*: One major benefit of critical conduction mode is the power switch turn on when the diode current reaches zero. Therefore the power switch on is lossless and soft and there is no need for a low reverse recovery time diode.

On the other hand, the critical conduction mode has some disadvantages:

1. Large peak currents that result in high $\frac{di}{dt}$ and RMS currents conducted throughout the PFC stage.
2. Large switching frequency variations.

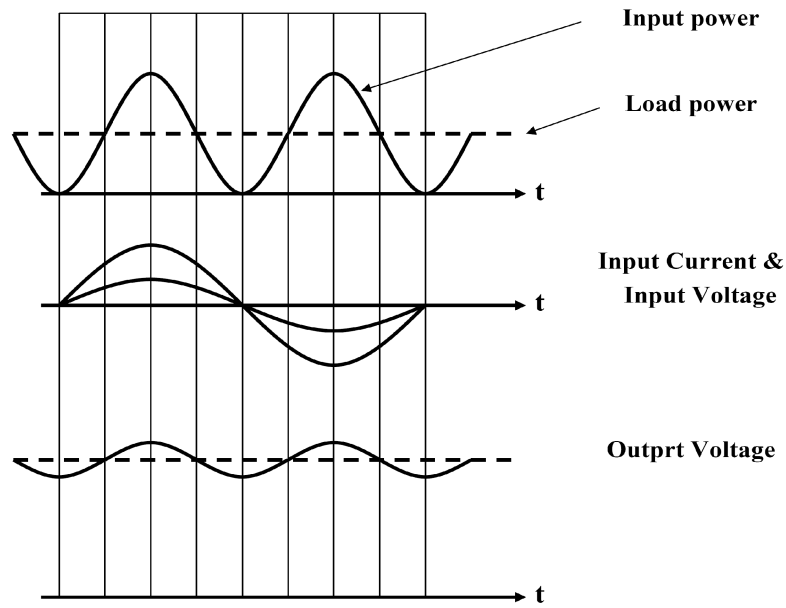


Figure 4.5: Low frequency ripple on the output voltage.

Buck Converter

As it is mentioned in previous section the output voltage of the PFC module is a constant dc voltage with the value of about 400 V which performs the dc bus voltage. The buck converter steps down this voltage to supply the lamp with the proper voltage regarding its different operation phases. In fact this stage controls the current delivered to the lamp and works as a controllable current source. Since this converter steps down the input voltage is called down-converter as well. The downconverter device serves as a current source, the output voltage of such converters being determined by impedance of a load connected to its output (Couwenberg and others, 2007). Fig. 4.6. schematically sketches the circuitry of a buck converter.

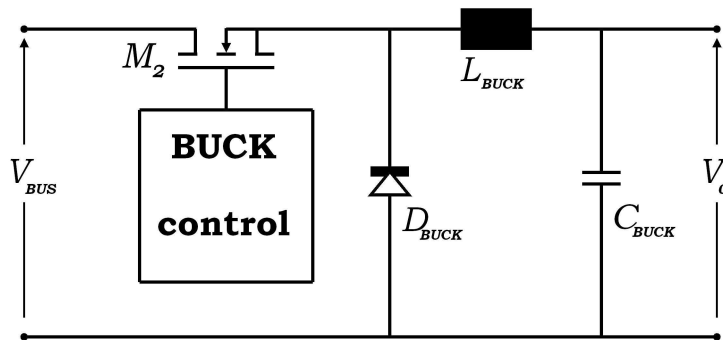


Figure 4.6: Schematic diagram of a buck converter.

When M_2 turns on current flows from dc bus through the buck inductor L_{buck} to the load (lamp). During ON time the current of the buck inductor increases linearly as it supplies load current. The reason is that the voltage over the buck inductor is a positive value since the

output voltage of the buck converter is lower than its input which is dc bus voltage. In contrast to the buck inductor, the current of the buck capacitor C_{buck} , may be in either direction, depending on the inductor current and the load current. When the inductor current rises, the energy stored in it increases. During this state, the inductor acquires energy. The equations that govern the operation of the circuit in the ON-time state are

$$\frac{di_{L_{buck}}}{dt} = \frac{V_{bus} - V_o}{L_{buck}} \quad (4.1)$$

$$\frac{dV_o}{dt} = \frac{i_{L_{buck}} - \frac{V_o}{R}}{C_{buck}} \quad (4.2)$$

where V_o is the output voltage of the buck converter and R is the ohmic load. When the ON time ends, the buck power switch turns off and load current continues to flow through the buck diode, D_{buck} , (free-wheels) and the buck inductor. The current of the inductor decreases linearly during the OFF time. In this state, the inductor discharges its energy and the capacitor current may be in either direction, depending on the inductor current and the load current.

In this state the governing equations are

$$\frac{di_{L_{buck}}}{dt} = \frac{-V_o}{L_{buck}} \quad (4.3)$$

$$\frac{dV_o}{dt} = \frac{i_{L_{buck}} - \frac{V_o}{R}}{C_{buck}} \quad (4.4)$$

When the switch is open, the inductor discharges its energy. When it has discharged all its energy, its current falls to zero and tends to reverse, but the diode blocks conduction in the reverse direction. During this state, the capacitor discharges its energy and the inductor is at rest, with no energy stored in it. The inductor does not acquire energy or discharge energy in this state. For this case the governing equation is

$$\frac{dV_o}{dt} = \frac{-\frac{V_o}{R}}{C_{buck}} \quad (4.5)$$

A buck converter operates in continuous mode if the current through the inductor never falls to zero during the commutation cycle. In some cases, the amount of energy required by the load is small enough to be transferred in a time lower than the whole commutation period. In this case, the current through the inductor falls to zero during part of the period. The only difference is that the inductor is completely discharged at the end of the commutation cycle.

I. Output Voltage Ripple of Buck Converter

The output voltage ripple of the buck converter is the main source of high frequency components in the lamp power spectrum. Such ripples are called switching ripple as they are generated due to switching of the current. As it is explained in the previous chapter such ripples may excite acoustic resonances in HID lamps. In this section the voltage ripple which is generated by buck stage is discussed in detail. The combination of the load resistance R (input impedance of the inverter circuit as is shown in Fig. 4.1) and the filter capacitor C_{buck} of the buck converter introduces a time constant of RC_{buck} .

The ripple calculation is carried out for two different states with respect to this time constant. If the RC_{buck} time constant is very large, compared to the cycle period of the switching frequency, the output voltage can be assumed to be constant. In this case the voltage ripple value is not noticeable. When both the input voltage and the output voltage are constant, the current through the inductor rises linearly when the switch is ON and it falls linearly when the switch is OFF. Under this condition, the current through the capacitor also varies linearly when it is getting charged or discharged. Operation of the buck converter under the above mentioned condition is shown in Fig. 4.7.

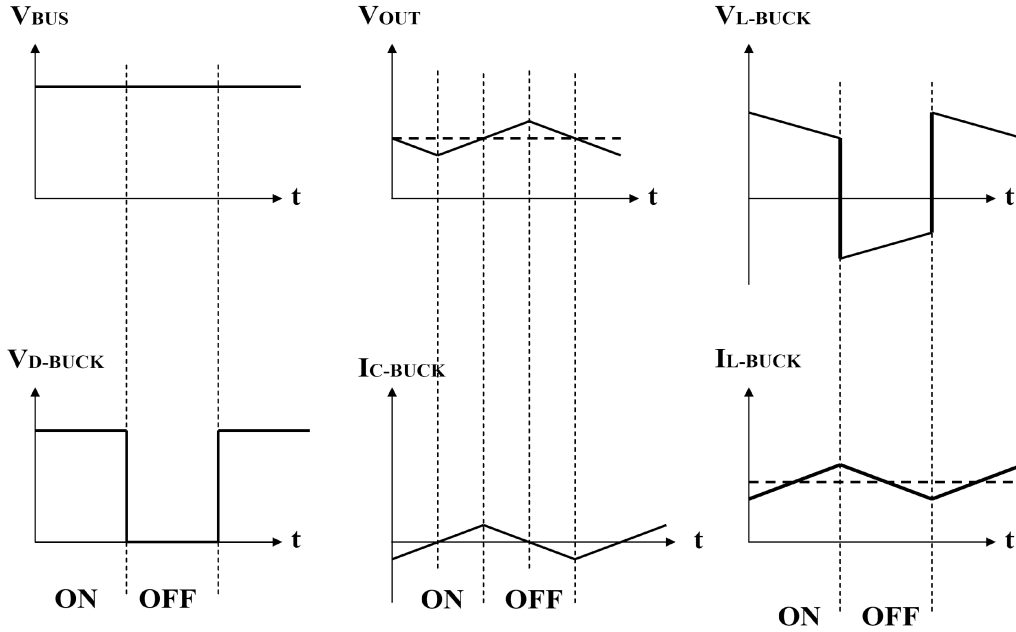


Figure 4.7: Operation of a buck converter with low time constant RC_{buck} . Dashed lines in V_{out} and I_{L-buck} show the average values of output voltage and buck inductor current respectively. It should be pointed out that for sake of clarity the value of ΔI and ΔV are exaggerated.

For a continuous mode operation of buck converter the average output voltage is calculated as

$$V_{o,avg} = \frac{1}{T} \int_0^{DT} V_{bus} dt = D \cdot V_{bus} \quad (4.6)$$

where T is the switching period and D is the duty cycle of switching. The duty cycle is defined as the ratio of the ON-time to the switching period. When the switch is ON, the change in inductor current can be calculated as follows. Let the change in inductor current be ΔI_{L-buck} , as shown in Fig. 4.8. During the ON-time, the voltage across the inductor can be expressed as

$$v_{L-buck}(t) = L_{buck} \frac{di_{L-buck}}{dt} = V_{bus} - V_{out} \quad (4.7)$$

When the output voltage remains steady at $V_{out,avg}$, the inductor current linearly increases during the ON-time period of the power switch. Therefore

$$\Delta I_{L-buck} = \frac{V_{bus} - V_{out,avg}}{L_{buck}} \cdot DT = \frac{D(V_{bus} - V_{out,avg})}{fL_{buck}} \quad (4.8)$$

where $f = \frac{1}{T}$ is switching frequency of the power switch. If the impedance of C_{buck} at the switching frequency is much lower than the load impedance (input impedance of the inverter circuit) then almost all ripple current flows through the capacitor. As a result the current of the capacitor would be equal to the buck inductor current with the dc component removed. That means

$$\Delta I_{C-buck} = \Delta I_{L-buck} = \frac{D(V_{bus} - V_{out,avg})}{fL_{buck}} \quad (4.9)$$

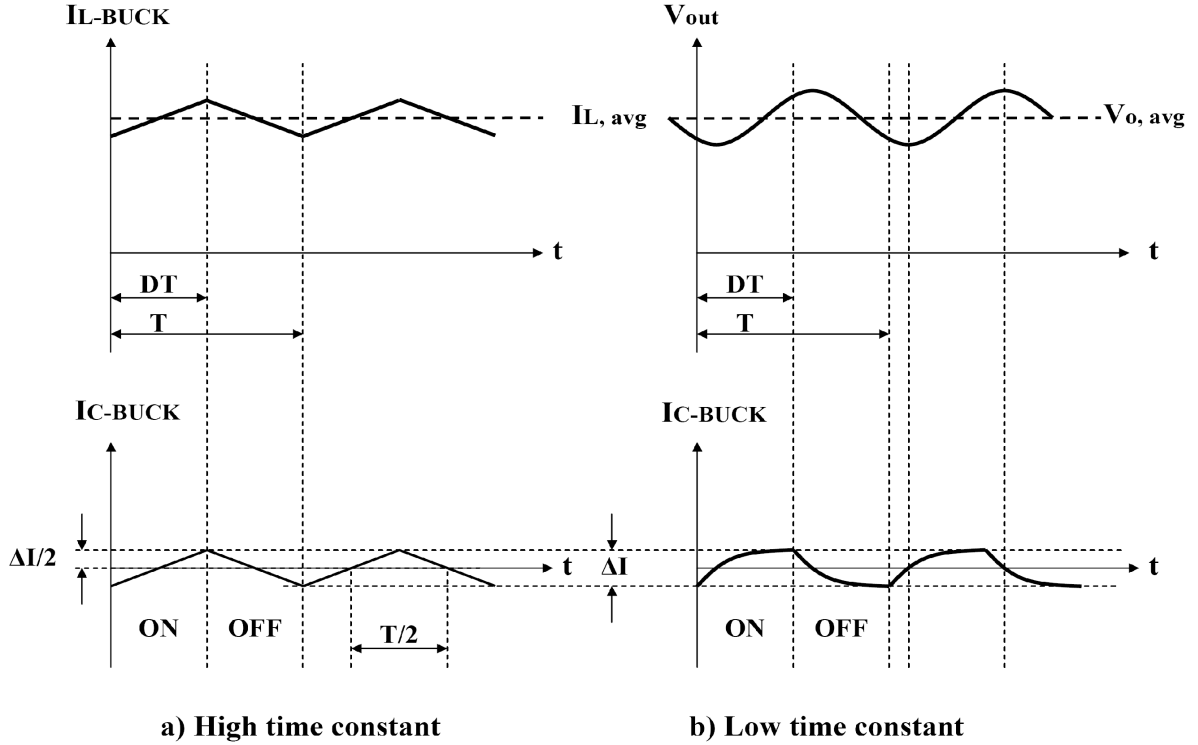


Figure 4.8: a) Linear change of buck inductor current and buck capacitor current under assumption of high time constant. The capacitor current is just the ac part of the inductor current. It is actually assumed that the capacitor is getting charged and discharged during ON and OFF periods respectively. b) Exponential change of buck inductor current and buck capacitor current when the buck converter operates under low time constant condition. The result of a low time constant is a sinusoidal voltage ripple.

For a periodic signal with zero dc value the average is defined based only on its positive portion. Hence, the average value of the buck capacitor current is defined as

$$I_{C-buck,avg} = \frac{1}{4} \cdot \Delta I_{C-buck} \quad (4.10)$$

Regarding Fig. 4.8, the current of the buck capacitor is a triangular waveform during each half period, $\frac{T}{2}$. For a capacitor the relationship between capacity, voltage, total charge, current and the time is written as

$$q = CV = i \cdot t \quad (4.11)$$

Combining (4.10) and (4.11) results in

$$\Delta V_{C-buck} = \frac{I_{C,avg} \cdot (T/2)}{C_{buck}} = \frac{(\Delta I_C) \cdot T}{8C_{buck}} = \frac{\Delta I_c}{8f C_{buck}} \quad (4.12)$$

Using equation (4.9) the voltage ripple is rewritten as

$$\Delta V_{C-buck} = \frac{D \cdot (V_{bus} - V_{o,avg})}{8f^2 L_{buck} C_{buck}} \quad (4.13)$$

As it is pointed out, the linear changes of inductor and capacitor current requires a very large time constant, RC_{buck} , of buck converter. Under the assumption of low time constant, these current waveforms changes show an exponential behavior with negative exponent. The result is that the voltage ripple appears to be sinusoidal. Under this assumption and considering the equation (4.13) as the peak to peak value, the RMS value of the voltage ripple is calculated as follows.

$$V_{rms,ripple} = \frac{D \cdot (V_{bus} - V_{o,avg})}{16\sqrt{2} f^2 L_{buck} C_{buck}} \quad (4.14)$$

II. Minimization of the Ripple

Output voltage ripple is one of the disadvantages of a switching power supply, and can also be a measure of its quality. In this section some considerations with respect to the design of the buck converter and also using additional filter to attenuate the output ripple will be discussed.

A. Ripple Reduction Based On Circuitry Design

Regarding (4.14) the ripple decreases by increasing

- The switching frequency
- Buck inductor
- Buck capacitor

and by decreasing

- The duty cycle
- The difference between input and output voltages.

Switching frequency selection is typically determined based on efficiency requirements, which tends to decrease at higher operating frequencies. Higher switching frequency can also reduce efficiency and possibly raise EMI concerns. The higher the chosen value of the switching frequency f , the smaller the size of the inductor. However the switching losses of the transistor also become larger as f increases.

A large inductor results in a physically larger and heavier inductor which is a disadvantage and furthermore makes the ballast more expensive. It is worth to recall that the output capacitor is chosen such that it provides significant filtering of the switching ripple. The selected

capacitor must be large enough so that its impedance is much smaller than the load at the switching frequency, allowing most of the ripple current to flow through the capacitor, not the load. The output capacitor's ESR must also be taken into account because this parasitic resistance, which is out of phase with its capacitance, will cause additional voltage ripple. Capacitor selection is normally determined based on cost, physical size and non-idealities of various capacitor types.

Two other parameters i.e. the duty cycle and the difference between input and output voltage can not be changed freely. The duty cycle is used to regulate the current of the lamp and is changed by the buck control unit for this task. The required breakdown and starting potential is always higher than the normal operation potential (Lister and others 2004). Therefore, the input voltage should be kept constant at about 400 V as the open circuit voltage of the ballast. This ensures that the voltage which is applied to the lamp is sufficient in order to safely start it. On the other hand the lamp voltage in the steady state operation and at nominal power is relatively constant at about 80-100 V depending upon the lamp type. This means that the output voltage of the buck converter is determined by the lamp and not the buck controller.

In addition, the input voltage of the buck converter is provided by the boost converter which increases the ac main voltage (with a peak value of 325 V). Hence, the input voltage of the buck converter is always higher than 325 V and it is not possible to get a dc bus voltage below this value. As a result, neither the input voltage nor the output voltage of the buck converter can be changed in order to reduce the voltage ripple.

B. Ripple Reduction Using Coupled Inductors Filter

(Balog and others, 2000) explains the principle of operation of the couple inductor filter. Fig. 4.9 illustrates a schematic diagram of this filter. Consider the input as dc component (V_{DC}) which is superimposed with a high frequency ac ripple (V_{ac}). Two inductors are coupled via a magnetic core and form a smoothing choke. The first winding which connects the input to the output is labeled L_{DC} and the other one which is connected to the dc blocking capacitor C_{ac} is labeled L_{ac} to indicate their purpose in the circuit. If C_{ac} is large then the ac voltage (V_{ac}) across it due to ripple current is zero. In other words the capacitor is short circuit for high frequency ripples. As a result the capacitor is charged up to V_{DC} without ac component. Applying KVL, the ripple voltage, V_{ac} appears across the inductor L_{ac} . Assuming perfect coupling between two windings and a one to one winding ratio, the ac ripple voltage across L_{ac} will transfer to the L_{DC} winding. Now applying KVL on the output of the filter confirms that the output voltage is only the dc component.

Thus, the coupled inductor serves as a 'signal transformer' for ripple current steering and at the same time as an 'energy storage element' for the switching power supply (Balog and others, 2000). These two properties make the coupled inductors a novel solution for the ripple problem of the buck converter. The idea is to replace the buck inductor L_{buck} with coupled inductors. Fig. 4.10 shows the modified buck converter topology which benefits from this filter construction.

In an example in (Balog and others, 2000) it is shown that using coupled inductors topology in buck converter can attenuate the ripple value practically up to 4.6 db comparing with the standard buck topology. The theoretical calculated value is 5 db. There are some considerations regarding the proper use of this filter.

The filter transfer function for ideal circuit components (Balog and others, 2000) is

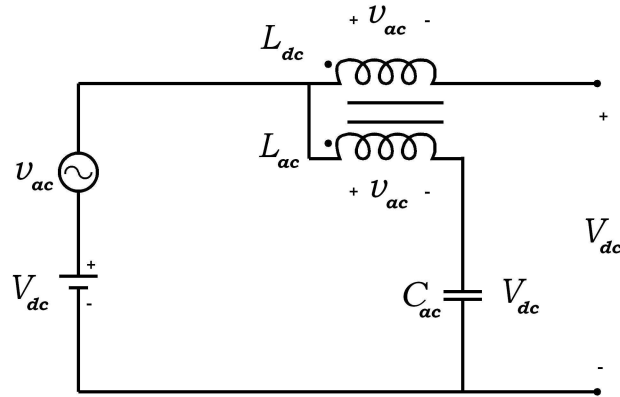


Figure 4.9: Coupled inductors filter.

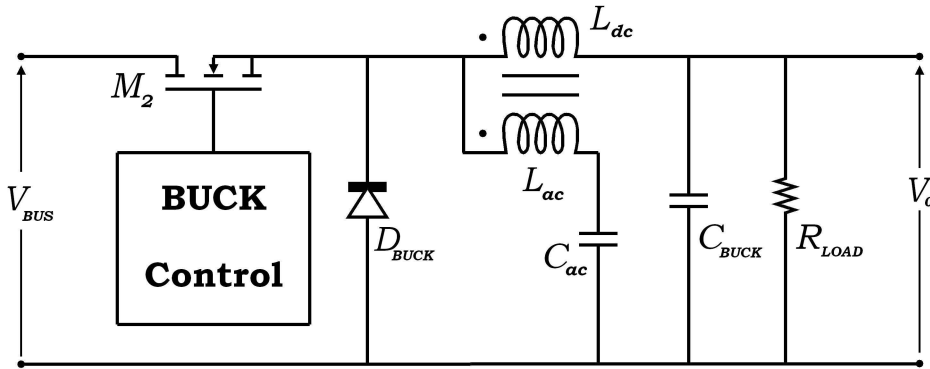


Figure 4.10: Schematic diagram of a buck converter with coupled inductor construction.

$$\frac{V_o}{V_{in}} = \frac{1 + s^2 C_{ac} L_{ac} \left(1 - k \sqrt{\frac{L_{dc}}{L_{ac}}}\right)}{1 + s^2 (C_{ac} L_{ac} + C_{dc} L_{dc}) + s^4 C_{ac} C_{dc} L_{ac} L_{dc} (1 - k^2)} \quad (4.15)$$

where $0 < k < 1$ is the coupling coefficient of two windings of the filter. According to (4.15) this is a fourth order filter which is realized only with three components which is a benefit of this arrangement.

If C_{ac} is by passed, the filter changes to a second order filter with L_{dc} and C_{dc} elements. In this case the circuit becomes the standard buck converter again. The pole and zero locations of the filter transfer function depends on the value of the coupling coefficient, k . There is a value k_{null} which causes the infinite frequency gain equal to zero.

$$k_{null} = \sqrt{\frac{L_{ac}}{L_{dc}}} \quad (4.16)$$

- By selecting $k = k_{null}$ the filter shows its steepest attenuation for higher frequencies since the filter slope is then governed by four poles and rolls off at the -80 db/decade.

When $k = k_{null}$ then the filter reacts as a fourth order lowpass filter and this mode is called *null condition*.

- For $k > k_{null}$ the filter frequency response at high frequencies is flat and there is no significant attenuation, which makes the filter useless.
- For k values less than k_{null} there is the appearance of frequency notch and this mode is called *notch mode*.

At high frequencies the effect of L_{dc} and C_{dc} pole is dominates and filter slope rolls off at -40 db/decade. If the frequency of the notch can be arbitrarily designed, then the coupled inductor can yield better results than the simple second order circuit, while using the same magnetic volume (Balog and others, 2000). This means it is desired to set the notch frequency of the filter equal to the switching frequency of the power switch.

It is important to note that there is a frequency peak below the notch frequency; if the switching frequency of the buck power switch varies then proximity of the peak may deteriorate the performance of the filter. Practically the value of k is set below k_{null} but very close to it to satisfy the notch mode condition and to bring the transfer function closer to the fourth order filter. This will satisfy the condition of good attenuation at high frequencies (above notch frequency). The disadvantage of this approach is that the design is extremely sensitive to the value of k . The reason of this sensitivity can be explained by considering the notch frequency of the filter (Balog and Krein, 2002)

$$\omega_{notch} = \frac{1}{\sqrt{C_{ac}L_{ac} \left(1 - k\sqrt{\frac{L_{dc}}{L_{ac}}}\right)}} \quad (4.17)$$

It should be noted that (4.17) gives the notch frequency of the filter neglecting C_{dc} . As it is mentioned, the value of k should be set very close to k_{null} , hence the term $\left(1 - k\sqrt{\frac{L_{dc}}{L_{ac}}}\right)$ would be a small value. As a result the notch frequency is extremely sensitive to changes of k , L_{dc} and L_{ac} . The other point to be considered about this filter is the effect of ESR of components. It is shown (Balog and others, 2000) that existence of parasitic resistance leads to elimination of the frequency notch. This effect can be reduced by changing the winding ratio of two windings of the coupled inductor. As it is reported in (Balog and others, 2000) increasing the number of turns in L_{ac} (1:5) leads to a 15 db notch with respect to the simple second order filter. The result is that the value of inductor increases with a factor of 25. However this means a larger inductor which is heavier as well. On the other hand the value of C_{ac} should be decreased with a factor of 25 to get the same $L_{ac} - C_{ac}$ resonant frequency.

In above mentioned paper a buck converter with switching frequency of 50 kHz is experimented with simple second order filter and with coupled inductors technique. The former shows a 50 kHz ripple with a peak to peak amplitude of 90 mV. The output voltage of the latter shows the elimination of 50 kHz. However there are other harmonics (higher frequencies) in the output voltage with the same or even larger amplitude.

4.2.2 Full Bridge Inverter and Ignition Stage

The output voltage of the buck converter is a regulated dc voltage. Since HID lamps are supposed to be operated with alternative current the buck stage output voltage, before applying to the lamp should be inverted. This stage (Fig. 4.11) inverts the input dc voltage to a low frequency square waveform. The top of the full bridge circuit connects to the buck output voltage and the two half-bridge midpoints oscillate 180 degrees out of phase from each other to produce the necessary ac voltage.

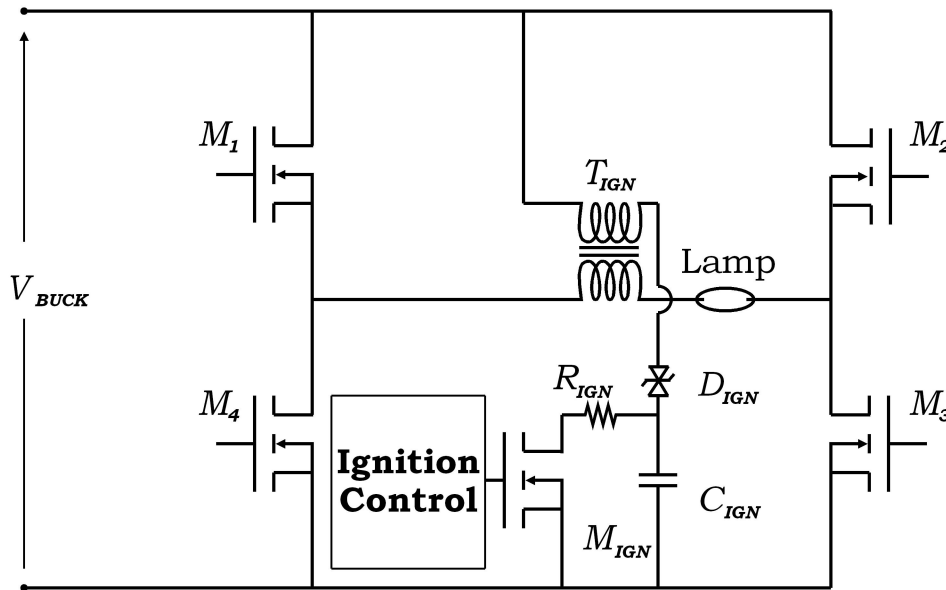


Figure 4.11: Full bridge and ignition circuitry.

The ignition circuit which is shown in Fig. 4.11 ignites the lamp with high voltage ignition pulses. During the ignition phase, the lamp is an open circuit and the buck output voltage is limited to a maximum value (typically 400 V). The ignition circuit contains a diac (D_{IGN}), transformer (T_{IGN}), capacitor (C_{IGN}), resistor (R_{IGN}) and switch (M_{IGN}). At the beginning C_{IGN} is charged with the voltage of the buck capacitor or V_{BUS} . When the ignition controller turns on switch M_{IGN} , capacitor C_{IGN} discharges through resistor R_{IGN} . This leads to a reduction of the ignition capacitor voltage and subsequently the voltage across the diac drops to its on-threshold value. When the diac turns on, a current pulse flows from the buck output through the primary winding of the ignition transformer and into C_{IGN} . This arrangement generates a high voltage pulse on the secondary of the transformer to ignite the lamp. The capacitor C_{IGN} charges up until the diac voltage reaches the off-threshold value and turns off. C_{IGN} discharges through the resistor R_{IGN} until the diac turns on again and another ignition pulse occurs. When the lamp ignites, the buck output voltage decreases quickly to the lamp voltage (typically 20 V) as the converter provides the lamp current necessary to keep the lamp on. The ignition controller disables the pulses by switching M_{IGN} off.

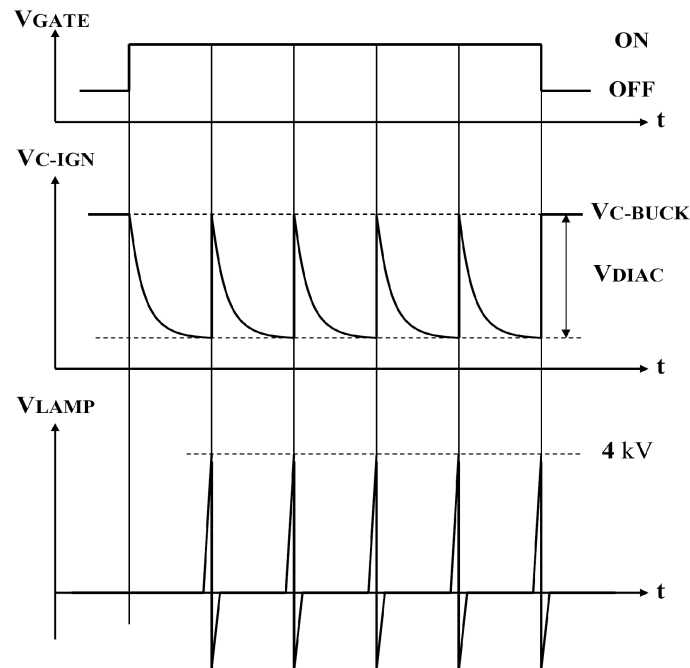


Figure 4.12: The HID ignition circuit produces high-voltage pulses that are discontinued once the ballast circuit detects the lamp has ignited.

4.2.3 Full Bridge Two-Stage Driver Topology

In a two stage topology the buck converter and the inverter circuit are integrated. A topology of an LFSW ballast of this type is proposed in (Faehnrich and Rasch, 1988). The ballast contains two inverters, one operating at 30 kHz and the second operates at 270 Hz. The first inverter which has a half bridge configuration limits the lamp current and the second one changes the polarity of the lamp current to avoid cathaphoretic effect. The output of the first inverter is rectified and smoothed to reduce any HF ripple. The proposed low frequency ballast in (Nishimura and others, 1988) uses a voltage doubler rectifier to produce a 282 V bus voltage from the main 100 V, ac 50/60 Hz.

As it is illustrated in Fig. 4.13, the lamp is supplied through a full bridge circuit. The switching frequency of Q_1 and Q_2 is 42 kHz and Q_3 and Q_4 are switched with the low frequency of 120 Hz. When Q_3 is ON, Q_4 and Q_2 are OFF and Q_1 is switched with the high frequency of 42 kHz. During the second half cycle, Q_4 is ON, Q_1 and Q_3 are OFF and Q_2 is switched with the high frequency. In this way the polarity of the lamp current is changed with the low frequency, and lamp voltage/current is regulated with high frequency switching simultaneously. As a result of high frequency switching of Q_1 and Q_2 , the current waveform flowing L_1 is a high frequency triangle waveform between zero and a positive peak in one half cycle and a negative peak in the second half cycle. The capacitor C_1 which is parallel with the lamp and ignition circuit is used to filter the high frequency ripples of L_1 current. As a result the lamp current waveform is a square wave which is superimposed with a high frequency ripple. It should be noted that the capacity of the parallel capacitor can not exceed a given value. Otherwise many high frequency components of the current will flow through the capacitor and the lamp current can not be a square waveform with sufficiently sharp edges any more.

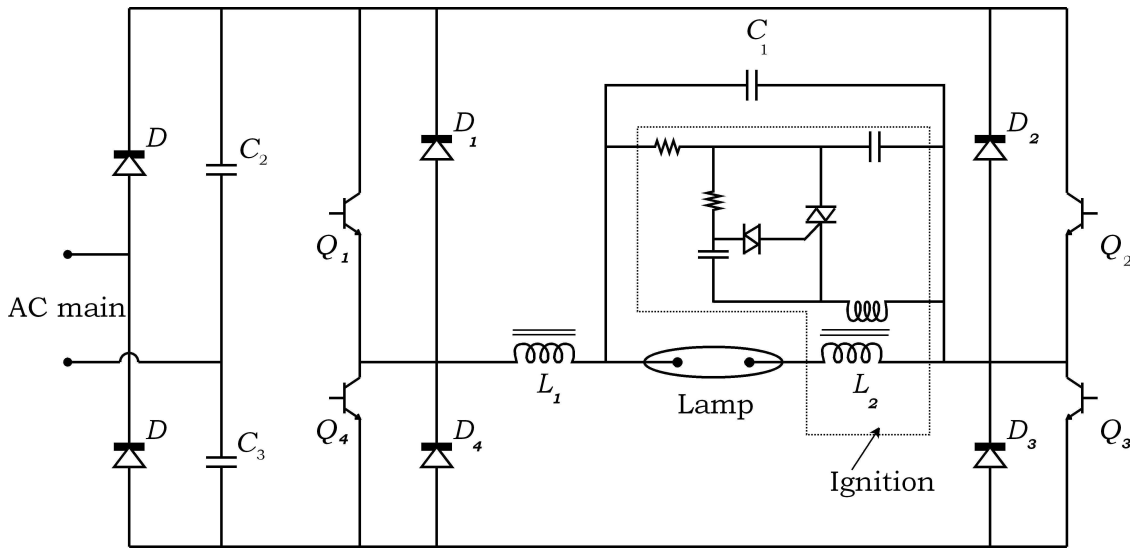


Figure 4.13: LFSW ballast topology proposed in (Nishimura and others, 1988).

4.2.4 Three-Stage Driver Topology

Based on (Faehnrich and Rasch, 1988; Nishimura and others, 1988) another low frequency ballast is designed and reported in (Melis, 1998). This topology uses a high power factor pre regulator connected to a sinusoidal AC power supply and a power controlled DC current source connected to the pre-regulator. A low frequency square wave DC to AC inverter is connected to the DC current source to change the polarity of the supplied current to the lamp.

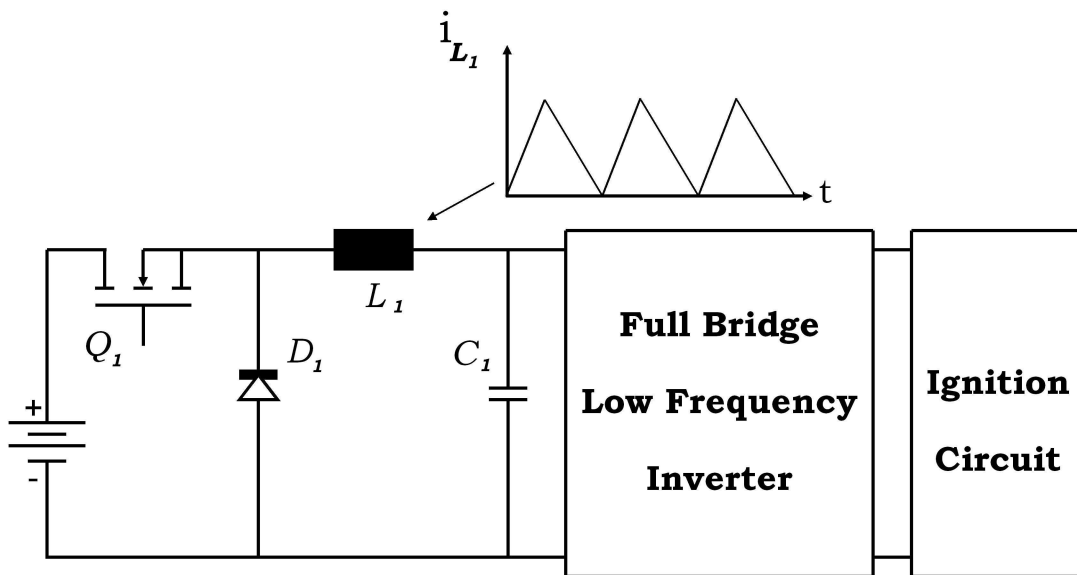


Figure 4.14: LFSW ballast topology proposed in (Melis, 1998)

Fig. 4.14 schematically shows the topology of a low frequency square wave ballast for HID lamps. The power delivered to the lamp is controlled using a buck power regulator with pulse ignition in discontinuous inductor current mode. A PWM control scheme is used to set the bus voltage of the full bridge circuit. When Q_1 is ON, the current flows through L_1 with

a positive slope and when Q_1 is OFF as long as the current of L_1 can not be switched off stepwise, D1 starts to conduct and the current of L_1 decreases. This cycle is repeated with a high frequency and as a result the current of L_1 has a large triangle ripple and therefore the bus voltage is superposed with high frequency ripple as well. This ripple can be reduced using a large capacitance C_1 in the output stage of the power supply and a small value of inductance L_1 . However, to sufficiently filter the AC high frequency current to be below an acceptable level, and to maintain discontinuous operation of the power supply, the capacitance C_1 and the inductor L_1 must be large (as it is described in previous section). The result could be a low characteristic impedance of the circuit as long as C_1 is large. The reduction of the characteristic impedance leads to other disadvantages (Sun and Goriki, 2000). Firstly, the resonant ignition method can not be used as long as the resonant voltage is approximated by the characteristic impedance multiplied by the resonant current. This means to reach a sufficiently high ignition voltage a huge resonant current is required and this is not possible due to physical restriction of the electronic components. Therefore the only way to ignite the lamp is pulse mode. The disadvantages of pulse ignition method are explained in (Maheshwari and others, 1999). Secondly, when the output capacitor is too large the switches of the full bridge circuit are loaded with a huge inrush current which can damage them. Therefore, it is necessary to compromise between the value of the output ripple and the maximum allowed inrush current. It is worth to point out that the discontinuous inductor current leads to switching efficiency as long as Q_1 is turned off only when the current passing through the inductance L_1 is zero.

4.2.5 Half Bridge Two-Stage Driver Topology

An alternative circuit for low frequency square wave with buck power regulator and high frequency resonant ignition is introduced in (Sun and Goriki, 2000) based on (US patent application No. 08/783,557). Fig. 4.15 illustrates a half bridge topology for an HID ballast. The bus voltage (V_b) is divided equally over two capacitors of Ca and Cb and therefore one lamp electrode has a constant voltage of $\frac{1}{2}V_b$. When Q_1 is ON and Q_2 is OFF the lamp current direction is from L_1 toward the lamp, and when Q_1 is OFF and Q_2 is ON the lamp current is in opposite direction. This switching is carried out in a low frequency rate. It should be noted that in the period in which Q_2 is OFF, Q_1 is switched ON and OFF with a high frequency switching rate. This is the concept of buck converter which regulates the voltage applied to L_1 and lamp due to controlling the duty cycle of Q_1 . The same is carried out during the second period for Q_2 . This arrangement leads to a very low high frequency current ripple of the inductor L_1 and the lamp current. The other advantage of this ballast topology is the possibility of implementation of the resonance ignition concept. The parallel capacitor C_1 with a small value is used for resonance ignition purpose and high frequency filtering effect is carried out approximately only by inductance L_1 .

For this reason, the low-pass filter is formed by L_1 and lamp impedance in series. The disadvantage of this filtering method is that the attenuation of higher frequencies (above the cut off frequency) is only -20 db/decade. As a result, to avoid any acoustic resonance problem, the value of L_1 should be sufficiently high which leads to a large physical size of the inductor. According to (Sun and Goriki, 2000) increasing the value of inductance L_1 , leads to an increase of the glow-to-arc transition time which is another disadvantage of this circuitry. Furthermore, due to the hard switching scheme the necessary switches and parallel freewheeling diodes are expensive and switching losses are relatively high.

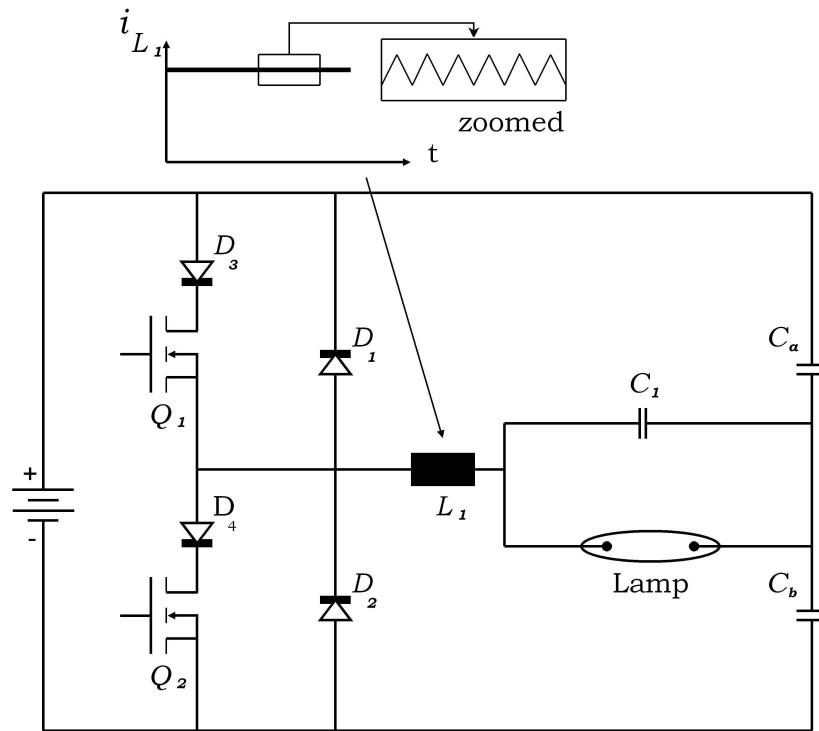


Figure 4.15: Half bridge topology for an HID ballast regarding (Sun and Goriki, 2000) based on (US patent application No. 08,783,557).

As it can be seen the generation of the high frequency current ripples in different ballast topologies due to use of buck converter is a structural characteristic. To reduce or eliminate harmful high frequency components of lamp current or power as it is explained many attempts have been carried out.

4.2.6 Integration of Buck and Boost Stages

In contrast to the above mentioned two-stage topologies, in which buck stage and inverter (full or half bridge) are combined, (Ribarich, 2007) proposes an HID ballast in which buck and boost stages are integrated. In this ballast a single buck-boost stage is used to fulfill the power factor correction and at the same time the dc bus voltage regulation tasks. The integrated circuit simplifies the design of the power converters and the ballast. Reducing part count, complexity and cost are benefits obtained in conjunction with the single stage buck-boost converter.

4.2.7 Two Stage Driver Topology with 2nd LC Stage

To overcome the above mentioned problems, (Sun and Goriki, 2000) suggests another low frequency square waveform ballast which is explained in this section. Fig. 4.16 schematically shows the structure of this buck type ballast which uses a 2nd LC stage. In ignition mode L_1 and L_2 resonate with C_2 to make high ignition voltage using high Q-factor. In this phase Q_1 and Q_2 are high frequency resonant switches that turn on and off alternatively in every half of the low frequency cycle. To avoid excessive high voltage across the first stage capacitor C_1 , the value of the characteristic impedance, $\sqrt{L_i/C_i}$, is chosen to be low for the first stage lowpass

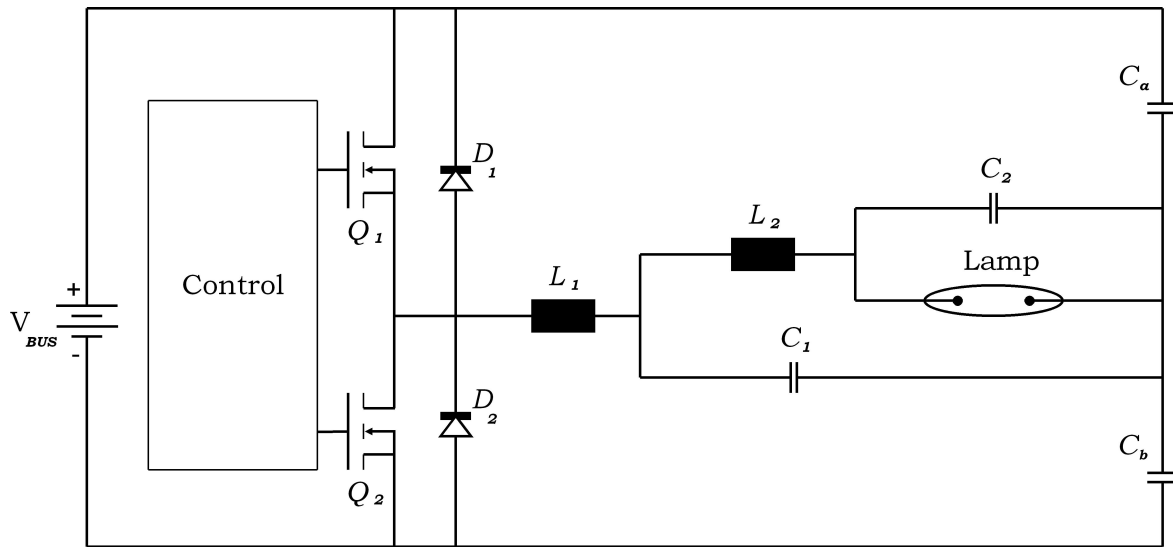


Figure 4.16: The buck type ballast using 2nd LC stage.

filter. In contrast characteristic impedance of the second stage is high to be able to ignite the lamp. In order to maximize the ignition voltage across the lamp the second stage capacitance C_2 is to be as small as possible and the second stage inductance L_2 is to be as large as possible as long as the lamp glow to arc transition time dose not deteriorate. Accordingly the first stage capacitance C_1 is higher in value than the second stage capacitance and the first stage inductance L_1 is much lower than the second stage inductance.

It is shown in (Sun and Goriki, 2000) that the ripple current of this buck converter is

$$i = \frac{v}{j2\pi f_o L_1 + (j2\pi f_o L_2 + R_{lamp}) \cdot \left(1 - \left(\frac{f_o}{f_{r1}}\right)^2\right)} \quad (4.18)$$

where f_o is the switching frequency of the power switches in normal operation, v stands for the RMS value of fundamental frequency component, R_{lamp} is the lamp impedance and f_{r1} is the resonance frequency of the first stage lowpass filter. The switching frequency in normal operation is higher than the resonant frequency of the first and the second lowpass filters. Otherwise the ripples never be suppressed with this filter. To compare this 2nd LC stage with a single stage lowpass filter one should consider $L_1 = 0$ and the term in the second parenthesis in denominator equal to unity. The result is a better attenuation in high frequency ripples. However this topology needs two separate inductors which, leads to an increase of the size and the weight of the ballast.

4.2.8 Two Stage Driver Topology with Coupled Inductors Filter

It is formerly discussed that a method to reduce the output voltage ripple of the buck converter is by using a coupled inductors filter. This method is used in (Allison and others, 1990; Cho and others, 2001). The former uses a pulse ignition method while the latter uses an internal LC resonance to ignite the lamp. Regarding (Cho and others, 2001) the lamp current ripple for a 150W ballast with a resistive load before using coupled inductors filter is about 500 mA (peak to peak) while after using this filter is reduced to about 100 mA. However, the ignition voltage

which is generated by this ballast is measured to be 1.25 kV for a CDM-TD 150W Philips lamp which is not satisfactorily high.

An important drawback of buck converters with coupled inductors filter is that the attenuation factor is highly sensitive to the frequency variation of the buck converter (Balog and others, 2000; Sun and Goriki, 2000). The reason is explained in detail when this type of filter is discussed. “It has been found both analytically and experimentally that the notch mode coupled inductors filter minimizes the output rms ripple when tuned so that switching occurs at the notch frequency “ (Balog and Krein, 2002). This paper proposes an automatic tuning technique to equalize the switching frequency of the buck converter and the notch frequency of the filter. Two methods are suggested to fulfil this task. Both methods use the ripple correlation control technique (Krein, 1999) in a feedback control system. In the first approach the aim of the control system is to adjust the switching frequency of the buck switch to minimize the difference between this parameter and the filter notch frequency. The second approach is to tune the filter notch frequency by changing the value of the filter components in such a way that the notch frequency meets the switching frequency. To be able to tune the notch frequency of the filter it is proposed to add a saturable inductor in the shunt branch of the filter.

A separate dc coil on the saturable inductor permits electrical adjustment of its inductance which tunes the notch frequency of the filter subsequently (Balog and Krein, 2002). As it can be seen the method of on-line tuning of the switching frequency or notch frequency of the filter is quite complicate and could be expensive to be implemented in electronic ballasts for low wattage HID lamps.

4.2.9 Pseudo-Random Switching Frequency

In chapter three it is discussed that a method to avoid excitation of acoustic resonance is to minimize the high frequency components in lamp power spectrum (spreading the lamp power spectrum). As it is told, this idea can be realized by several techniques of frequency modulation such as periodical, complex or white noise modulation method. The idea of spreading the power spectrum is used in (Sun, 2000) to spread the frequency spectrum of the ripple which is superimposed on the square waveform of the voltage or current in a LFSW ballast. The ballast which is used in this approach is a half bridge inverter with a single stage lowpass filter, as shown in Fig. 4.15. The only difference is the way of controlling the power switches. According to (Sun, 2000) a pseudo-random noise generator is connected to the voltage controlled PWM ramp generator to modulate the frequency of the PWM signal by pseudo-random signal. This PWM signal is used to drive the gate of two switches of inverter during normal operation of the lamp. As a result the mono-frequent ripple changes to multi-frequent ripple which reduces the power of the signal at any given frequency. In this way, it is possible to supply the lamp with a significantly higher level of ripple without excitation of acoustic resonance in lamp. Regarding (Sun, 2000) the mentioned method was applied to a 100 W metal halide lamp without excitation of acoustic resonances. Under nominal power of the lamp, the measured value of the lamp current is 960 mA with 380 mA (peak to peak) high frequency ripple. Accordingly the ratio of ripple to RMS value of the lamp current for the whole frequency range is 39%. The center frequency of the pseudo-random noise was considered to be 60 kHz and the ratio of ripple to RMS value of the lamp current at this frequency is reported to be 22%.

4.2.10 Modulated Switching Frequency

Another method to reduce the effect of the high frequency ripples is to modulate the switching frequency of power switches. This method attenuates the amplitude of high frequency components of the lamp power spectrum. In this way, although the switching ripples are not filtered, their potential power to excite acoustic resonances is reduced. (Greenwood and Soar, 2002) presents a square wave low frequency half bridge HID ballast with modulated switching frequency. The method suggests a modulation method based on the voltage across the series inductor (L_1 in Fig. 4.15). Regarding this proposed method, the rate of change in the current through the inductor depends on the voltage across the inductor and the inductance value. Since the inductance value is constant the rate of current depends only on the voltage across the inductor. The voltage between two capacitors (C_a and C_b in Fig. 4.15) increases during the positive half cycle of low frequency and decreases during the negative half cycle of the low frequency switching. This results in an decrement of the voltage across the inductor during the ON time of switches for both positive and negative low frequency half cycle. This decreasing voltage is used to modulate the switching frequency in a rate in which the acoustic resonance does not occur.

4.3 Methodology for Measurement of Acceptable Level of the Power Ripple

It is shown that the power ripple of LFSW ballasts is a characteristic problem which is originated in use of switch-mode DC-DC converters. Complete elimination of such ripples seems to be impossible and many design efforts are carried out to attenuate them or to suppress their effect on the lamp. In the introduction of this chapter it is pointed out that the acceptable value of the power ripple which is allowed to transfer from ballast to the lamp is under debate. The purpose of the second section of this chapter is to introduce an experimental method with the aim of measurement of acceptable power ripple for an HID lamp in a given frequency range.

4.3.1 Criterion and Concept of the Experiment

To fulfill the above mentioned mission, it is necessary to drive the lamp with a power waveform which resembles a low frequency square waveform electronic ballast. In this regard the lamp should be operated at its nominal power rate, with a dc power spectrum. To evaluate the effect of the power ripple in different frequencies, high frequency components with known values of frequency and amplitude should then be added to the lamp power spectrum.

The metal halide lamp is supplied with a 200 Hz square-wave current superposed with a high frequency sinusoidal ripple. The frequency and the amplitude of the ripple can be set during the experiment. Arising acoustic instability in the lamp can distort the normal flow of the lamp species in the arc tube. This will lead to a change of the discharge path and may change the lamp impedance and the irradiated light of the lamp as well. Therefore, the acoustic instability will be recognized by analyzing the emitted light of the lamp and changes of the lamp impedance.

In the second chapter and in (Afshar, 2006 I.), a measuring method to recognize the perceptible light transients and flickering light has been described. The method introduces the quantity of ‘Light Flicker Factor’ as a measure of instability strength with respect to the human response to the light transients. By modeling the human eye-brain response to the intermittent stimulus, light flicker factor determines the perceptibility/imperceptibility of the unsteady luminance signal. The input signal is the temporal evolution of the luminance and the output signal quantifies the flicker factor. If the flicker factor exceeds a threshold level, then the light transient is perceptible otherwise it is imperceptible to the normal human eye. The overall gain of the eye-brain model determines the value of the threshold level, which is considered to be unity. Therefore, any intermittent luminance with a light flicker factor greater than one will be considered as a perceptible change of light intensity.

If the superimposed ripple is sufficiently strong then a perceptible light transient can arise. Thus the maximum tolerable amplitude of the ripple at any frequency can be determined in such a way that the flicker factor remains below unity. Using this criterion, one can be sure that superimposed ripples does not arise any discharge instability leading to a perceptible change of output light of the lamp.

4.3.2 Experimental Setup

The experimental setup is sketched in Fig. 4.17. A function generator (THURLBY THANDAR INSTRUMENTS TGA 1240) which is controlled by the computer generates two signals; the first signal is a DC voltage and the second one is a sinusoidal voltage. The Amplitude and the frequency of the sinusoidal ripple and the level of the DC voltage can be controlled by the computer. The DC signal goes to the power amplifier (FM Elektronik FM1295) which operates in current mode. The input signal is amplified to supply the lamp as the main power. The sinusoidal signal is amplified using a high frequency amplifier (TOELLNER TOE 7608). The amplifier works in the frequency range of 0-500 kHz. Amplified DC and sinusoidal ripple signals are added using a low-pass filter in the DC current path and a high-pass filter in the high frequency path. The low-pass filter is implemented using a single inductor (2.20 mH; 0.32 Ω) and as a high-pass filter a capacitor (0.5 μ F; 600 V) is used. The result is a DC current which is superimposed with a single frequency sinusoidal ripple. By using a full-bridge the current signal is converted into a low frequency square-wave superimposed with the ripple. The desired value of the amplitude and the frequency of the ripple can be set with the computer. This current is used to supply the lamp. The lamp is located in an integrating sphere. Using a fast Lux-meter sensor (LMT System Flash Meter SF100), the light signal which is proportional¹ to the luminance is captured. The output of the Lux-meter is a 0-10 V signal. A 16-bit A/D card (National Instruments PCI 6014) is used to acquire the signal for the further process of light transient evaluations. To get the actual voltage and current of the lamp an oscilloscope (Ultima Gould500) is used.

To implement the communication between computer and other instruments LabVIEW software and GPIB protocol is used. In order to determine the frequency response of the experimental setup, the lamp is substituted with a 103 Ω resistor. The amplitude of the sinusoidal ripple is set to 5 Volts and is kept constant during the measurement. The current is set to 0.34 A to achieve about 35 W power over the resistor. The value of the power ripple in a frequency range of 10-400 kHz is measured. The result is illustrated in Fig. 4.8. As it can be seen, the

¹For more details see the second chapter

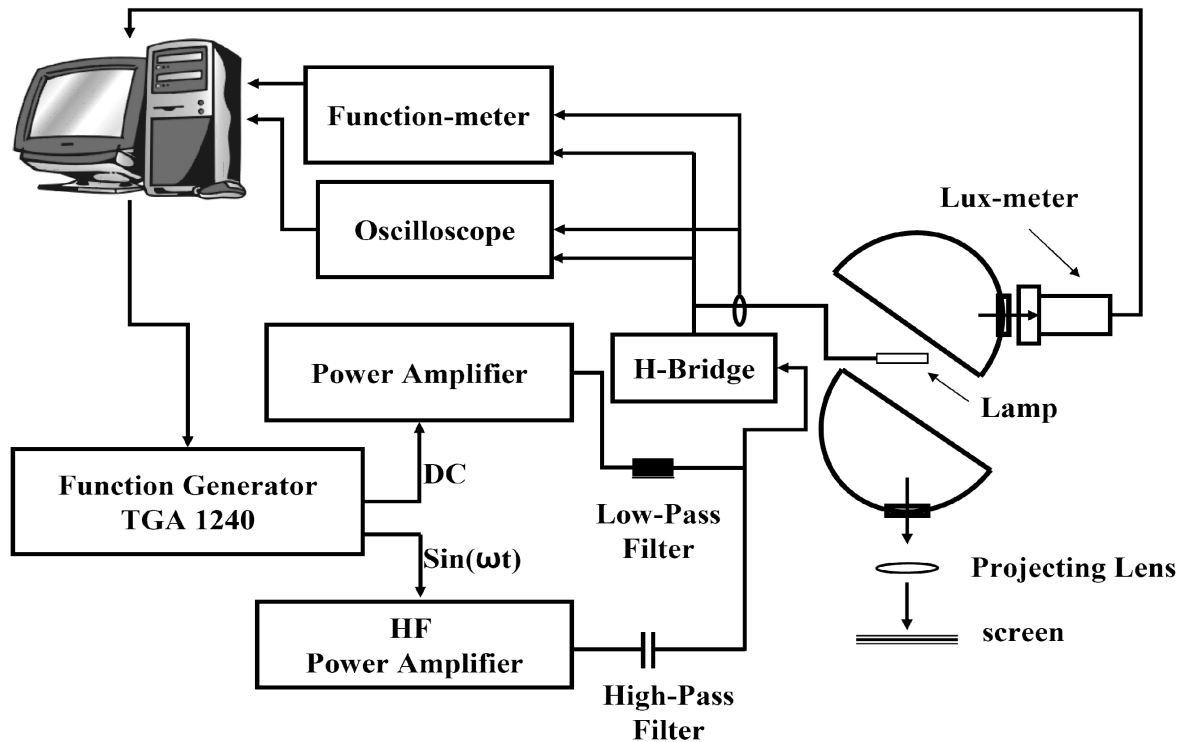


Figure 4.17: Schematic diagram of experimental setup

equivalent high frequency impedance of the measuring circuit is increasing up to about 375 kHz and after that starts to decrease. There is a stepwise change of frequency response around 40 kHz as well.

There is a non-linear behavior of the measuring circuit with respect to the ripple frequency. Because of this non-linearity, having the amplitude of the sinusoidal ripple, which is generated by function generator (for example 5V), is not sufficient to precisely determine the actual ripple value of the lamp power. The value of the ripple should be determined by direct measurement of the lamp voltage and current. This way, the non-linearity does not deteriorate the measurement's results.

4.3.3 Experimental procedure

As mentioned formerly, the goal of this experiment is to find a threshold value for the ripple amplitude in the acoustic resonance frequencies with respect to the perceptible light fluctuations. This will be achieved if the flicker factor as a quantitative equivalent of light transient perceptibility is located in a predefined tolerance band from 0.8 to 1. At the beginning the power applied to the lamp is kept at the nominal value for the lamp under investigation with a predefined tolerance (2% for 35 W, 1.5% for 70 W and 1% or less for 150 W lamps). We start with a high ripple amplitude, for example 5-10%, the flicker factor will then be calculated. If this value is less than one, we will change to other frequencies because the lamp does not show any instability with this strong ripple amplitude. If the value is located in the desired tolerance band then the goal is achieved. Because this means the amplitude of the ripple is a threshold value to excite a perceptible discharge instability. If the flicker factor is greater than one, we

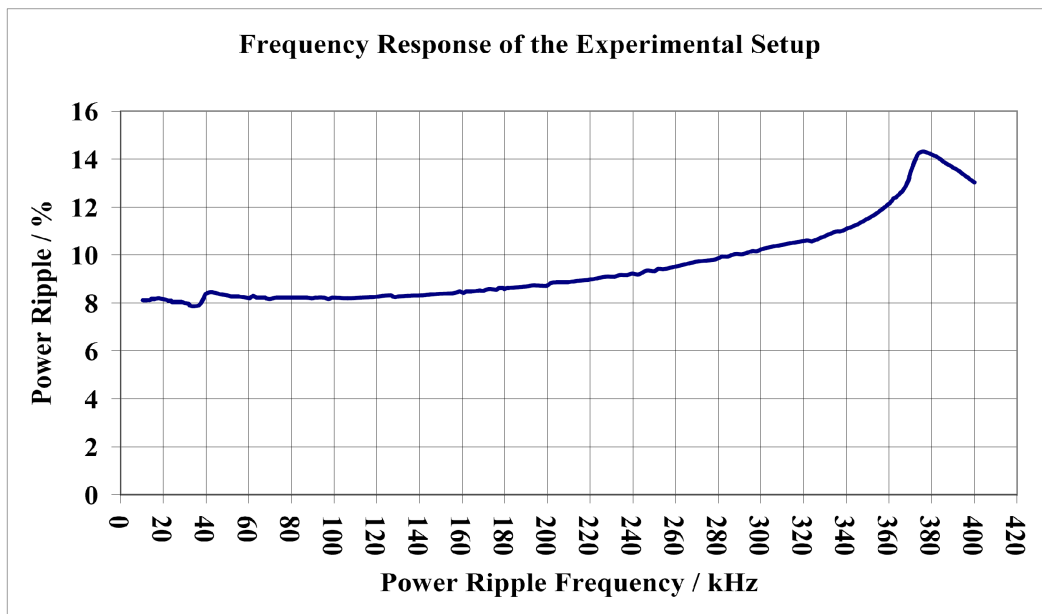


Figure 4.18: Frequency response of the experimental setup with a 103Ω resistance.

will try a new ripple value with reduced amplitude to the half of the starting value. If still the flicker factor is not in the desired tolerance, amplitude depth should be changed sequentially. Using PEST² algorithm, the modulation depth will be increased or decreased. The procedure will be continued, until the flicker factor achieves a value inside the tolerance band, or will be terminated if changing of the modulation dept from one state to the other is less than a predefined value.

This case can occur when the acoustic instability has a step-wise behavior: up to some threshold value there is no acoustic excitation and after reaching the threshold, a pronounced instability arises. In this case the flicker factor is much lower than unity for ripples with an amplitude less than the threshold and much greater than unity for ripples with an amplitude exceeding the threshold. In such cases the last value of the ripple amplitude (highest) which can not excite an acoustic instability (flicker factor below unity but not necessarily in the desired tolerance band) will be selected as the acceptable ripple at that frequency. Since the acoustic frequencies of different lamps are not known in advance, the above procedure is carried out for the entire frequency range i.e. 5-400 kHz. The procedure is applied to the whole range with the steps of 200 Hz. Alternatively, the frequency could be swept over the entire desired range. However, this is not practical because for some frequencies the lamp shows a hysteretic behavior for frequency sweeps of different directions (Schäfer and Stormberg, 1982).

This method is implemented in the main procedure of the program and is summarized in the next section.

The Main Block

1. The ripple amplitude is set to zero. This removes the ripple and the lamp is operated with a square-wave current.

²Parameter Estimation by Sequential Testing

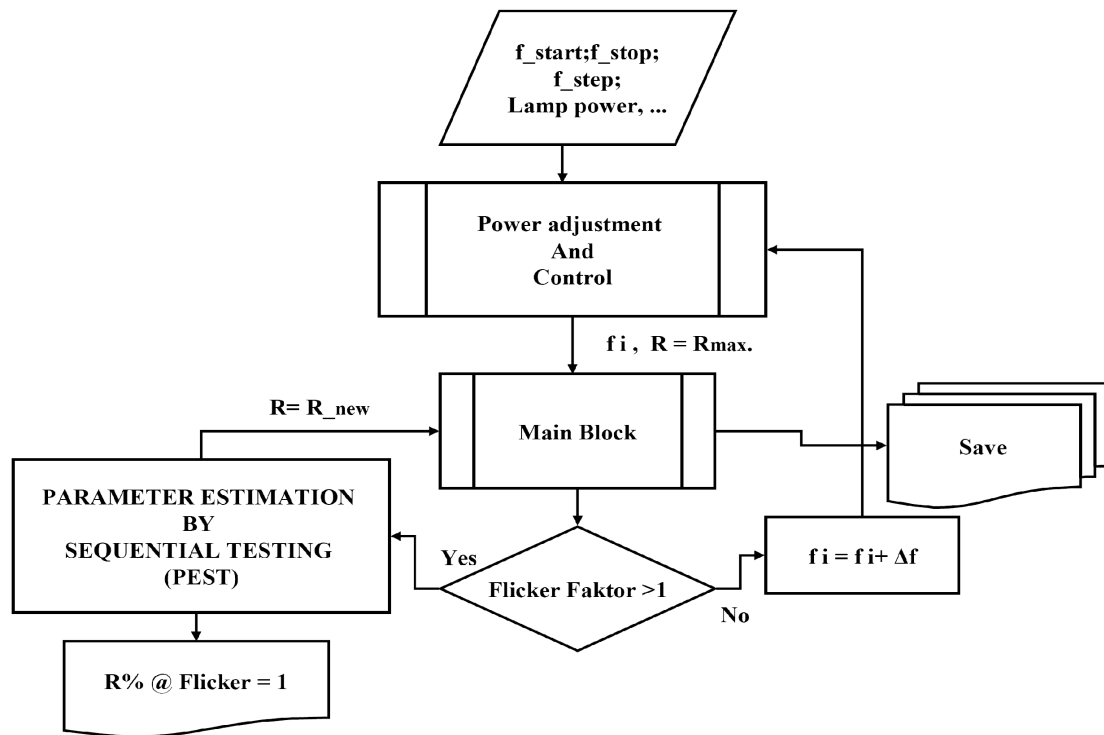


Figure 4.19: Flow-chart of the program which automates the measurement process

2. Lamp impedance and lamp power are determined using the oscilloscope in a 20 ms snapshot (Z_0 and P_0). To obtain the impedance and the power of the lamp, RMS values of the current and voltage waveforms are used. This is implemented using a measurement function of the oscilloscope returning the RMS value of the waveform.
3. The ripple with a predefined amplitude is superimposed. Initially the ripple amplitude is set to 5 volts (this is the input signal of the HF generator). This ripple is amplified using the HF generator and superimposed on the lamp current or voltage.
4. For slightly more than 5 seconds, the lamp is supplied with this current which is superimposed with the ripple. During this time interval the light signal (proportional to the luminance) is captured. Acquisition of the light signal is started 125 ms before applying the ripple.
5. Lamp impedance and lamp power (Z_r , P_r) are measured, with the same method as described in the second item.
6. While having ripple superimposed on the current, the oscilloscope is used to acquire the current and the voltage waveforms during a 20 ms time period.
7. By setting the ripple amplitude to zero the ripple is removed. If the discharge has been changed due to the acoustic excitation it will now return to its original state. At this stage the actual value of the impedance is measured (Z_i).
8. Comparing Z_0 and Z_i makes it possible to decide whether the lamp has returned to its original state or not. If the deviation of the lamp impedance exceeds a predefined value

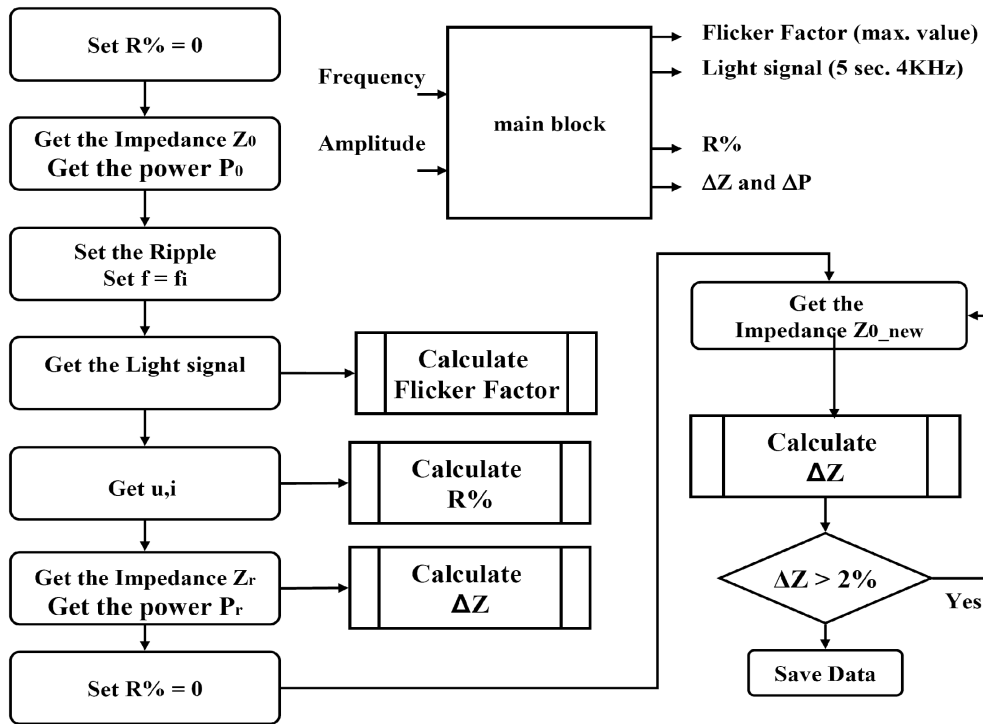


Figure 4.20: Flow-chart of the main-block of the program.

(for example 2%), then the measurement of impedance is continued until it falls below the desired impedance deviation. At this level of the program, the power control unit is active as well, and this ensures that the discharge will reach its nominal state (impedance and power), before continuing the procedure.

9. The light signal from item 4 is used to determine the flicker factor.
10. Using voltage and current waveforms of item 7, the percentage of the power ripple (R%) is calculated.

Calculation of the Power Ripple Percentage

The calculation method of the power ripple is discussed in (Moskowitz and Olsen, 2004). According to Moskowitz, the Fourier transform of the power waveform should be measured for the duration of the acoustic damping time. The acoustic damping time is considered to be about 1 ms which is 50 times greater than the period of a 50 kHz acoustic resonance. The transformed power spectrum of such intervals should then be averaged over the whole waveform. In our case a 20 ms snapshot of the current and voltage waveform is acquired. The power waveform is then calculated by multiplying current and voltage samples. Using the method suggested by Moskowitz, the whole length of the power waveform is divided into 39 1 ms intervals with 50% overlap. After a Blackman window has been applied to each interval, the Fourier transform is calculated. The spectra calculated by this method are averaged and the ratio of the spectral amplitude to the DC value is defined as the power ripple.

In a simple case of a power waveform according to

$$P(t) = P_{dc} + a \cos \omega t \quad (4.19)$$

the calculated value of the power ripple (PR%) is:

$$\text{PR}\% = \frac{1}{2} \cdot \frac{a}{P_{dc}} \cdot 100 \quad (4.20)$$

Assuming voltage and current waveforms containing a dc part and a sinusoidal ripple, this value is approximately equal to the voltage or current amplitude depth.

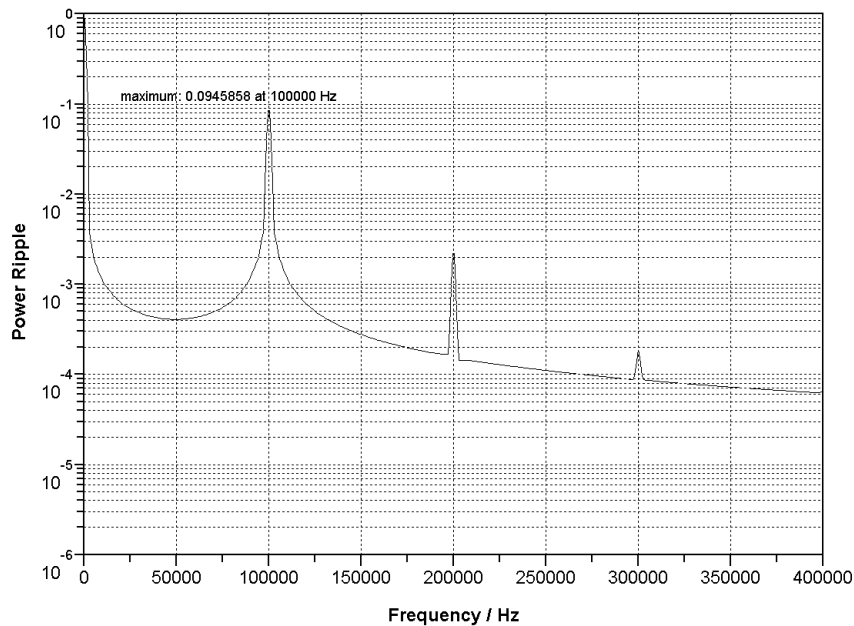


Figure 4.21: Power Ripple calculated using the method suggested by Moskowitz for a 20ms voltage and current waveform (200 Hz square wave) with superimposed sinusoidal ripple. The ripple waveform is a 100 kHz sinusoidal oscillation with an amplitude of 10% with respect to the amplitude of the square-wave of both, current and voltage.

4.3.4 Results

Using the procedure described in the previous sections the maximum acceptable value of the power ripple for different lamps with different nominal power up to 150 W is determined. Fig. 4.22 illustrates an example of the complete measurement of a 70 W metal halide lamp. As can be seen, the most critical resonance occurs at two frequencies: 33 kHz and 70 kHz. At both frequencies, a power ripple greater than about 0.7% is sufficient to excite an acoustic instability. In contrast, for the frequencies of 50 kHz, 150 kHz and 175 kHz this is about 2%. For higher frequencies the excitation level of ARs gradually increases. This can be seen comparing the allowed power ripple at 175 kHz, 250 kHz and 330 kHz with 2%, 3.5% and 5.5% respectively.

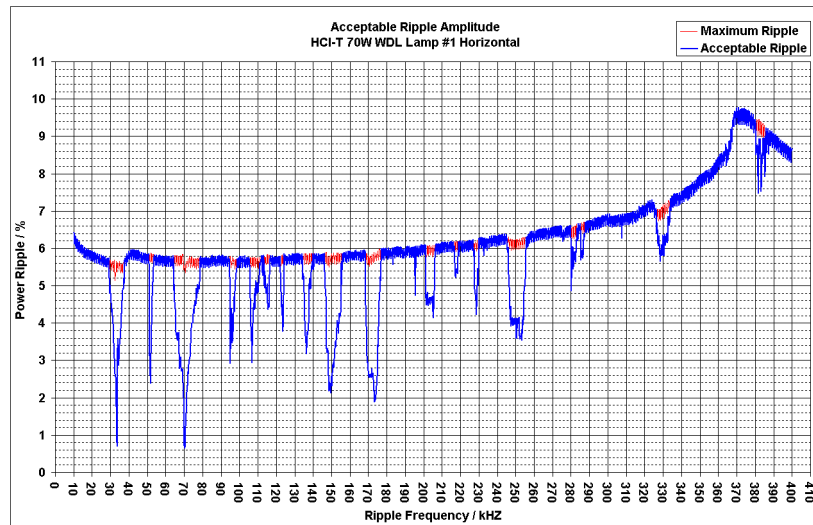


Figure 4.22: Acceptable power Ripple versus the ripple frequency.

Fig. 4.24 shows the measured current and voltage waveform of an OSRAM HCl-T 70W WDL lamp with a 33.1 kHz sinusoidal current/voltage ripple. These curves were obtained using a 12bit digital oscilloscope with a sample frequency of 2.5 Ms/s. The instant power is then calculated by point-by-point multiplication of the current and voltage samples. The value of the power ripple for the curves illustrated in Fig. 4.24 is 5.65%. The light signals of Fig. 4.25 illustrate the effect of the power ripple. As can be seen, before applying the ripple (at $t = 250$ ms) the light intensity (luminance) is constant, after that, depending on the value of the ripple, the light intensity shows some transients.

The higher the value of the ripple the stronger is the change of the light signal. In this acoustic mode, increasing the value of the ripple results in a faster and stronger change of the light. The first curve in Fig. 4.25 (corresponding to the 5.65% ripple) shows a damped oscillating behaviour with a frequency of about 16 Hz and a damping time of approximately 190 ms. Superimposing the ripple also has a slight effect on the DC part of the light signal and this is recognized by measuring the lamp impedance before and after applying the ripple. This is more significant in the second curve which has 3% ripple. The lamp impedance before adding the ripple is 115 Ω and its steady value (after 5 s) with ripple is 118 Ω . Since the lamp is operated with the power amplifier in current mode, the current is kept constant before and after adding the ripple. If an acoustic mode results in an increment of the lamp impedance, the lamp power and consequently, the emitted light of the lamp is increased as can be seen in Fig. 4.25.

Corresponding light flicker factor curves are illustrated in Fig. 4.26. The first light signal with 22.5% overshoot shows a very high flicker factor of about 800, with the lower values of the ripple of 1.64% flicker factor is below unity. Therefore, the flicker factor curves are sketched in a semi-log diagram in Fig. 4.26. This diagram shows that a threshold level for the ripple with the frequency of 33.1 kHz for an OSRAM HCl-T 70W WDL lamp in a horizontal burning position is 2.02%.

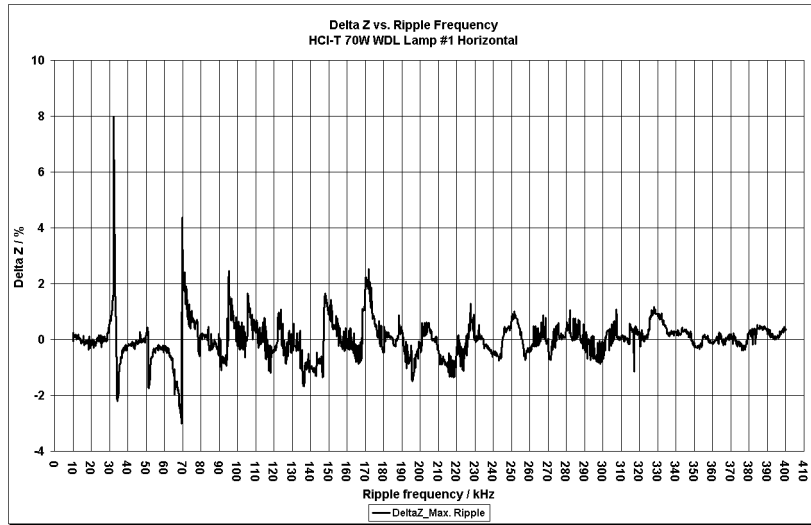


Figure 4.23: Impedance deviations versus the ripple frequency.

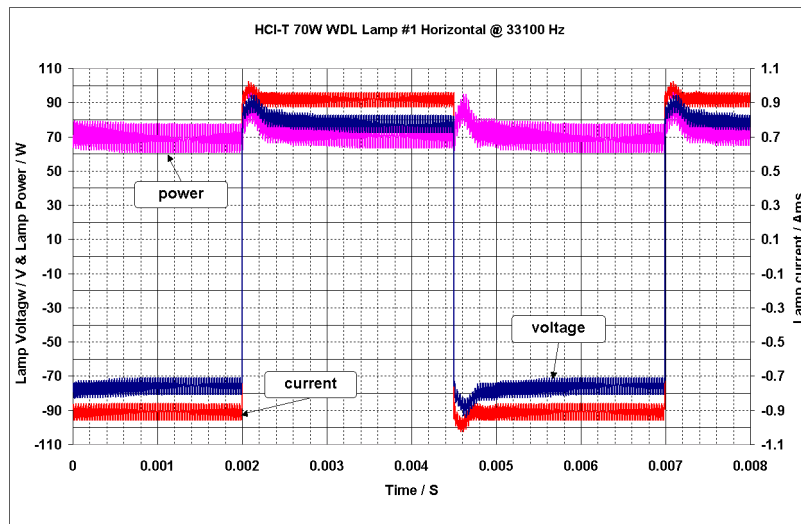


Figure 4.24: The current and voltage waveform of the lamp with a 33.1 kHz sinusoidal ripple and the corresponding power waveform. The power ripple is 5.65%.

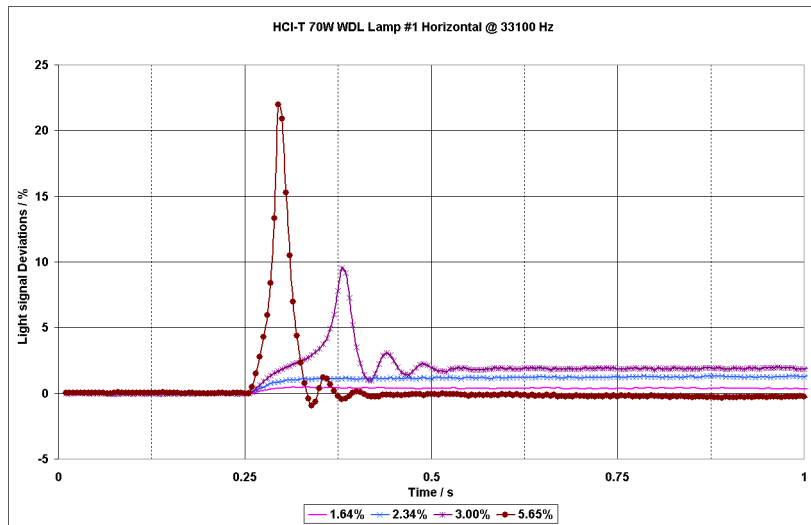


Figure 4.25: Light signal (output of the Lux-meter) vs. time for different values of the power ripple.

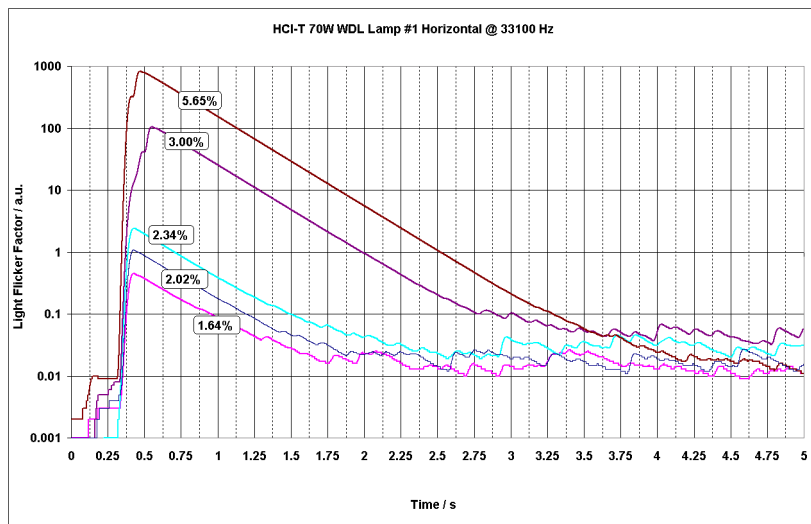


Figure 4.26: Light Flicker Factor curves (semi-log) for the light signals shown in Fig. 4.25.

Arc Straightening Using the Results of This Method

In the third chapter it is explained that a useful application of acoustic resonance is the arc straightening of a horizontal operated lamp. According to Fig. 4.23 the lamp impedance within the frequency region of 50 to 70 kHz of the power ripple is reduced with respect to its nominal value (negative values in the graph). Since in the normal operation of the lamp the discharge has an upward deflection, the reduction of the lamp impedance means that the discharge has a lower length or it is straightened. This means applying the current ripple in this frequency range with sufficient amplitude can push the discharge toward the centerline of the lamp. By sweeping the ripple frequency within mentioned frequency range it is possible to fulfill this application.

4.4 Effect of Ripple Superposition on the Lamp Power

According to this proposed method, a sinusoidal current ripple is superposed to the lamp current. Considering the lamp as a resistor, the lamp voltage is superposed with a sinusoidal waveform as well. Assuming the current and the voltage waveforms in a half cycle of the low frequency switching one can write:

$$i(t) = I_{dc} + a \cos(\omega t) \quad (4.21)$$

$$v(t) = V_{dc} + b \cos(\omega t) \quad (4.22)$$

where ω is the ripple frequency and a and b are the amplitude of the current and voltage ripples respectively. Then the instant power of the lamp is calculated as follows

$$p(t) = I_{dc}V_{dc} + [V_{dc}a + I_{dc}b] \cos(\omega t) + ab \cos^2(\omega t) \quad (4.23)$$

Assume that the lamp is operating at its nominal power before adding the ripple. The average value of the second term in a half cycle is zero. In contrast, from the last term of equation (4.23) it can be seen that adding the sinusoidal ripple to the lamp current results in an increase of the lamp power. The increase of the lamp power increases the emitted light of the lamp as well. If this sudden increase of the light is significant, the flicker model interprets it as a light flicker which is caused by the excitation of the acoustic resonance. It is obvious that this is just a misleading error.

For small values of the ripple amplitude, as is the case in this work, the third term of the (4.23) is quite low. For example if the current and voltage ripple amplitude are 5% with respect to their dc value, the amplitude of the third term of (4.23) would be 0.25% of the lamp power base line. Especially for low wattage lamps this value is very low and negligible.

If for any reason this method is desired to be used with higher values of the ripple amplitude, some modifications should be carried on in the measuring procedure to overcome this problem.

4.5 Conclusion and Discussion

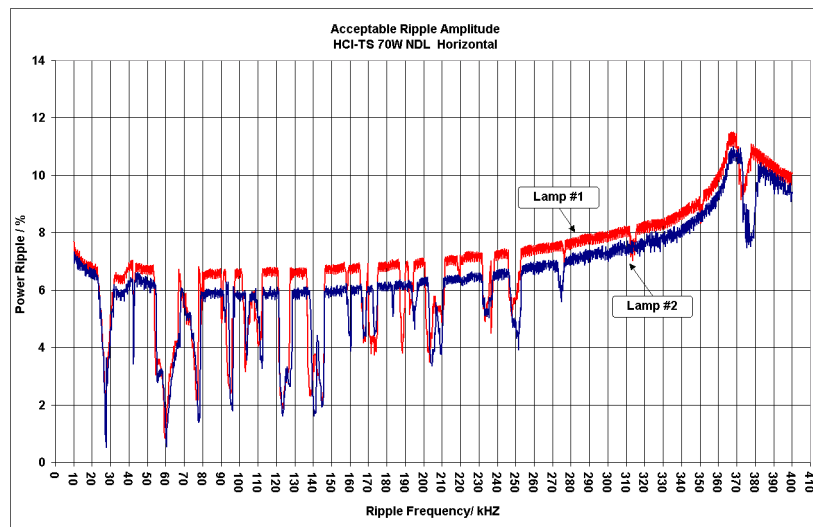


Figure 4.27: A comparison of the measurement results of two similar OSRAM HCl-T 70W NDL lamps.

This section is dedicated to explain a practical method to determine the threshold value of the power ripple for LFSW electronic ballasts. The optical behavior of the lamp is the key parameter to detect the existence and strength of the acoustic excitation.

Based on the light flicker factor an automatic measuring system has been implemented to determine the above mentioned threshold for different lamps in the frequency region of interest. The method of the measurement has been described and some measurement results are illustrated. This measuring method shows a very good reproducibility and very similar results for lamps of the same type. Fig. 4.27 shows the measurement results of two similar OSRAM HCl-TS 70W NDL lamps. As it can be seen, both lamps show a very similar sensitivity to the ripple with respect to the frequency regions and the threshold values. A difference in the impedance of the two lamps results in a vertical shift of the two curves. The measured impedance of the lamp #1 is about 87Ω while for the lamp #2 this value is about 97Ω . Besides manufacturing tolerances which leads to this variation of the lamp impedance, the other possible reason for this observation is as follows. After excitation of acoustic resonance it is possible that the arc attachment position on the electrode tip is changed. In some cases the discharge attachment position is changed from electrode tip to the winding on the electrode and remains at this new position. This condition leads to the enlargement of the discharge and subsequently increases the lamp impedance.

From Fig. 4.27 it can be found that the difference in lamp impedances is more significant for the ripple frequencies greater than 30 kHz. This frequency is the upper bound of the first acoustic mode, it is highly possible that after excitation of this acoustic mode the position of the arc attachment in lamp #2 was changed from electrode tip to the winding and therefore due to an increment of the discharge length the lamp impedance was increased. Fig. 4.23 shows change of the lamp impedance with respect to the frequency of the power ripple. Regarding this graph, a very significant change of the lamp impedance around that frequency region is noticeable. The impedance increment is reflected in reduction of the ripple percentage as long as the maximum amplitude of the high frequency ripples during all measurements is constant.

Measurements of different lamps give the following general results:

In most cases the power ripple in the frequency region in which the strong acoustic resonances are observed should be kept less than 1% . This is in accordance with the result of Olsen's experiment in (Olsen and Moskowitz, 2005). Olsen found that a power ripple of 0.84% at the resonance frequency can change the maximum arc tube temperature up to 5C. This means that already such a low power ripple has a detectable effect on the lamp discharge. The first acoustic resonance for 150 W lamps occurs around 20 kHz, for 70 W lamps around 30 kHz and for 35 W lamps around 45 kHz.

Acoustic modes with lower frequencies are the most sensitive in the whole frequency range. Burning position of the lamp has a dramatic effect on the results. This can be an effect connected to the significant change of the temperature distribution (and flow of the filling) in the arc tube. The temperature distribution determines the acoustic velocity and acoustic resonance frequencies in the lamp. The following characteristic responses with respect to the light signal are observed:

1. Continuing periodic light flicker which persists as long as the power ripple exists. Usually the lamp shows some transients before starting to this periodic flickering.
2. Damped periodic light flicker (see Fig. 4.25) in which by applying power ripple the lamp discharge shows a great change but the instability is damped gradually. In this case the lamp impedance before and after applying the ripple can be different.
3. Stepwise (increasing or decreasing) change of the light signal. This is the dominant case according to our experiments. For most resonance frequencies, an increasing stepwise change of the light intensity is detectable. In such cases, the lamp discharge has a change of shape and/or position and is stable in its new state. This is followed by a measurable impedance deviation with respect to the nominal impedance of the lamp. This is the case especially with lower values of the power ripple and increasing the power ripple leads to a greater and faster step response of the discharge which can be followed by a periodic flicker.

Depending on the lamp sensitivity, every complete test takes between 10 to 30 hours. The proposed measuring system introduces a precise and at the same time simple method to determine the power ripple threshold in HID lamps.

A similar approach like the measuring method proposed in this work has been reported in (Dalla Costa and others, 2005; Dalla Costa and others, 2007). There are two major shortcomings with the evaluating method (as briefly described in the introduction of this chapter) suggested in that paper. Firstly, the method does not provide an absolute threshold value for the light flicker. This way light flicker gives only a relative quantity. For example in one acoustic mode the light flicker is 2% and in the other mode it is 5%. This shows that the second acoustic mode is 2.5 times stronger than the first one. Knowing this is not sufficient to judge the threshold value of the ripple amplitude. A minimum value of the light flicker should be defined to be able to decide whether a light transient should be considered as a flicker or not.

Secondly, using a single low-pass filter does not account for the attenuation characteristics of the human eye (Kelly, 1961). The human eye shows 5 times more sensitivity to the flickering light with the frequency of 10 Hz comparing to a 35 Hz flicker (Henger, 1986). Using the proposed method of (Dalla Costa and others, 2005), one gets equal flicker values for both cases if amplitudes and mean values are kept constant. This will lead to overestimation or underestimation of the flicker level depending on the definition of the acceptable flicker level.

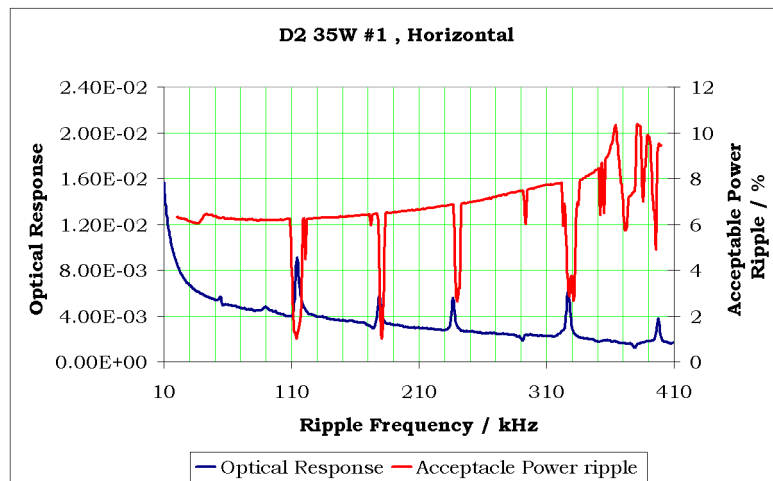


Figure 4.28: A comparison of the method which is proposed in this work with Olsen's method (Olsen and Moskowitz, 1997).

A direct comparison of the proposed method of this work with the method of optical measurement of acoustic resonances in HID lamp proposed in (Olsen and Moskowitz, 1997) is illustrated in Fig. 4.28. Both methods are used to find the acoustic resonant frequencies in a 35 W automotive headlight lamp. The lower curve shows the optical response of the lamp to the high frequency components of the lamp power as it is described³ in (Olsen and Moskowitz, 1997). The upper curve is the measurement result of the same lamp which is carried out using the method which is proposed in this chapter. A good agreement between these two methods with respect to the resonant frequencies is noticeable. The advantage of the proposed method of this work is that besides the resonant frequencies, the sensitivity of the lamp in such resonant bandwidths is determined as well.

³It should be noted that this measurement is carried out by Moskowitz and is used in this work to compare two methods.

Chapter 5

Temporal Response of Acoustic Resonance Instabilities

5.1 Introduction

The whole process of acoustic instability, from formation of standing pressure waves in the arc tube to occurrence of visible discharge instabilities, can be completed after a time interval (onset time of the AR excitation). Measuring of this onset time interval for different acoustic modes helps us to get a better understanding of the physical backgrounds of AR instability phenomenon.

It is worth to recall the process of acoustic resonance and acoustic streaming briefly. In presence of the standing pressure waves the arc tube of the HID lamp can be considered as a standing wave resonator. In such a resonator, close to the solid boundary, shear viscosity of the filling gas induces acoustic streaming (Hamilton and others, 2003). Generally speaking, establishment of acoustic streaming is a result of the dissipation of acoustic energy. The acoustic energy is converted into a momentum of the filling material in the lamp arc tube. The bulk viscosity of the filling material is the other cause for the dissipation and conversion of the acoustic energy in the arc tube (Boluriaan and Morris, 2003).

The linear acoustic velocity has a time dependent oscillatory behavior with the frequency of the arc tube eigenfrequency. On the other hand, the resulting streaming represents a non-linear one-directional (or in case of a lamp arc tube circulating) time-independent movement with a much slower velocity (Sastrapradja, 2004).

Establishment of the acoustic streaming which may lead to discharge instability occurs after a certain time constant. Arising of acoustic streaming represents a coherent movement of the filling particles along a trajectory. Movement trajectories are determined by the corresponding acoustic modes. Presence of acoustic resonances introduces an extra force (acoustic force as it is called in Fig. 5.1) acting in a specific direction (depends on the acoustic mode) to the particles. The vector addition of the acoustic force and the forces acting on the particles during normal operation of the lamp (in the absence of ARs) determines the new movement trajectory of the particles. When the acoustic force is applied, the movement path changes immediately but the particles need time to move along this path to achieve a significant deviation from their original path. According to this concept, the time constant for the arc instability growth is the time which is needed for ARs to significantly divert the normal movement of the particles.

As it is schematically illustrated in Fig. 5.1, a short duration of the power ripple (t_1) has an insignificant effect on the particle movement (state 1-2). In contrast, a power ripple with sufficient duration (t_2) may significantly change the motion parameters of the particle. When a sufficient number of the particles move coherently along a new trajectory they get enough energy to destabilize the discharge. In other words the excitation of an acoustic mode which exists for a specific time is able to establish a significant abnormal mass displacement of the filling material in the arc tube. In this case, the discharge is affected regarding the new flow pattern of the filling material in the arc tube. This means that the electrical conductivity of the discharge is changed. As a result, the electrical parameters and, subsequently, the emitted light of the lamp is changed as well. After removing the power ripple the source of the acoustic instability is removed as well, but its effect will diminish with a certain offset time. The reason could be the inertia of the particles (which were moving along abnormal trajectories) and the effect of the stabilizing forces on the discharge.

By analyzing the electrical parameters of the lamp or its emitted light after applying a ripple at a known AR frequency the occurrence of an instability can be determined. The purpose of this chapter is to introduce an experimental method to estimate the onset time of the arc

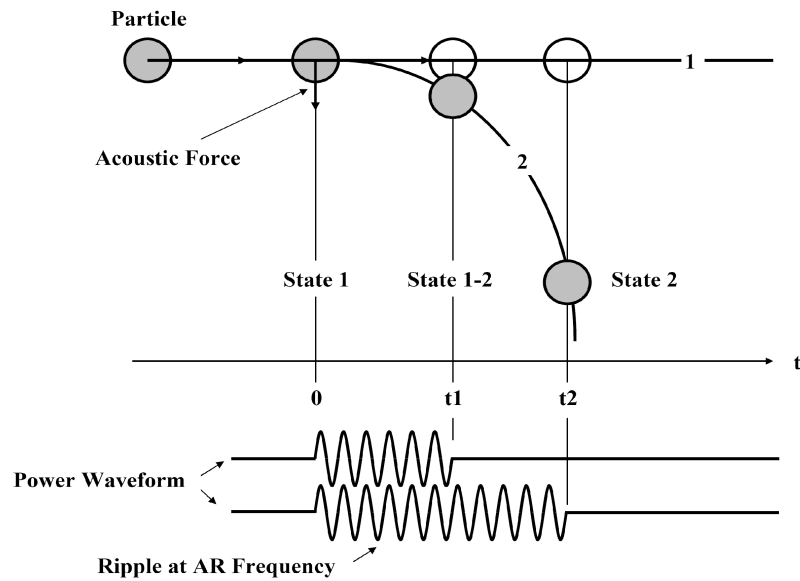


Figure 5.1: Schematic diagram of changing the motion trajectory of a particle as a result of presence of an acoustic (streaming) force. The power ripple is applied at $t = 0$, at this time the particle moves along trajectory 1 which is considered as a normal operation of the lamp (state 1). As the acoustic force is applied to the particle, the movement trajectory is changed to 2 (state 1-2). After passing the time constant of t_2 the position and the movement parameters of the particle is changed significantly (state 2) which satisfies the discharge destabilization conditions.

instability in the frequency regions of interest. The time constant for arc instability growth is an important parameter of the acoustic resonance instability in HID lamps. The only reference known to the author which addresses this time constant is (Wada and others, 1987). Wada gives a value of 10 ms to 1 s for this time constant and refers to (Hasebe and Matsumoto, 1976) as the origin of this data. Since after publication of the mentioned papers many new generations of HID lamps have been developed, this value should be measured for the new HID lamps.

The temporal response of the discharge after applying the power ripple at AR frequencies is the other subject discussed in this chapter. An important concept in high frequency operation of HID lamps is the real time detection of acoustic resonance (Calderia and others, 1999; Oh and others, 2002). Detection of AR excitation and changing of the inverter frequency to avoid acoustic instability should be carried out before any perceptible light deviations arise. To fulfill this goal, one should know the time response of the discharge to the AR instabilities. In (Calderia and others, 1999) a method is suggested to measure the time constant of the discharge deflection when it is subjected to a force. In this method an extra electromagnetic force is applied to the discharge and its time constant for achieving a certain deflection is measured. The value of the $\tau = 50$ ms is reported for this time constant. However, applying the electromagnetic force may have some unknown effects on the discharge and the deflection is achieved due to the other phenomenon than AR excitation.

In contrast to the above mentioned approach, the method proposed in this work is more straightforward, because the deflection time constant of the discharge is measured directly

during AR excitation.

5.2 Concept of the Experiment

The lamp is operated with a low frequency (200 Hz) square wave (LFSW) current. This guarantees a stable operation of the lamp without any light fluctuations. Afterwards, a sinusoidal ripple with the frequency of the acoustic resonance of the lamp is superposed on the current. At a given value of the ripple amplitude an increase of the duration time of the ripple leads to an unstable lamp discharge. This can be detected by analyzing the emitted light of the lamp.

To detect a perceptible disturbance of the luminance, the concept of the light flicker factor with the threshold value of unity (Afshar, 2006 I.) is used. The flicker factor analysis needs the luminance (or a proportional signal) as input and provides as an output a signal that indicates the flicker level. In case the output signal exceeds unity the flicker is perceptible to the human eye.

The highest sensitivity of a lamp to fluctuations of the power invested into the lamp is reached at acoustic resonance frequencies. There are some methods suggested in literature to detect AR frequencies, for example (Olsen and Moskowitz, 1997; Schäfer and Stormberg, 1982; Kaiser and others, 2003). In a recent paper (Afshar, 2006 II.), a measuring method is introduced to determine the allowable level of power ripple for a lamp versus the ripple frequency. Using the results of that experiment, the acoustic resonance frequencies for lamps of interest are already known.

It should be noted that it is not possible to operate the lamp with a sinusoidal current at AR frequency and nominal power. For this reason, it is operated with a LFSW current superposed with ripple at AR frequency. This means, the value which is measured with this method should be interpreted as the upper limit of the time constant.

We start with the lowest possible duration of the ripple which is only one period of the ripple signal. As long as the disturbance remains imperceptible (flicker factor below unity) the duration is considered to be shorter than the onset time. Any perceptible change of emitted light is considered as a significantly abnormal mass displacement of the filling material in the arc tube which should be avoided. It is therefore possible to use the flicker factor analysis as a sensitive tool to detect perceptible influence of the duration of the ripple signal.

5.3 Experimental Setup

The experimental setup is schematically shown in Fig. 5.3. A function generator (THURLBY THANDAR INSTRUMENTS TGA 1240), which is controlled by a computer, generates two signals: the first signal is a DC voltage and the second one is a sinusoidal voltage. The Amplitude, the frequency and the duration of the sinusoidal ripple and the level of the DC voltage can be controlled by the computer. The DC signal is the input signal for an power amplifier (FM Elektronik FM1295) which operates in current mode. The DC signal is amplified to provide the main power supply to the lamp. The sinusoidal signal is amplified using a high frequency amplifier (TOELLNER TOE 7608), which works in the frequency range of 0-500 kHz. Amplified DC and sinusoidal ripple signals are added using a low-pass filter in the DC current path and a high-pass filter in the high frequency path. The low-pass and high pass filters are implemented using a single inductor (2.20 mH; 0.32 Ω) and a capacitor (0.5 μ F; 600 V)

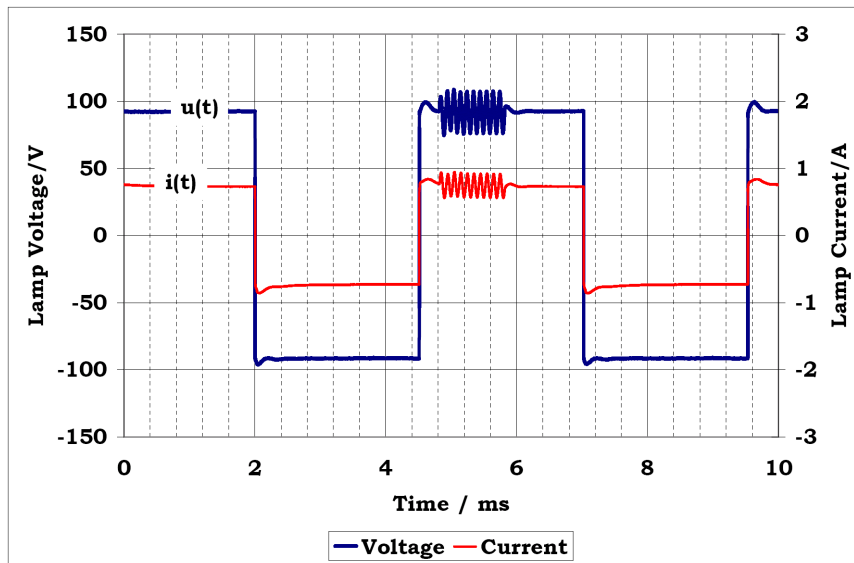


Figure 5.2: Voltage and current waveform of an OSRAM HCI T 70W WDL Lamp. The lamp is operated with a 200 Hz, LFSW current at nominal power of 70W. A ripple with a frequency of 10 kHz and duration of 1 ms (10 periods of high frequency ripple) is superposed on the main waveform.

respectively. The result is a DC current which is superimposed with a single frequency sinusoidal ripple with given amplitude and duration. By using a full-bridge the current signal is converted into a low frequency square-wave. To determine the duration of the ripple, the total number of its periods is specified. The ripple with given parameters as mentioned above is superposed on the main signal when the function generator receives the trigger signal from the computer. The lamp is placed in an integrating sphere. Using a fast Lux-meter sensor (LMT System Flash Meter SF100), the light signal which is proportional¹ to the luminance is captured. The output of the Lux-meter is a 0-10 V signal. A 16-bit A/D card (National Instruments PCI 6014) is used to acquire the signal for the further process of light transient evaluations. The actual voltage and current waveform of the lamp are recorded using oscilloscope (Ultima Gould500). To measure the power of the lamp and keep it constant a Function-meter (ZES ZIMMER LMG95) is used.

5.4 Procedure of the Measurement

At the beginning the power of the lamp is set to its nominal value. The time duration of the ripple can be set as an integer value times its period. Hence, the minimum possible value of the ripple duration is equal to its period. We start with this duration of the ripple for a given AR frequency of the lamp. After adjusting the lamp power within an acceptable tolerance around its nominal value, the computer sends the trigger command to the function-generator.

Upon triggering the function-generator, the ripple is superimposed on the current and, simultaneously the light signal is captured. After analysis of the light signal, the maximum value of its corresponding flicker factor signal is considered as the value of the flicker factor.

¹This concept is explained in the second chapter.

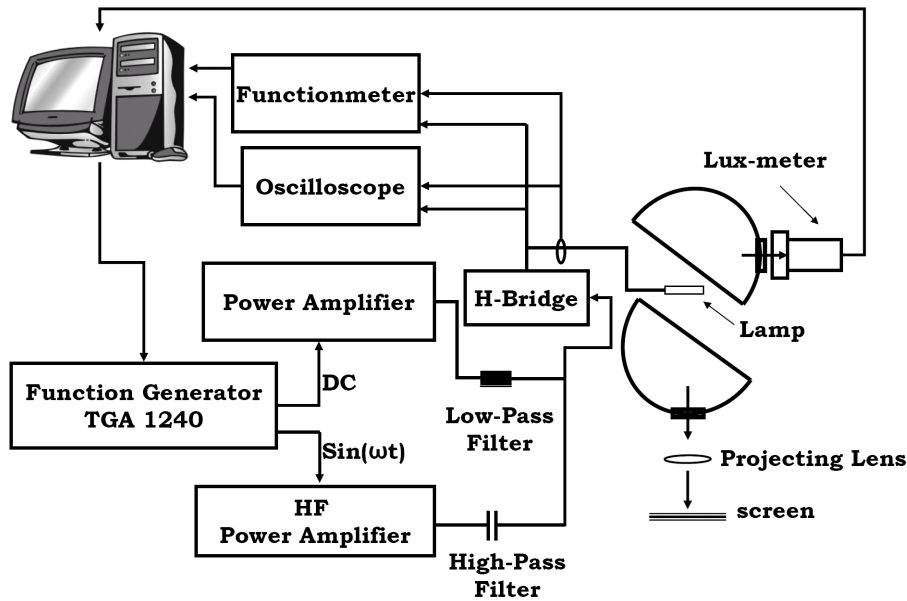


Figure 5.3: Schematic diagram of the experimental setup.

The percentage of the power ripple is determined using the method proposed in (Moskowitz and Olsen, 2004). As it is explained in (Afshar, 2006 II.), the minimum length of the current and voltage signal for calculating the power ripple percentage is at least 20 ms. Thus, by applying a ripple with a very short duration, e.g. 0.01 ms for one period of a 100 kHz sinusoidal ripple, the calculated actual power ripple percentage is very low².

For this reason the value of the power ripple is determined by applying the same ripple with duration of about 50 ms to get the voltage and current waveform with the same ripple within a 20 ms interval. It should be noted that regarding the suggested method by Moskowitz, the value of the power ripple which is calculated with the short duration of the ripple is the actual value. This actual value is not of interest in this measurement. What should be considered is the value of the ripple in a time window in which the ripple is applied to the lamp (considering the waveform of Fig. 5.2 this time interval would be from 4.8 ms to 5.8 ms).

Considering the lamp power waveform the percentage of the power ripple should be half of the ratio of the ripple amplitude to its DC term. This result is achievable only if the ripple duration is expanded to the whole length of the power waveform. As it is sketched in the diagram of Fig. 5.4 a trigger command, which is generated by the computer, synchronizes the process of applying the ripple and achieving the current and voltage waveform. Afterwards the value of the power ripple will be calculated.

The procedure is continued with a new duration of the ripple and the same amplitude. To cover a wide range of measurement regarding duration of the ripple this parameter is changed in a logarithmic manner up to the highest predefined value.

²Because in this method the value of the power ripple is an average of power ripple in small intervals (1 ms) of the signal. When the duration of the ripple is very short only in a few intervals the power ripple achieves its estimated value and in other intervals the power ripple is zero. Therefore, the total value of the power ripple is very low.

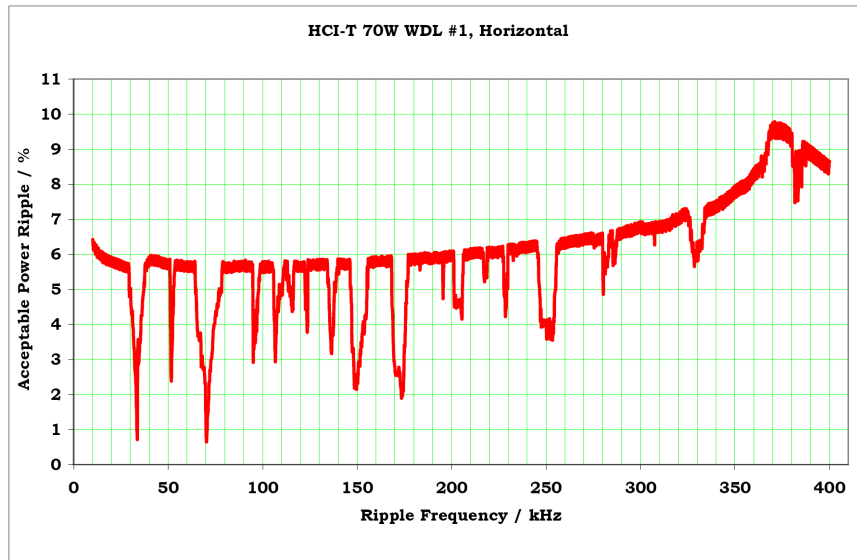


Figure 5.5: Acceptable power ripple versus frequency of an OSRAM HCI T 70W WDL lamp. This diagram is used to know the frequencies in which the acoustic resonances excite (Afshar, 2006 II.).

tube is exemplified in Fig. 5.7. Considering the horizontal operation of the lamp, the curve No. 2 shows the normal length (L) of the discharge. The upward deflection of the discharge in normal operation is due to the thermal convection effect of the filling material. The curve No. 1 illustrates the case that the discharge path is enlarged and the arc is deflected upward. This case corresponds to an increment of the impedance and emitted light. If the acoustic force pushes the discharge downward, this leads to a straightening of the discharge (curve No. 3) and a reduction of the discharge length ($L - \delta L$). Therefore, emitted light will be decreased as well. For greater downward forces the discharge may be deflected toward the bottom of the arc tube. The curve No. 4 shows the discharge which is deflected downward but has the same length as its normal position. In this position there is no change of impedance and emitted light. Finally the last curve (No. 5) stands for a downward deflection in which the length of the discharge is increased. According to the different acoustic modes, many other shapes or positions of the discharge in the arc tube are possible. However, since the basic mechanism is the same they are not discussed herein.

In Fig. 5.6, it can be seen that for ripple duration of 31.25 ms the instability starts with increasing the emitted light, according to the above considerations, this is an upward deflection of the discharge ($L + \delta L$). The deflection takes about 35 ms for completion (the light deviation signal achieves its max. value). Afterwards, the curve goes down, which means the discharge resumes its original position (L) which takes about 20 ms (light deviation is zero). The downward movement is continued for 50 ms and the emitted light decreases to its minimum value. At this moment the discharge has its minimum length and the discharge is straightened. During the last 100 ms interval, the discharge resumes its original stable position.

Considering the ripple duration of 31.25 ms for this measurement, the offset time for this instability mode is about 170 ms. There are two possible scenarios to explain the discharge behavior illustrated in fig. 5.8. First scenario: The acoustic force pushes the discharge downward. The first minimum of the curve shows that the discharge length attains a minimum (no

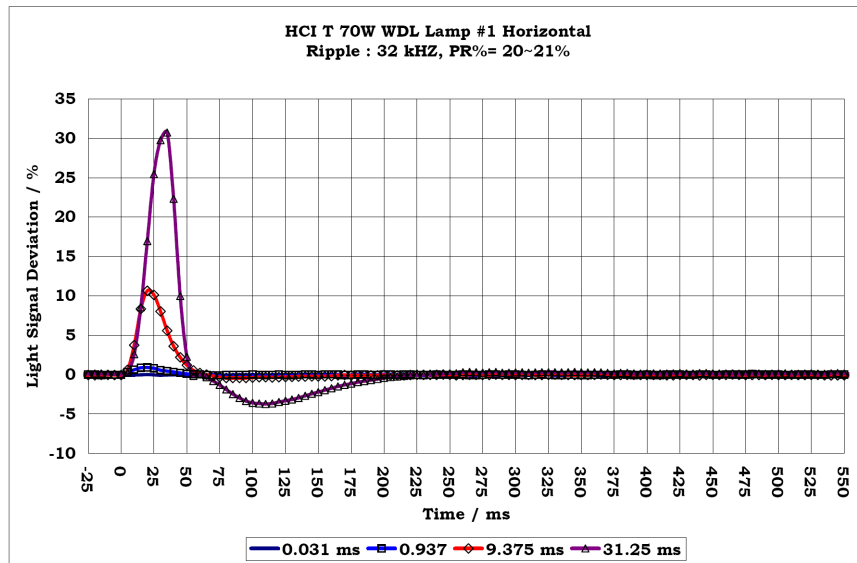


Figure 5.6: Light signal deviation (output of the Lux-meter normalized to its DC value) vs. time for different values of the ripple durations at the frequency of 32 kHz. The power ripple is set to 20-21%.

deflection). The downward movement is then continued and the discharge length is increased. The first zero-crossing indicates that the discharge length is equal to its original value but it is deflected in the opposite direction. The increase of the discharge length is continued until the first maximum of the curve. At this point the discharge has its maximum length and the distance between lower wall of the arc tube and discharge is minimal.

The stabilizing forces (mainly wall stabilizing forces) push the discharge upward leading to a decrease of the discharge length. The second zero-crossing shows the transition through its original length and the second minimum corresponds the minimum length of the discharge (no deflection) and finally the discharge reaches its original position. Second scenario: The discharge is pushed downward, up to the first minimum. After that the discharge goes up with a corresponding increase of its length. This is continued up to the first maximum. In contrast to the first scenario, in this position, the discharge is close to the upper wall of the arc tube. Then it is pushed down and reaches its original position (second zero-crossing). The downward movement is continued up to the second minimum and finally the discharge reverts to its original position. There are two local minima in the light deviation curve of Fig. 5.8. Since these two minima have different values, they can not belong to a unique position of the discharge as is the case for the first scenario. For this reason, the plausible explanation of the discharge movement for this case is the second scenario.

The acoustic mode which is excited at the AR frequency of 175 kHz (Fig. 5.9) is similar to the acoustic mode at the frequency of 32 kHz. Fig. 5.10 shows the time response of the lamp discharge at the frequency of 250 kHz. In this case for a short duration of the power ripple a similar response of the discharge is recognizable. In the last curve (80 ms of power ripple) it can be seen that at the beginning the discharge is pushed upward and starts to fluctuate and change its position. The discharge is subject to two different forces, the acoustic force tends to push it upward whereas the stabilizing force tends to push it back toward the center of the arc tube. After removing the AR excitation the stabilizing force is able to bring it back to its

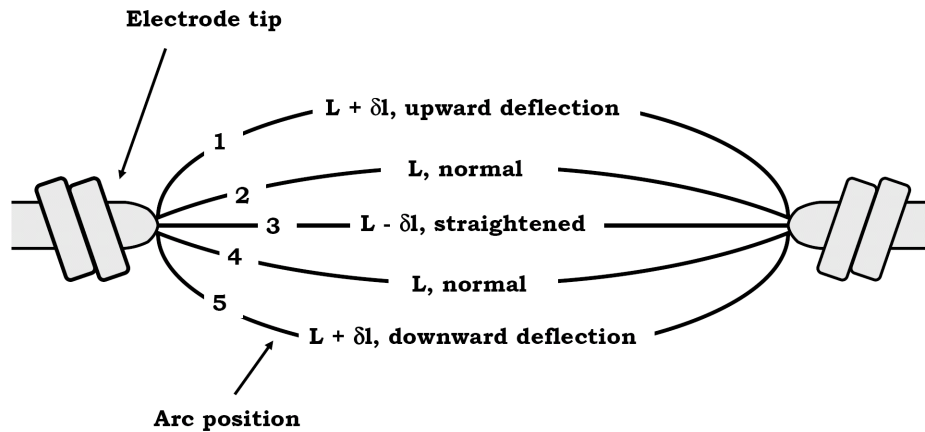


Figure 5.7: Schematic diagram of the discharge position between electrode tips for a lamp operated horizontally. 1: upward deflection of the discharge with length extension 2: normal position of the discharge 3: straightened position 4: downward deflection with the same length of the discharge as its normal position 5: downward deflection with length extension.

original position and make it stable.

In all cases the last part of the light deviation curve has a characteristic form. The last local minimum of the emitted light indicates that the discharge is straightened. This position is not stable and after about 100 ms, thermal convection forces deflect the discharge upward.

5.6 Evaluation of the Experimental Results

The section introduces an experimental method to determine the time constant of exciting acoustic resonances in HID lamps. A theoretical hypothesis based on the establishment of acoustic streaming is given to explain the retardation of discharge instabilities excited by AR. The experimental results of this research show that exciting acoustic resonance in an OSRAM 70W HCI lamp leads to a perceptible light deviation after less than 1 ms.

Fig. 5.11 sketches the light flicker factor (Afshar, 2006 I.) against the duration of the power ripple for different AR frequencies. Any point with the flicker factor greater than unity represents a perceptible light fluctuation as a result of the AR excitation. Obviously, a value of 10ms for this time constant as it is reported in (Wada and others, 1987) is not realistic, the discharge instability occurs much faster.

The temporal response of the lamp discharge to the acoustic instability is investigated. A direct method to measure the time constant of the discharge deflection caused by acoustic instability is proposed. The deflection time constant varies depending on the acoustic mode and the duration of the power ripple. This value ranges from 10 ms for excitation with 70 kHz (power ripple duration: 7.143 ms) to about 35 ms for the frequency of 32 kHz (power ripple duration: 31.25 ms). This is comparable to a typical time constant of 50 ms which is reported in (Calderia and others, 1999) for a 100W metal halide lamp. Figures 12 and 13 illustrate an example of superposition of high frequency ripple on a low frequency square waveform of current and voltage. The RMS value of the lamp current is kept constant. The effect of the acoustic resonance can be observed in voltage, power and emitted light signal. It should be noted that

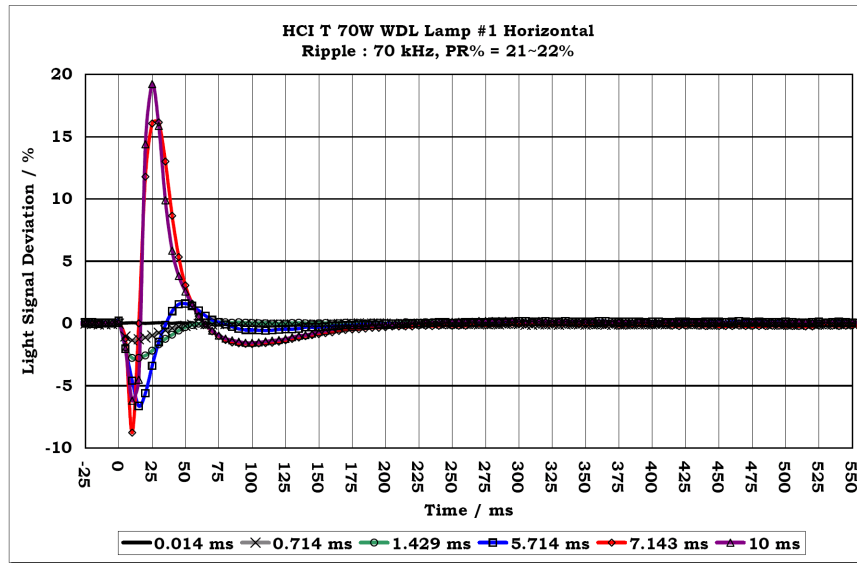


Figure 5.8: Light signal deviation (output of the Lux-meter normalized to its DC value) vs. time for different values of the ripple durations at the frequency of 70 kHz. The power ripple is set to 21-22%.

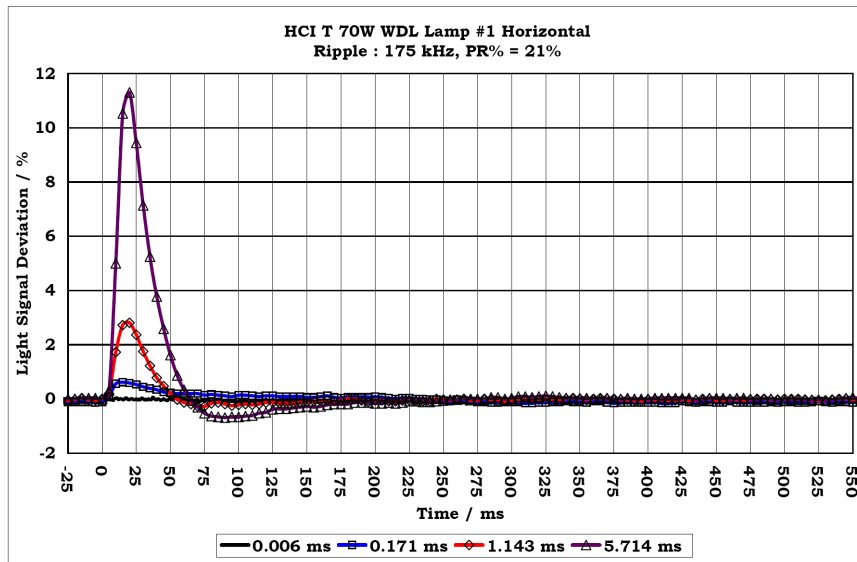


Figure 5.9: Light signal deviation (output of the Lux-meter normalized to its DC value) vs. time for different values of the ripple durations at the frequency of 175 kHz. The power ripple is set to 21%.

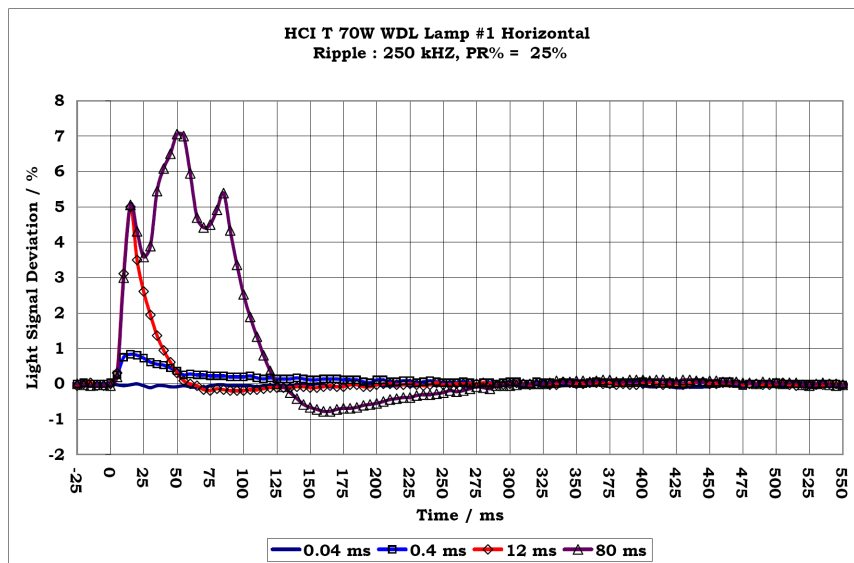


Figure 5.10: Light signal deviation (output of the Lux-meter normalized to its DC value) vs. time for different values of the ripple durations at the frequency of 250 kHz. The power ripple is set to 25%.

the response of lamp to the power ripple could be different (compared to Fig. 5.12 and 5.13) for operation with commercial electronic ballasts, because electronic ballasts use different methods, for example power regulation or current regulation, to control the supplied power to the lamp. The clock time of the controller which is used in the control loop of the electronic ballast plays a significant role in this regard.

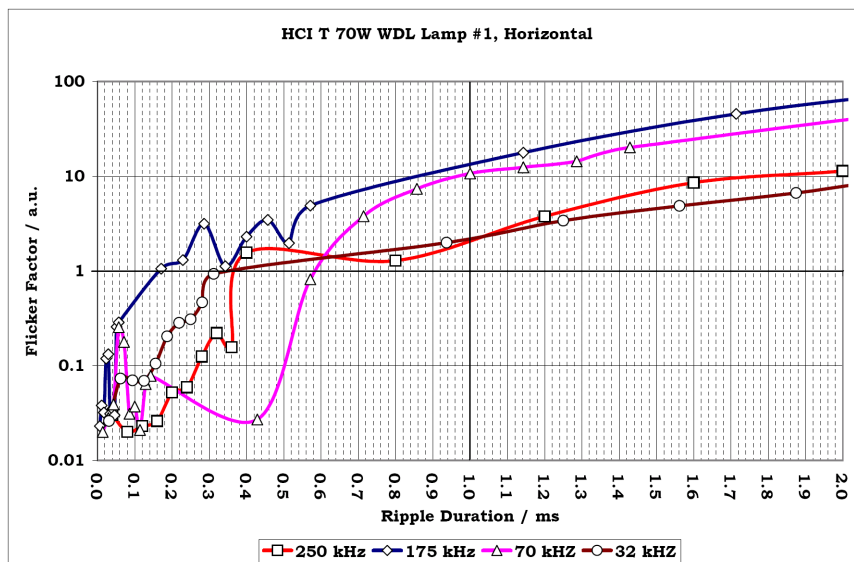


Figure 5.11: Flicker factor vs. ripple duration (semi Log) for different AR frequencies. The power ripple is 20~25%.

The results of such measurements are quite helpful for applications which are related to both avoidance and excitation of acoustic resonances in HID lamps. For applications that the

excitation of AR must be avoided, the time duration in which the conditions of excitation of AR are satisfied should be always kept below the onset time. In contrast, for applications in which the excitation of AR is desired, it should be known that a certain time interval is required for AR to be excited after satisfying its conditions.

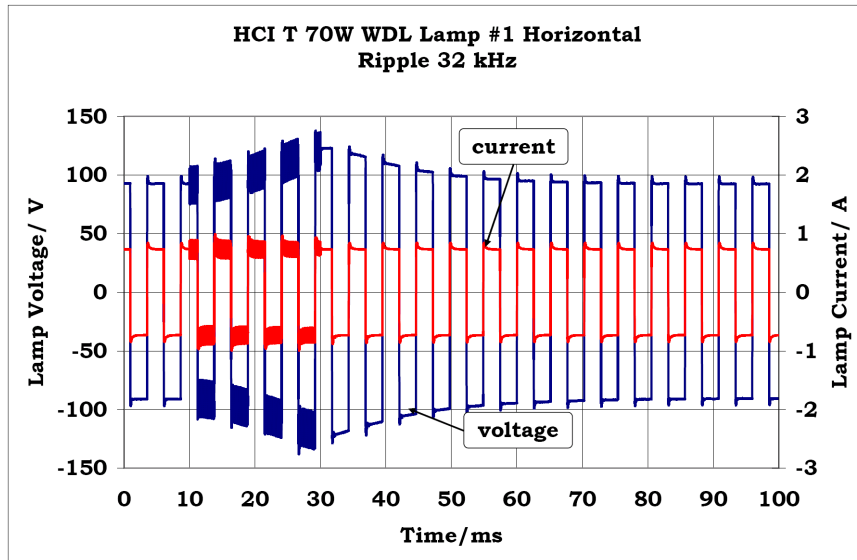


Figure 5.12: Voltage and current waveform of an OSRAM HCI 70W lamp subjected to a 20ms sinusoidal ripple at the frequency of 32 kHz and power ripple of 21%.

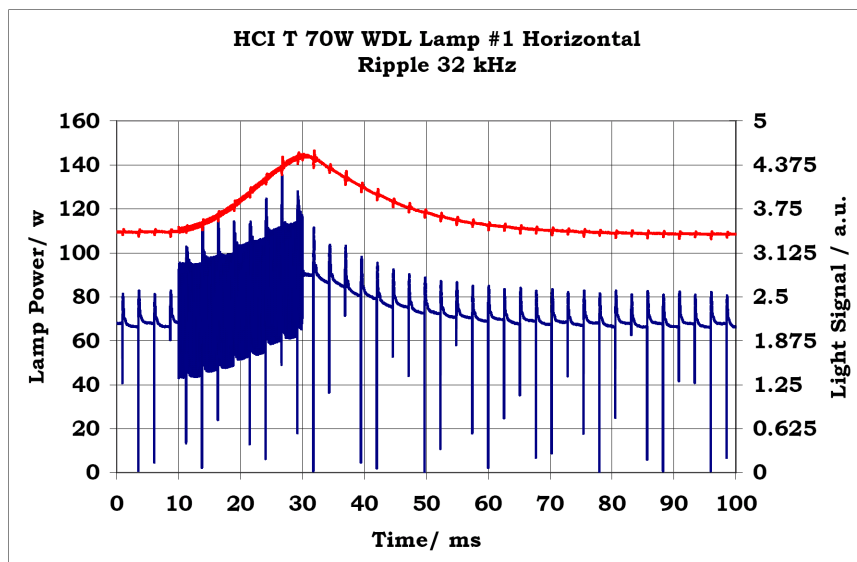


Figure 5.13: Light signal (upper curve) and calculated power waveform (lower curve) for an OSRAM HCI 70W lamp subjected to a 20 ms sinusoidal ripple at the frequency of 32 kHz and power ripple of 21%.

Chapter 6

Experimental Results and Conclusion

6.1 Experimental Results

This section is dedicated to present some experimental results and the discussion about the outcome of the measurements. The aim of these measurements is to find acoustic resonance frequencies and the allowed level of the power ripple as a function of the power ripple frequency. The scope of the measurements is low wattage metal halide lamps in a range of 35 to 250 W and in a frequency range of 10 to 400 kHz.

For each lamp there are four graphs indicating important parameters which are affected due to the existence of high frequency components in the lamp's power spectrum. That is, the parameters are sketched versus the power ripple frequency. It is worth to note that if for some applications the lamp is supposed to operate with a sinusoidal voltage and current waveform, the frequency of the current and voltage should be considered half of the power ripple frequency. This is due to duplication of the power frequency when the current and voltage waveforms are sinusoidal.

For each lamp:

- The first graph is the value of acceptable power ripple by which the excitation of acoustic instability remains imperceptible or there is no instability due to excitation of acoustic resonances. This curve compares the measured value with the value of 1.5% which is currently considered as the upper limit of the power ripple in some lighting communities.
- The second graph illustrates the lamp power fluctuations as a result of excitation of acoustic resonances with the highest value of the power ripple which was applied to the lamp.
- The third graph shows changes of the lamp impedance (percentage of the relative impedance of the lamp with respect to the lamp impedance without high frequency ripple) with the highest value of the power ripple. A useful application of this measurement is to finding the acoustic frequency regions within which the possibility of the arc straightening exists. The frequency regions with negative relative impedance are possible candidates for this application.
- The fourth graph is the value of the light flicker factor with the highest value of the power ripple which was applied to the lamp. A comparison of this value with unity represents the perceptible/imperceptible transient of emitted light of the lamp at each ripple frequency.

Afterwards for each lamp category, with respect to their nominal wattage, a general graph is given. This graph combines the results of all measurements (different lamps and different

burning positions) of acceptable power ripple. In fact the information which is given by these graphs is the essence of the experimental attempts of this research.

Practically this means that:

the frequency spectrum of the power ripple of an electronic ballast which is supposed to drive all lamps of each category should be located under the given acceptable power ripple curve in the whole frequency span.

6.1.1 Measurements' Results for 35 W Metal Halide Lamps

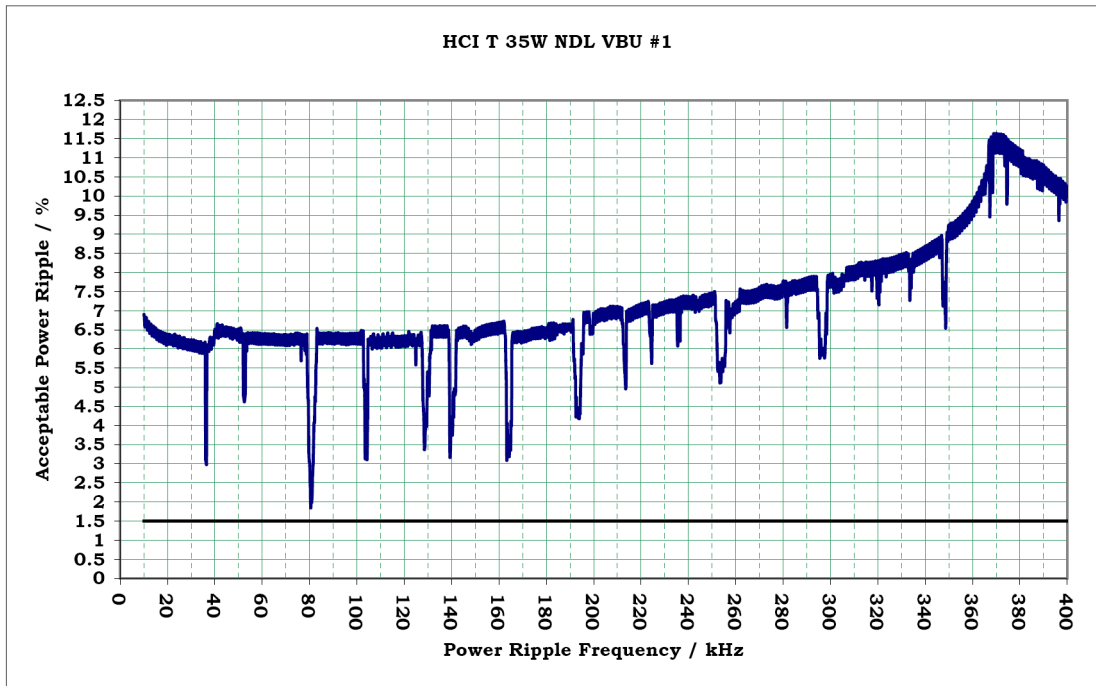


Figure 6.1: Acceptable power ripple vs. power ripple frequency for an OSRAM HCI T 35W NDL lamp operated vertically based up.

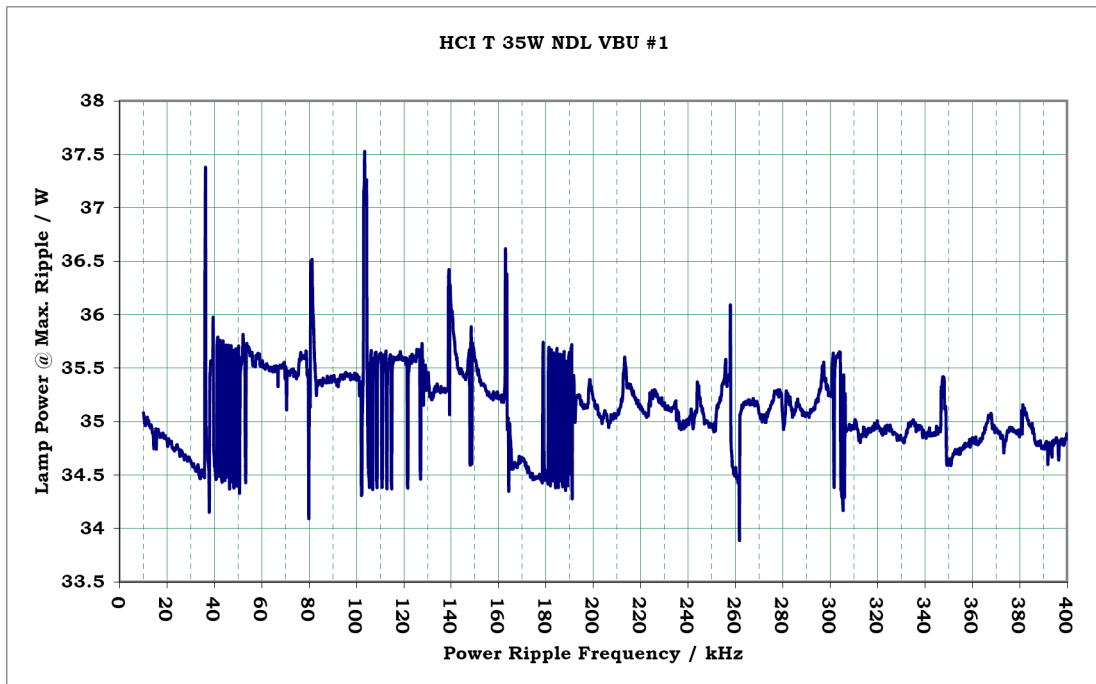


Figure 6.2: Fluctuations of the lamp power vs. power ripple frequency for an OSRAM HCI T 35W NDL lamp operated vertically based up.

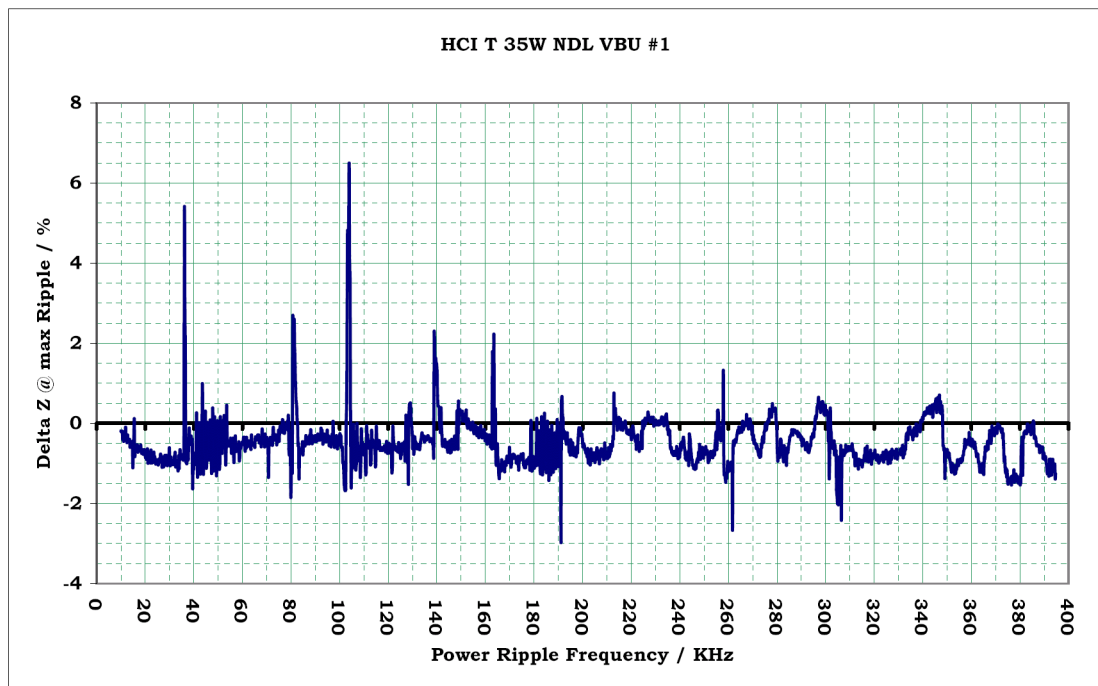


Figure 6.3: Relative impedance of the lamp vs. power ripple frequency for an OSRAM HCI T 35W NDL lamp operated vertically based up.

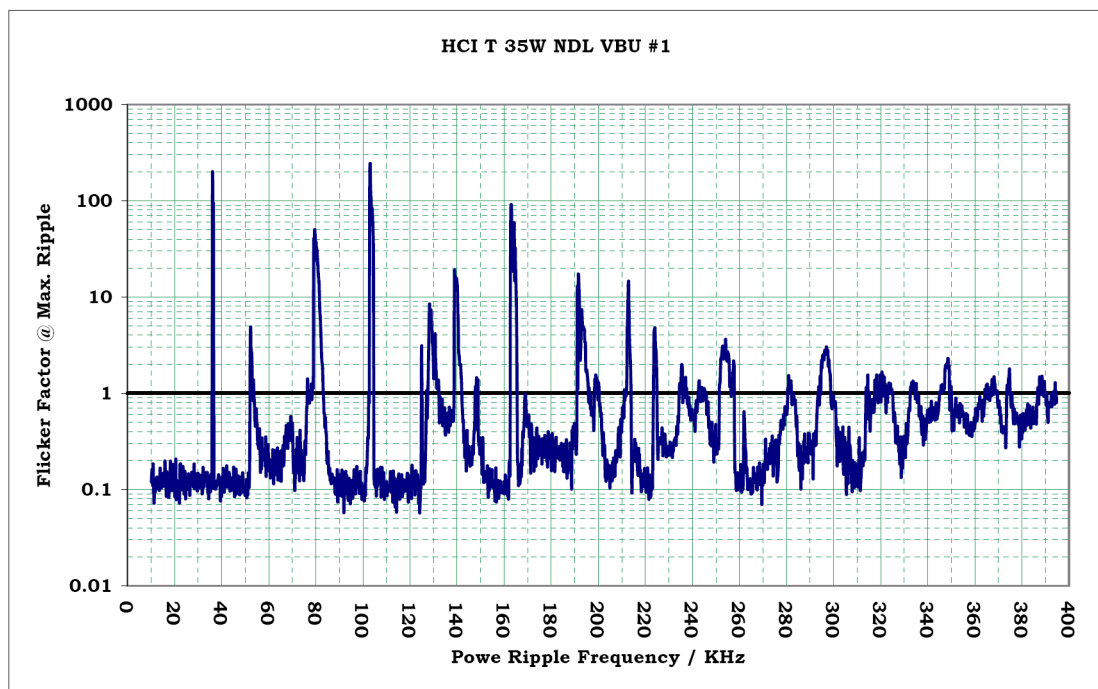


Figure 6.4: Light flicker factor vs. power ripple frequency for an OSRAM HCI T 35W NDL lamp

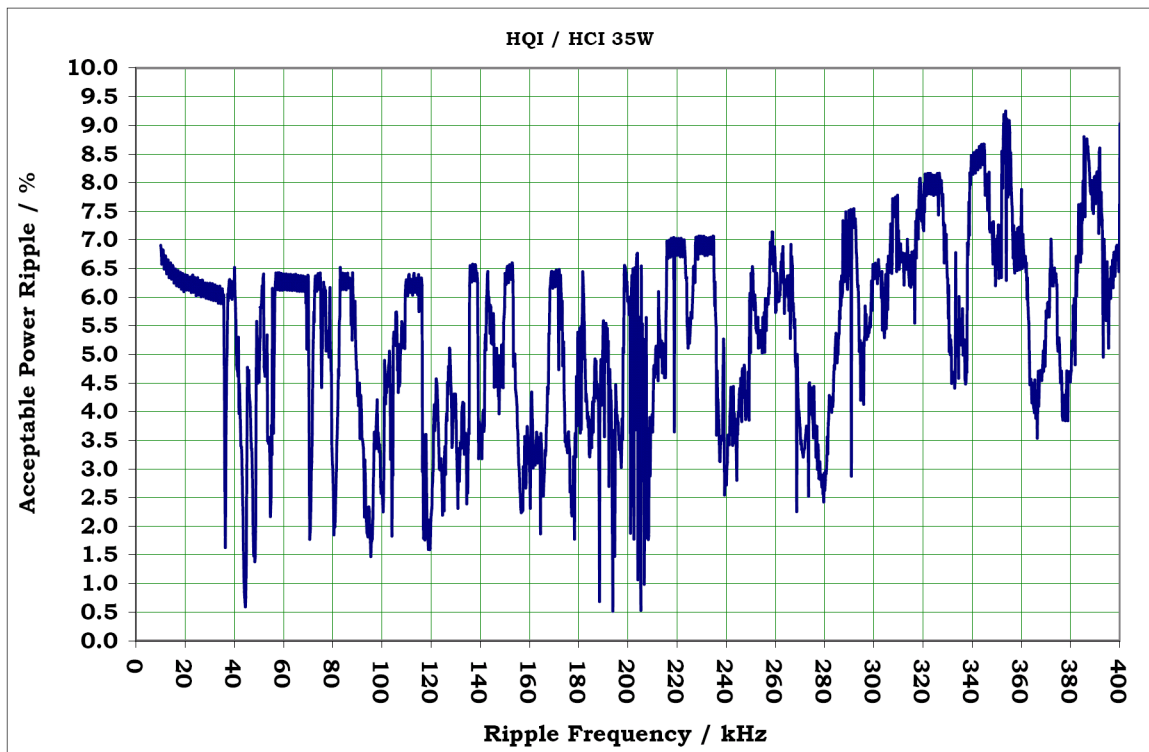


Figure 6.5: Acceptable power ripple for 35 W lamps based on the all measured 35 W lamps.

6.1.2 Measurements' Results for 70 W Metal Halide Lamps

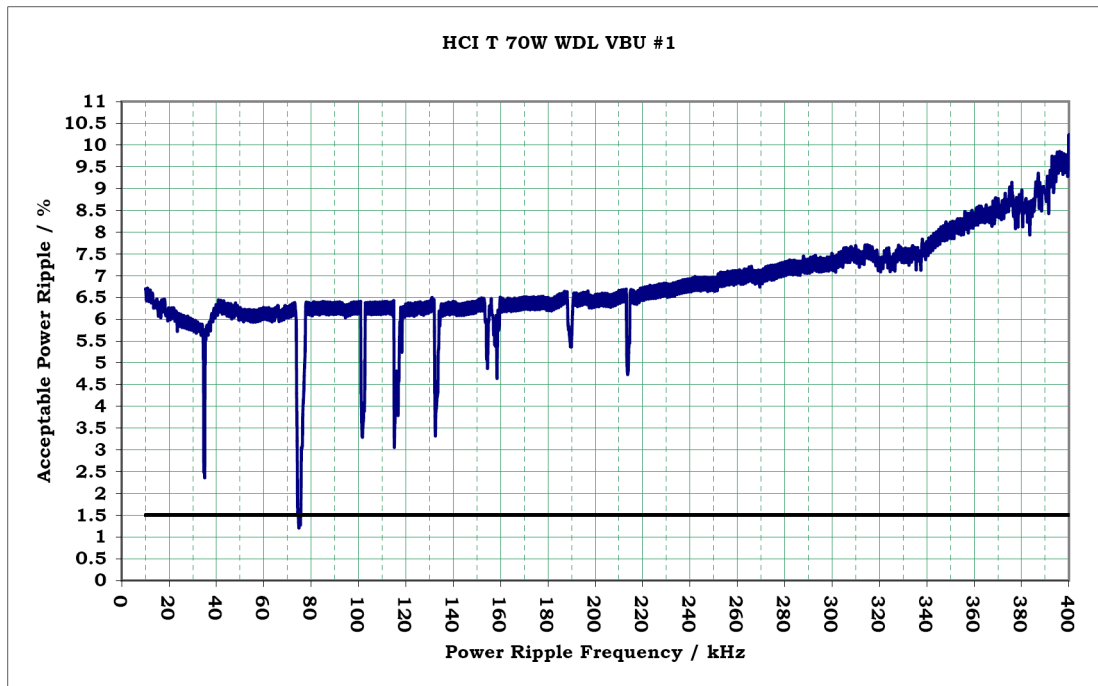


Figure 6.6: Acceptable power ripple vs. power ripple frequency for an OSRAM HCI T 70W WDL lamp operated vertically based up.

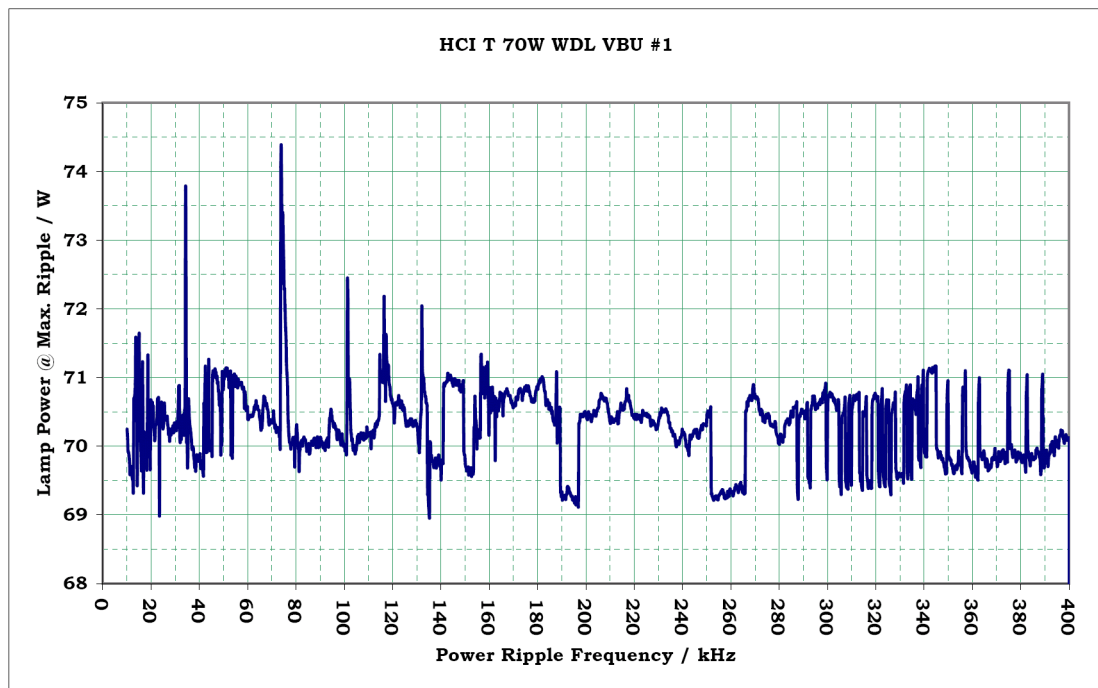


Figure 6.7: Fluctuations of the lamp power vs. power ripple frequency for an OSRAM HCI T 70W WDL lamp operated vertically based up.

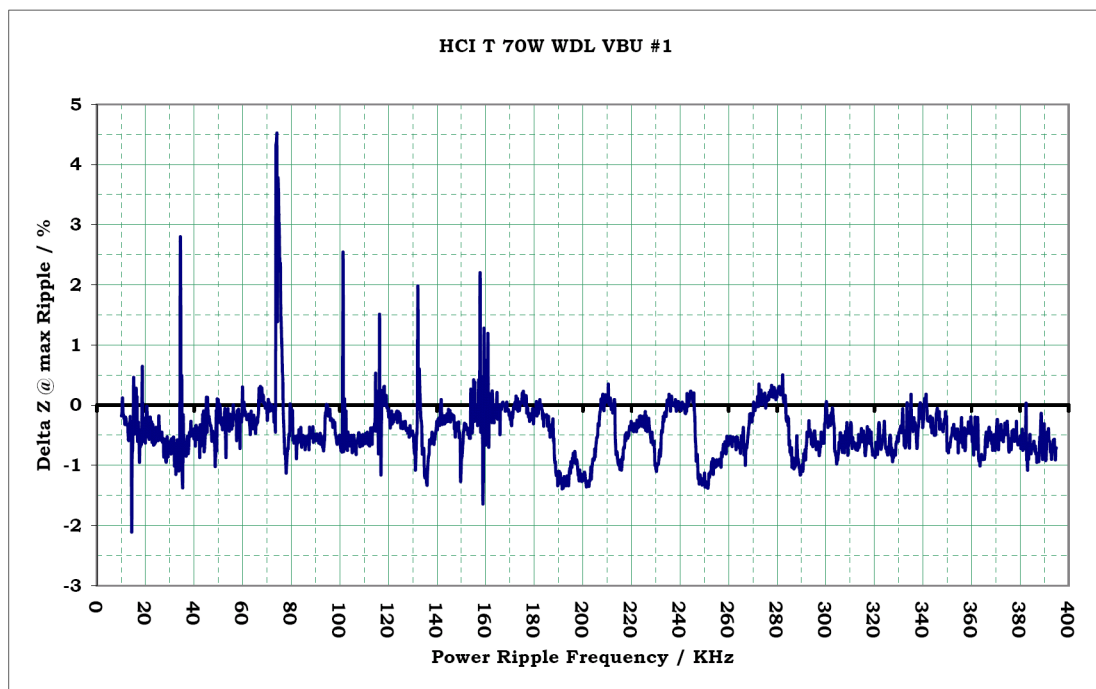


Figure 6.8: Relative impedance of the lamp vs. power ripple frequency for an OSRAM HCI T 70W WDL lamp operated vertically based up.

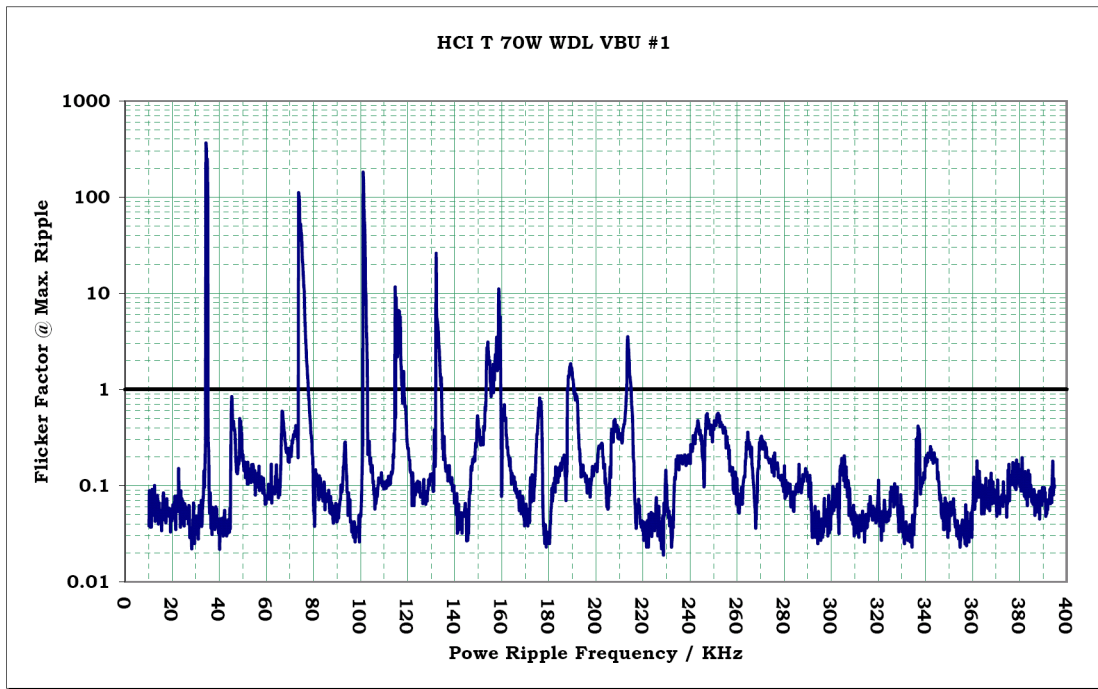


Figure 6.9: Light flicker factor vs. power ripple frequency for an OSRAM HCI T 70W WDL lamp

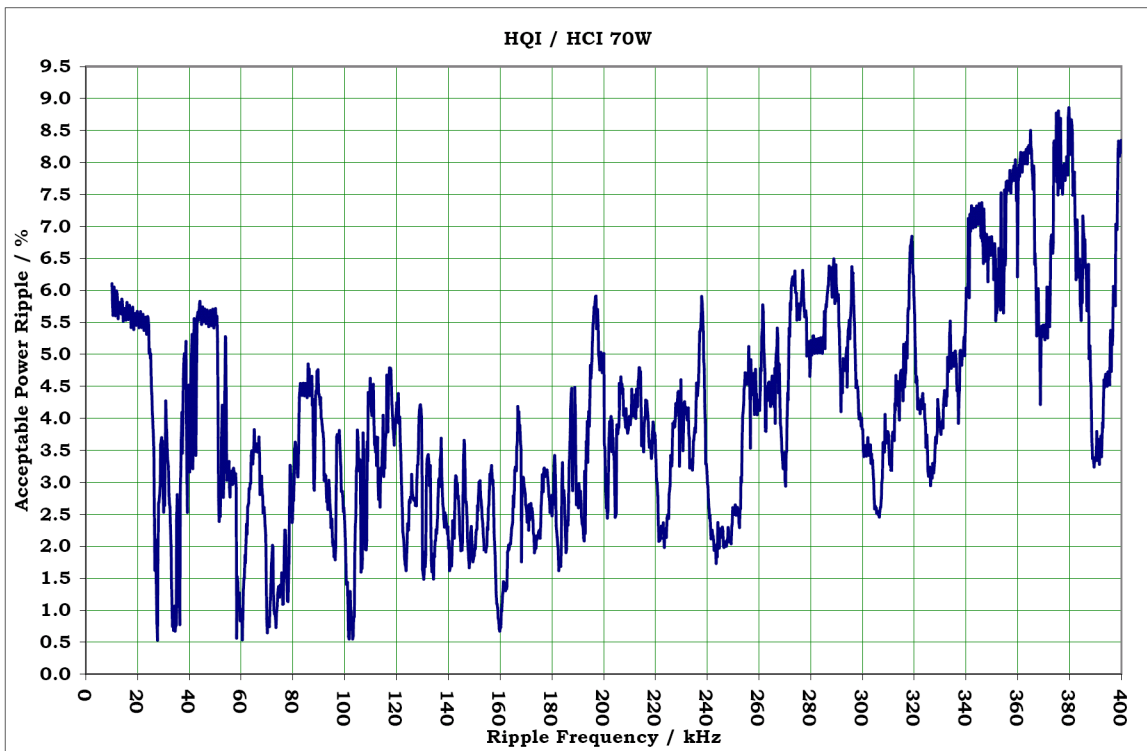


Figure 6.10: Acceptable power ripple for 70 W lamps based on the all measured 70 W lamps.

6.1.3 Measurements' Results for 150 W Metal Halide Lamps

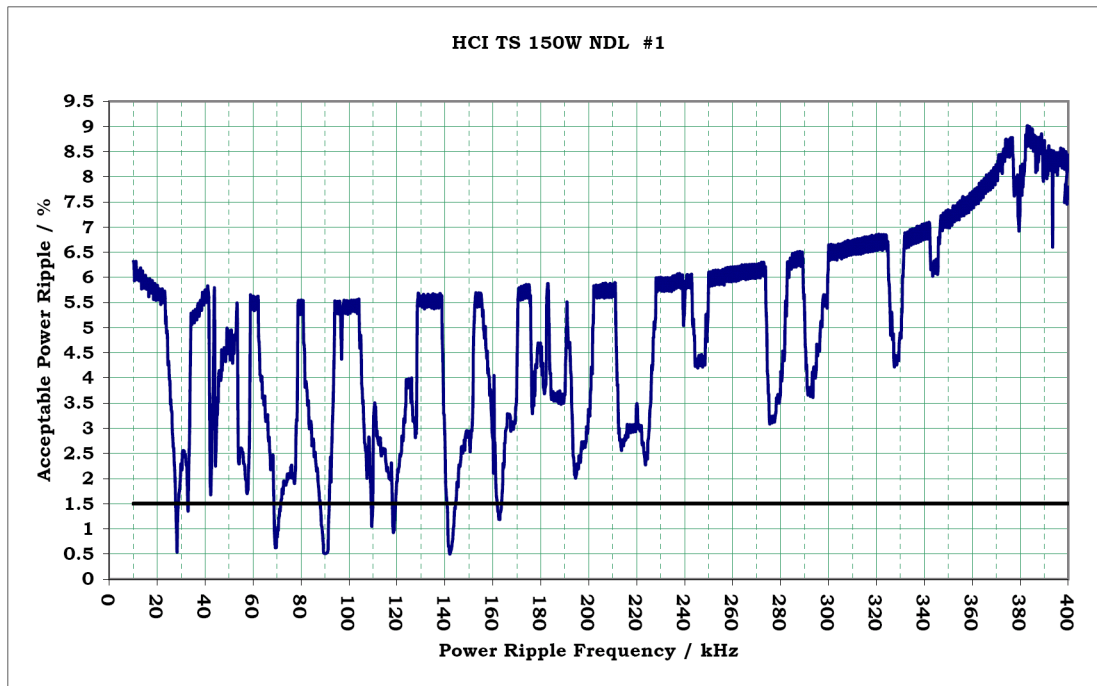


Figure 6.11: Acceptable power ripple vs. power ripple frequency for an OSRAM HCI TS 150W NDL lamp operated vertically based up.

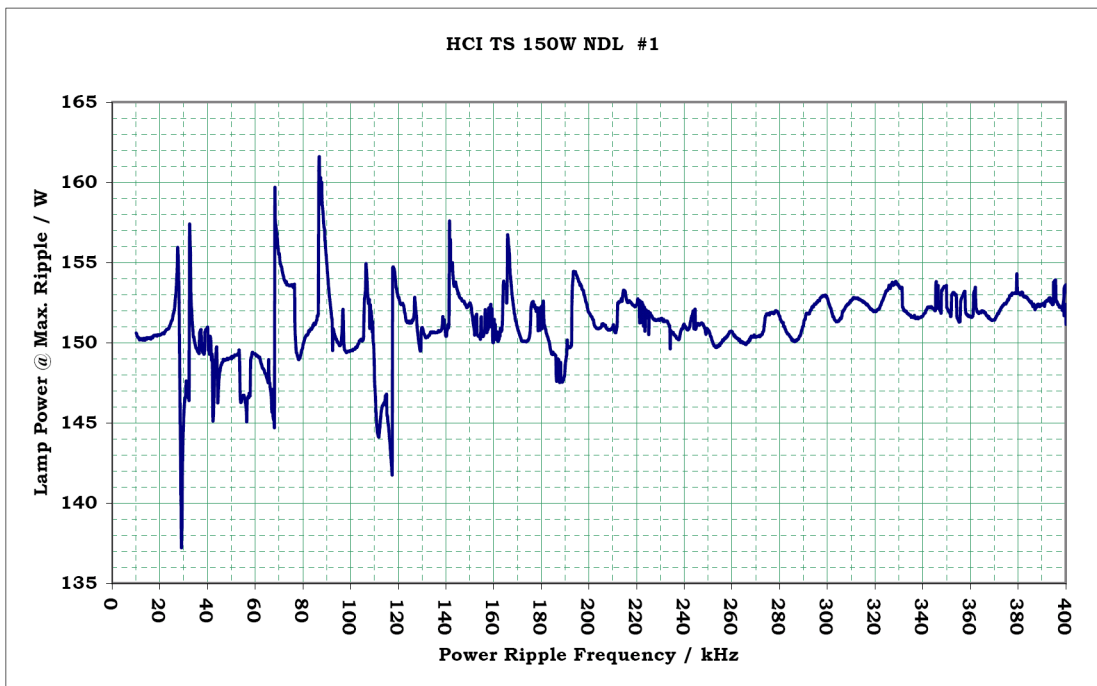


Figure 6.12: Fluctuations of the lamp power vs. power ripple frequency for an OSRAM HCI TS 150W NDL lamp operated vertically based up.

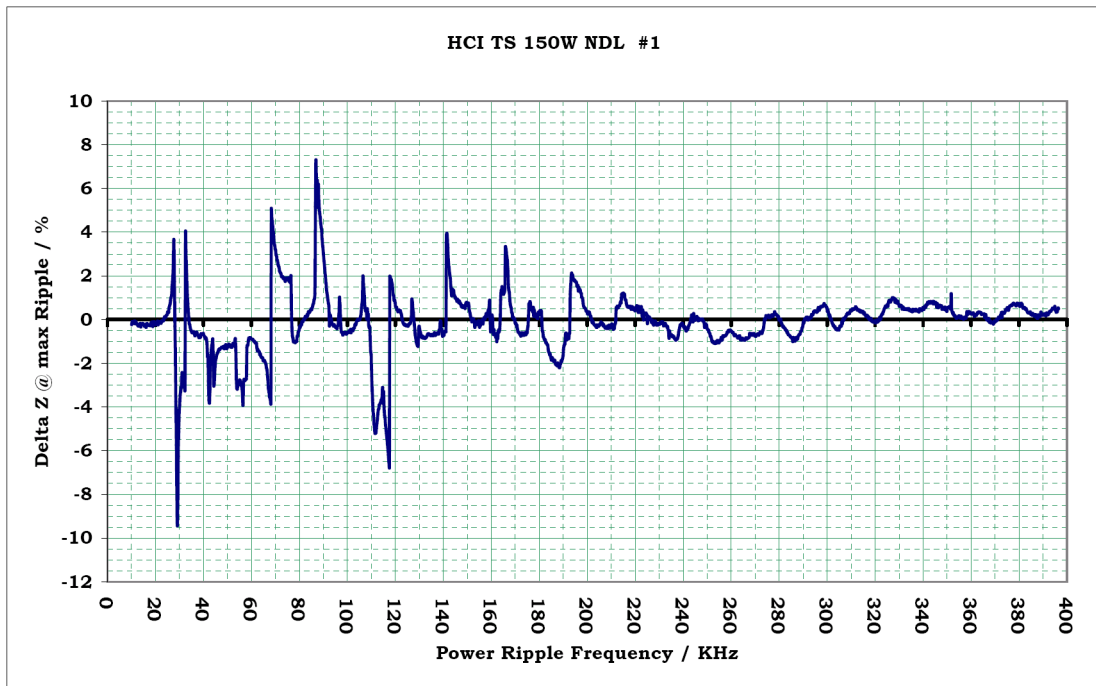


Figure 6.13: Relative impedance of the lamp vs. power ripple frequency for an OSRAM HCI TS 150W NDL lamp operated vertically based up.

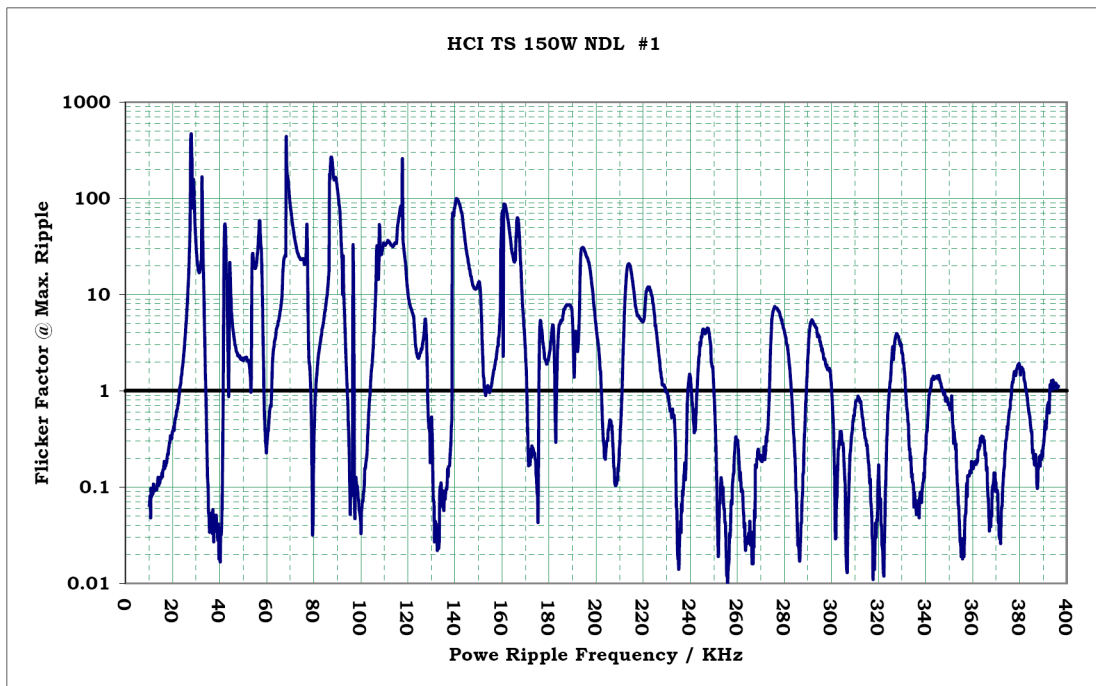


Figure 6.14: Light flicker factor vs. power ripple frequency for an OSRAM HCI TS 150W NDL lamp

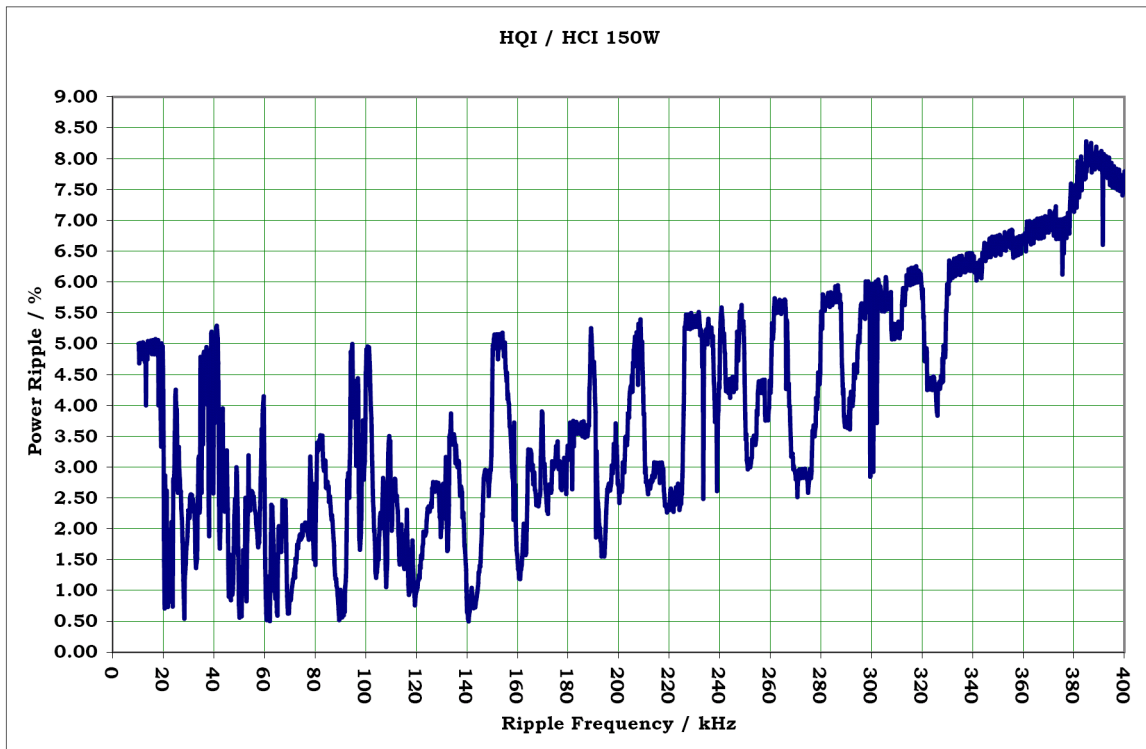


Figure 6.15: Acceptable power ripple for 150 W lamps based on the all measured 150 W lamps.

6.1.4 Measurements' Results for 250 W Metal Halide Lamps

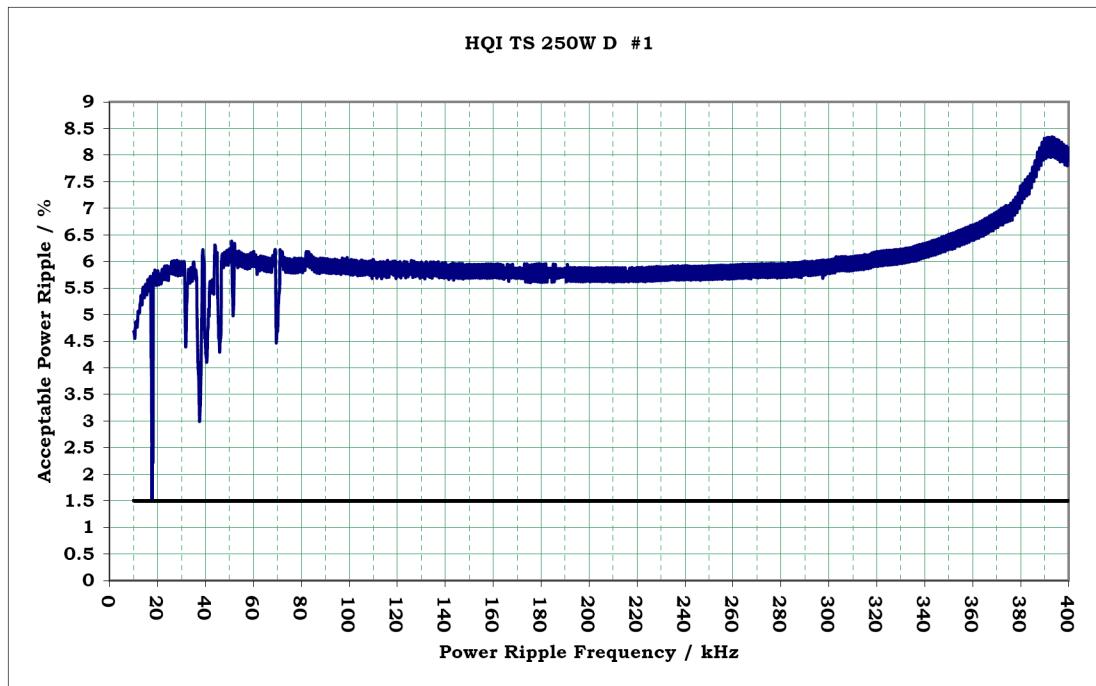


Figure 6.16: Acceptable power ripple vs. power ripple frequency for an HQI TS 250W D lamp operated vertically based up.

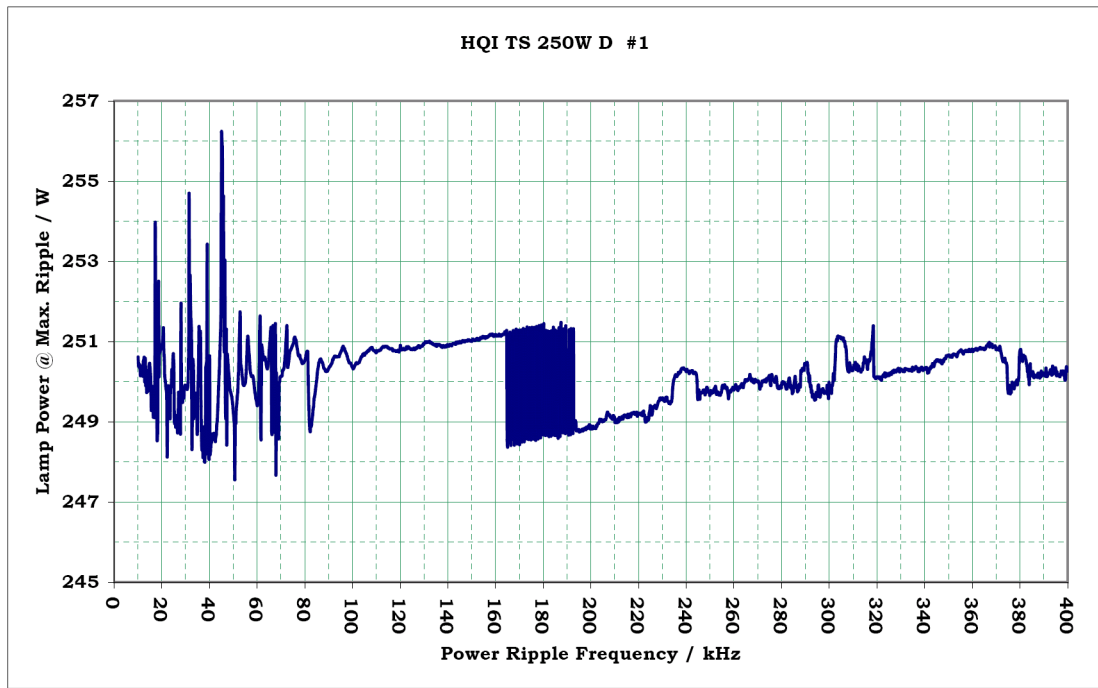


Figure 6.17: Fluctuations of the lamp power vs. power ripple frequency for an HQI TS 250W D lamp operated vertically based up.

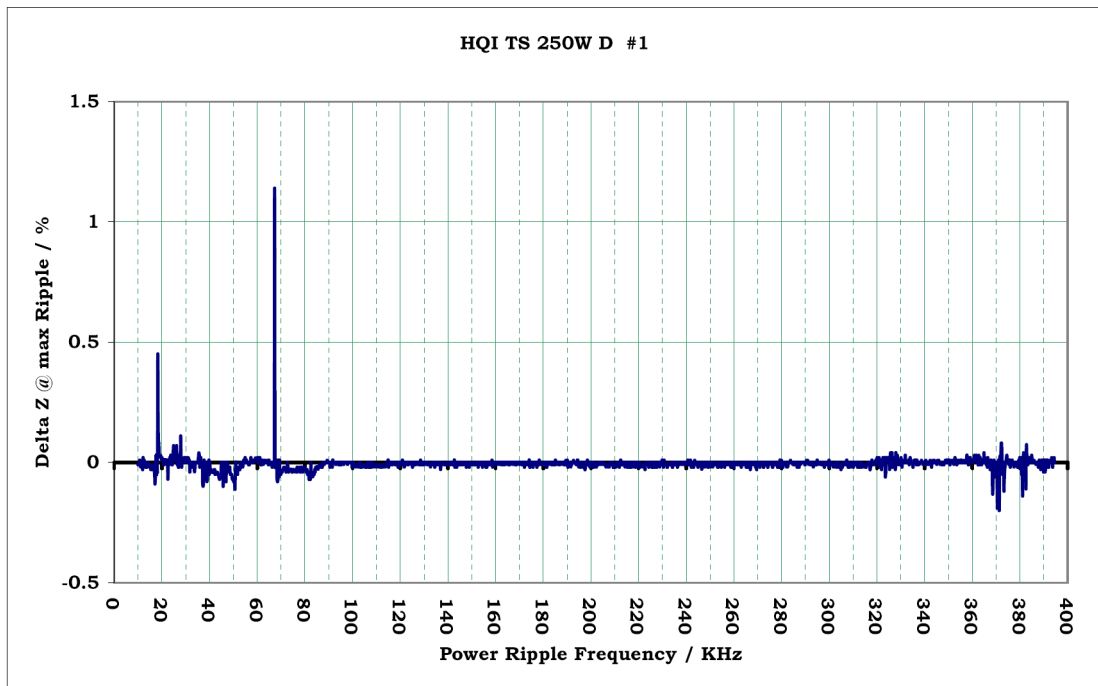


Figure 6.18: Relative impedance of the lamp vs. power ripple frequency for an HQI TS 250W D lamp operated vertically based up.

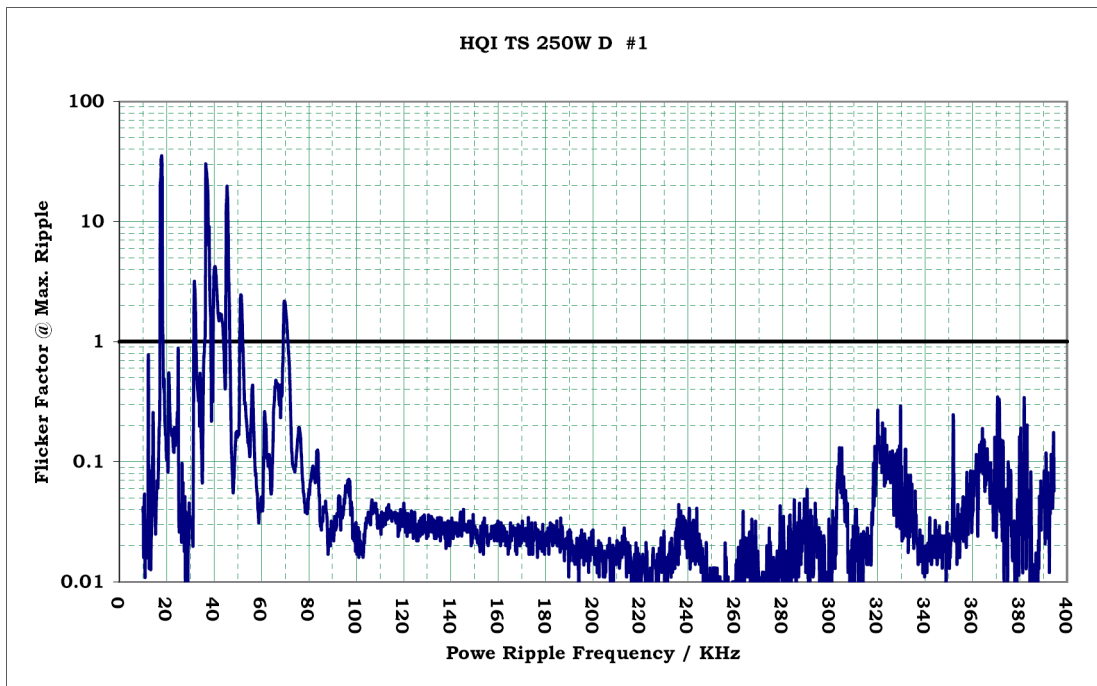


Figure 6.19: Light flicker factor vs. power ripple frequency for an HQI TS 250W D lamp

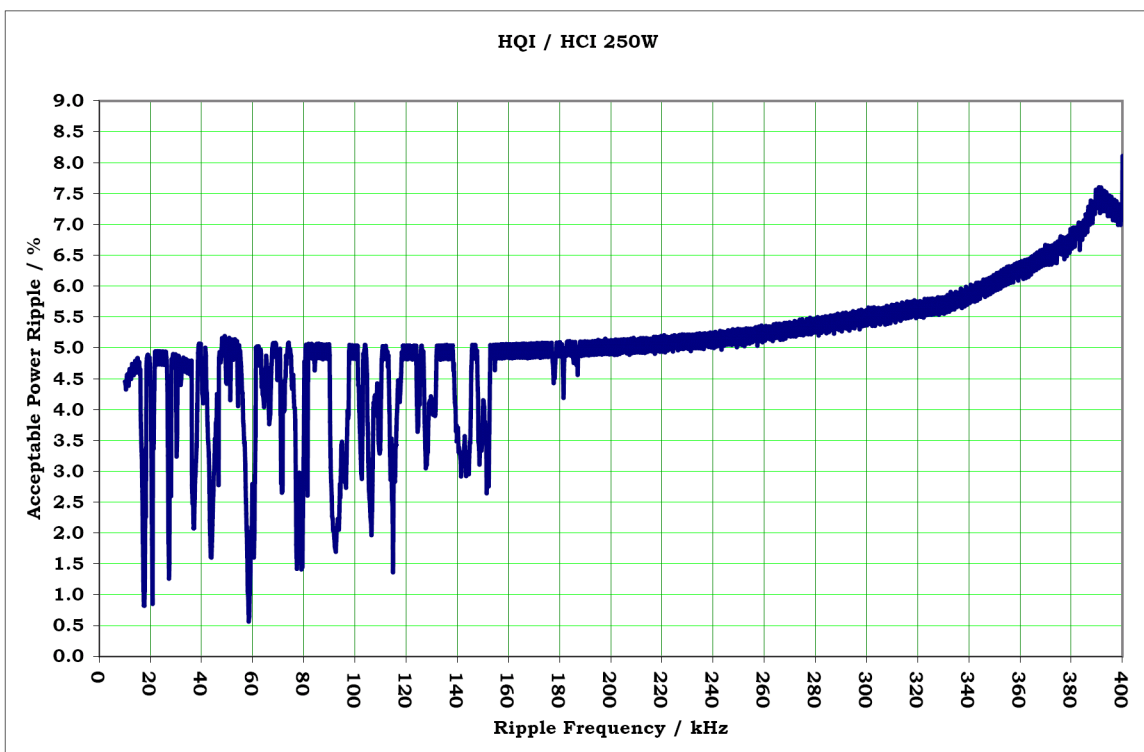


Figure 6.20: Acceptable power ripple for 250 W lamps based on the all measured 250 W lamps.

6.2 Conclusion

This work explores the concept of acoustic resonance in HID lamps theoretically and experimentally. A phenomenological investigation was carried out to contribute and promote existed theories which try to explain the physical backgrounds of excitation of acoustic instabilities. An explanatory theory of acoustical instabilities based upon the establishment of acoustic streaming in HID lamps was developed and discussed. The problem of acoustic resonance, concerning a given temperature distribution inside the arc tube of the lamp, was numerically solved. The solution confirmed some practical observations such as:

- The strength of acoustic modes decreases with increase of the acoustic resonance frequency.
- By increasing the frequency, the spectrum of resonance frequencies approaches a continuum, while at low frequencies the resonant frequencies are more widely spread.
- Consideration of temperature distribution shows a considerable effect on calculated acoustic resonance frequencies (and acoustic mode-shapes). This explains the significant difference between the lamp sensitivity to acoustic resonance excitation for different burning positions of the lamp.

The classic method, (Witting, 1978; de Groot and van Vliet, 1986) based on (Morse, 1948) for calculation of acoustic resonant frequencies, deals only with cylindrical geometry of arc tube and does not account for temperature distribution. In contrast, the method of this work which uses the proposed method of (Davenport and Petti, 1985) considers the real geometry of the arc tube and the temperature distribution inside the arc tube.

Numerical calculation of wave equation inside the arc tube helps us find the position of nodes and antinodes of standing pressure wave and linear acoustic velocity. Regarding the acoustic streaming theory direction and position of streams of filling materials can be determined. This may help understand and predict the effect of excitation of acoustic resonances on discharge at different acoustic modes.

In a real case, the hypothesis of "effect of acoustic streaming on the discharge" is used to explain the behavior of the lamp discharge as a result of excitation of acoustic resonance. It is shown that the proposed hypothesis is able to explain some observations regarding acoustic instability of discharge.

The practical aspect of this work, aims to determine the acceptable level of the high frequency components of the power waveform which is allowed to flow from the ballast into the lamp. Any perceptible changes of emitted light of the lamp caused by excitation of acoustic resonances must be avoided. Based on this criterion, a method and a measuring system is designed and implemented to quantify the light flicker with respect to the human eye perceptibility to the transient light. This measuring system can be used for any other application in which the investigation of the light intermittent with respect to the human vision system is desired.

A fully automated measuring system, including the light flicker meter, is developed to experimentally determine the sensitivity of any HID lamp to the high frequency components of the power waveform regarding the excitation of acoustic resonances.

Based on the laboratory measurements carried out in OSRAM GmbH, the acceptable value of the power ripple for low wattage metal halide lamps is determined. As it was expected, the allowed level of the power ripple extremely depends on the ripple frequency and the burning position of the lamp. Generally speaking a ripple with an amplitude of less than one percent at the resonant frequency can excite a perceptible arc instability.

In chapter four it is shown that the proposed method has an acceptable reproducibility. A comparison of the measurements results (see Fig. 4.28) of the proposed method of this work with that of the method of (Olsen and Moskowitz, 1997) illustrates the reliability of this measuring system.

Fig. 6.21 sketches the acceptable power ripple of all measured 150W lamps and the measured power ripple of POWERTRONIC PTi 150 electronic ballast, against the ripple frequency.

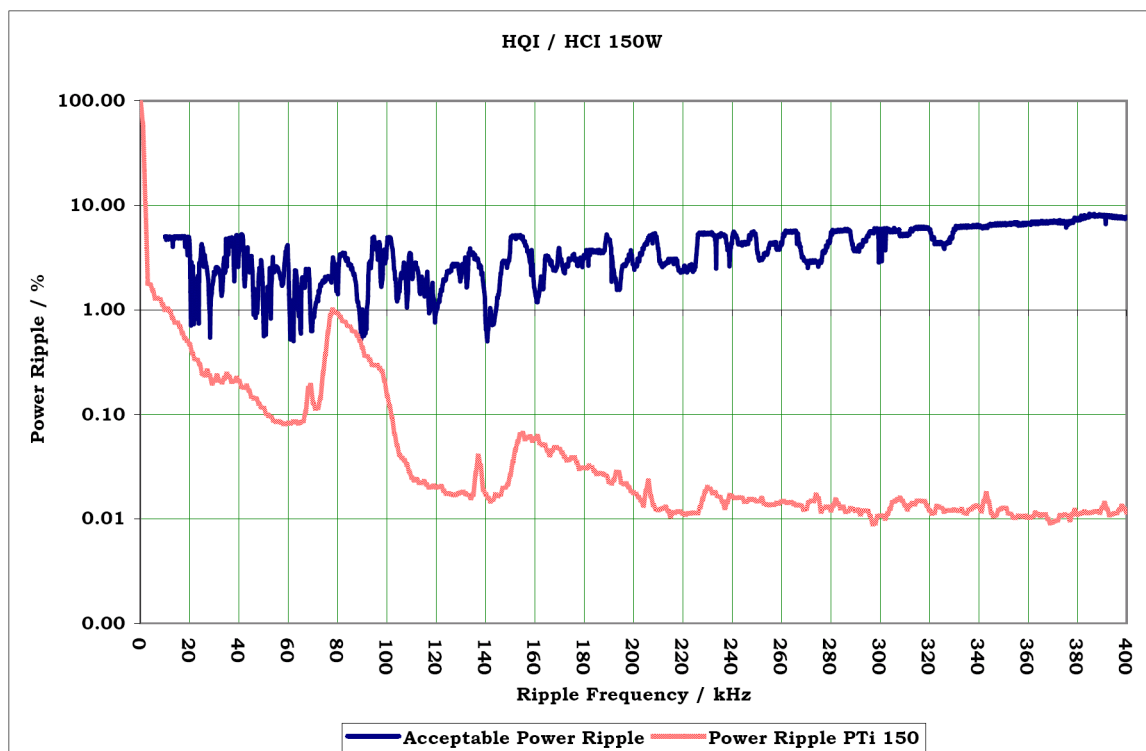


Figure 6.21: Acceptable power ripple for 150W lamps compared with POWERTRONIC PTi 150 Power Ripple.

As can be seen, the overall value of the power ripple of POWERTRONIC PTi 150, is still below the threshold value of power ripple for all measured 150W lamps. This means that although the ballast transfers high frequency components to the lamp (see figures 1.1 to 1.3), a lamp operation free of acoustic instabilities is expected by using this ballast.

Such measurements for any electronic ballast is decisive in order to determine whether the ballast may cause acoustic instability or not.

Table 6.1 summarizes the minimum and the maximum (measured up to 400 kHz) acoustic resonant frequency for any lamp category. As it was expected 250W lamps show the lowest minimum resonant frequency. This is mainly the effect of lamp arc tube's geometry. Since 250W lamps have the largest arc tube (in this group of lamps) the first acoustic mode in these lamps occurs at lower frequencies. In contrast, for 35W lamps with the smallest size of the arc

Lamp Category	min. Resonant Freq. kHz	max. Resonant Freq. kHz
35W	36.3	393
70W	27.7	390.7
150W	20.5	325
250W	17.5	152.3

Table 6.1: Max. and min. acoustic resonant frequency for low wattage metal halide lamps in a frequency range of 10-400 kHz.

tube this frequency is significantly higher.

The other concept which is theoretically and experimentally investigated is the onset time of the excitation of acoustic instabilities. According to the measurements which is discussed in the fifth chapter for some acoustic modes the time duration required to establish a perceptible change of the lamp discharge is less than 1 ms. This measured value is much lower than the time constant of about 10 ms which is reported in (Wada and others, 1987).

It should be noted that although the concept of acoustic resonance in HID lamps is known and reported since 1960's, there are still many unrevealed physical backgrounds which are needed to be able to explain the observations or model this phenomenon. This thesis tries to gather existing theories in the field of acoustic and physics of the HID lamps to give a better understanding of this subject.

As long as this thesis deals with a very specific measurements, which were not already existed, a significant part of this work is dedicated to define the methodology of measurements and to design and implement of the measurement systems.

Appendix A

Coefficients of IIR Filter

Coefficients of IIR filter which resembles the Attenuation Characteristic of the Human Eye

Step	a_0 for $f_s = 200 Hz$ and $f_s = 4kH$	a_1 for $f_s = 200 Hz$ and a_{20} for $f_s = 4kH$	a_2 for $f_s = 200 Hz$ and a_{40} for $f_s = 4kH$
1	1.0000000000000000	0.0000000000000000	0.0000000000000000
2	1.0000000000000000	0.0000000000000000	0.0000000000000000
3	1.0000000000000000	0.0000000000000000	0.0000000000000000
4	1.0000000000000000	0.0000000000000000	0.0000000000000000
5	1.0000000000000000	-1.438411252704130	0.570446281564561
6	1.0000000000000000	-1.880645035909870	0.884208206188637
7	1.0000000000000000	-1.899998100000000	0.902500000000000
8	1.0000000000000000	-1.899998100000000	0.902500000000000
Step	b_0 for $f_s = 200 Hz$ and $f_s = 4kH$	b_1 for $f_s = 200 Hz$ and b_{20} for $f_s = 4kH$	b_2 for $f_s = 200 Hz$ and b_{40} for $f_s = 4kH$
1	1.0000000000000000	1.989547081698220	0.999999800000010
2	1.0000000000000000	1.290526169778280	0.826441730999967
3	1.0000000000000000	0.207417519258380	0.363652885608599
4	1.0000000000000000	-0.267596690778833	0.181789640903222
5	1.0000000000000000	-1.294258775376100	0.457529211746861
6	1.0000000000000000	-1.964111892118920	0.965419502401698
7	1.0000000000000000	-1.984314774542740	0.984376477992438
8	1.0000000000000000	-1.906409179443660	0.913047766088119
		Scale Factor	0.048253300822139

Table A.1: Coefficients of eight 2^{nd} order and the corresponding 40^{th} order IIR filters.

Appendix B

Acoustic Resonance Frequencies for HQI TS 150W WDL

Allowed level of the power ripple for an OSRAM HQI TS 150W WDL is illustrated in Fig. B.1.

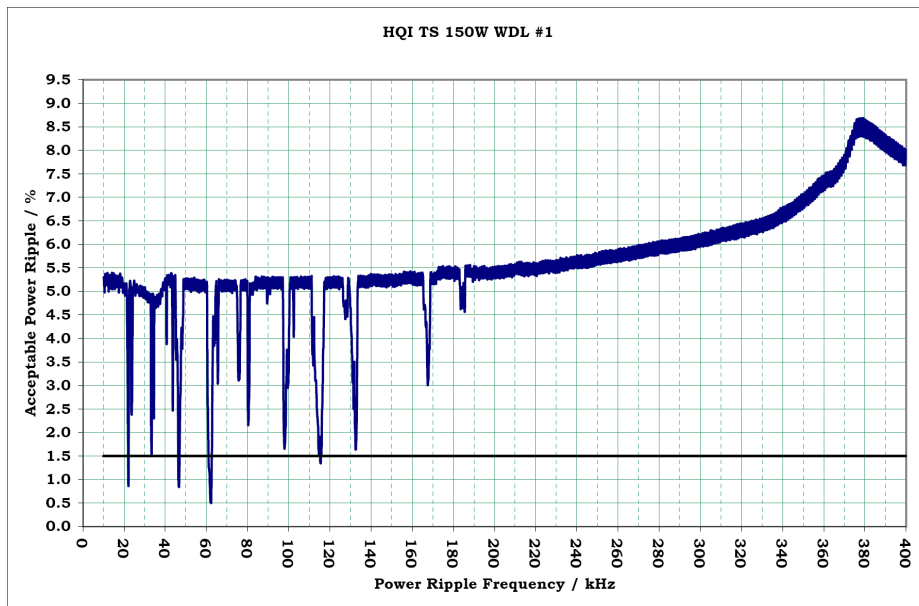


Figure B.1: Acceptable power ripple for HQI TS 150W WDL No. 1.

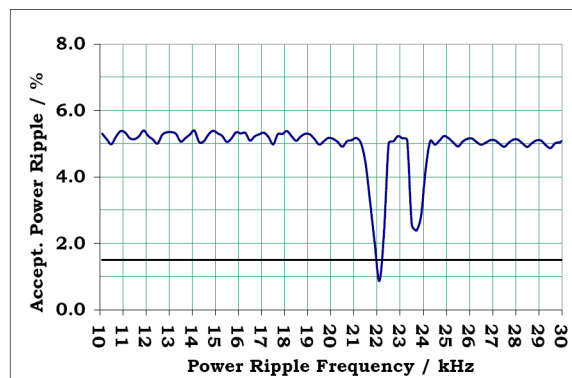


Figure B.2: Acceptable power ripple for HQI TS 150W WDL No. 1 for frequency range of 10-30 kHz to show the first longitudinal acoustic mode.

According to the diagrams of Fig. B.1 and B.2, the first acoustic resonant frequency is 22 kHz. Since this is the first resonant frequency, it is supposed that this is the frequency in which the first longitudinal acoustic mode is excited. It is known that the first longitudinal acoustic mode corresponds to the length of the arc tube as the longest dimension of it.

Appendix C

LabVIEW Program to determine the Allowed Level of the Power Ripple

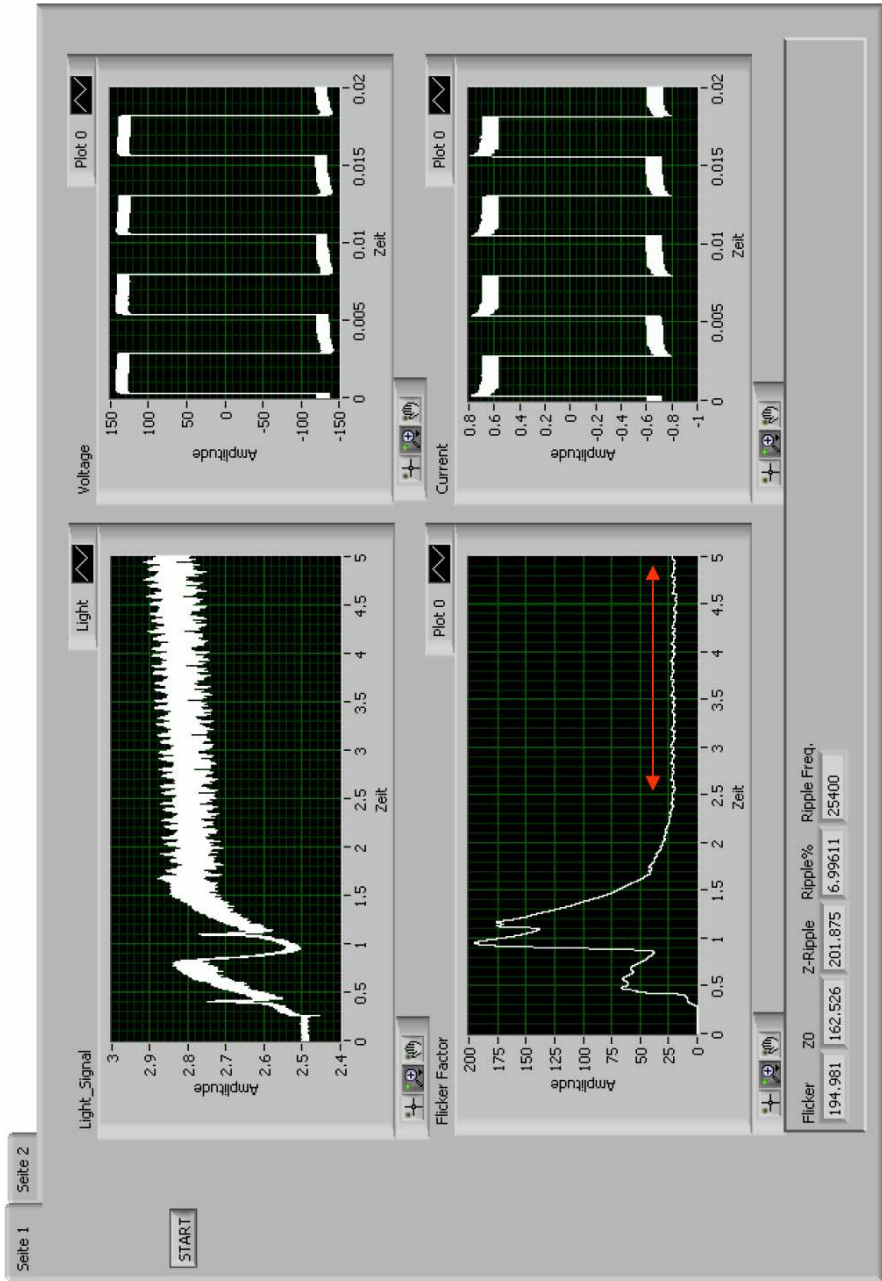


Figure C.1: LabVIEW program which is used to determine the allowed level of the power ripple.

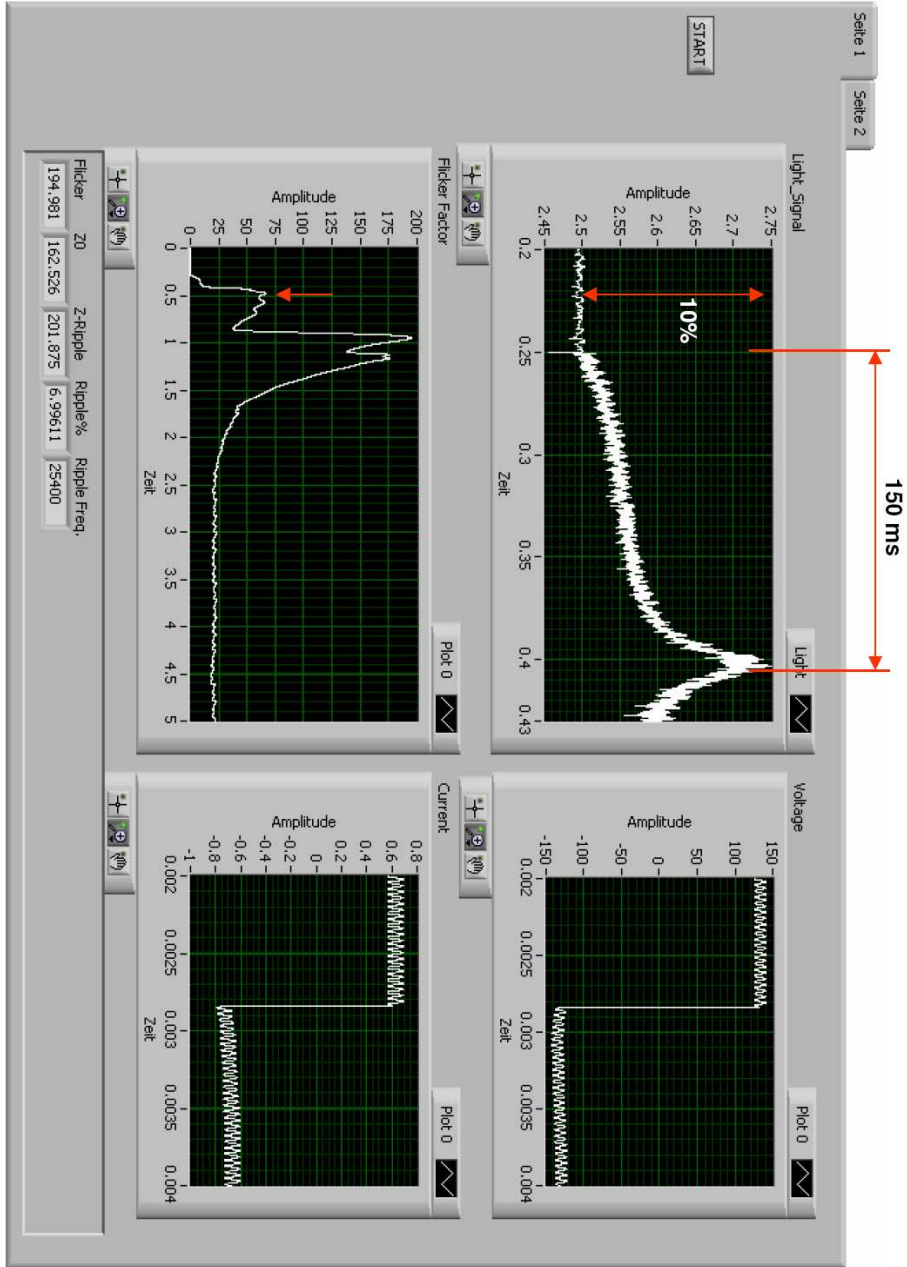


Figure C.2: LabVIEW program which is used to determine the allowed level of the power ripple.

Appendix D

List of Publications

- 1. Light Flicker factor as a Diagnostic Quantity for the Evaluation of Discharge Instabilities in HID Lamps**
LEUKOS, Journal of the Illuminating Engineering Society of North America, Vol. 3 No. 1 July 2006
Online:
<http://www.iesna.org/leukos/Volume3/number1.cfm>
- 2. Allowed Level of the Power ripple in Low Frequency Square Wave Ballasts of Metal Halide lamps.**
LEUKOS, Journal of the Illuminating Engineering Society of North America, Vol. 3 No. 2 October 2006
Online:
<http://www.iesna.org/leukos/Volume3/number2.cfm>
- 3. Measurement of the Onset Time of Acoustic resonance instabilities in HID Lamps.**
LEUKOS, Journal of the Illuminating Engineering Society of North America, Vol. 3 No. 3 January 2007
Online:
<http://www.iesna.org/leukos/Volume3/number3.cfm>
- 4. The Theory of Acoustic Resonance and Acoustic Instability in HID Lamps.**
LEUKOS, Journal of the Illuminating Engineering Society of North America, Vol. 5 No. 1 July 2008
Online:
<http://www.iesna.org/leukos/Volume5/number1.cfm>

Index

- Acoustic Resonance, 56
 - Acoustic Instability, 56
 - Analytical Solution, 63
 - Avoidance, 89
 - Benefits, 96
 - Damping Effect, 62
 - Pressure Effect, 62
 - Wall Effect, 62
 - Describing Equation, 61
 - Detection Methods, 85
 - Eigenfrequencies, 66
 - Importance of Acoustic Modes, 75
 - Interference with Acoustic Streaming, 83
 - Numerical Solution, 65
 - Theory of Acoustic Resonance, 56
- Acoustic Streaming, 58, 59
 - Analytical Solution, 81
 - Calculation of ..., 79
- Arc Straightening, 96, 133
- Buck Converter, 110
 - Buck Boost, 123
 - Ripple, 112
- Coupled Inductors, 116
- Critical Flicker Frequency, 13
- Diffusion Theory
 - Ives' Theory, 16
 - Veringa's Theory, 20
- Double Flash Test, 23, 43
- Effective Sound Velocity, 64
- Electrode Instability, 8
- Ferry-Porter Law, 15, 44
- Filter Characteristics of the Human Eye, 27
- Genetic Algorithm, 30
- Helical Instability, 8
- HID Ballast
 - Topology, 106
- Human Eye Temporal Modulation Sensitivity
 - Curve, 25
- Human vision Model
 - Model of De Lange, 19
 - Model of Kelly, 22
 - Model of Rashbass, 23
 - Model of Sperling and Sondhi, 20
- Light Flicker Factor, 8
 - F_{10} , 9, 26
- Model of the human vision, 28
- Onset Time of Acoustic Instability, 141
- Paley-Wiener Criterion, 20
- Power Ripple Percentage, 131
- Psychophysical Measurements, 45
- Re-ignition peak, 8
- Retina, 10
 - Construction of Retina, 10
- Sound Wave, 57
- Standing Wave, 57
- Stevens' Power Law, 13, 52
- Talbot-Plateau Law, 14
- Trolands, 16
- Voltage Flicker Meter, 10
- Weber's Law, 12
- Weber-Frchner Law, 13

Bibliography

- Adler, H. G. : 2000, *Diagnostic In Lamp Research to Evaluate HID Electrode and Ballast Performance.*, IEEE, Conference Record of the Industry Applications, Vol.: 5, On pages: 3309-3313
- Afshar, F. : 2006 (I.), *Light Flicker Factor as a Diagnostic Quantity for Evaluation of Discharge Instabilities in HID Lamps*, LEUKOS, The Journal of the Illuminating Engineering Society of North America. Vol. 3 No 1
- Afshar, F. : 2006 (II.), *Allowed Level of the power Ripple in Low Frequency Square Wave Ballast of Metal Halide Lamps.*, LEUKOS, The Journal of the Illuminating Engineering Society of North America. Vol. 3 No 2
- Afshar, F. : 2007, *Measurement of the Onset Time of Acoustic Resonance Instabilities in HID Lamps.*, LEUKOS, The Journal of the Illuminating Engineering Society of North America. Vol. 3 No. 3
- Allen, G. R. and others : 1992, *Acoustic Resonance Operation of Xenon-Metal Halide Lamps.*, US Patent 5,131,034
- Allison J. M. and others : 1990, *Ballast Circuit for Metal Halide Lamps.*, US Patent 4,904,907
- Alonso, j. M. : 2002, *Evaluation of High-Frequency Sinusoidal Waveform Superposed with 3rd Harmonic for Stable Operation of Metal Halide Lamps.*, IEEE Power Electronics Specialists Conference, PESC 2002, On Pages: 1483-1488
- Anton, J.C. and others: 2003, *Measurement System for Characterization of High Intensity Discharge Lamps (HID) operating at High frequency.*, Proceedings on the 20th IEEE Instrumentation Technology Conference 2002, On pages: 1359-1363
- Aramyan, A. R. and Galechyan, G. A. : 1997, *Characteristics of sound wave generation in gas discharge.*, Tech. Phys., August 1997. On pages: 901-904.
- Asi, H. and Perlman, I. : 1992, *The relationships between the ERG a-wave, b-wave and oscillatory potentials and their application to clinical diagnosis.*, Documenta Ophthalmologica 79, On pages: 125-139
- Balog, R. and others : 2000, *Coupled inductors - a basic filter building block.* Electrical Manufacturing and Coil Winding Association Conf., OH, 2000; and Electrical Manufacturing and Coil Winding Association Letters, 2002.

Internet web site:

http://www.hamill.co.uk/pdfs/ciabfbb_.pdf

- Balog, R. and Krein, P.T. : 2002, *Automatic Tuning of Coupled Inductor Filters.*, IEEE, The 3rd Annual Power Electronics Specialists Conference. Pesc 02. Vol 2, On pages: 591-596
- Beasley, D. D. : 1999, *Method of Avoiding Acoustic Compression Wave Resonance in High Frequency, High Intensity Discharge Lamps.*, US Patent 5,883,475
- Boluriaan S. and Morris P.J. : 2003, *Acoustic Streaming : From Rayleigh to today.*, Aeroacoustics Vol. 2 No. 3,4
- Brundrett, G. W. : 1992, *Human Sensitivity to flicker.*, Lighting Research and Technology Vol. 6 No. 3. On pages: 127-143
- Calderia, P. and others : 1997, *Controller for a Gas Discharge Lamp with Variable Inverter Frequency and with Lamp Power and Bus voltage control.*, US Patent 5,623,187
- Campbell, J.H. : 1969, *High Intensity Discharge lamp on High Frequency Power.*, Illuminating Engineering Society, December 1969. On pages: 713-722
- CCOH : *Canadian National Center for Occupational Health and Safety.*,
Internet web site:
http://www.ccohs.ca/oshanswers/ergonomics/lighting_flicker.html
- Chiu, H. J. and others : 2006, *A Frequency-Modulation Control Method for Elimination of Acoustic Resonance in HID Lamps.*, Proceeding of IASTED International conference on Intelligent System and Control. Honolulu Hawaii. On pages: 124-129
- Cho, B. C. and others : 2001, *A new HID Ballast using Internal LC Resonance and Coupled Inductor Filter.*, ICPE 2001, On pages: 737-740
- Conner, J.D. and MacLeod, D.I.A. : 1976, *Rod photoreceptors detect rapid flicker.*, Science 195, On pages: 698-699
- Correa, J. and others : 2004, *Evaluation of Close Loop Digital Control Based in a Microcontroller and Used to Eliminate Acoustic Resonances in HID Lamps.*, IEEE, 35th Annual Power Electronics Specialists Conference, PESC 04, Vol.: 1, On pages: 401-405
- Couwenberg and others : 2007, *Method and Apparatus for Driving a Gas Discharge Lamp.*, US patent 7,164,241 B2
- Dagnelie, G. : 1992, *Temporal Impulse Response from Flicker Sensitivities: Practical Considerations.*, Journal of the Optical Society of America A, On pages: 659-672
- Dalla Costa, M.A. and others : 2005, *Acoustic Resonance characterization of low wattage Metal Halide Lamps Under Low Frequency Square Waveform Operation.*, Conference Record of the Fourtieth IAS Annual Meeting. Volume 3, On pages: 1575-1580

- Dalla Costa, M.A. and others : 2007, *Acoustic Resonance characterization of low wattage Metal Halide Lamps.*, IEEE Transactions on Plassma Science. Vol. 35, No. 1 On pages: 43-58
- Davenport J.M. and Petti, R.J. : 1985, *Acoustic Resonance Phenomena in Low Wattage Metal Halide Lamps.*, Journal of Illuminating Engineering Society April 1985
- de Groot, J. J. and van Vliet, J.A.J.M. : 1986, *The High Pressure Sodium Lamp.*, Philips Technical Library.
- De Lange, H. : 1958, *Research into the Dynamic Nature of the Human Fovea Systems with Intermittent and Modulated Light. I. Attenuation Characteristic with White and Colored Light.*, Journal of the Optical Society of America, Vol. 48, Nr. 11 On pages: 777-784
- DIN EN 61000-3-3 : 2002, *Electromagnetic compatibility (EMC) – Part 3-3: Limits – Limitations of voltage changes, voltage fluctuations and flicker in public low-voltage supply systems.*
- Denneman, J.W. : 1983, *Acoustic Resonance in High Frequency Operated low Wattage Metal Halide lamps.*, Philips J. Res., 38, On Pages: 263-272
- Dubuc, B. : *The Brain from top to bottom, Vision, The Eye.*, Published by: Canadian Institutes of Health Research. (CIHR)
Internet web site:
http://thebrain.mcgill.ca/flash/d/d.02/d.02_cr/d.02_cr_vis/d.02_cr_vis.html
- Elholma, L. and others : 2004, *Luminance and Visibility in Road Lighting, Conditions, Measurements and Analysis*, Helsinki University of Technology, Lighting Laboratory. ISBN: 951-22-7232-6
Internet web site:
<http://www.lightinglab.fi/publications/files/report30.pdf>
- EN 61000-4-15 : 1998, *Electromagnetic compatibility (EMC) – Part 4-15: Testing and measurement techniques - Flickermeter - Functional and design specifications.*
- Epron, S. and others : 1998, *Acoustic Resonance Phenomena in High Pressure Discharge Lamps.*, Proceedings of the 8th International Symposium on the Science and Technology of Light Sources (LS-8). On pages: 348-349
- Faehnrich, H. J. and Rasch, E. : 1988, *Electronic Ballast for Metal Halide lamps.*, Journal of Illuminating Engineering Society. On pages: 131-140
- Fellows, M. and others : 1998, High Frequency HID Lamp System with Lamp Driven at a Frequency Above the Audible and Below the Lowest Lamp Resonant Frequency. US Patent 5,828,185
- Fellows, M. W. : 2003, *A Study of the High Intensity Discharge Lamp Electronic Ballast Interface.*, IEEE, Conference Record of the Industry Applications Conference, 38th IAS Annual Meeting vol.2. On pages: 1043-1048

- Flesch, P. and Neiger, M. : 1999, *Modeling of High Pressure Discharge Lamps Including Electrodes.*, IEEE Transactions on Plasma Science, Vol. 27, NO. 1. On pages: 18-19
- Fromm, D. C. and Hohlfeld, A. : 1993, *Reduced Flickering of Metal Halide Lamps by Optimized Electrode Design.*, JOURNAL of the Illuminating Engineering Society. On pages: 69-76
- Fuortes, M.G.F. and Hodgkin A.L. : 1964, *Changes in time scale and sensitivity in the ommatidia of Limulus.*, J Physiol. 1964 Jul.; 172(2) On pages: 239-263
- Galechyan, G. A. : 1995, *Acoustic Waves in plasma.*, Physics-Uspekhi 38(12). On pages: 1309-1330
- Galo, C. F. and Courtney, J. E. : 2004, *Acoustical Resonances in Modulated XenonKrypton Compact Arc Lamps.*, Applied Optics Vol. 6, No. 5. On pages: 939-941
- Garcia, J. and others : 2004, *New HF Square Waveform Ballast for Low Wattage Metal Halide Lamps Free of Acoustic Resonance.*, Records of the 39th Annual Meeting of Industry Applications Conference, Vol.: 1, On pages: 655-662
- Giese, H. : 1997, *Theoretische Untersuchungen zur Konvektion in Quecksilber-Hochdruckgasentladungslampen.*, Auflage Aachen: Verlag der Augustinus Buchhandlung.
- Gillis, K.A. and others, *Measurements of the Bulk Viscosity of Xenon (BVX).*, Chemical Science and Technology Laboratory. National Institute of Standards and Technology (NIST). Industrial and Analytical Instruments and Services.
Internet web site:
<http://www.cstl.nist.gov/projects/fy05/iais05gillis.pdf>
- Goodenough, F. : 1996, *Novel DC-DC Converter Keeps Power Constant.*, Electronic Design. On pages: 51-62
- Gomez, J. C. and Morcoz, M. M. : 2002, *Flicker Measurement and Light effect.*, IEEE Power Engineering Review November 2002. On pages: 11-15
- Graint, R. and Hammond, E.L. : 1931, *Comparative Studies on the Peripheral and Central Retina- V. The sensation time curve and the time course of the fusion frequency on intermittent stimulation.*, American Journal of Physiology 98, On pages: 654-663
- Greenwood, S.R. and Soar, S. : 2002, *High Intensity Discharge Lamp Ballast.*, US Patent: 6,384,544 B1
- Haitz, P. : 1986, *Ein Verfahren zur nomierten Flimmerbeurteilung von Bildschirmgeräten, basierend auf experimentellen Untersuchungen zur Flimmerverschmelzungsfrequenz des menschlichen Auges.*, Technische Universität München, Fakultät für Maschinenwesen. (Dissertation)
- Hamilton M.F. and Blackstock D.T. : 1998, *Nonlinear Acoustics.*, ISBN 0-12-321860-8

- Hamilton M. F. and others : 2003, *Thermal Effects on Acoustic Streaming in Standing Waves.*, Journal of Acoustical Society of America. Vol. 114 No. 6
- Hasebe T. and Matsumoto K. : 1976, *The Instability of High Intensity Discharge Lamp on High Frequency Operation.*, Preprint of the Technical meeting of Sources and Related Applications LS-76-7
- Henger, U. : 1986, *Untersuchungen zur Entwicklung eines Messgerätes zur Bestimmung des Flickerfaktors.*, Licht 86 7. Lichttechnische Gemeinschaftstagung Baden bei Wien, 13. to 16. Mai 1986
- Hentschel, H. J. : 2002, *Licht und Beleuchtung: Grundlagen und Anwendungen der Lichttechnik*, 5., neu bearb. u. erw. Aufl. - Heidelberg : Hüthig, 2002. ISBN 3-7785-2817-3
- Hofmann, D. : 1982, *Internal OSRAM Report.*
- Hsieh Y. C. and others : 2005, *Detection of acoustic resonance in metal halide lamps.*, Holon Academic Institute of Technology, Journal of Science and Engineering B, Volume 2
- Hubel, D. H. : 1989, *Augen und Gehirn Neurobiologie des Sehens.*, Erscheinen bei Spektrum der Wissenschaft in Heidelberg.
- Huynh, T. P. : 1999, *Electronic Ballast for a High Intensity Discharge Lamp with Automatic Acoustic Resonance Avoidance.*, US Patent 5,942,860
- Ingard, U. : 1966, *Acoustic Wave Generation and Amplification in a Plasma.*, Physics Rev., Vol. 145, On pages: 41-46
- Ives, H. E. : 1922, *A Theory of Intermittent Vision.*, Journal of the Optical Society of America and R.S.I., Vol. 6, On pages: 343-361
- Jiang, Y. and others : 2003, *An Adaptive Acoustic Resonance Free Electronic Ballast for HID Lamps.*, IEEE, Conference Record of the Industry Application Conference. 38th Annual meeting. On pages: 1020-1024
- Jongerius, M. J. and Ras, A. J. M. J. and Vrehan, Q. H. F. : 1984, *Optogalvanic Detection of Acoustic Resonances in a High-Pressure Sodium Discharge.*, Journal of applied Physics 55(7), 1 April 1984
- Kaiser, W. and others : 2003, *Sound Emission from Pulse Operated High-Pressure Sodium Lamps.*, Industry Applications Conference, Volume: 2 On pages: 1036-1042
- Kalloniatis, M. and Luu, C. : 2005, *Psychophysics of Vision.*,
Internet web site:
<http://retina.umh.es/Webvision/Psych1.html#Psychophysical>
- Keijsers, R. A. J. : 2001, *Electronic operation of HID lamps.*, LS9, Ithaca pp. 103-111.

- Kelly, D. H. : 1961, *Visual Response to Time-Dependent Stimuli. I. Amplitude Sensitivity Measurements.*, JOURNAL OF THE OPTICAL SOCIETY OF AMERICA Vol. 51, Nr 4
On pages: 422-429
- Kelly, D. H. : 1969, *Diffusion Model of Linear Flicker Responses.*, JOURNAL OF THE OPTICAL SOCIETY OF AMERICA Vol. 59 Nr. 12 On pages: 1665-1670
- Kelly, D. H. : 1971, *Theory of Flicker and Transient Response. I. Uniform Fields.*, JOURNAL OF THE OPTICAL SOCIETY OF AMERICA Vol. 61 Nr.4 On pages: 537-546
- Koenderink, J.J. and Van Doorn A.J. : 1977, *Detectability of Power Fluctuations of Temporal Visual Noise.*, Vision Res. Vol. 18 On pages: 191-195
- Kolb, H. : 2003, *How the Retina Works.*, American Scientist, Vol. 91. On pages: 28-35
- Koshimura, Y. and others : 1983, *Stable High Frequency Operation of High Intensity Discharge Lamps and Their Ballast Design.*, Proc. CIE 20th Session. On pages: E/36-1 E/36-2
- Kramer, J.M. : 2001, *Reduction of Vertical Segregation in a Discharge Lamp.*, US Patent 6,184,633
- Kramer, J. M. : 2002, *Systems and Method for Detecting the Frequency of Longitudinal Mode Required for Color Mixing in a Discharge Lamp.*, US Patent 6,400,100 B1
- Kramer, J. M. : 2003, *Reducing Vertical Segregation in a HID Lamp Operated at VHF Frequencies Using Simultaneous Arc Straightening and Color Mixing.*, US Patent 2003/0117085 A1
- Krein, P.T. : 1999, *Ripple correlation control, with some applications*, Proceedings of the 1999 IEEE International Symposium on Circuits and Systems. On pages: 283-286
- Kuge, T. : 2002, *Wavelet Picture Coding and its Several Problems of the Application to the Interlace HDTV and the Ultra-High Definition Images.*, NHK Laboratories Note No. 481
Internet web site:
<http://www.nhk.or.jp/strl/publica/labnote/lab481.html>
- Lake, W.H. and Davenport, J.M. : 1982 *Low wattage Metal Halide Lamps.*, Journal of Illuminating Engineering Society. January 1982
- Lama, W. and Hammond, T. : 1981, *Arc-acoustic Interaction in Rare Gas Flashlamp.*, Applied Optics, Vol. 20 No. 5 On pages: 765-769
- Lapatovich, W. P. and others : 1996, *Method for Deflecting The Arc of an Electrodeless HID Lamp.*, US Patent 5,508,592
- Laskai, L. and others : 1998, *White-Noise Modulation of High-Frequency High-Intensity Discharge Lamp Ballasts.*, IEEE Transactions on Industry Applications, Vol. 34, No. 3. On pages: 597-605

- Lichtenberg, S. and others : 2002, *Observation of different modes of cathodic arc attachment to HID electrodes in a model lamp.*, JOURNAL OF PHYSICS D: APPLIED PHYSICS 35. On pages: 1648-1656
- Lighthill, M.J. : 1978, *Acoustic Streaming.*, Journal of Sound and Vibration. vol. 61, No. 3. On pages: 391-418
- Lindner, H. : 1992, *Lichtwelligkeit von Gasentladungslampen.*, Licht 7- 8/1992 On pages: 631-638
- Lister, G.G. and others : 2004, *The physics of the discharge Lamps.*, Reviews of Modern Physics. Vol. 76. April 2004. On pages: 541-598
- Rayleigh, Lord : 1883, *On the circulation of air Observed in Kundt's Tubes, and On Some Applied Acoustical Problems.*, Phylos. Trans. Roy. Soc. London Ser. A, Vol. 175 On pages: 1-21
- Maheshwari, A. and others : 1999, *Discharge Lamp Driving.*, US Patent: 5,932,976
- Mason, S. J. and Zimmerman, H. J. : 1960, *Electronic Circuits, Signals and Systems.*, John Wiley Sons, Inc., StateplaceNew York, 1960
- McKim, J. : 1992, *The UIE Flickermeter Demystified.*,
Internet web site:
<http://www.cemag.com/archive/1999/mayjune/McKim.html>.
- Melis, j. : 1998, *Electronic Ballast Design for HID lamps.*,
Internet web site:
<http://www.ballastdesign.com/index.shtml>
- Mitome, H. : 1998, *The mechanism of Generation of Acoustic Streaming.*, Electronics and Communications in Japan, Part 3. Vol. 81 No. 10
- Moo, C.S. and others : 2003 *High-frequency electronic ballast with auto-tracking control for metal halide lamps.*, IEEE, Industry Applications Conference. Conference Record of the 38th IAS Annual Meeting. Vol. 2, Issue, 12-16 On pages: 1025-1029
- Montag, E.D. : 2002 I., Stevens' Power Law.,
Internet web site:
http://www.cis.rit.edu/people/faculty/montag/vandplite/pages/chap_6/ch6p10.html
- Montag, E.D. : 2002 II., Psycophysics.,
Internet web site:
http://www.cis.rit.edu/people/faculty/montag/vandplite/pages/chap_1/ch1p2.html
- Montag, E.D. : 2002 III., weber's Law.,
Internet web site:
http://www.cis.rit.edu/people/faculty/montag/vandplite/pages/chap_3/ch3p1.html

- Moskowitz, P.W. and Olsen, J. : 2004, *Method for Measuring Ripple Generated by an HID Ballast.*, 10th International Symposium on the Science and Technology of Light Sources, Toulouse, France, July 2004
- Morse, P.M. : 1948, *Vibration and Sound.*, 2nd ed., McGraw-Hill, New York
- Nishimura, H. : 1988, *A New Electronic Ballast for HID Lamps.*, Journal of the Illuminating Engineering Society. Summer 1988
- Obitko, M. : 1998, *Introduction to Genetic algorithms.*,
Internet web site:
<http://cs.felk.cvut.cz/xobitko/ga/>
- Oh, D. J. and others : 2002, *A Novel Complex Modulation Method for the Metal Halide Lamp Ballast.*, IEEE I28th Annual Conference of the Industrial Electronics Society, Vol.: 1, On pages: 377-382
- Olsen, J. and Moskowitz, P.W. : 1997, *Optical Measurement of Acoustic Resonance Frequencies in HID Lamps.*, IEEE Industrial Application Society. 1997. Thirty-second IAS Annual Meeting Vol. 3. On Pages: 2263-2269
- Olsen, J. and Moskowitz, P.W. : 2005, *Detrimental effect of a small amount of ripple in a metal halide system.*, IEEE, Industry Application Conference. Fourtieth IAS Annual Meeting. Vol. 3, On pages: 1581-1587
- Pabst, W. : 1986, *Analoge und digitale Filter für Flickermessungen an Lampen.*, Technische-wissenschaftliche Abhandlungen der Osram-Gesellschaft. Zwölfter Band. On pages: 256-267
- Peng, H. and others : 1997, *Evaluation of Acoustic Resonance in Metal Halide Lamps and an Approach to detect its Occurrence.*, IEEE, Record of the 32nd Annual Meeting of the Industry Application Conference.
- Perlman, I. : 2005, *The Electroretinogram: ERG*,
Internet web site:
<http://retina.umh.es/Webvision/ERG.html>
- Ponce, M. and others : 2004, *Electronic Ballast for HID Lamps with High Frequency Square Waveform to Avoid Acoustic Resonances*, Journal of circuits, systems, and Computers. Vol. 13, No. 3. On pages: 651-663
- Rackensperger, W. and Grüsser, O. : 1966, *Sinuslichtreizung der rezeptiven Felder einzelner Retinaneurone.*, Experienta 22, Basel.
- Rashbass, C. : 1970, *The Visibility of Transient Changes of Luminance.*, Journal of Physiol. 210, On pages: 165-186
- Ribarich, T. : 2006, *Shedding Light on HID Ballast Control.*, Power Electronic Technology.
Internet web site:
<http://powerelectronics.com/mag/610PET22.pdf>

- Ribarich, T. and others : 2007, High Intensity Discharge Lamp Ballast Circuit., US patent 7,190,151
- Rinalducci, E. and others : 1999, *Mechanism of photopic, mesopic and, scotopic vision.*, Proceedings of Vision at low light Levels. EPRI/LRO. TR-110738 On pages: 13-24
- Rovamo, J. and others : 1999, *The effects of Temporal noise and retinal illuminance on foveal flicker sensitivity*, Vision Research 39 (1999). On pages: 533-550
- Sastrapradja D. : 2004, *Rayleigh Streaming Simulation Using the Vorticity Transport Equation.*, Ph.D. Thesis. The Pennsylvania University
- Schäfer, R. and Stormberg, H. P. : 1982, *Investigation on the Fundamental Longitudinal Acoustic Resonance of High Pressure Discharge Lamps.*, Journal of Applied Physics 53(5) May 1982
- Schieber, F. : 2006, *Weber's Law of Just Noticeable Differences.*, Internet web seit:
<http://www.usd.edu/psyc301/WebersLaw.htm> and <http://www.usd.edu/schieber/>
- Scholz, C.F. : 1970, *Characteristics of Acoustical Resonance in HID Lamps.*, Illuminating Engineering Society, December 1970
- Schuster, V.K. and Matz, W. : 1970, *Über Stationäre Strömungen im Kundtschen Rohr.*, Akus. Zeitschrift, Vol. 5 On pages: 349-352
- Shen, E. : 2002, *Method for Coloring Mixing of HID lamps Operated at VHF Frequencies Using duty Cycle Modulation.*, US Patent 6,498,441 B1
- Simons, G. : 1917, *Das Flackern des Lichtes in Elektrischen Beleuchtungsanlagen.*, ETZ Nr. 37, On pages: 453-455 and Nr. 38, On pages: 465-468 and Nr. 39, On pages: 474-476
- Sperling, G. and Sondhi, M.M. : 1968, *Model for Visual Luminance Discrimination and Flicker Detection.*, Journal of the Optical Society of America Vol. 58, No. 8 On pages: 1133-1145
- Statnic, E. : 1986, *Zum Hochfrequenzbetrieb von Halogen-Metaldampflampen kleiner Leistung.*, Technisch-Wissenschaftliche Abhandlungen der Osram-Gesellschaft. 12.Band
- Stockwald, K. : 2007 *operating Method, Electronic Ballast ans System for the Resonant Operation of High Pressure Lamps in the Longitudinal Mode.*, US patent 7,157,867 B2
- Stevens, S. S. : 1975, *Psychophysics: Introduction to its perceptual, neural and social prospects.*, New York: Wiley.
- Stormberg, H.P. and Schäfer, R. : 1983, *Excitation of Acoustic Instabilities in Discharge Lamps with Pulsed Supply Voltage.*, Lighting Research and Technology. Vol. 15 No. 3 On pages: 127-132

- Sturm, C.H. and Klein, E. : 1992, *Betriebsgeräte und Schaltungen für Elektrische Lampen.*, 6., neubearbeitete Aufgabe, 1992
- Sun, Y. : 2000, Method and Driving Circuit for HID Lamp Electronic Ballast., US patent 6,144,172
- Sun, Y. and Goriki, T. :2000, *Driving Circuit for High Intensity discharge Lamp Electronic Ballast.*, US Patent No. 6,020,691
- Tanahashi, T. : 1975, *On the Damping Factor of Acoustic Waves Due to Viscosity and Heat Conduction.*, Japan National Congress for Applied Mechanics, 23rd, Tokyo, Japan, October 1973, Proceedings. (A75-46726 24-31) Tokyo, University of Tokyo Press, 1975, p. 357-374.
- Turchi, J. : 2003, *Power Factor Correction Stages Operating in Critical Conductance Mode.*, Semiconductor Components Industries, LLC, 2003.
Internet web site:
<http://www.onsemi.com/pub/Collateral/AND8123-D.PDF>
- Veringa, F. : 1970, —, JOURNAL OF THE OPTICAL SOCIETY OF AMERICA Vol.60, On page: 286
- Victor, J. D. : 1989, *Temporal Impulse Response from Flicker Sensitivities : Causality, linearity and Amplitude Data Do not Determine Phase.*, JOURNAL OF THE OPTICAL SOCIETY OF AMERICA A6, On pages: 1302-1303
- Wada S. and others : 1987, *Study of HID lamps with Reduced Acoustic Resonances.*, Journal of the illuminating Engineering Society winter 1987, On pages: 162-175
- Wang, C. H. and Devaney, M. J. : 2004, *Incandescent Lamp Flicker Mitigation and Measurement.*, IEEE Transactins on Instrumentation and Measurement. Vol. 53, No. 4, August 2004. On Pages: 1028-1034
- Wang, J and others : 2004, *Low-Frequency Sine Wave Modulation of 250W High-frequency Metal Halide Lamp Ballasts.*, IEEE, Nineteenth Annual Applied Power Electronics Conference and Exposition, APEC apos;04. Vol.: 2 Issue 2004 On Pages: 1003-1007
- Waymouth, J. F. : 1971, *Electric Discharge Lamps.*, The Massachusetts Institute of Technology Press.
- Witting, Harald L. : 1978, *Acoustic Resonances in Cylindrical High-Pressure Arc Discharge.*, Journal of Applied Physics 49. On Pages: 2680-2683
- Yan, W. and Hui, S.Y.R. : 2000, *Investigation on Methods of Eliminating Acoustic Resonance in Small Wattage High Intensity Discharge Lamps.*, IEEE Industrial Application Conference, Volume 5, 8-12 Oct. 2000 On pages: 3399-3406
- Yan, W. and Hui, S.Y.R. : 2004, *Aging Effect on the Stability Performance of Small Wattage Metal Halide Lamps.*, IEEE, Nineteenth Annual Applied Power Electronics Conference and Exposition, APEC '04. Vol.: 2, On pages: 978-983
- Zhou, and others : 1999, *A Novel Method for Testing acoustic Resonance of HID Lamps.*, IEEE Applied Power electronics Conference and Exposition. AEPC 99, Vol. 1. On pages: 480-485